WRDC-TR-89-2046

STUDIES ON THE STARTUP TRANSIENTS AND PERFORMANCE OF A GAS LOADED SODIUM HEAT PIPE

R. Ponnappan

Universal Energy Systems, Inc.
4401 Dayton-Xenia Road
Dayton, Ohio 45432

June 1989

Technical Report for Period June 1987 - November 1988

AERO PROPULSION LABORATORY
WRIGHT RESEARCH AND DEVELOPMENT CENTER
AIR FORCE SYSTEMS COMMAND
WRIGHT-PATTERSON AIR FORCE BASE, OHIO 45433-6563

REPORT DOCUMENTATION PAGE

Form Approved
OMB No. 0704-0188

1a. REPORT SECURITY CLASSIFICATION Unclassified	1b. RESTRICTIVE MARKINGS N/A
2a. SECURITY CLASSIFICATION AUTHORITY N/A	3. DISTRIBUTION/AVAILABILITY OF REPORT Approved for public release; Distribution is unlimited
2b. DECLASSIFICATION/DOWNGRADING SCHEDULE N/A	
4. PERFORMING ORGANIZATION REPORT NUMBER(S) UES-799-TR-87-001	5. MONITORING ORGANIZATION REPORT NUMBER(S) WRDC-TR-89-2046
6a. NAME OF PERFORMING ORGANIZATION Universal Energy Systems, Inc. 6b. OFFICE SYMBOL (If applicable) SS/TTSG	7a. NAME OF MONITORING ORGANIZATION Wright Research and Development Center, Aero-propulsion and Power Laboratory (WRDC/POOS)
6c. ADDRESS (City, State, and ZIP Code) 4401 Dayton-Xenia Road Dayton, OH 45432	7b. ADDRESS (City, State, and ZIP Code) Wright-Patterson Air Force Base OH 45433-6563
8a. NAME OF FUNDING/SPONSORING ORGANIZATION 8b. OFFICE SYMBOL (If applicable)	9. PROCUREMENT INSTRUMENT IDENTIFICATION NUMBER F33615-87-C-2738
8c. ADDRESS (City, State, and ZIP Code)	10. SOURCE OF FUNDING NUMBERS PROGRAM ELEMENT NO. 62203F; PROJECT NO. 3145; TASK NO 30; WORK UNIT ACCESSION NO. 51

11. TITLE (Include Security Classification)
Studies on the Startup Transients and Performance of a Gas Loaded Sodium Heat Pipe

12. PERSONAL AUTHOR(S)
Rengasamy Ponnappan

13a. TYPE OF REPORT	13b. TIME COVERED	14. DATE OF REPORT (Year, Month, Day)	15. PAGE COUNT
Interim	FROM 29JUN87 TO 30NOV88	JUNE 1989	251

16. SUPPLEMENTARY NOTATION
Prepared as a doctoral dissertation (Ph.D.) for the University of Dayton, Dayton, Ohio.

17. COSATI CODES			18. SUBJECT TERMS (Continue on reverse if necessary and identify by block number)
FIELD	GROUP	SUB-GROUP	
22	02	00	Artery, Startup, Noncondensible Gas, Frozen Start, Diffusion Model, Reservoir Wick, Heat Front, High Temperature, Liquid Metal, Sodium, Transient Analysis.
10	01	00	

19. ABSTRACT (Continue on reverse if necessary and identify by block number)

High temperature liquid metal heat pipes have exhibited difficulties starting up from frozen state due to inherent low near-room temperature vapor pressures associated with working fluids. Inert gas loading is a possible solution to the frozen state startup problem. A few research papers give results of this technique. The applicability of the method to heat pipes with arterial grooves and long adiabatic lengths is unknown. The present study deals with the design, fabrication and startup testing of a gas loaded sodium heat pipe of the double walled type with grooved artery channel and long adiabatic section.

A 2 m long, 2.22 cm diameter stainless steel heat pipe was designed to transport 1800 W at 1000 K and charged with 1.35 torr argon at room temperature. A two dimensional, quasi steady state, binary vapor gas diffusion model determined energy transport rate of

(continued)

20. DISTRIBUTION/AVAILABILITY OF ABSTRACT ☒ UNCLASSIFIED/UNLIMITED ☐ SAME AS RPT. ☐ DTIC USERS	21. ABSTRACT SECURITY CLASSIFICATION Unclassified
22a. NAME OF RESPONSIBLE INDIVIDUAL Michael Morgan	22b. TELEPHONE (Include Area Code) (513) 255-2922 22c. OFFICE SYMBOL WRDC/POOS

Item 19. ABSTRACT (cont'd)

vapor at the diffusion front. The hot vapor front did not move until the vapor pressure became equal to the initial gas charge pressure. At the beginning of startup, the diffusion rate was high and decreased exponentially to a very low value as steady state was approached. A one-dimensional transient thermal model of the startup process considered energy balances on hot and cold zones individually with the vapor diffusion process as the heat transfer coupling between the two zones. The diffusion model was solved analytically to give the vapor flux which in turn was used in the thermal model to predict the time rate of change of temperature and position of the hot front. A computer code developed to solve the transient problem calculated fluid depletion in the evaporator during startup which dictated the maximum limit on gas pressure. Startup temperature and time were also determined.

The experimental heat pipe was tested in a vacuum chamber for steady state and transient performances. In both vacuum and gas filled modes, good agreement between the theory and experiment was observed. It was concluded that a gas loaded liquid metal heat pipe could be easily started from the frozen state without adverse effects even if the heat pipe had a long adiabatic artery channel.

FOREWORD

This technical report describing the design, fabrication and startup testing of a 2 m Double Wall Artery Gas Loaded Sodium Heat Pipe was prepared under the Air Force Contract No. F33615-87-C-2738, "Thermal Energy Storage and Heat Transfer Support." This contract was administered by the Aero-Propulsion and Power Laboratory (APPL) of the Wright-Patterson Air Force Base and funded by the Aerospace Power Division (WRDC/POOS-3) and Strategic Defense Initiative Organization (SDIO). Dr. E. T. Mahefkey was the Technical Area Manager. Ms. J. E. Johnson and Mr. Michael Morgan were the Program Monitors.

The heat transport study, Task 001 of this effort, was conducted on-site at the Thermal Laboratory (APPL) by Universal Energy Systems, Inc. with Mr. R. Ponnappan as the Principal Investigator. This report satisfied the partial fulfillment requirement for his doctoral degree from the University of Dayton.

Messrs. J. Tennant and M. D. Ryan (UES) and D. Reinmuller (APPL) provided the technical support for the various phases of the experimental work. Miss Cathy Baker (UES) helped on the computational aspects. UES Publications and Drafting groups provided their services for preparing this technical report.

TABLE OF CONTENTS

TABLE OF CONTENTS (continued)

TABLE OF CONTENTS (concluded)

LIST OF ILLUSTRATIONS

LIST OF ILLUSTRATIONS (continued)

LIST OF ILLUSTRATIONS (concluded)

LIST OF TABLES

SPECIAL NOMENCLATURE

Symbol	Definition
A	area
A_o, A_r, A_v	parameters, Eqs. (27)', (28)', (29)'
A_v	vapor core cross-sectional area, Eq. (65)
c	total molar density of mixture
c_c	c evaluated at temperature T_c
c_h	c evaluated at temperature T
c_i	initial molar density of the noncondensible gas
C	heat capacity per unit length
C_p	specific heat capacity at constant pressure
d	diameter
d_i	inner diameter of inner tube
d_o	outer diameter of inner tube
d_v	vapor core diameter
d_w	wick diameter
D	binary diffusion coefficient
D_i	inner diameter of outer tube
D_o	outer diameter of outer tube
f_ℓ	drag coefficient for liquid flow
f_u	ultimate tensile stress
$F_c(g)$	function, Eq. (16)
$F_h(g)$	function, Eq. (17)

Symbol	Definition
F_{HC}	radiation shape factor between hot and cold zones
F_{ℓ}	friction factor for liquid flow
F_v	friction factor for vapor flow
g	dimensionless vapor flux (diffusion parameter), Chapter II
g	gravitational acceleration, Chapter III
h_{fg}	heat of vaporization per unit mass
H	capillary height potential, Eq. (44)
k	thermal conductivity
k_{eff}	wick effective thermal conductivity
K	wick permeability
ℓ	dimensionless length
L	length
m	fluid inventory
$\dot{m}$	rate of fluid mass depletion during startup, Eq. (33)
M	total mass of fluid depleted, Eq. (34)
M_A, M_B	molecular weight of vapor, Appendix A
M_v	vapor flow Mach number
n	number of grooves

SPECIAL NOMENCLATURE (continued)

Symbol	Definition
N	screen mesh number
$\vec{N}_g$	molar gas flux
$\vec{N}_o$	initial vapor flux
$\vec{N}_v$	molar vapor flux
P	pressure
P_c	capillary pressure
P_{cm}	maximum capillary pressure
P_i	initial pressure of noncondensible gas at room temperature
P_{pm}	maximum available pumping pressure
P_v	vapor pressure
q_i, q_o, q_r, q_v	dimensionless Q_i, Q_o, Q_r, Q_v, respectively
Q	heat flow rate
Q_i	heat input rate
Q_o	heat rate radiated at the condenser
Q_r	heat rate exchanged between the hot and cold zones internally
Q_v	heat transport rate of the vapor diffusing into the noncondensible gas at the vapor-gas front
r	radius
$\bar{r}$	dimensionless r
r_c	capillary radius

Symbol	Definition
$r_{h,\ell}$	hydraulic radius for liquid flow
r_m	mean radius
r_n	nucleation radius for boiling
r_v	vapor core radius
$R_1, R_2, \ldots, R_8$	resistance to liquid flow, Appendix G
$\bar{R}$	universal gas constant
Re_ℓ	Reynolds number for liquid flow
Re_v	Reynolds number for vapor flow
R_v	gas constant for vapor
s_1, s_2	parameters, Eq. (23)'-(26)'
t	thickness, Chapter III and Appendix F
t	time
t_i	rise time
t_s	startup time
T	temperature
T_c	room temperature
T_H	lumped hot zone temperature
T_{Hi}	rise temperature
T_{Hs}	startup temperature
T_o	initial temperature
T_s	test chamber shroud temperature

SPECIAL NOMENCLATURE (continued)

Symbol	Definition
T_v	vapor temperature
v	specific volume, Eq. (73)
w	groove width
x_g	mole fraction of noncondensible gas
x_v	mole fraction of vapor
y	noncondensible gas concentration variable, Eq. (12)
z	distance along pipe
$\bar{z}$	dimensionless z

Greek Symbol	Definition
γ_v	vapor specific heat ratio
δ	groove depth
ΔP	pressure drop
Δr	radial thickness
ΔT	temperature difference
ϵ	emissivity
ϵ	porosity of screen wick, Eq. (49) and (83)
ϵ_H	emissivity of hot zone internally
ϵ_p	emissivity of pipe external surface
ϵ_{AB}	Lennard-Jones parameter, Appendix A
θ	dimensionless temperature, Eq. (23)'-(26)'

SPECIAL NOMENCLATURE (continued)

Greek Symbol	Definition
θ	wetting angle, Eq. (44)
κ	Boltzmann constant, Appendix A
λ	latent heat of vaporization, Chapter III
$\lambda(\theta,\ell)$	parameter, Eq. (11)
μ	dynamic viscosity
ν	kinematic viscosity
ρ	density
σ	Stefan-Boltzmann constant
σ_{AB}	collision diameter
σ_{ℓ}	surface tension coefficient, Eq. (40)
ψ	heat pipe tilt to the horizontal, Eqs. (41) and (42)
$\Omega_{D,AB}$	collision integral, Appendix A

Subscript	Definition
ax	axial
A	adiabatic
Ar	argon
c	cold zone
C	condenser
E	evaporator
eff	effective

Subscript	Definition
h	hot zone
i	inner
in	input
I	insert
ℓ	liquid
m	mean
Na	sodium
NCG	noncondensible gas
o	outer, output
P	pipe
r,R	radial, reservoir, radiative (as noted in text)
s	sonic, screen
ss	stainless steel
v	vapor
w	wick, wire, wall

Abbreviation	Definition
DWAHP	double wall artery heat pipe
dia.	diameter
eq.	equation
ID	inner diameter

SPECIAL NOMENCLATURE (concluded)

Abbreviation	Definition
LHS	left hand side
NCG	noncondensible gas
OD	outer diameter
RHS	right hand side
TC#	thermocouple location number
TIG	tungsten-inert-gas
VCHP	variable conductance heat pipe

CHAPTER I

INTRODUCTION

1.1 About the Heat Pipe in General

The heat pipe is a wonderful and conceptually simple two-phase (liquid and vapor) thermodynamic/heat transport device invented to circumvent the barrier of solid metallic conductance. The heat pipe working principle was first proposed in 1944 but the fruit of the research in this area was realized only during the past couple of decades starting from the original work on heat pipes at Los Alamos National Laboratory, which coined the word "heat pipe" [1-3]. Though the original work was in conjunction with the thermionic converters (to work out-of-core in nuclear reactors), heat pipes were used extensively in spacecraft for thermal control applications in the pre-Apollo and post-Apollo missions. The rapid development of this device caught up with many other terrestrial (solar, energy regeneration and electronics cooling) applications as well. Today this device is a commercial off-the-shelf item with dozens of manufacturers in the United States, Europe and Japan.

The name heat pipe should not be confused with the "heat pump" (which has a separate role in thermodynamics) where there is net work done whereas in a heat pipe there is no net work and no moving parts. The heat pipe is a closed tube or chamber with one of many different shapes whose inner surfaces are lined with a porous

capillary wick. The wick is saturated with the liquid phase of the working fluid and the remaining volume of the chamber contains the vapor phase. Heat applied at the evaporator vaporizes the liquid in that section causing the pressure difference to drive the vapor down to the condenser section where it condenses releasing the latent heat of vaporization to a heat sink. The condensate is returned back to the evaporator by the capillary pumping action of the wick and this process continues as long as the wick does not become dry. This is the basic working principle of a heat pipe. The heat pipe is functionally a "heat transport pipe" as well as:

- A high conductance device. It surpasses the best metallic conductors such as gold, silver and copper in thermal conductance. Its conductance could be anywhere from 30-4800 times that of an equivalent size copper bar in various temperature ranges.
- Near-isothermal. From end-to-end, the temperature drop (ΔT) is very small; much smaller than that of a metallic conductor.
- Has no moving parts. It is a hermetically sealed stationary device; works as it rests.
- Transports heat. From one end to the other end without the expense of any external work done on it, the transport mechanism being the closed loop flow pattern of the evaporating liquid and the condensing vapor set up by the capillary wick and the working fluid contained inside it.

- Not an engine. Since it does not have any net work, there is no efficiency defined for this. Its performance is judged by the maximum heat transport ability and the distance of transport under minimum temperature drop.
- Analogous to a transformer (electrical). It can accept heat input at certain flux and deliver at a different flux.
- A maintenance free, no-noise device. Once installed, it does not require maintenance and does not make any noise during operation.
- A vapor chamber. It may build up high pressure inside if heated inappropriately leading to hazardous explosion.

Heat pipes can be categorized into several types based on their working principle, configuration of the wick structure and working temperature range [4].

(1) Working Principle:
- Conventional heat pipe mode
- Thermo syphon
- Variable conductance heat pipe
- Osmotic heat pipe
- Wickless rotating heat pipe
- Capillary pumped loop heat pipe
- Electrodynamic heat pipe

(2) Configuration:
- Shape - cylindrical, flat, annular, bent in forms - U,L,C, etc.
- Structure - rigid or flexible
- Material - metallic or ceramic

- Wicks - conventional, composite and arteries

(3) Temperature:

- Cryogenic (<122 K)
- Moderate temperature (122-628 K)
- High temperature (>628 K)

Figure 1 illustrates the heat pipe temperature regimes and working fluids.

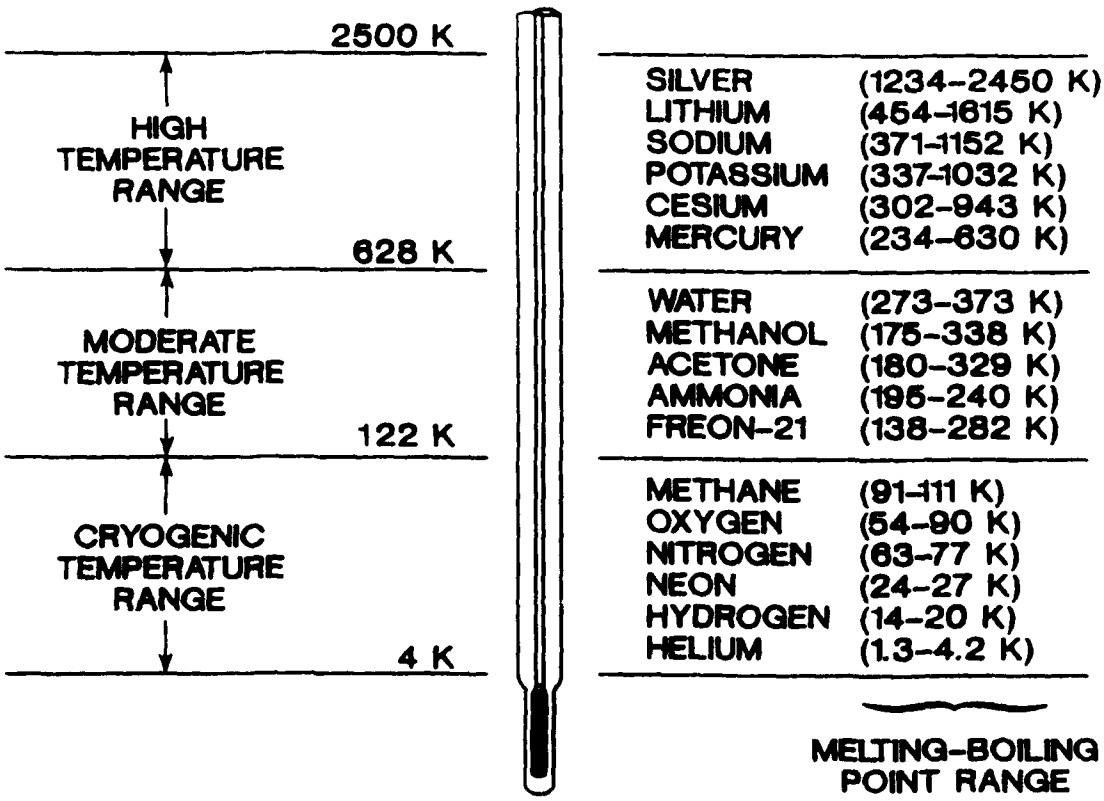

Figure 1. Heat Pipe Temperature Regimes and Working Fluids.

1.2 Outstanding Problem

In recent years, the demand for high capacity, high performance, and reliable heat pipe systems has increased with the advent of newer space missions such as space stations and terrestrial applications, including power plants, electronic cooling, highway deicing, etc. Fairly well established design, fabrication, material compatibility, and steady state performance testing procedures for all types of heat pipes exist in the industry [4 8]. However, a thorough understanding of the transient characteristics is lacking. An area of major concern for heat pipe applications, particularly liquid metal, high temperature heat pipes, is the behavior of these devices under transient load conditions during startup, shutdown and operational variation of the thermal loads. The startup process may not be successful when the working fluid is in the frozen state since there will be no liquid return from the condenser to the evaporator. A sudden removal of the heat input to the evaporator (shutdown) without removing the condenser load may freeze the working fluid at the condenser and create evaporator dryout [9]. These transient operating problems are further complicated by special artery wick designs which provide superior performance during normal operation. An example of a special wick design, shown in Figure 2, is the Double Wall Artery Heat Pipe (DWAHP) developed by Ponnappan and Mahefkey [10].

The DWAHP was introduced in 1982 and a modified design was developed subsequently [11]. In the modified DWAHP, a screenless adiabatic length is used in order to make very long heat pipes

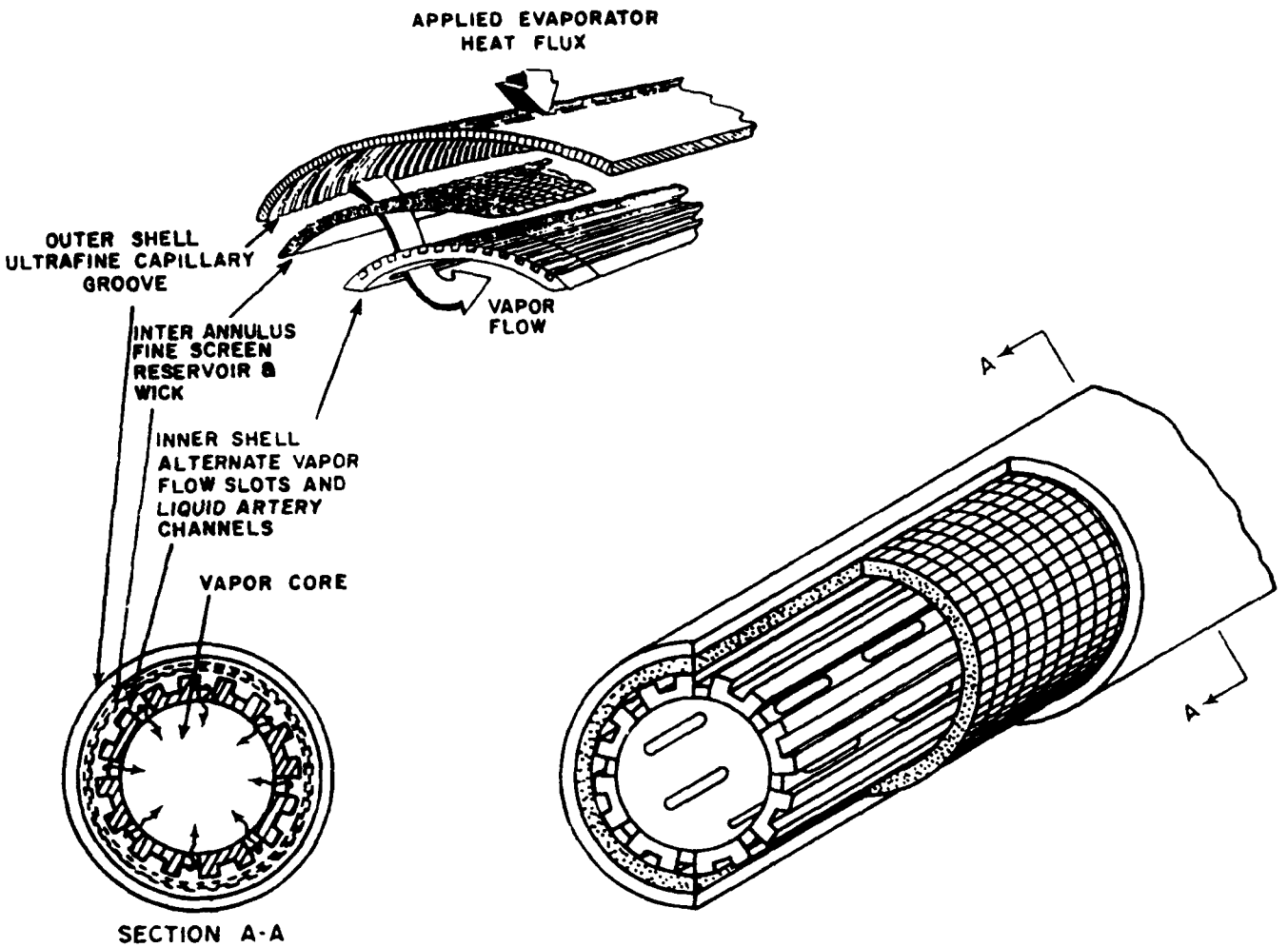

Figure 2. Double Wall Artery Wick Concept

simpler. Other unique advantages of this design are entrainment-free transport and the availability of lean wick evaporator configurations. Though this design concept works well in the low temperature regime (25-200°C) copper water system, it was not known whether the same design could be scaled up to the high temperature regime liquid metal system. The issues concerning the extension of the DWAHP development which form the basis of the present investigation are as follows:

(1) The choice of the wick structure.

(2) The methods of coupling the evaporator input and the condenser output.

(3) The thermal load requirements.

(4) The initial conditions of thawing or priming status of arteries.

(5) Whether a noncondensible gas filling will help startup from frozen state.

(6) What effects the gas will have on artery priming.

(7) The modeling of the startup from frozen state using the coupled diffusion and energy balance equations.

(8) The design, fabrication and testing of an appropriate hardware to verify the theoretical modeling.

1.3 Review of Literature

A literature search was conducted and a brief review is presented here. Though the heat pipe technology is only 25 years old, an abundant number of technical publications covering the broad spectrum of this technology exists in the open literature. A closer scrutiny of works related to transient behavior, unsteady power,

pulsed operation, startup, shutdown, and analysis/modeling narrowed down the publications to a sizeable number covering the period between 1967 and 1988. Online Information Retrieval (computer search) of data bases covering Physics Abstracts, Aerospace Abstracts, NTIS, DTIC, etc. was used for the literature search.

Cotter [12] was the first to quantify the dynamics of a heat pipe startup using a lumped-parameter one-dimensional model. An effective thermal conductivity in the axial direction of the heat pipe dependent upon the state of the vapor for the free molecular flow regime was introduced. Characteristic response times (condenser rate and axial rate of responses) were defined. He predicted the required length of the heat pipe, once the input and output conditions were determined.

Sockol and Forman [13] visually observed the moving temperature front during startup in a lithium heat pipe (1273-1673 K). Cotter's model was reassessed and modified. They predicted and confirmed that the temperature of the hot zone was fairly independent of the power input to the evaporator until the hot zone reached the end of the pipe.

Marcus [14,15] conducted an extensive investigation on the theory and design of room temperature gas loaded variable conductance heat pipe (VCHP). His study concentrated mainly on the steady state theory. Marcus noted that "seeking an accurate predictive capability for heat pipe transient behavior is substantially a more ambitious task than the development of the steady state theory."

Tower [16] performed an analysis of oxygen diffusion into metal alloys pertaining to the startup of T-111 (tantalum alloy) heat pipe filled with lithium.

Sockol [17] presented a model for the rapid startup of a high temperature gas loaded heat pipe. A two-dimensional analysis was used. Startup was not initiated until the vapor pressure P_v in the hot zone reached a value proportional to the initial gas pressure P_i. Through proper choice of P_i, startup could be delayed until P_v was large enough to match with the thermal load on the heat pipe. However, the analytical results were not verified with any experimental data.

The use of the liquid-trap as a secondary heat pipe for forward mode operation during a heat pipe diode shutdown was studied by B&K Engineering [18]. Thermal switching was defined as the shutting down of the thermal diode in case of a reversal of heat flow direction.

Camarda [19] used a simple analytical technique to determine startup, transient and steady state performance of the heat pipe during testing. The temperature ranged from 883 K to 922 K and heat flux 23.9 to 39.5 W/cm^2.

Colwell [20] developed a method for predicting the behavior of cryogenic heat pipes during startup or changes in thermal transport.

Williams [21,25) evaluated the forward (heat flow from evaporator to condenser) and reverse-mode (heat flow from condenser to evaporator) operation for an ethane heat pipe working in 170 to 220 K. Results indicated that the heat pipe might not reliably

startup in the forward mode. However, startup could be initiated when preceded by a diode reversal.

Groll and Munzel [22,23,26] presented an analysis and design of all aluminum and all stainless steel ammonia heat pipe diode. The liquid trap principle was used. The shutdown ratio, defined as the ratio of the forward mode conductance to the reverse mode conductance (W/K), was 384. Test program comprised transient shutdown behavior and restart from the shutdown condition.

Alario [24] developed a stainless steel ethane heat pipe diode and used it for investigating the startup dynamics of arterial cryogenic thermal diodes.

Shukla [27] conducted a combined analytical and experimental investigation of the transient response of a gas-controlled heat pipe with an absorption gas reservoir.

Groll and Supper [28] showed a shutdown technique which consisted of heating up the condenser with a constant heat flux while having the evaporator and trap thermally free-floating.

Bystrov et al. [29] presented the results of experimental studies of the startup of vacuum and of gas-loaded sodium heat pipes by sudden and smooth application of heat to the evaporator. A qualitative analysis of the dynamics of startup of such pipes was also presented.

Bystrov and Goncharov [30] examined an approximate method of calculating the unsteady temperature fields and the startup characteristics for a quick startup and switch to the heat pipe regime, using a lumped-parameter model for the vapor predicted on a

planar vapor-gas boundary and the possibility of neglecting the thermal inertia of the vapor flux. The analytical results were in good agreement with the experimental results of an argon filled annular artery sodium heat pipe.

Colwell and Chang [31] examined the transient behavior of a slab type wick in a low temperature heat pipe. It was found that under some conditions, the heat pipe might approach steady state operation with a portion of the capillary structure dried and that rewetting could be quickly accomplished. However, when the entire wick structure at the evaporator dried, rewetting was much more difficult.

Chang and Colwell [32] developed a computational model based on finite-difference approximations for predicting the transient operating characteristics of low temperature heat pipes. It was shown that the width of fluid gap between screen layers had a significant effect on the transient operation.

Colwell and Hartley [33] emphasized the need for developing the capability to predict operational behavior of liquid metal heat pipes under adverse operating conditions such as when drying, rewetting, choking, noncontinuum flow, freezing, thawing, etc., occurred within the heat pipe.

Beam [34] developed a lumped-parameter transient model of a heat pipe and verified his model with data obtained from a screen wick copper-water heat pipe. Two response times, one corresponding to the thermal response of the heat pipe and the other to the hydrodynamics of the wick with an applied heat flux, were defined.

An upper limit for the pulse size (so as not to create a dryout) was also determined in this analysis.

Cullimore [35] described the Advanced Simulation Analysis of Heat Pipes (ASAHP) program, that simulated the transient operation of heat pipes. The transient capabilities included wicking and entrainment-limited dryout and recovery simulation with the corresponding condenser flooding. The program provided a means to evaluate the effects of adverse transients (rapid changes in orbital environments, or high-power/short-duty cycles) on a spacecraft heat pipe radiator.

Ambrose et al. [36] have presented a simplified one-dimensional model to predict the drying and rewetting of the wick during a pulsed startup. Their model included a thermal capacitance term. They compared model predictions with the experimental results obtained with a copper water screen wick heat pipe. It was verified that the ability of the heat pipe to transport a pulsed heat load was equal to the maximum design capillary heat transport rate without dryout.

Tilton et al. [37] analyzed the transient behavior of a steady operating Inconel 617 sodium heat pipe with superimposed external thermal loading at the condenser. The analytical model predicted the direction of the mass flow of vapor and the location of the condensation and evaporation zones along the heat pipe as a function of time for different condenser heat loads. Heat pipe flow reversal and incipient dryout could be predicted. Experimental results of a

45-cm long 1.27-cm diameter screen wick heat pipe using radiant heaters were used to verify the analytical prediction.

Merrigan et al. [38] reported transient performance characteristics of a 4 m moly-lithium heat pipe with annular screen wick. Shutdown tests were conducted to establish the requirements of restarting the pipe from frozen condition. A freeze plug could form in the condenser during the cooldown and cause liquid depletion of the evaporator thereby causing restart difficulty.

Bobco [39] developed a closed form expression for estimating the location of the minimum temperature in the inactive condenser of a VCHP under steady state. Equations were presented to show how the gas reservoir design may be based on the operating conditions for maximum heat load and incipient freezeout. The experimental data of Marcus [14] were used to verify the theory.

Costello et al. [40] developed a comprehensive model but did not report calculation results. Hall and Doster [41] introduced the transient computer code called THROPUT (Thermal Hydraulic Response of Heat Pipe Under Transients) and applied it to verify the performance of a 4 m lithium heat pipe charged with a noncondensible gas at 10^{-4} Pa and 300 K. This code required large CPU time (24 hours on a VAX 8000 system for 2 hours of transients). In addition, it is reported that the liquid does not return fast enough to keep up with evaporation, resulting in an ever decreasing liquid inventory in the evaporation section.

Jang et al. [42] used finite element techniques with explicit and implicit solution procedures to solve the mathematical model of

a liquid metal heat pipe used in leading edge cooling. They compared model predictions with experimental data of Camarda [19] and found good agreement.

Seo and El-Genk [43] developed a two-dimensional transient model for liquid metal heat pipes that is capable of predicting the operating limits of the heat pipe during steady state and transient operations. Their model assumes a completely thawed heat pipe with no noncondensible gas in the vapor core of the annular wick heat pipe. They also show how the slow cooling rate (0.1 kW/s) or fast heat rate (1.0 kW/s) from a stable operating point can encounter the sonic or entrainment limit respectively in a 4 m long 1.9 cm outside diameter lithium heat pipe built at Los Alamos National Laboratory [38].

Peterson and Tien [44,45] found numerical and analytical solutions for two-dimensional gas distribution in gas loaded heat pipe in the room temperature regime. No frozen startup or transient behavior is studied here. The authors claim that the errors in "flat-front" diffusion models are eliminated and that the condenser shutoff length is computed accurately.

It is concluded from the literature review that a combination of analytical and experimental works on the transient behavior of various types of heat pipes exists. Most of the referenced papers deal with thermal diodes and cryogenic or room temperature heat pipes. There are only three publicatcns on the gas filled liquid metal heat pipe transient behavior; those of Sockol [17] and Bystrov et al. [29,30].

It is difficult to apply the analysis pertaining to a particular heat pipe design to another constructionally different heat pipe. Conventional or the homogeneous wick heat pipes are no longer useful for high capacity application. The state-of-the-art heat pipe designs have developmental and material problems. Making the heat pipes suitable for adverse operating conditions is a technological challenge. In view of this, it is of interest to develop the Double Wall Artery Heat Pipe into a liquid metal high capacity design and evaluate its performance theoretically and experimentally for steady and transient thermal loads.

1.4 Need and the Uniqueness of the Research

Future space missions will require large area space radiators constructed out of liquid metal heat pipes to reject large amounts of waste heat at rejection temperatures of 1000 K or more. Peak electric power, in excess of 1 MWe, is required which generates waste heat in the form of pulses with a peak-to-average ratio of 10^4 to 10^5 based on the mission and orbital duty cycles envisioned [46,47]. Essentially these heat pipes have to withstand directed energy impacts such as micrometeoroids, or pulsed input loads. A space nuclear power system is a typical example of a power supply requiring such high capacity liquid metal heat pipes [48].

Another example is NASA's space station which is being designed to be powered by a solar dynamic cycle. A solar dynamic system will require thermal energy storage and some form of energy transport device (liquid metal heat pipe) for transporting energy to the power conversion unit. The transition from illuminated to

eclipse portion of the orbit will introduce transient thermal loads on the heat pipe device [49]. In addition, cold start or thawing of a liquid metal heat pipe is a unique problem for space or terrestrial applications. Uniform distribution of the working fluid within the heat pipe wick structure is important during shutdown of any heat pipe device. An abrupt shutdown during a dryout may cause irrecoverable damage [9]. Long transport lengths cause priming and flow resistance problems. In essence, the need of a reliable liquid metal heat pipe is apparent from the above applications, and the uniqueness of investigating a liquid metal DWAHP for its startup and shutdown characteristics is exemplified by the operational requirements shown in Figure 3.

Though the general problem of transient operation is common to all the liquid metal heat pipes as well as low temperature heat pipes, the same problem is unique to the liquid metal DWAHP proposed to be investigated presently for the following reasons:

(1) Long transport section length without screen wick, no direct contact between liquid and vapor flows in the transport sections;

(2) Composite wicking arrangement with arterial grooves nonconstant groove widths; and

(3) Noncondensible gas loading and reservoir wick in evaporator to aid startup from frozen state.

1.5 Statement of the Problem

The startup of a liquid metal heat pipe (sodium, potasium or lithium) from the frozen state is an area of concern for potential

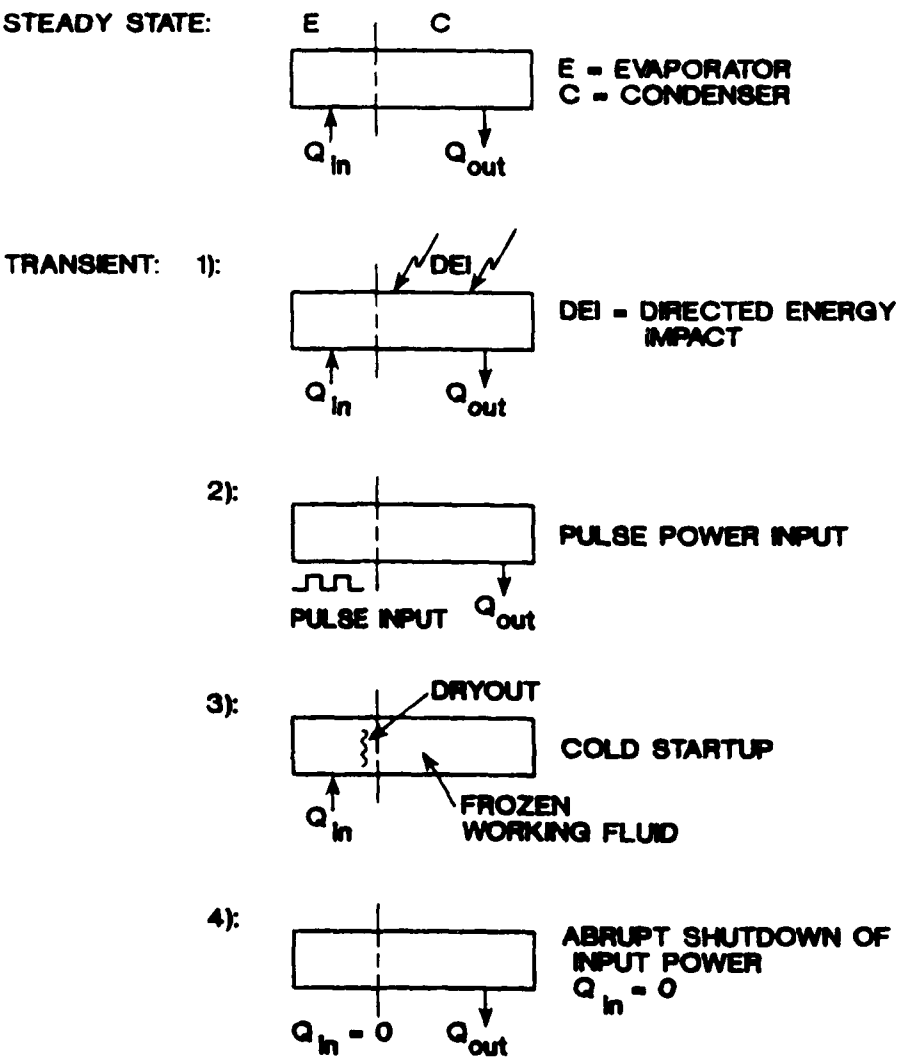

Figure 3. Operational Requirements of a Liquid Metal Heat Pipe

applications in space radiators since the heat pipe may dry out due to the working fluid depletion in the evaporator during startup. Though active methods such as electrical trace heating or prelaunch thawing can be adapted for starting, they are neither convenient nor desirable. A passive and reliable startup technique which will not require onboard electrical power is preferable. Researchers have recommended filling the liquid metal heat pipe with noncondensible gas in order to make it start easily [17,30]. The heat pipe geometry they used was quite different from the one tested in the present work. A composite wick high capacity liquid metal heat pipe of the DWAHP type with long adiabatic section has not been built and tested so far.

The DWAHP gains further attention for investigation because of its entrainment free and capillary wickless transport section, high radial heat flux evaporator design, and ease of manufacture. The present problem is to investigate and find answers to the following basic questions on this subject area.

(1) Will the noncondensible gas charging provide reliable startup of a liquid metal arterial heat pipe of the DWAHP type?

(2) What analytical methods could be used or need to be developed to solve the transient problem of the above mentioned heat pipe, e.g., the mass diffusion and thermal problems?

(3) How do the vapor front propagation and the temperature vary with time and input power variation?

(4) What experimental methods can be devised to explore the above?

1.6 Objectives of the Present Study

The scope and objectives of the present study are grouped and defined under two categories, namely, analytical and experimental:

- Analytical. Develop an analytical model and solve to predict the frozen state startup and the transient thermal characteristics of a high temperature heat pipe with long adiabatic section and filled with noncondensible gas charge. The study of the effects of different initial charge pressures and power input is also of interest.
- Experimental. Design, fabricate and test suitable experimental hardware to verify the analytical predictions on the startup transients. Investigate the dynamics of the diffusion zone during the transient condition and determine the condenser shutoff length during the steady state condition.

CHAPTER II

THEORETICAL ANALYSIS OF STARTUP

2.1 Startup Characteristics

In general, heat pipes are intended for isothermal operation at a fixed temperature and energy transport. Starting up a heat pipe does not present any difficulty if it is heated isothermally to the operating temperature with the power then gradually increased to the allowable limit. Often in practical situations, this method of startup is inconvenient or even impossible and also the condenser zone heat removal is effected simultaneously with the evaporator heating. Other aspects which concern startup are:

(1) The allowable rate and duration of heat supply;

(2) The method of heat transfer coupling between the source and the evaporator, and the sink and the condenser;

(3) The initial state (solid, liquid or vapor) of the working fluid within the wick structure;

(4) The heat transport capacity versus temperature characteristics of the heat pipe; and

(5) The wick design in the transport zone.

Three characteristic startup types have been categorized for heat pipes:

(1) Uniform startup (e.g., water and ammonia heat pipes);

(2) Frontal startup without noncondensible gas (NCG) (e.g., sodium heat pipe); and

(3) Frontal startup with NCG (e.g., sodium heat pipe with argon).

These are very well described in the heat pipe literature [4,8]. Figure 4 illustrates these startup characteristics schematically.

Heat pipes with working fluids having high vapor pressures at startup temperatures typically exhibit uniform startup, while those with low vapor pressures exhibit frontal startup. Use of NCG in the vapor core has been found to ease the startup difficulties in liquid metal heat pipes [8,17,30]. There are however advantages and disadvantages in charging a heat pipe with NCG:

Advantages

(1) The heat pipe is enabled to operate as a variable conductance heat pipe (VCHP).

(2) The NCG acts as a buffer to the working fluid vapor while expanding into the vapor core and helps the starting or shutting down of the heat pipe.

(3) The size of the gas slug in the heat pipe at a given temperature can be predetermined and this flexibility allows the designer to control the length of inactive condenser.

(4) The need for special starting up/shutting down arrangements such as trace heaters and condenser decoupling from a heat sink is eliminated.

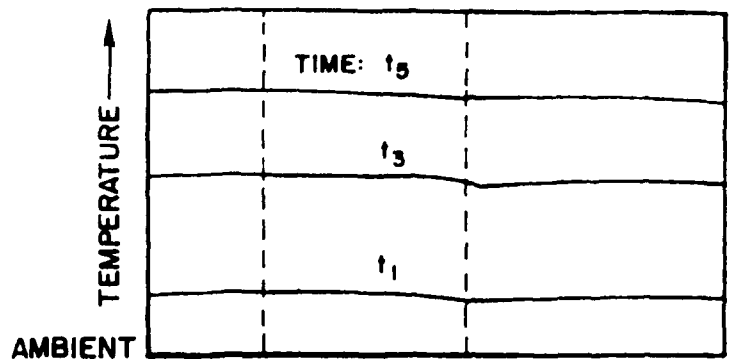

a) UNIFORM STARTUP

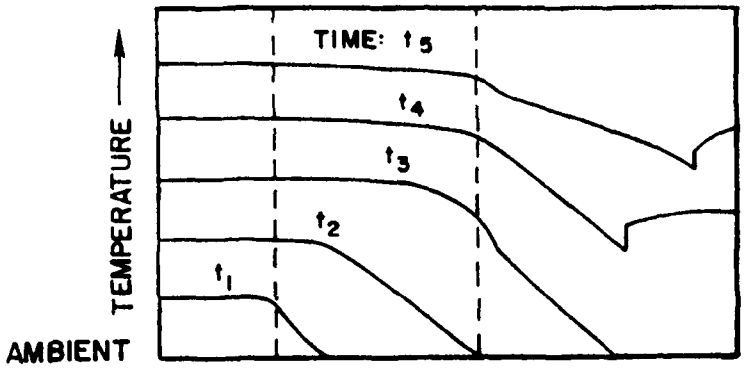

b) FRONTAL STARTUP (NO NONCONDENSIBLE GAS)

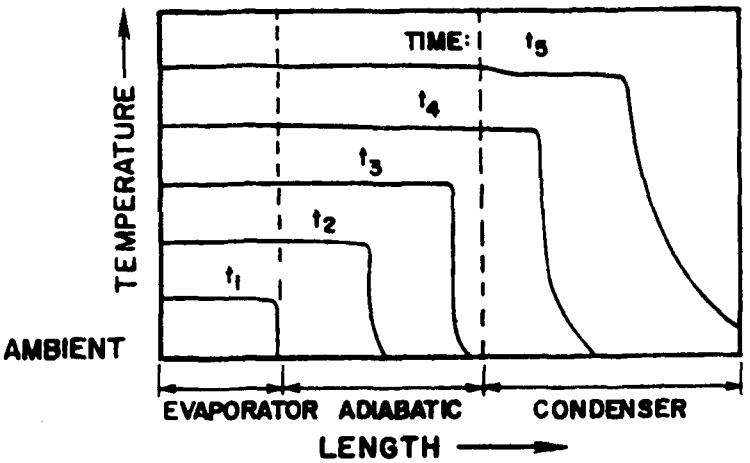

c) FRONTAL STARTUP (WITH NONCONDENSIBLE GAS)

NOTE. Time: $t_5 > t_4 > t_3 > t_2 > t_1 > 0$

Figure 4. Heat Pipe Startup Characteristics

Disadvantages

(1) There is a potential danger of NCG bubble trapment in artery wicks which may lead to depriming of the artery.

(2) The choices of compatible fluid and NCG pair may be limited for high temperature applications. The pair should be chemically non-reacting and non absorbing (non-soluble) types even under high pressure and temperature conditions.

(3) Even with careful design, the non-use of a portion of the condenser (inactive length) under steady state operation may have to be tolerated.

Stages of Frozen State Startup

A gas filled heat pipe in general (or the present DWAHP in particular) undergoes several stages of energy transport during the startup from the initial frozen state to the operating regime [4,30].

Stage 1: Melting and evaporation of heat transfer fluid.

With the supply of uniform heat input to the evaporator, the frozen working fluid thaws and eventually evaporates at the liquid meniscus in the capillary pores of the wick. Gradual withdrawal of NCG from the evaporator to the adiabatic section begins.

Stage 2: Formation of axial vapor flux.

As the heat power supplied increases, the temperature of the evaporator increases and the vapor pressure compresses the NCG away from the evaporator. The speed of vapor flow at the evaporator exit increases up to sonic speed.

Stage 3: Sonic regime.

Continuation of power input to the evaporator takes the heat pipe along the boundary of the sonic limit. In this regime, considerable non-isothermal conditions prevail along the heat pipe. Evaporator fluid inventory continues to deplete as the adiabatic section, if any, thaws and no fluid recirculation from condenser commences.

Stage 4: Sonic to supersonic vapor flow.

With increase in vapor pressure, the vapor-gas front moves toward the condenser end. Vapor velocity variations result from a variable mass flow through a constant vapor core area. The velocity can increase further and become supersonic, or a recompression of the vapor may occur, resulting in a pressure recovery. The amount of pressure recovery depends on the heat removal rate in the condenser section.

Stage 5: Isothermal operating regime.

Once the vapor flow returns to the subsonic levels, the liquid return flow establishes recirculation, and the condenser heat removal rate equals the evaporator input rate, the pipe switches to steady isothermal operating condition.

2.2 Parametric Analysis

Homogeneous and annular wick liquid metal heat pipes are reported to have been analyzed or tested in NCG filled mode without problems [17,29,30]. However, it is not yet established in the liquid metal heat pipe research literature that if a grooved artery heat pipe (of the DWAHP type with unvented artery and screenless

adiabatic section) would start from frozen state and work with NCG filled mode. In order to answer this question, a preliminary analysis addressing the design and testing parameters is done in the following question-and-answer format.

(1) Whether freezing of sodium in a closed artery channel will create any problem?

Sodium shrinks on freezing since the density of the solid is larger than that of the liquid at the freezing point (97.83°C), while the volume change is only 2.63%. The void created within the artery channel (which is fully primed during normal operation) may be vacuum or NCG depending upon the propagation of the solidification front of the sodium during shutdown of the heat pipe. On thawing (initial startup), the void will be filled back if vacuum or the gas will be expelled out of the artery if NCG was present to start with.

(2) Whether the problem of vapor back-flow into the artery exists in the liquid metal DWAHP?

This is not likely under low radial evaporator heat fluxes (<50 W/cm^2) since the critical superheat (ΔT_{crit}) required to create bubble nucleation/boiling in the wick is approximately 40 C at 700°C (see Table 11). On the other hand, the evaporator ΔT across the sodium saturated stainless steel wick (with typical equivalent thermal conductivity, k_e = 40 W/m°C) is about 3 C for a heat input of 1797 W at 800°C (see Section 3.5.5). At higher heat fluxes (>50 W/cm^2), capillary flow inserts at the evaporator/adiabatic transition may be needed to stop vapor back flow (see Reference 55 for details).

(3) What are the conditions under which the NCG bubbles can get into the artery? Under what conditions are they deleterious to the heat pipe operation?

This depends on the solubility of the NCG into the working fluid and the construction of the artery at the condenser. If solubility of NCG in the working fluid is high, the gas will tend to disperse in the fluid and stay under subcooled conditions within the artery. If the fluid is frozen in this condition, it may lead to bubble growth problems later while thawing. In the present case, argon is not soluble in sodium since the Ostwald coefficient is low ($\alpha = 2.27 \times 10^{-5}$ at 500°C) [50].

If the construction of the artery at the condenser section is such that the artery wall is a fine porous structure (such as a screen or sinter), the vapor-gas mixture may pass through the porous wall and get trapped due to the capillary pressure difference across the artery wall. In the case of vented artery channels (such as in the DWAHP condenser), the liquid/vapor meniscus exists inside the groove at each of the vent slots which are large enough to let the gas vent back into the vapor core while the condensation of the vapor takes place. Hence, conceptually, gas bubbles cannot be trapped in the artery channels of the present design.

(4) In case the NCG bubble is trapped in the closed artery channel, will it affect the priming? Will the bubble grow and prevent startup?

Upon thawing of the sodium, the volume of the bubble will expand. A further increase in temperature could expand the bubble more and

might cause artery depriming. Hence, under this hypothesis, the heat pipe may not start. The other possibility is that the bubble may be initially stagnant at an axial position during the thawing process, but start moving toward the evaporator (the direction of higher capillary potential) soon after the moving hot front crosscs the adiabatic zone and the heat pipe action starts. Both possibilities exist in the practical situation and hence experimental study is necessary. In order to avoid the multiple artery averaging effects from confusing the experimental results, it was planned to construct a single channel artery heat pipe as shown in Figure 5. The details of this design are given in Chapter III.

(5) During startup mode, will there be condensate formation at the upstream side of the moving temperature front? If so, what are the effects on the startup?

This is a unique situation with respect to the ventless adiabatic artery channels as opposed to a porous (sinter or screen wall) artery. The vapor traveling down the vapor core will lose its latent heat to the incremental length of the adiabatic section as the vapor/gas front moves. This movement depends on the axial conduction and the diffusion rates of the vapor into the NCG. Initially, there will be some amount of condensate collection at the vapor/gas front but as more and more vapor is generated and the vapor pressure builds up, the already formed droplets will be vaporized back and moved toward the advancing front. The thawing proceeds progressively and the front moves down the vapor core. As

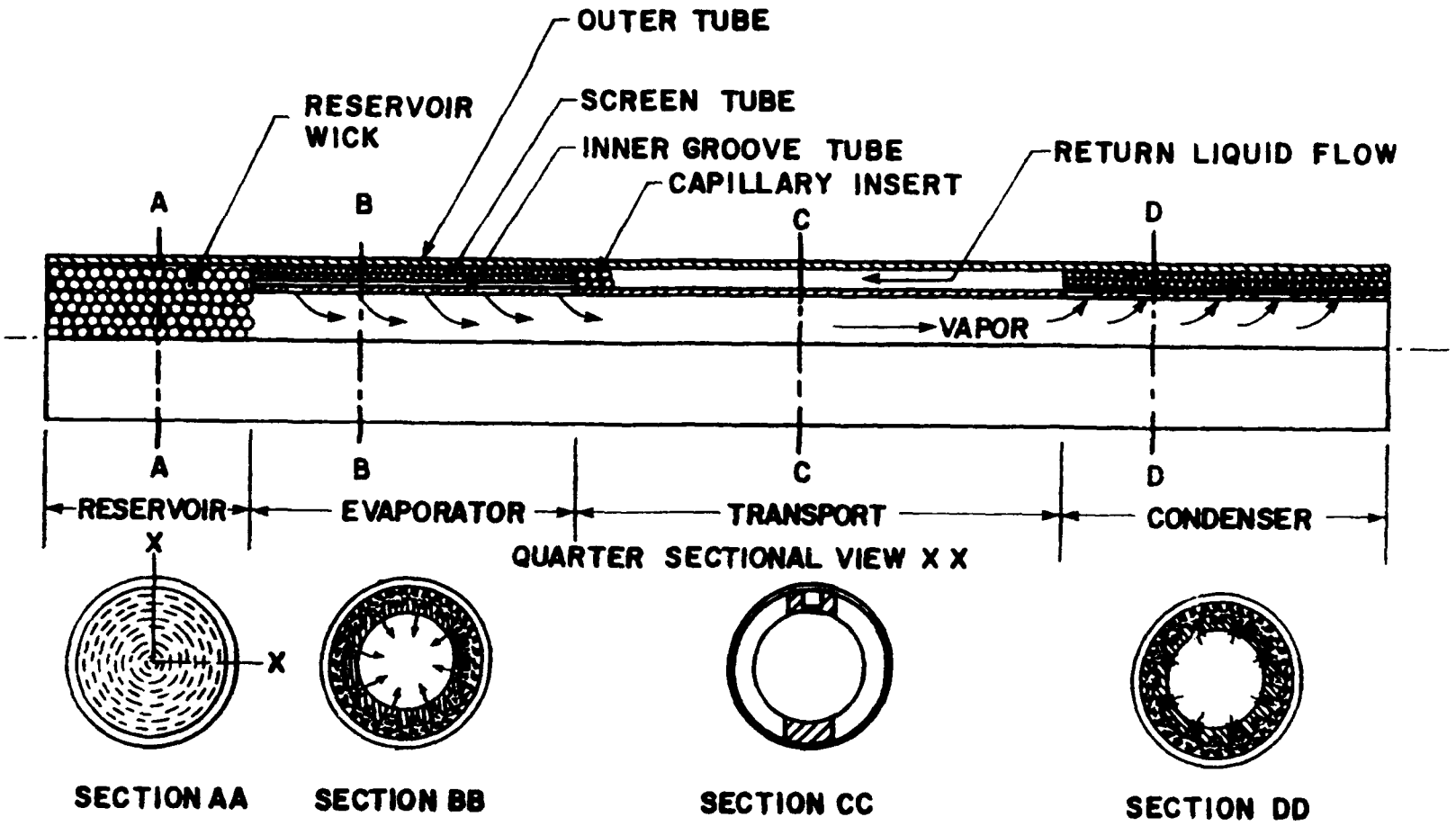

Figure 5. Single Channel Artery Heat Pipe Verfication Model

the front reaches the condenser vent slot zone, the heat pipe action starts.

The key analytical design issue here is to satisfy the requirement that the evaporator should not be depleted of working fluid before the thawing of the transport section is completed. The diffusion gas front analysis for this situation will determine the maximum possible adiabatic length for the case of frozen startup. In addition to the axial conduction (along the heat pipe wall) and the diffusion mechanism available for the energy transfer during start-up, there also is the radiation mode to help the thawing process.

2.3 Heat Transfer Model of the Startup Process

A gas loaded heat pipe contains a fixed quantity of NCG in addition to the working fluid. The purpose of the gas is to facilitate the startup from frozen state. All the three modes of heat transfer, namely, conduction, convection and radiation, occur during the startup. Identifying and estimating the dominant mode is the key to the solution of the startup analysis. Figure 6 shows the heat transfer paths of a gas-filled heat pipe during startup. The heat input (Q_i) to the evaporator is transferred to the adiabatic and condenser sections by 1) axial conduction (Q_{ax}) through the wall and wick, 2) convective transfer by hot vapor diffusing into the NCG and condensing at the downstream side of the diffusion front (Q_v), and 3) radiation exchange between the hot and cold zones (Q_r).

Generally, in the moderate temperature (122 628 K) VCHP research, Q_v has been reported to be much smaller than the axial

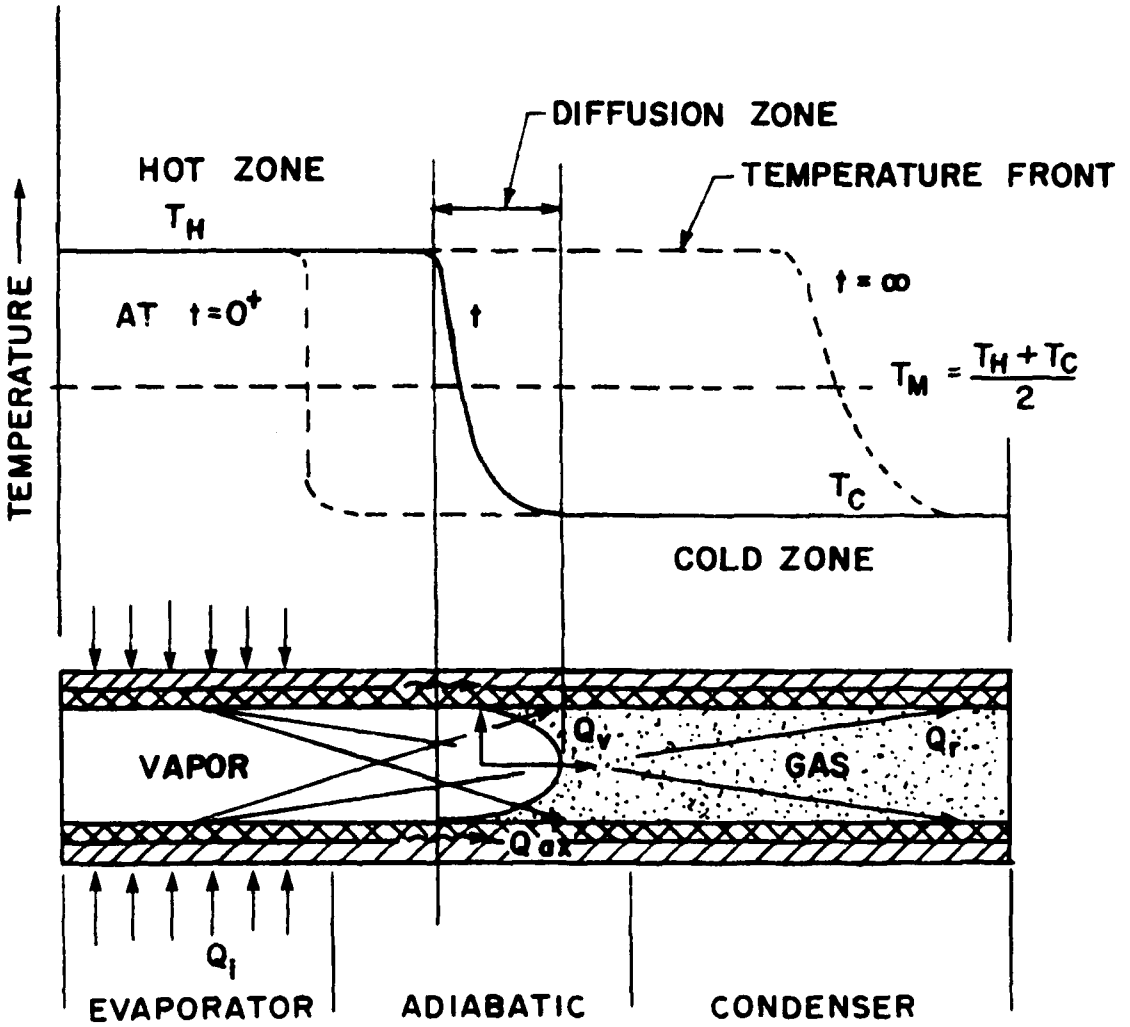

Figure 6. Heat Transfer Model for a Gas Loaded Heat Pipe During Startup

conduction (Q_{ax}), with the diffusion rate assumed constant [4,14,39]. For high temperature heat pipes, Sockol [17] found that Q_v is much larger than Q_{ax} and that Q_v approaches Q_i at the beginning of the startup and drops to almost zero when steady state is approached. This theory justifies the stationary vapor-gas front at steady state. On the contrary, if axial conduction term were dominant, the hot front may move even after the diffusion process stopped. High wall conductance tends to spread the front over the condenser masking the diffusion zone temperature profile. High temperature wall materials such as stainless steel and refractory metals have poor thermal conductivity; hence, the temperature gradient at the diffusion front will be sharper than that for high conductivity materials such as copper and aluminum commonly used for low temperature heat pipes.

A qualitative picture of the temperature profiles at the diffusion zone is shown in conjunction with the heat transfer model sketched in Figure 6. At the beginning of the startup, the gradient is very steep indicative of strong vapor diffusion activity and at steady state, it is spread out due to axial conduction effects. Hence, it appears that the transient state is governed by the diffusion process and the steady state by axial conduction. This hypothesis is verified through numerical and experimental results (see results in Section 5.2.2).

The radiation exchange (Q_r) between the hot and cold zones is less significant than Q_v or Q_{ax} since the length to diameter ratio of the pipe is very large.

In the present work, a two-dimensional analysis of the vapor diffusion through the NCG is performed. The diffusive energy transport rate thus obtained is coupled with a thermal model of the startup of the radiatively cooled sodium-argon double wall artery heat pipe.

2.4 Diffusion Model and Analysis

The objective of the diffusion analysis is to determine the vapor diffusion rate past the hot front as a function of the length and temperature of the hot zone. The model is based on Fick's law for binary gas system explained in detail by Bird et al. [51] and developed by Sockol [17]. Assumptions used in this analysis are as follows:

(1) The local condensation rate upstream of the front is assumed to be negligible.

(2) The cold wall acts as a perfect sink for the vapor.

(3) The transition region between the cold and hot zones is vanishingly thin.

(4) The upstream vapor velocity is uniform over the cross section.

(5) The gas is stagnant throughout the pipe.

(6) The axial vapor pressure drop is negligible.

(7) The vapor velocity during startup is limited to much less than sonic speed.

(8) In a long cylinderical heat pipe, the vapor concentration should relax to a quasi-steady profile in time of order $(r_v/2.4)^2/D$. If the distance moved by the front during this time is small, steady-flow equations can be used for the

diffusion analysis. For the sodium-argon system at 1000 K, with $r_v = 0.635$ cm and $D = 4.591$ cm^2/sec, the relaxation time is 15.25 milliseconds. As it will be seen in the numerical analysis results section later, the rate of front movement is 0.04 to 0.37 cm/sec for a power input of 1000 W with the gas charge pressure of 0.2 torr. Hence, the front movement in 15.25 milliseconds is very small and the steady state diffusion assumption is justified.

Fick's law for binary diffusion in the form of molar flux is given by [51]

$$\vec{N}_v = x_v(\vec{N}_v + \vec{N}_g) - cD_{vg}\vec{\nabla}x_v \qquad (1)$$

For a stagnant gas $\vec{N}_g = 0$ and Eq. (1) becomes,

$$\vec{N}_v = x_v\vec{N}_v - cD_{vg}\vec{\nabla}x_v$$

or

$$(1 - x_v)\vec{N}_v = -cD_{vg}\vec{\nabla}x_v$$

Total mass fraction of the system, $x_g + x_v = 1$.

Therefore, the vapor flux $\vec{N}_v$ can be written in terms of the mole fraction of the gas x_g as:

$$\vec{N}_v = - \frac{cD_{vg} \vec{\nabla}(1 - x_g)}{x_g}$$

or $$\vec{N}_v = - cD_{vg} \frac{(-\vec{\nabla} x_g)}{x_g}$$

which also can be written as

$$\vec{N}_v = cD_{vg} \vec{\nabla} \ln x_g \tag{2}$$

From the principle of conservation of mass applicable to the vapor flow,

$$\text{div } \vec{N}_v = 0$$

or $$\vec{\nabla} \cdot \vec{N}_v = 0 \tag{3}$$

Substituting for $\vec{N}_v$ from Eq. (2),

$$cD_{vg} \vec{\nabla}^2 \ln x_g = 0$$

Since $cD_{vg} \neq 0$, $\vec{\nabla}^2 \ln x_g = 0$ (4)

In order to solve this equation and to set up the necessary boundary conditions, a cylindrical coordinate system is introduced as shown in Figure 7. According to Assumption (3), the axial distance over

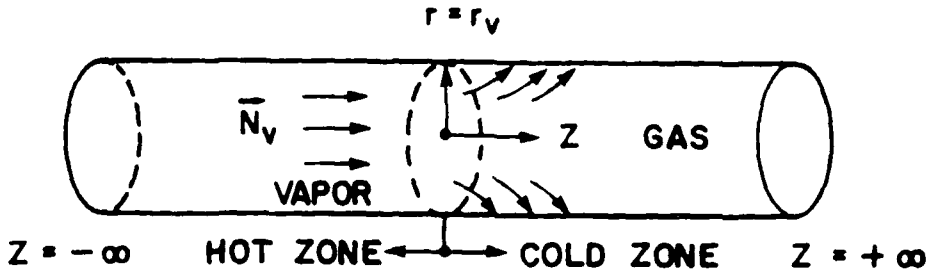

Figure 7. Coordinate System for Diffusion Analysis.

which x_g departs from 0 or 1 is small compared to the hot zone or cold zone lengths. From the location of the front, the boundaries of z are at $\pm\infty$. The boundary conditions are as follows:

$z < 0$:

(1) As $z \to -\infty$, the vapor flux $\vec{N}_v$ is given by an unknown constant flux $\vec{N}_o$.

$$\vec{N}_v \to \vec{N}_o$$

That is from Eq. (2),

$$cD \frac{\partial}{\partial z} (\ln x_g) \to \vec{N}_o \quad \text{as} \quad z \to -\infty \tag{5}$$

(2) At the wall, the vapor flux ($\vec{N}_v$) in the radial direction is zero as there is no condensation in the hot zone.

$$\frac{\partial}{\partial r} (\ln x_g) = 0 \quad \text{at} \quad r = r_v \tag{6}$$

$z \geq 0$:

(1) At the condenser end, there is no vapor; only gas exists.

$$x_g \to 1 \quad \text{as} \quad z \to +\infty \tag{7}$$

(2) At the wall (perfect sink), there is no sodium vapor due to complete condensation. $x_v = 0$ and $x_g = 1$

$$x_g = 1 \quad \text{at} \quad r = r_v \tag{8}$$

A mass balance on the gas is done to obtain the unknown vapor flux $\vec{N}_o$ in terms of the initial molar concentration c_i of the NCG at T_c.

$$\begin{pmatrix}\text{mass of}\\ \text{gas}\\ \text{in pipe}\end{pmatrix} = \begin{pmatrix}\text{mass of}\\ \text{gas}\\ \text{in hot zone}\end{pmatrix} + \begin{pmatrix}\text{mass of}\\ \text{gas}\\ \text{in cold zone}\end{pmatrix}$$

$$= \begin{pmatrix}\text{mass of}\\ \text{gas}\\ \text{in hot zone}\end{pmatrix} + \begin{pmatrix}\text{mass of}\\ \text{vapor + gas}\\ \text{in cold zone}\end{pmatrix} - \begin{pmatrix}\text{mass of}\\ \text{vapor}\\ \text{in cold zone}\end{pmatrix} \tag{9}$$

If the total length of the heat pipe is L_p and the hot zone length is L, then Eq. (9) can be expressed in the integral form as,

$$c_i L_p = \int_{-L}^{L_p - L} \overline{cx}_g \, dz$$

$$\approx \int_{-\infty}^{0} \overline{cx}_g \, dz + \int_{0}^{L_p - L} c \, dz - \int_{0}^{\infty} \overline{cx}_v \, dz$$

where c is the total molar density of the mixture and the bar indicates an average over the cross section. Simplifying the integrals and bringing the constant c (as c_c and c_h evaluated at T_c and T, respectively) outside the integral, one obtains

$$c_i L_p = c_h \int_{-\infty}^{0} \bar{x}_g \, dz + c_c(L_p - L) - \int_{0}^{\infty} (\overline{1 - x_g}) \, dz \qquad (10)$$

From ideal gas law, the molar densities at various temperatures are expressed as,

$$c_i = \frac{P_i}{RT_c} \quad ; \quad c_c = \frac{P_v(T)}{RT_c} \quad ; \quad c_h = \frac{P_v(1)}{RT}$$

where P_i = initial charge pressure of NCG.

Introduce dimensionless variables as follows:

$$\bar{r} = \frac{r}{r_v} \quad ; \quad \bar{z} = \frac{z}{r_v} \quad ; \quad \ell = \frac{L}{r_v} \quad ; \quad \ell_p = \frac{L_p}{r_v} \quad ;$$

$$\theta = \frac{T}{T_c} \quad ; \quad g = \frac{\vec{N}_o r_v}{cD} \quad \text{(Diffusion Parameter)}$$

$$\lambda(\theta,\ell) = \frac{c_c(L_p - L) - c_l L_p}{c_c r_v} = \ell_p - \ell \cdot \frac{p_i}{p_v(1)} \tag{11}$$

A new dependent variable y is introduced in place of $\ell n\ x_g$ as,

$$y(\bar{r},\bar{z}) = -\frac{\ell n\ x_g}{g} \tag{12}$$

Eq. (4) in cylindrical coordinates transforms to

$$\frac{1}{\bar{r}}\frac{\partial}{\partial\bar{r}}\left(\bar{r}\frac{\partial y}{\partial\bar{r}}\right) + \frac{\partial^2 y}{\partial\bar{z}^2} = 0 \tag{13}$$

Boundary conditions, Eq. (5) to (8) become,

$$\left.\begin{aligned} &\bar{z} < 0: \quad \frac{\partial y}{\partial\bar{z}} \to -1 \quad \text{as} \quad \bar{z} \to -\infty \\ &\qquad\quad \frac{\partial y}{\partial\bar{r}} = 0 \quad \text{at} \quad \bar{r} = 1 \\ &\bar{z} > 0: \quad y \to 0 \quad \text{as} \quad \bar{z} \to \infty \\ &\qquad\quad y = 0 \quad \text{at} \quad \bar{r} = 1 \end{aligned}\right\} \tag{14}$$

Rearranging and normalizing Eq. (10),

$$\lambda(\theta,\ell) = \int_0^\infty \overline{(1 - x_g)}\, d\bar{z} - \frac{c_h}{c_c}\int_{-\infty}^{0} \bar{x}_g\, d\bar{z}$$

Averaging the gas concentration over the cross section,

$$\lambda(\theta,\ell) = 2\int_0^1 \bar{r}\,d\bar{r}\int_0^\infty (1 - e^{-gy})d\bar{z}$$

$$- \frac{2}{\theta}\int_0^1 \bar{r}\,d\bar{r}\int_{-\infty}^0 e^{-gy}d\bar{z} \qquad (15)$$

Letting

$$F_c(g) = 2\int_0^1 \bar{r}\,d\bar{r}\int_0^\infty (1-e^{-gy})d\bar{z} \qquad (16)$$

$$F_h(g) = 2\int_0^1 \bar{r}\,d\bar{r}\int_{-\infty}^0 e^{-gy}d\bar{z} \qquad (17)$$

Eq. (15) becomes,

$$\lambda(\theta,\ell) = F_c(g) - \frac{1}{\theta}F_h(g) \qquad (18)$$

Solution Method

The partial differential Eq. (13) and the boundary conditions Eq. (14) are solved for $y(\bar{r},\bar{z})$ in the closed form using Bessel functions as described by Sockol [17]. Once y is known, g can be obtained by solving Eq. (18). The mass flux in terms of θ and ℓ

are obtained by performing the radial integral numerically. A simplifying approximation is used for this purpose. For large values of g, $F_h(g)$ is negligible compared to $F_c(g)$ and the radial integral yields,

$$F_c(g) = \frac{1}{\beta_1} (\ell n\ g - 1.339) \tag{19}$$

where $\beta_1 = 2.4048$ is computed from the zeros of Bessel function. Now, the approximate equation for $F_c(g)$ is

$$F_c(g) \approx \lambda(\theta,\ell) \approx \frac{1}{\beta_1} (\ell n\ g - 1.339) \tag{20}$$

Or

$$g = \exp(1.339 + \beta_1 \lambda) \tag{21}$$

The energy transport by vapor diffusion from the hot to cold zone Q_v is given by

$$Q_v = A_v M_v \vec{N}_o h_{fg} \qquad \left[cm^2 \times \frac{g}{gmole} \times \frac{gmole}{cm^2\ sec} \times \frac{J}{g}\right]$$

$$= \pi r_v^2 M_v \vec{N}_o h_{fg} \qquad [W]$$

Or in terms of cD and g,

$$Q_v = \pi r_v M_v cD h_{fg} g \tag{22}$$

The values of cD for sodium-argon mixture as a function of temperature are computed from the kinetic theory of gases using the Chapman-Enskog relation as outlined in Appendix A. The diffusion parameter g has to be very large at the beginning of the startup in order to have large Q_v and must drop to zero toward the end of startup.

2.5 Transient Thermal Analysis

The transient state of the gas loaded liquid metal heat pipe with a long adiabatic section at time t after the application of evaporator power input Q_i is shown in Figure 8. The top sketch Figure 8(a) shows the heat pipe during the thawing process when there is no heat output at the condenser. Figure 8(b) shows the condition when the pipe is transporting and radiating out Q_o at the condenser.

2.5.1 Assumptions

(1) Axial conduction is negligible compared to Q_v during startup.

(2) The evaporator and adiabatic sections are perfectly insulated (shielded) such that no heat loss occurs in the radial direction.

(3) Axial and radial temperature variations within the same zone (hot or cold) are not considered. The hot zone is at a uniform temperature T and the cold zone (gas slug region) is uniformly at T_c. Only the time dependence of temperature and the location of the hot front are analyzed, i.e., $T = T(t)$; $L = L(t)$.

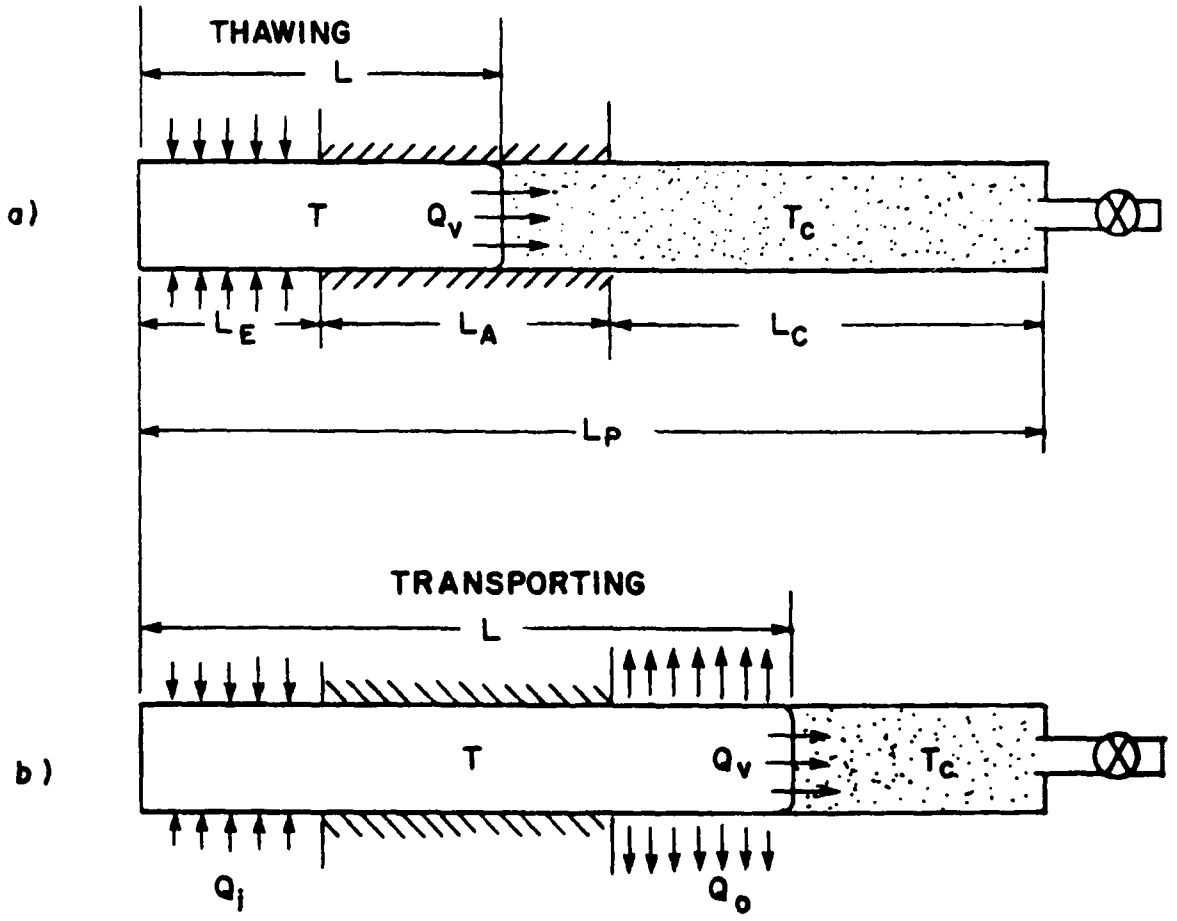

Figure 8. Transient State of the Heat Pipe at Time t During a) Thawing and b) Transporting

(4) There is no liquid return flow to the evaporator during the thawing stage and there is enough fluid inventory to last till the pipe starts up.

(5) Initially, the wick structure is saturated with the working fluid which is in a frozen state.

(6) The heat pipe vapor core is filled with a NCG (argon) charge at a pressure P_i and temperature T_c. There is no separate gas reservoir in the pipe.

(7) No chemical reaction occurs between the fluid and gas.

(8) The mechanism of vapor diffusion into the gas within the vapor core is as outlined in the previous section.

(9) Horizontal orientation of the pipe is assumed during startup.

(10) Heat input to the evaporator is uniform along its length and it can be conductively or radiatively coupled whereas the heat removal at the condenser is radiatively coupled to the cold sink at T_s.

(11) The reservoir wick at the end of the evaporator is in good capillary contact with the evaporator wick.

2.5.2 Definitions

(1) Initial hot zone temperature, or rise temperature (T_{Hi}) is the temperature at which the sodium vapor pressure is equal to the adjusted initial NCG charge pressure P_i such that

$$P_v(T_{Hi}) = P_i \left(\frac{L_p}{L_p - L_E}\right)$$

(2) Startup temperature (T_{Hs}) is the temperature of the hot zone when the hot front has reached the beginning of the condenser.

(3) Rise time (t_i) is the time required to raise the temperature of the evaporator to T_{Hi} from T_c (room temperature) after the Q_i is applied.

(4) Startup time (t_s) is the time taken after t_i for the hot front to move to the beginning of the condenser, i.e., to move through the adiabatic length, L_A.

2.5.3 Governing Differential Equations

Energy balances are conducted for the control volumes enclosing the hot and cold zones of the heat pipe during the transient states of hot zone diffusing into the cold zone as depicted in Figure 8. Two sets of equations corresponding to the thawing stage and transporting stage for each of the control volumes are written with the initial and boundary conditions. The symbols are explained in the nomenclature.

Hot Zone:

Thawing stage: $0 < t < t_s$; $L_E \leq L \leq (L_E + L_A)$

$$[C_E L_E + C_A(L - L_E)] \frac{dT}{dt} = Q_i - Q_v - Q_r \qquad (23)$$

with boundary condition : $T = T_c$ at $t = 0$

Transporting Stage: $t_s < t < \infty$; $(L_E + L_A) \leq L \leq L_p$

$$[C_E L_E + C_A L_A + C_C(L - L_E - L_A)] \frac{dT}{dt} = Q_i - Q_v - Q_r - Q_o \qquad (24)$$

with boundary condition : $L = (L_E + L_A)$ at $t = t_s$

Cold Zone:

Thawing Stage: $0 < t < t_s$; $L_E \leq L \leq (L_E + L_A)$

$$C_A(T - T_c) \frac{dL}{dt} = Q_v \qquad (25)$$

with boundary condition : $L = L_E$ at $t = 0$

Transporting Stage: $t_s < t < \infty$; $(L_E + L_A) \leq L \leq L_p$

$$C_C(T - T_c) \frac{dL}{dt} = Q_v \qquad (26)$$

with boundary condition : $L = (L_E + L_A)$ at $t = t_s$

Other known relations are,

$$Q_v = \pi r_v M_v c D h_{fg} g \qquad \text{(Diffusion Equation)} \qquad (27)$$

$$Q_o = \pi D_o(L - L_E - L_A)\, \varepsilon_p \sigma(T^4 - T_s^4) \qquad \text{(External Radiation)} \qquad (28)$$

$$Q_r = 2\pi r_v L F_{HC} \varepsilon_H \sigma(T^4 - T_c^4) \qquad \text{(Internal Radiation)} \qquad (29)$$

Eqs. (23) to (29) are normalized using the following nondimensional variables.

$$\theta = \frac{T}{T_c} \quad ; \quad \theta_s = \frac{T_s}{T_c}$$

$$\ell = \frac{L}{r_v} \;,\; \ell_E = \frac{L_E}{r_v} \;,\; \ell_A = \frac{L_A}{r_v} \;,\; \ell_C = \frac{L_C}{r_v} \;,\; \ell_p = \frac{L_p}{r_v}$$

$$q_i = \frac{Q_i}{C_E\, r_v\, T_c} \;,\; q_v = \frac{Q_v}{C_E\, r_v\, T_c} \;,\; q_r = \frac{Q_r}{C_E\, r_v\, T_c}$$

$$q_o = \frac{Q_o}{C_E\, r_v\, T_c} \;,\; s_1 = \frac{C_A}{C_E} \;,\; s_2 = \frac{C_C}{C_E}$$

The normalized equations and the boundary conditions are,

$$[\ell_E + s_1(\ell - \ell_E)]\, \frac{d\theta}{dt} = q_i - q_v - q_r \qquad (23)'$$

with boundary condition : $\theta = 1$ at $t = 0$

or $0 < t < t_s$; $\ell_E \leq \ell \leq (\ell_E + \ell_A)$

$$[\ell_E + s_1\ell_A + s_2(\ell - \ell_E - \ell_A)]\, \frac{d\theta}{dt} = q_i - q_v - q_r - q_o \qquad (24)'$$

with boundary condition : $\ell = (\ell_E + \ell_A)$ at $t = t_s$

for $t_s < t < \infty$; $(\ell_E + \ell_A) \leq \ell \leq \ell_p$

$$s_1(\theta - 1)\, \frac{d\ell}{dt} = q_v \qquad (25)'$$

boundary condition : $\ell = \ell_E$ at $t = 0$

$$s_2(\theta - 1)\, \frac{d\ell}{dt} = q_v \qquad (26)'$$

boundary condition : $\ell = (\ell_E + \ell_A)$ at $t = 0$

$$q_v = A_v g \tag{27}'$$

where $$A_v = \frac{\pi M_v c D h_{fg}}{C_E T_c}$$

$$q_o = A_o(\ell - \ell_A - \ell_E)\ (\theta^4 - \theta_s^4) \tag{28}'$$

where $$A_o = \frac{\pi D_o \epsilon_p \sigma T_c^3}{C_E}$$

$$q_r = A_r \ell(\theta^4 - 1) \tag{29}'$$

where $$A_r = \frac{2\pi F_{HC} \epsilon_H \sigma T_c^3}{C_E}$$

From the diffusion analysis we have,

$$g = \exp[1.339 + 2.4048\ \lambda(\theta,\ell)] \tag{21}$$

$$\lambda(\theta,\ell) = \ell_p - \ell - \frac{\ell_p P_i}{P_v(T)} \tag{11}$$

With this, the formulation of the transient problem is completed and the numerical solution technique is described in Section 2.6.

2.6. Numerical Computations

The governing differential equations and the initial conditions, Eqs. (23)' to (29)', are solved by numerical integration using the fourth order Runge-Kutta method for the 2 m sodium argon

heat pipe design described in the next chapter [52]. A FORTRAN program called SODART was developed for this purpose. SODART works in conjunction with several subroutines written for specific purposes. Table 1 lists all those subroutines and their functions. A flow chart illustrating the sequence and logic is given in Figure 9. A listing of the SODART program and subroutines are given in Appendix B.

2.6.1 Input Data

The input data required for the program is given in Table 2. The temperature dependent properties such as the diffusion coefficient (cD) and the enthalpy of vaporization (h_{fg}) are input as coarse table and interpolated within the program for fine intervals. Since $P_v(T)$ is an exponentially varying property, the empirical relation [Eq. (30)] by Ditchburn and Gilmour [53] is used.

$$P_v = 2.29 \times 10^{11} (T^{-0.5}) (10^{-5561/T}) \qquad (30)$$

where T is in degrees K and P_v in N/m^2. A sample input data file is also given along with the program in Appendix B.

2.6.2 Computation of Startup Parameters

The startup parameters to be computed are the rise time and temperature (t_i, T_{Hi}), startup time and temperature (t_s, T_{Hs}) and the sodium mass depletion rate from the evaporator ($\dot{m}$). The NCG initial charge pressure [$P_i(T_c)$] and the evaporator power input (Q_i) are the main input parameters to start the computations. For the given P_i, the startup vapor pressure is found from:

TABLE 1. LIST OF SUBROUTINES AND THEIR PURPOSES

NO.	SUBROUTINE	FUNCTION
1.	INPSUB	Reads the input data and transfers to the main program. Calls WRITEUP to printout the input data.
2.	RUNGE	Performs the numerical integration of the differential equations (first order time derivatives of length and temperature dL/dt and dT/dt) with the precision of time step (TSTEP) specified. Runge-Kutta method is used.
3.	CALC	Computes g, Q_v, Q_r, and Q_o from the governing differential equation. Uses INTPOLT and PVCALC to compute the temperature dependent properties, h_{fg}, cD and P_v.
4.	DERV	Converts the differential equations to differential quantities for numerical integration.
5.	INTPOLT	Interpolates property data for any temperature during the integration.
6.	WRITEUP	Prints the input and output data.
7.	PVCALC	Uses an empirical relation to calculate P_v of sodium as a function of temperature.
8.	STARTUP	Calculates the starting temperature for the given gas charge pressure (P_i).

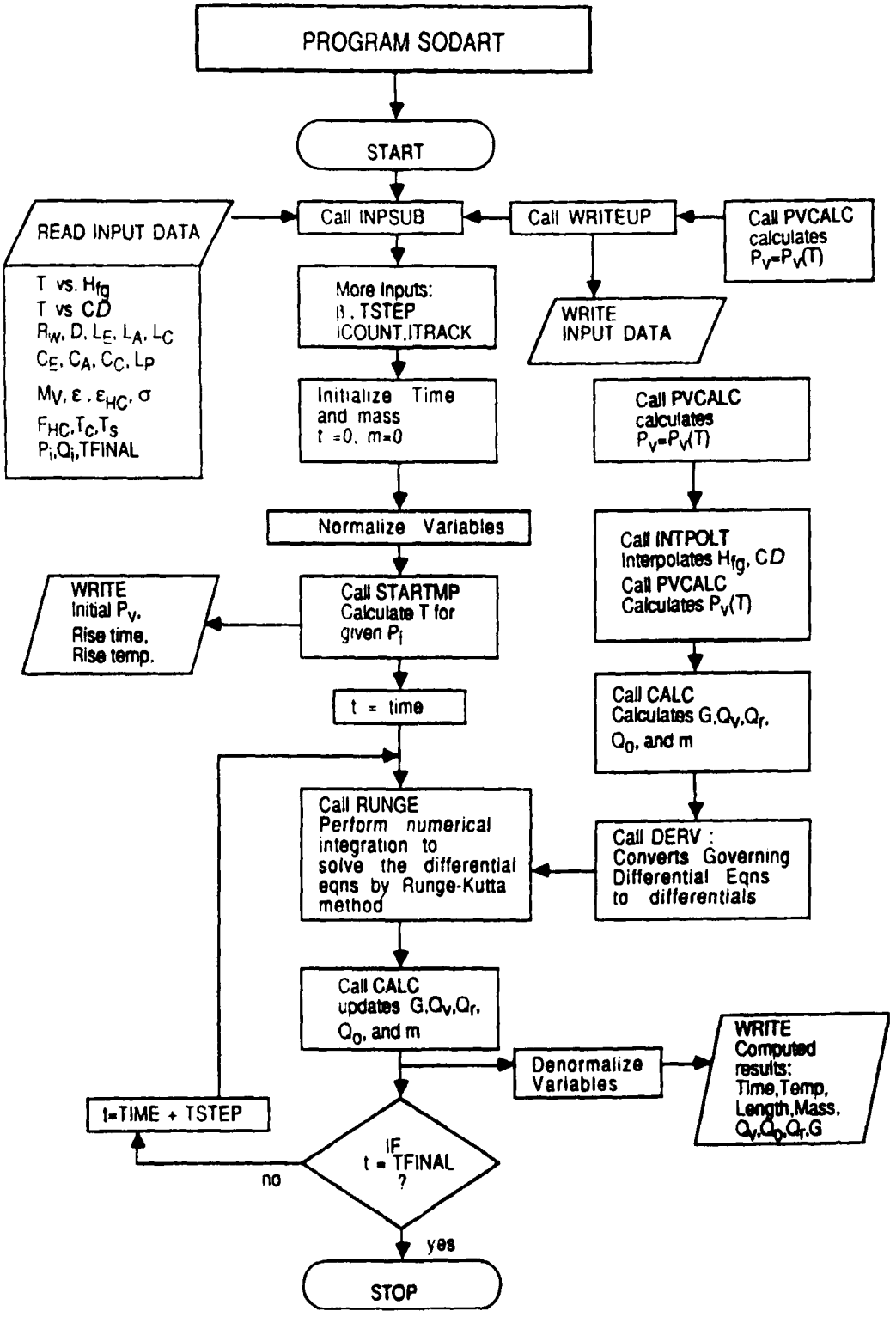

Figure 9. Flow Chart for the Computer Program SODART

TABLE 2. INPUT DATA FOR PROGRAM SODART FOR 2 m LIQUID METAL DWAHP

1.	Vapor Core radius (r_v)	= 0.635×10^{-2} m
2.	Evaporator length (L_E)	= 0.375 m
3.	Adiabatic length (L_A)	= 0.745 m
4.	Condenser length (L_C)	= 0.910 m
5.	Total length (L_P)	= 2.030 m
6.	Evaporator unit thermal capacity (C_E)	= 911.717 J/m K
7.	Adiabatic unit thermal capacity (C_A)	= 598.934 J/m K
8.	Condenser unit thermal capacity (C_C)	= 886.340 J/m K
9.	Molecular weight of sodium (M_v)	= 23
10.	Emissivity of condenser surface (ϵ_ℓ)	= 0.66
11.	Stefan-Boltzmann constant (σ)	= 5.669×10^{-8} W/m^2 K^4
12.	Emissivity of vapor core surface (ϵ_H)	= 0.1
13.	Shape factor between hot and cold zone (F_{HC})	= 0.01159
14.	Room temperature (T_c)	= 300 K
15.	Chamber sink temperature (T_s)	= 300 K
16.	NCG charge pressure (P_i):	0.05, 0.10, 0.20, 0.50, 1.00, 2.00 torr
17.	Evaporator input (Q_i):	100, 250, 500, 1000 W
18.	Heat input increments (ITHEAT)	= 0
19.	Solution stop time (TFINAL)	= 3000 sec

$$P_v(T_{Hi}) = P_i(T_c) \frac{L_p}{(L_p - L_E)} \tag{31}$$

From the sodium vapor pressure relation [Eq. (30)], T_{Hi} corresponding to $P_v(T_{Hi})$ is computed. Applying the energy conservation principle to the hot zone and neglecting the losses, one obtains the equations for t_i and t_s.

$$t_i = \frac{Q_i}{C_F L_E (T_{Hi} - T_c)} \tag{32}$$

$$t_s = \frac{Q_i}{(C_E L_E + C_A L_A)(T_{Hs} - T_c)} - t_i \tag{33}$$

T_{Hs} is computed from the SODART program by solving the governing differential equations (Section 2.5.3)

During the time of thawing, vapor mass flow rate is governed by Q_v. If $\dot{m}$ is the rate of mass depletion in the evaporator during startup, Q_v can be written as,

$$Q_v = \pi r_v^2 M_v \vec{N}_o h_{fg} = \dot{m} h_{fg}$$

or

$$\dot{m} = \frac{Q_v}{h_{fg}} \tag{33}$$

By integrating $\dot{m}$ with respect to time, the total mass of sodium vaporized from the evaporator and transferred to the adiabatic section is obtained.

$$M = \int_0^{t_s} \dot{m}\, dt \qquad (34)$$

This integration is automatically available from the Q_v computation in SODARI.

2.6.3 Results of Computations

A matrix of computations was done varying the P_i and Q_i values. For every value of Q_i (i.e., 100, 250, 500, and 1000 W), six P_i values (0.05, 0.1, 0.2, 0.5, 1.0, 2.0 torr) were varied, and a total of 24 computations was done. In each set of computation, the transient results t versus L, T, Q_v, Q_o, Q_r, and M were computed for 3000 sec and graphed. The time step used was 10^{-3} sec and the CPU time consumed in a CDC mainframe computer was 220 sec.

Table 3 lists the results of the startup parameters. It is observed that the parameters time, temperature and mass increase with increase in NCG charge pressure, P_i, while the location of the hot front decreases. Figure 10 shows the variation of the hot front length with power input for various NCG charge pressures while Figure 11 shows the same result in different form. The sodium mass depletion from evaporator during startup as a function of NCG charge pressure is plotted in Figure 12. The important design input variable for heat pipe operating condition in terms of selecting the NCG charge pressure is obtained from these results, i.e., the integrated sodium mass depletion values. Only the mass depletion

TABLE 3. RESULTS OF THE STARTUP ANALYSIS

Sl. No.	Startup Parameters	Evaporator Power Input Q_i (Watts)	Noncondensible Gas Initial Charge Pressure, P_i (Torr)					
			0.05	0.10	0.20	0.50	1.00	2.00
1	Rise Time, t_i (sec)	100	1076.8	1150.9	1230.7	1345.6	1440.7	1543.9
		250	430.7	460.4	492.3	538.2	576.3	617.6
		500	215.4	230.2	246.1	269.1	288.1	308.8
		1000	107.7	115.1	123.1	134.6	144.1	154.4
2	Startup Time, t_s (sec)	100	1563.0	1673.0	1791.0	1961.0	2105.0	2261.0
		250	625.0	669.0	715.0	783.0	841.0	903.0
		500	313.0	335.0	359.0	391.0	421.0	451.0
		1000	157.0	167.0	179.0	197.0	211.0	225.0
3	Rise Temperature, T_{Hi} (K)	100	614.9	636.6	659.9	693.6	721.4	751.6
		250	614.9	636.6	659.9	693.6	721.4	751.6
		500	614.9	636.6	659.9	693.6	721.4	751.6
		1000	614.9	636.6	659.9	693.6	721.4	751.6
4	Startup Temperature, T_{Hs} (K)	100	634.3	657.4	682.4	718.4	748.3	780.8
		250	614.3	657.4	682.4	718.4	748.3	780.8
		500	634.3	657.4	682.4	718.4	748.3	780.8
		1000	634.3	657.4	682.4	718.4	748.3	780.8
5	Sodium mass depletion from the evaporator integrated over the startup time t_s sec, M (grams)	100	32.9	35.3	38.0	41.7	45.1	48.5
		250	32.9	35.3	38.0	41.7	45.1	48.5
		500	32.9	35.3	38.0	41.7	45.1	48.5
		1000	32.9	35.3	38.0	41.7	45.1	48.5
6	Location of hot front in 3000 sec after rise time, L (meter)	100	1.317	1.291	1.267	1.238	1.218	1.200
		250	1.620	1.564	1.511	1.446	1.401	1.360
		500	1.901	1.846	1.784	1.695	1.626	1.560
		1000	2.011	1.999	1.980	1.935	1.886	1.882

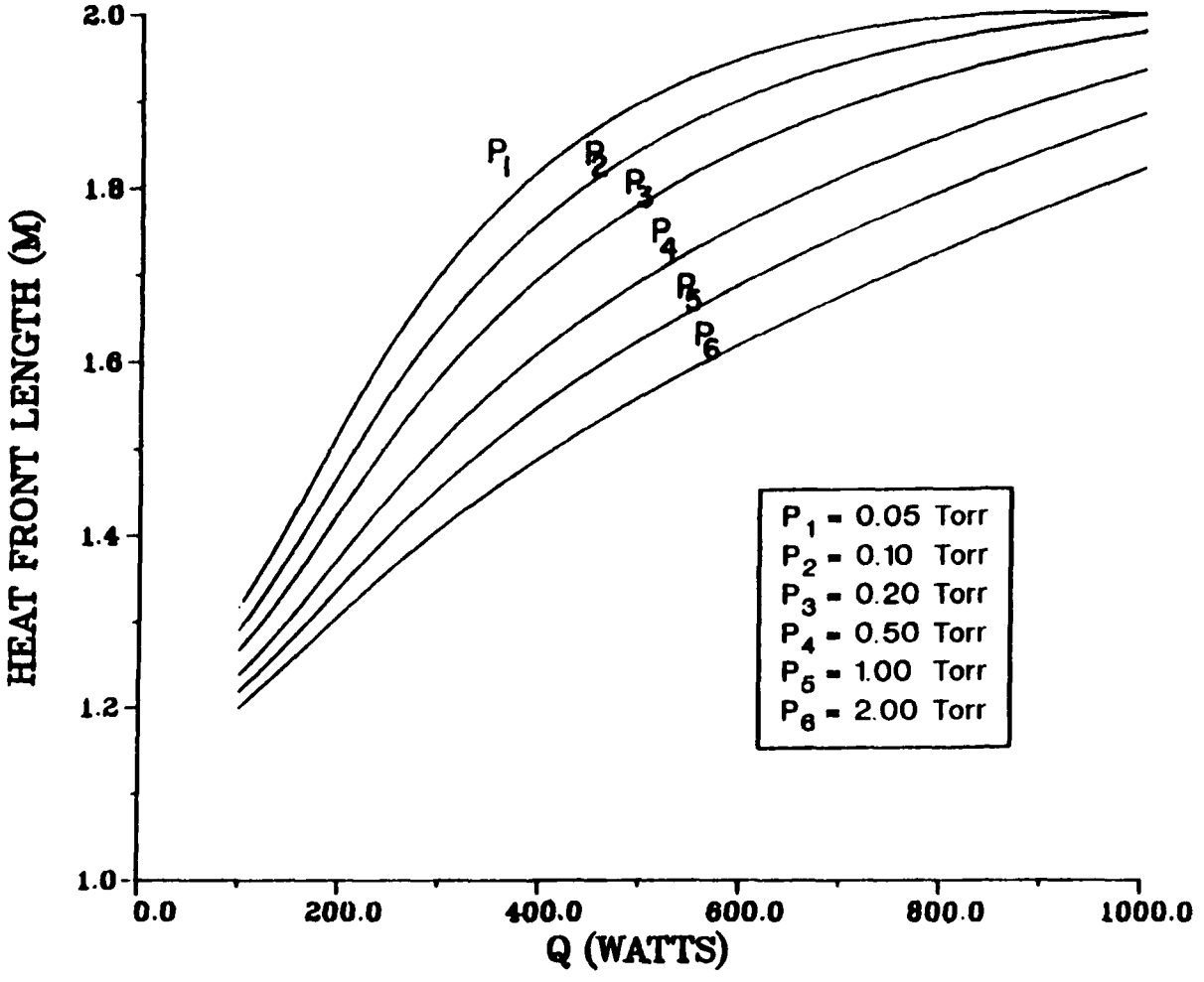

Figure 10. Heat Front Length Versus Heat Input

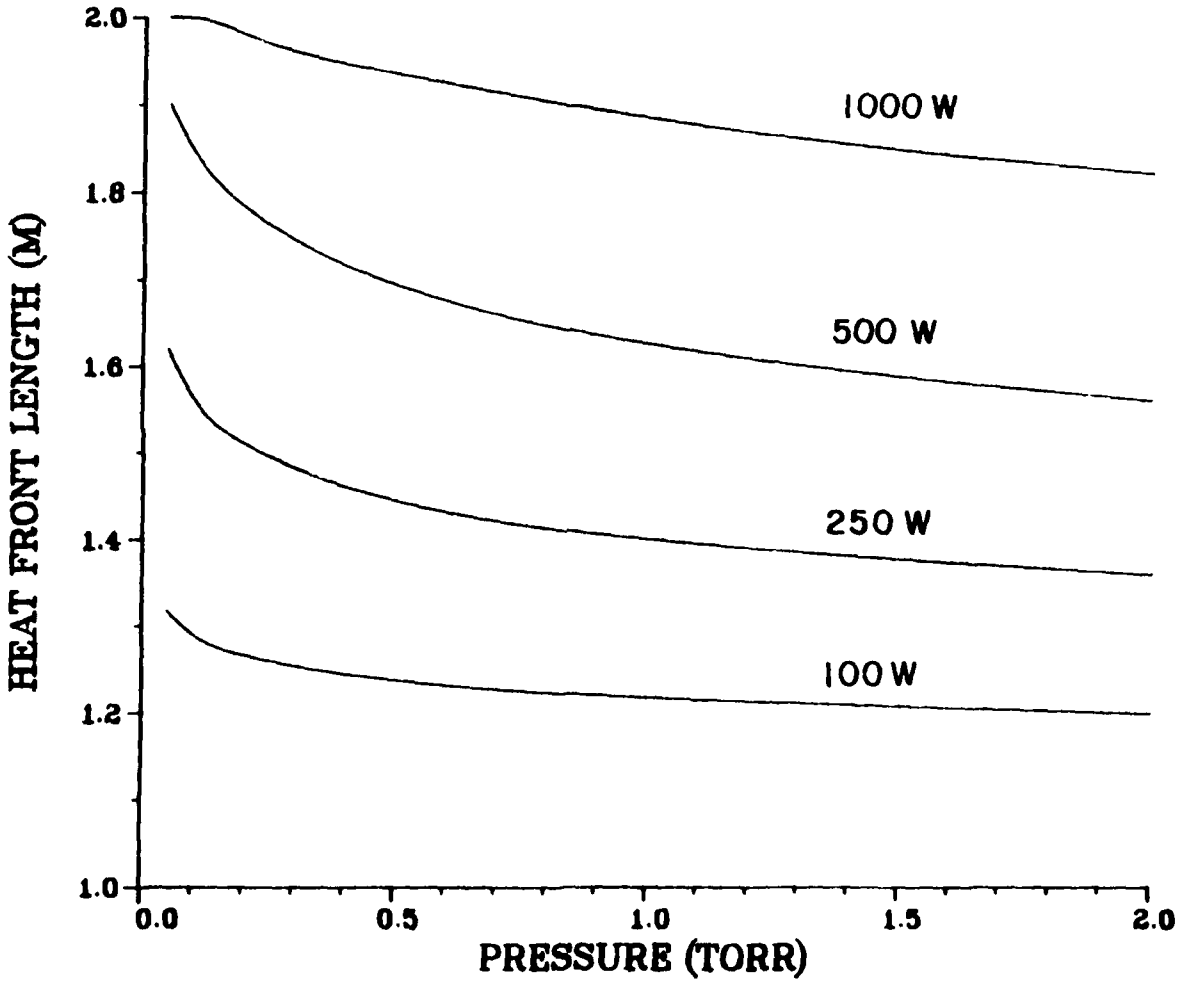

Figure 11. Heat Front Length Versus NCG Pressure

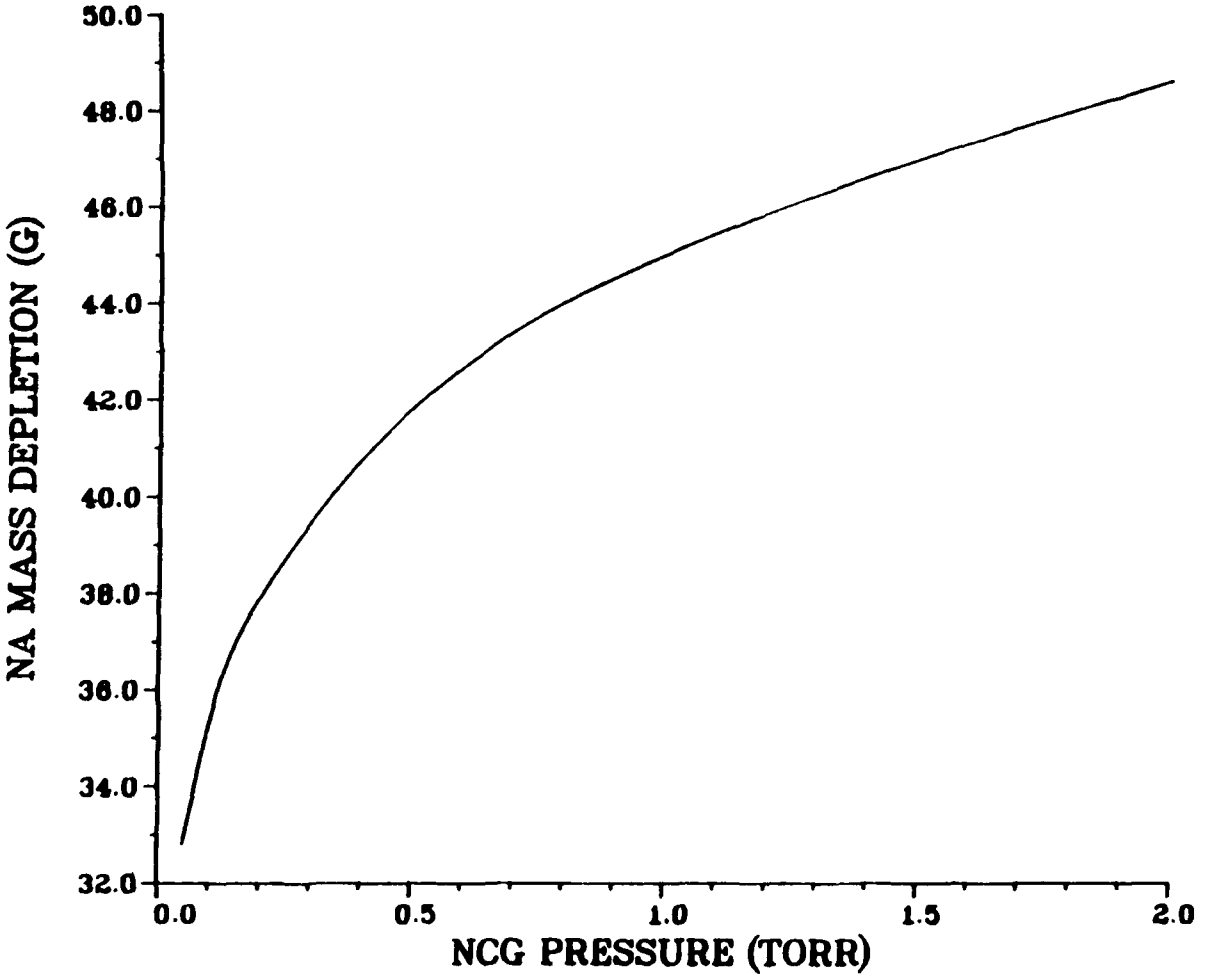

Figure 12. Sodium Mass Depletion Versus NCG Pressure

value of 38.0 g for P_i 0.2 Torr satisfied the design conditions (evaporator and reservoir wick hold 38.23 g); hence, this value of the charge pressure was recommended. Other charge pressures (0.05 2.0 Torr) also could be tried during the experimental phase. The startup temperature necessary for a successful start with reference to the characteristics of liquid metal heat pipe startup (Section 2.1) was obtained.

The major aspects of the transient results of the computation are presented in the graphs of Figures 13 through 28. Each graph shows six curves corresponding to the six charge pressures and represents one of the four parameters (L, T, Q_v, or Q_o). Figures 13 through 16 correspond to Q_i = 100 W and show L vs t, T vs t, Q_v vs t, and Q_o vs t, respectively. Three other sets of figures (Figures 17 through 28) show the results for 250, 500 and 1000 W in order.

The general trend of the Q_v vs t curves is important. At the starting time, Q_v is as high as Q_i and as the hot front moves, Q_v drops exponentially to very low value at the end. The kink in the curve where the slope changes signifies the abrupt change in the thermal capacity of the adiabatic to condenser sections. On the other hand, Q_o remains zero until the hot front reaches the condenser and increases fast to a maximum toward the end. The variation of hot zone temperature during startup is only marginal. The rise temperature is as high as the startup temperature and this signifies the frontal nature of the startup.

These results are compared and corroborated with the experimental data in the results and discussion section.

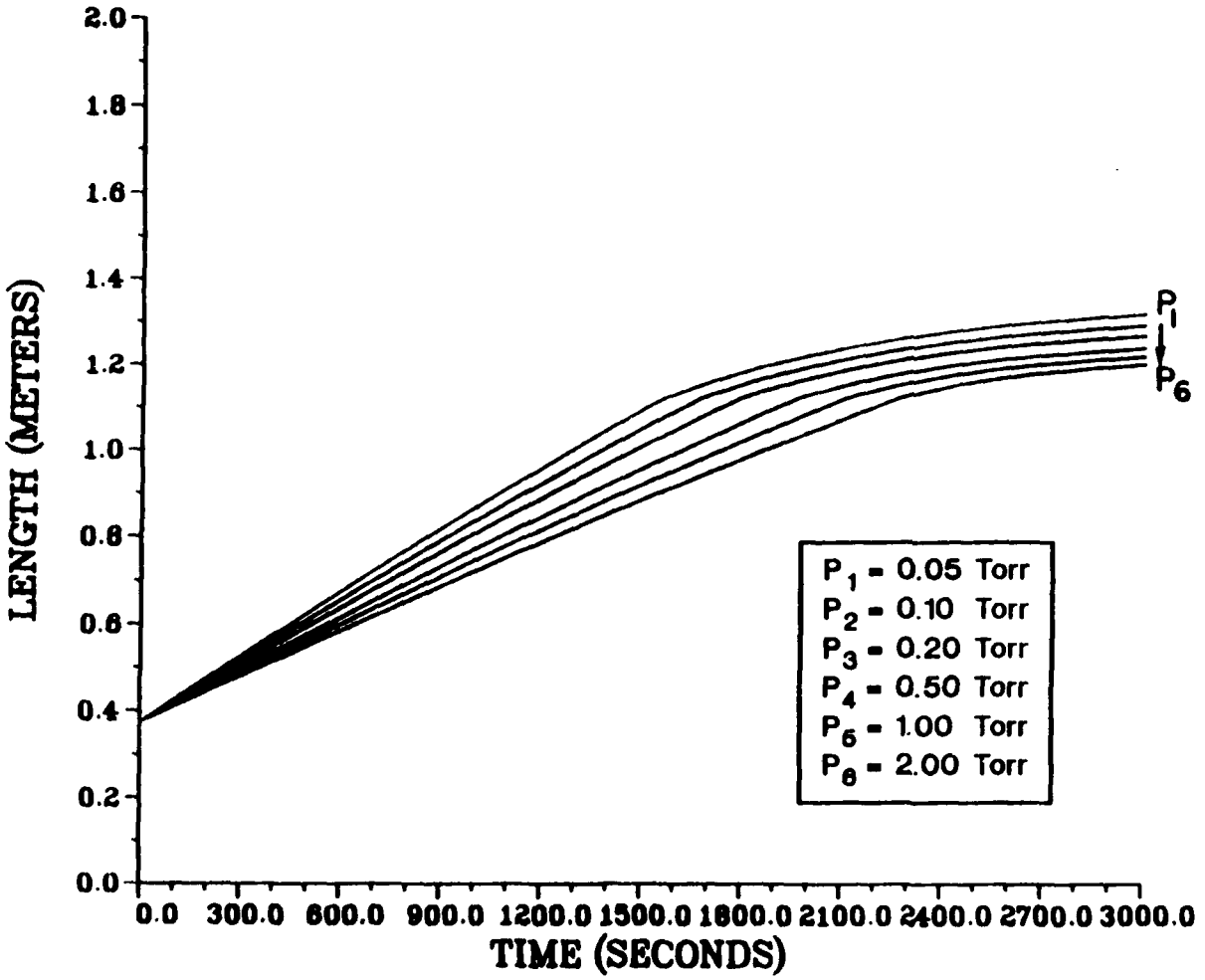

Figure 13. Heat Front Length Versus Time for 100 W

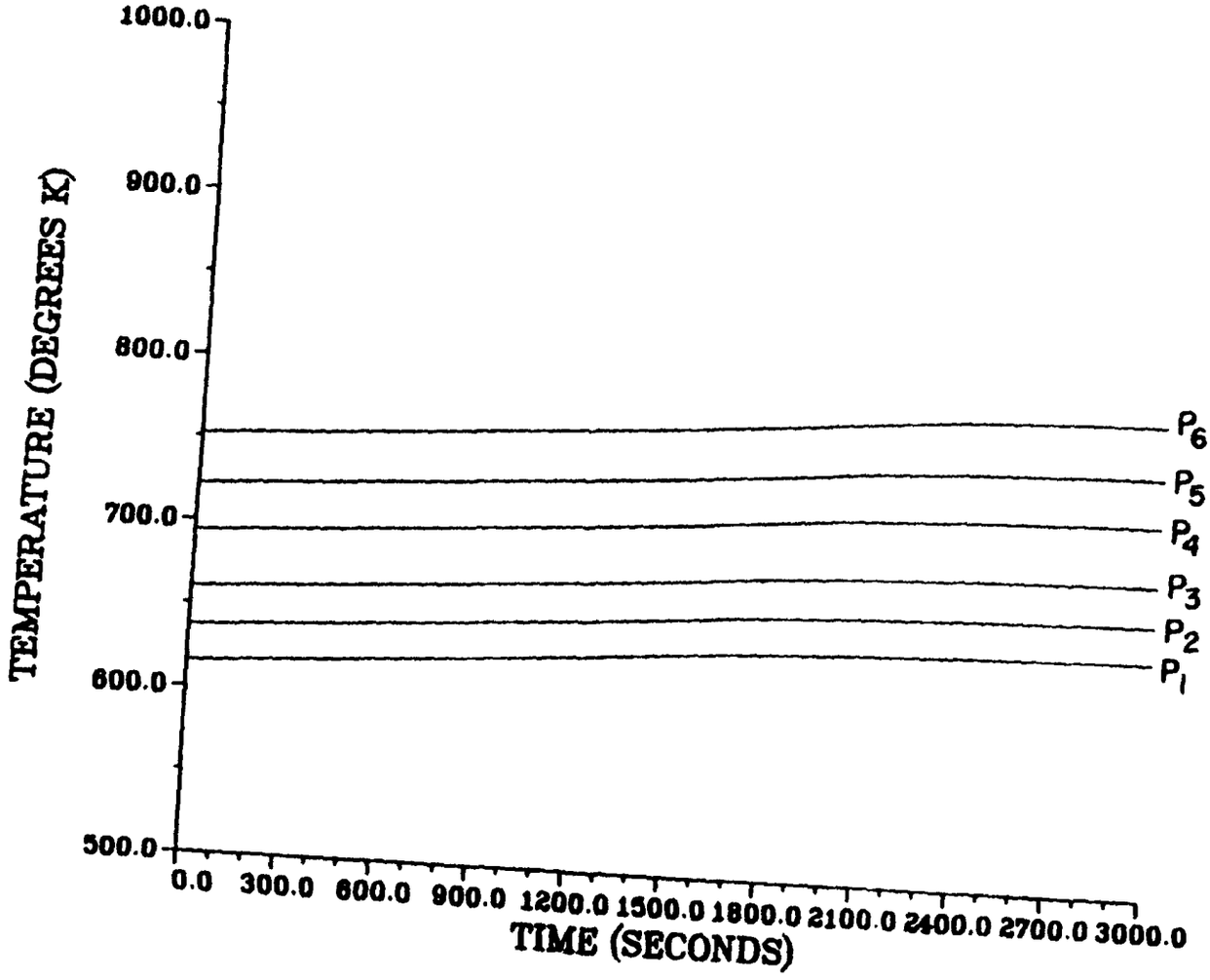

Figure 14. Hot Zone Temperature Versus Time for 100 W

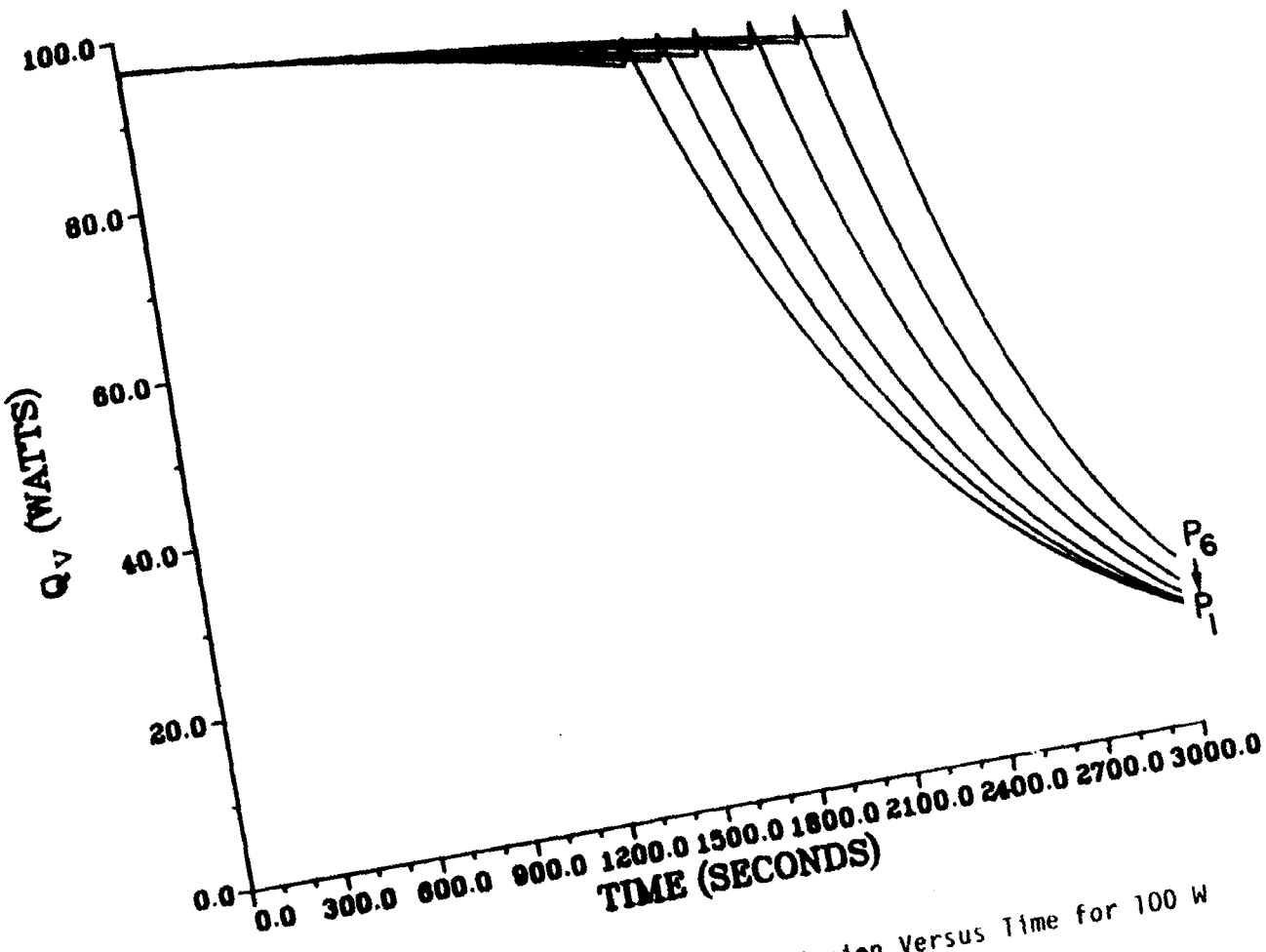

Figure 15. Heat Transport by Vapor Diffusion Versus Time for 100 W

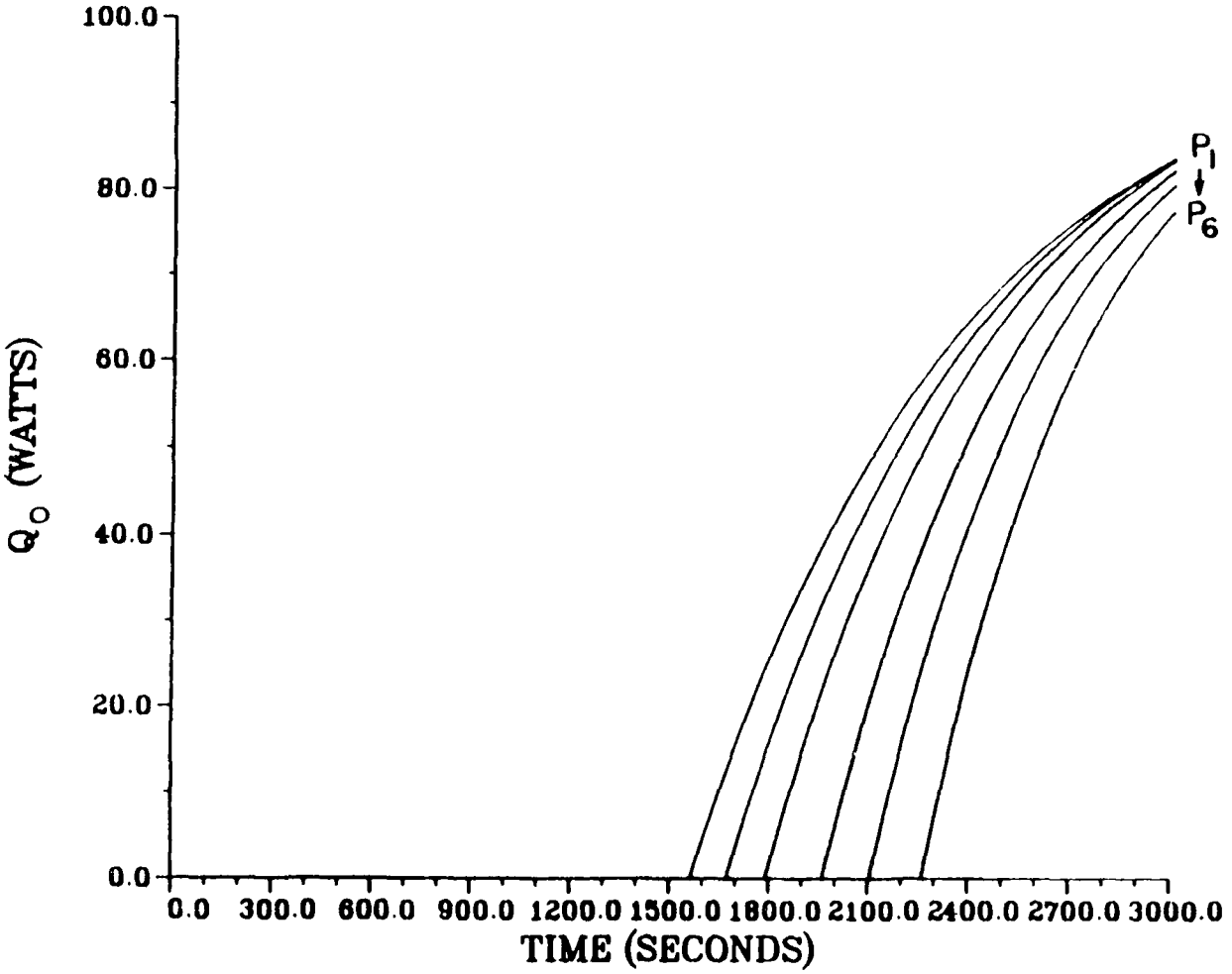

Figure 16. Heat Radiated Out Versus Time for 100 W

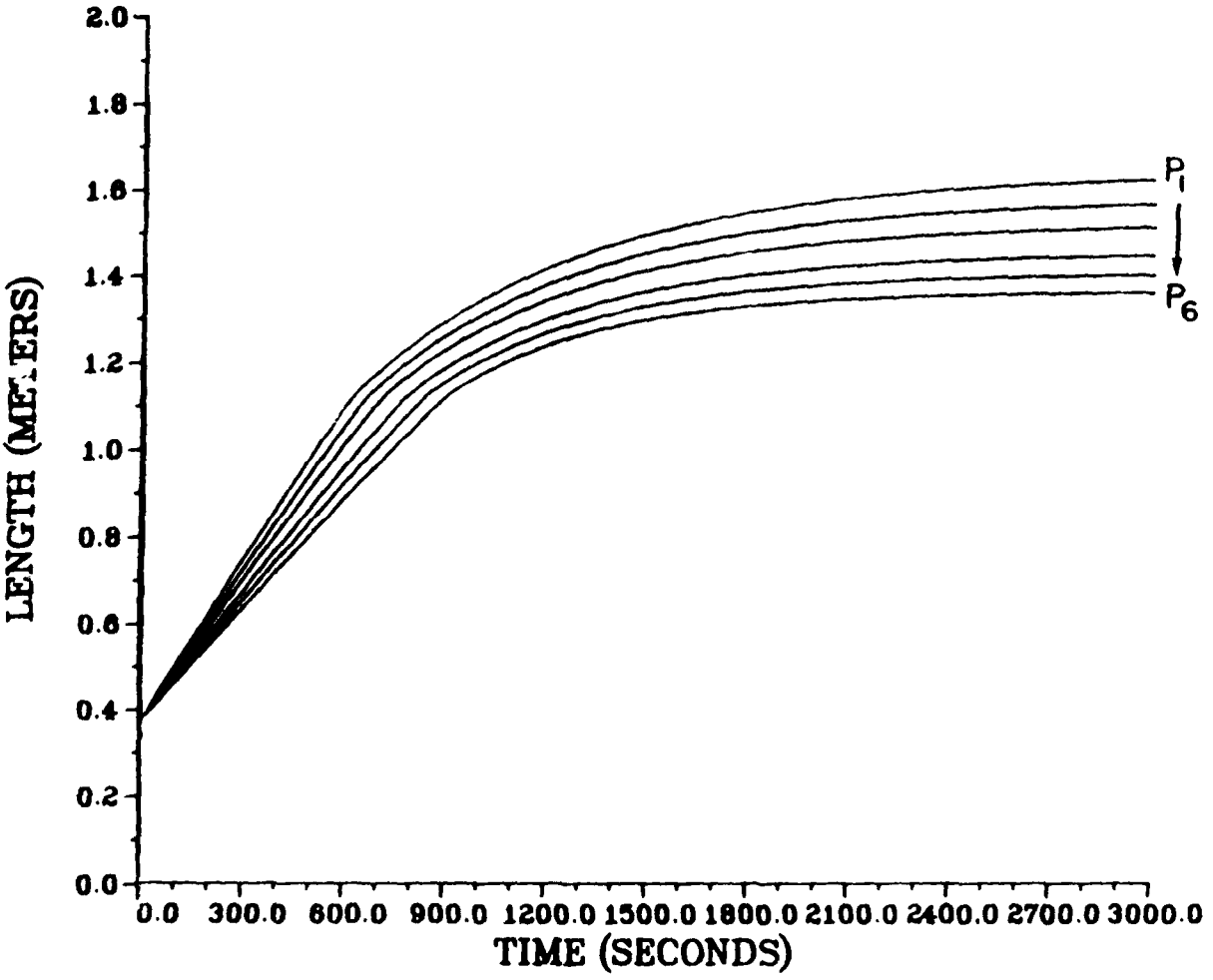

Figure 17. L Versus t for 250 W

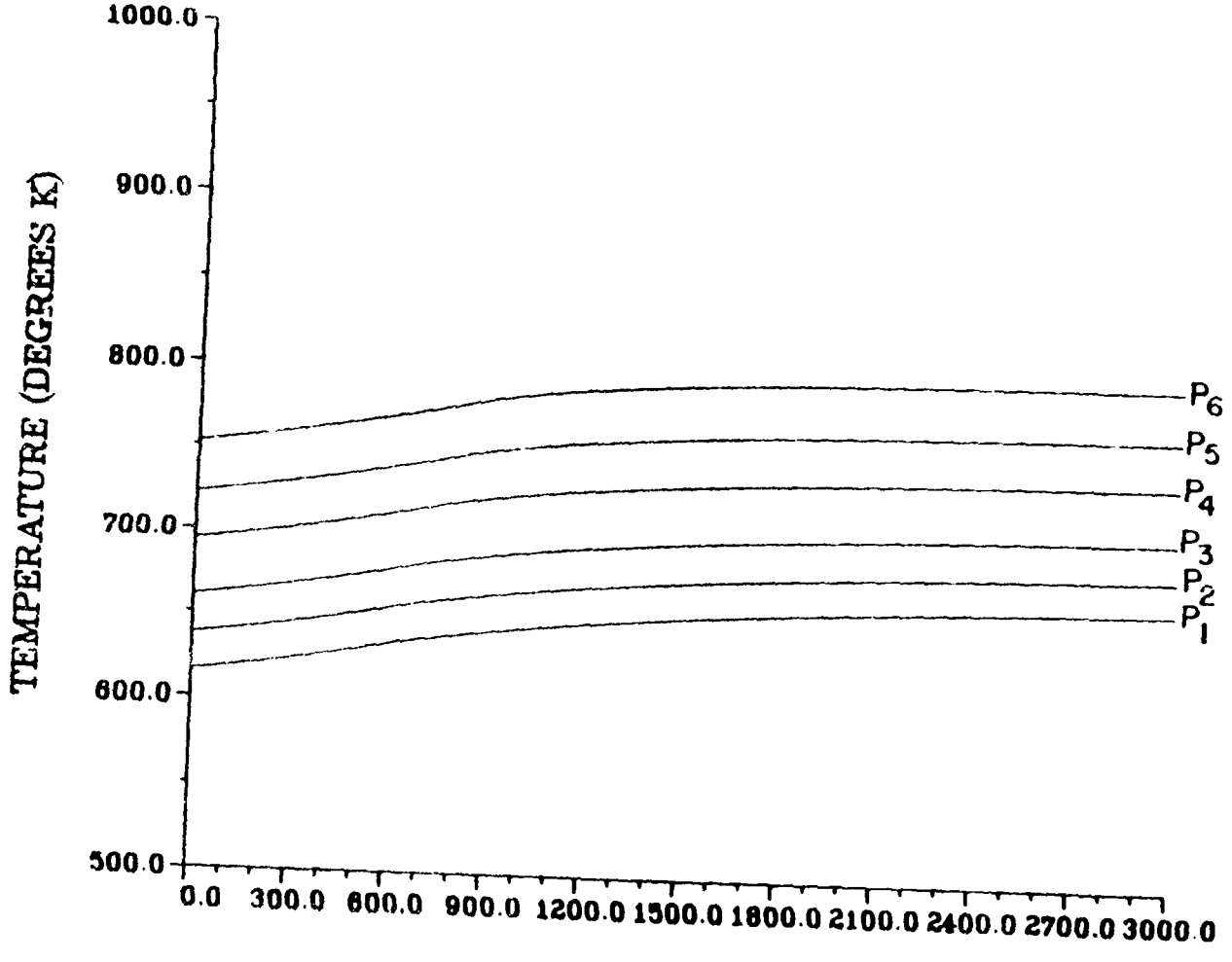

Figure 18. T Versus t for 250 W

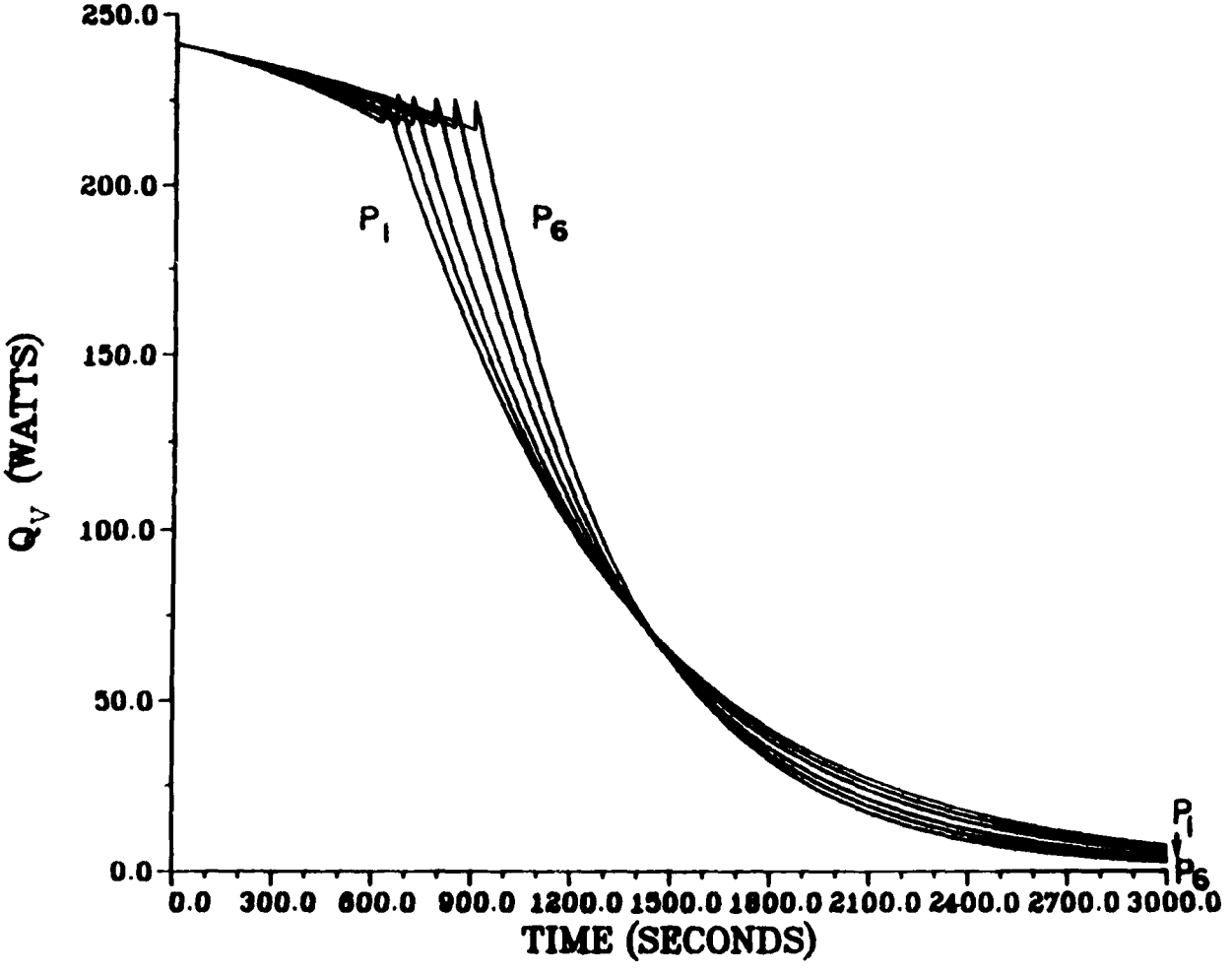

Figure 19. Q_v Versus t for 250 W

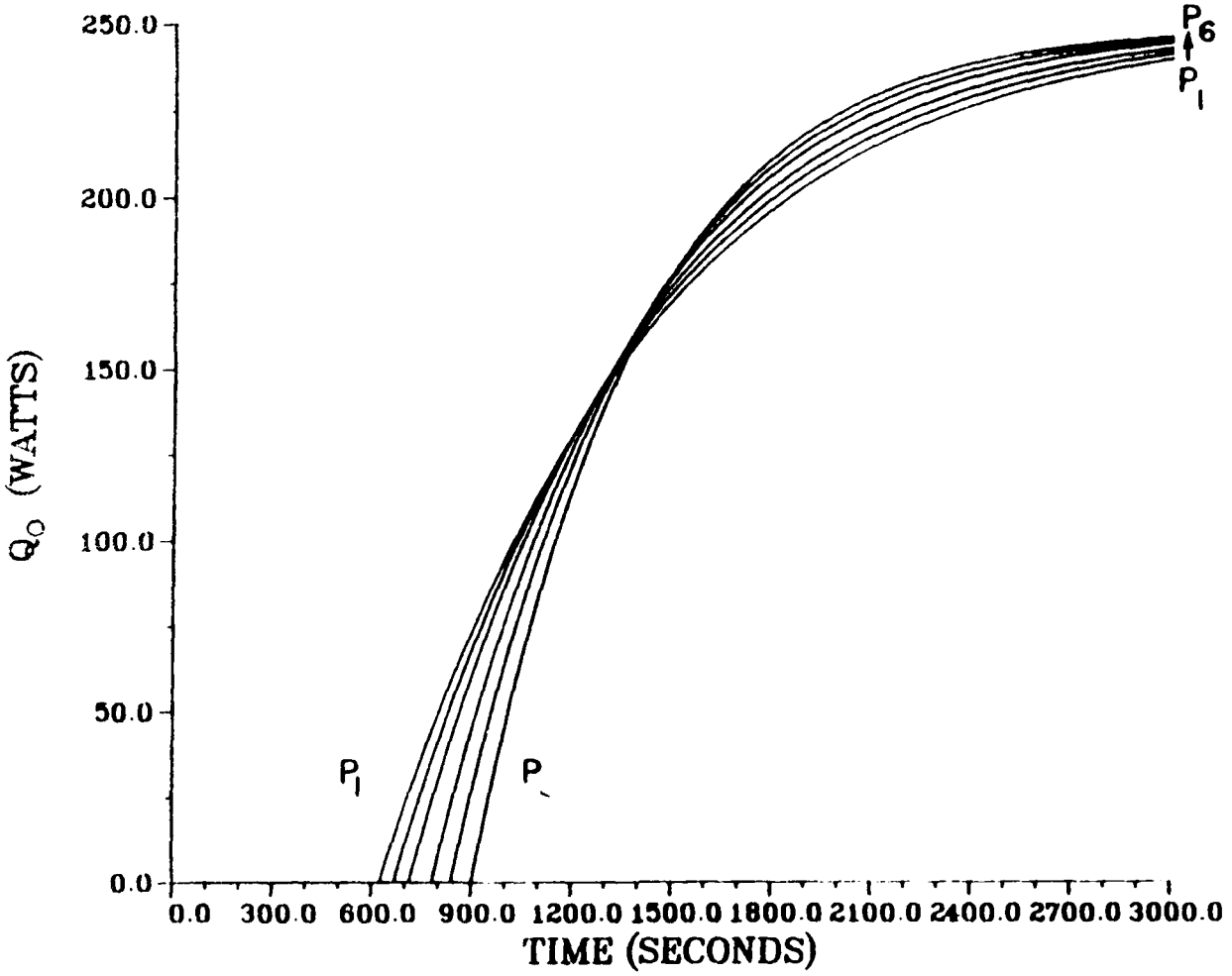

Figure 20. Q_0 Versus t for 250 W

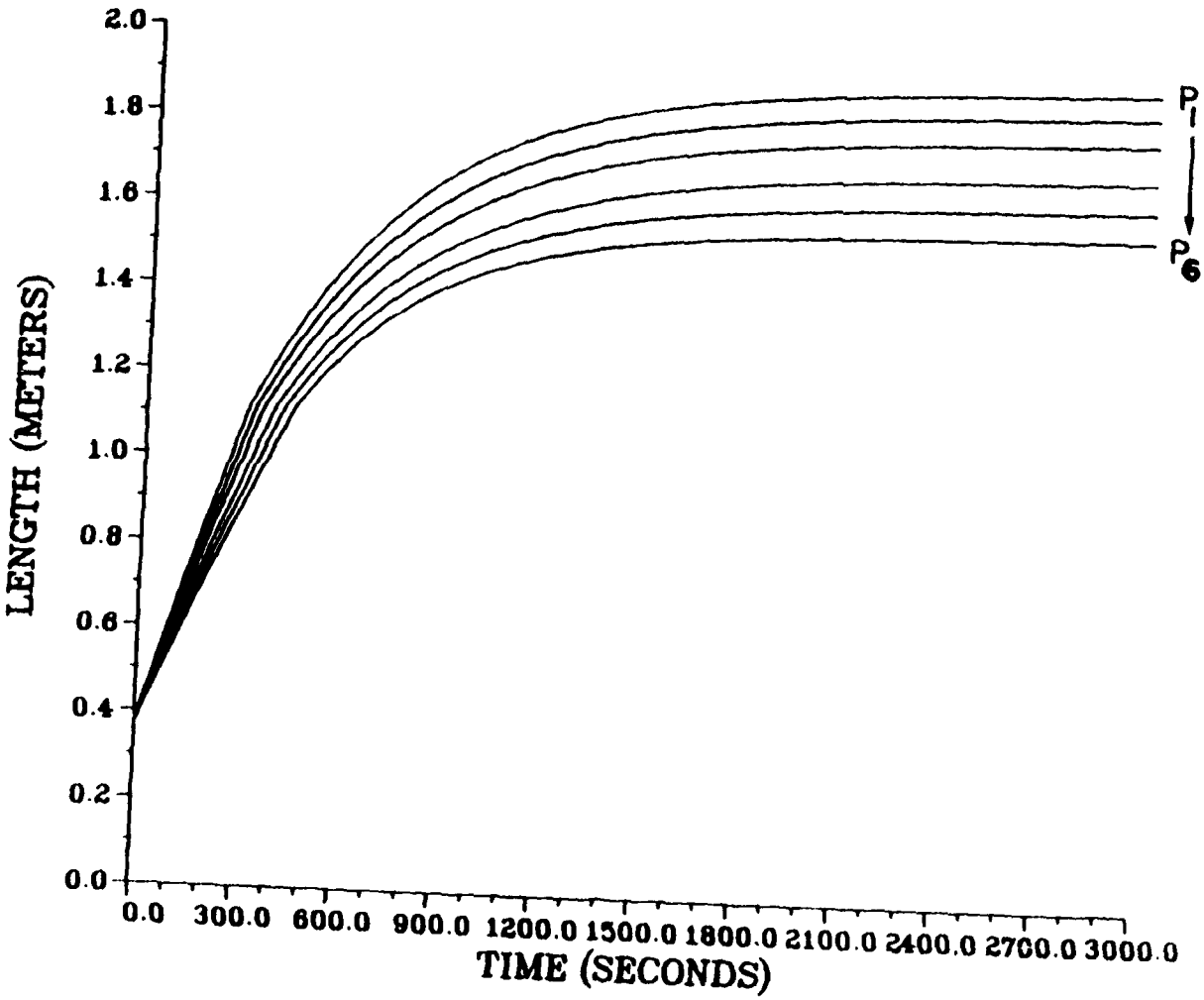

Figure 21. L Versus t for 500 W

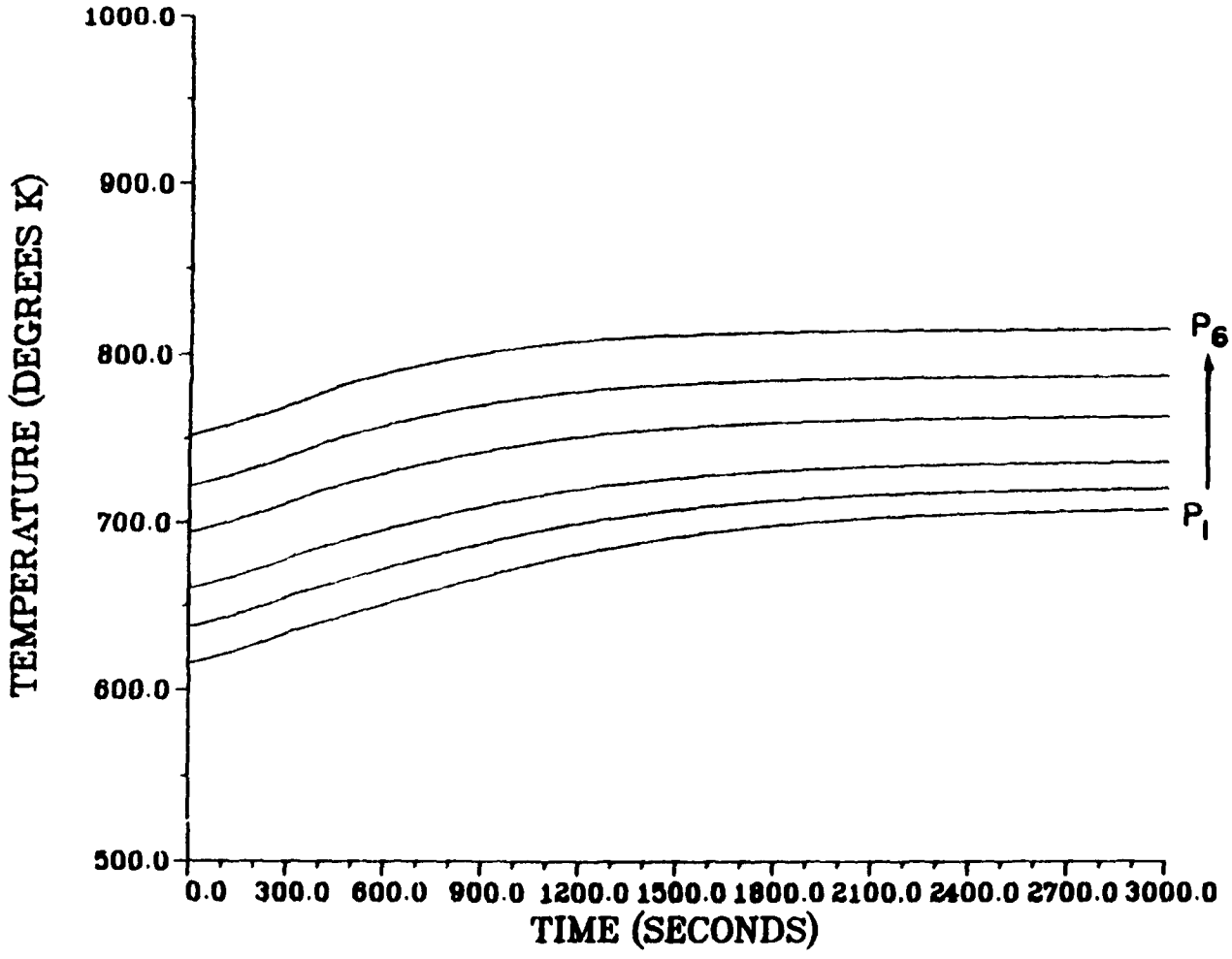

Figure 22. T Versus t for 500 W

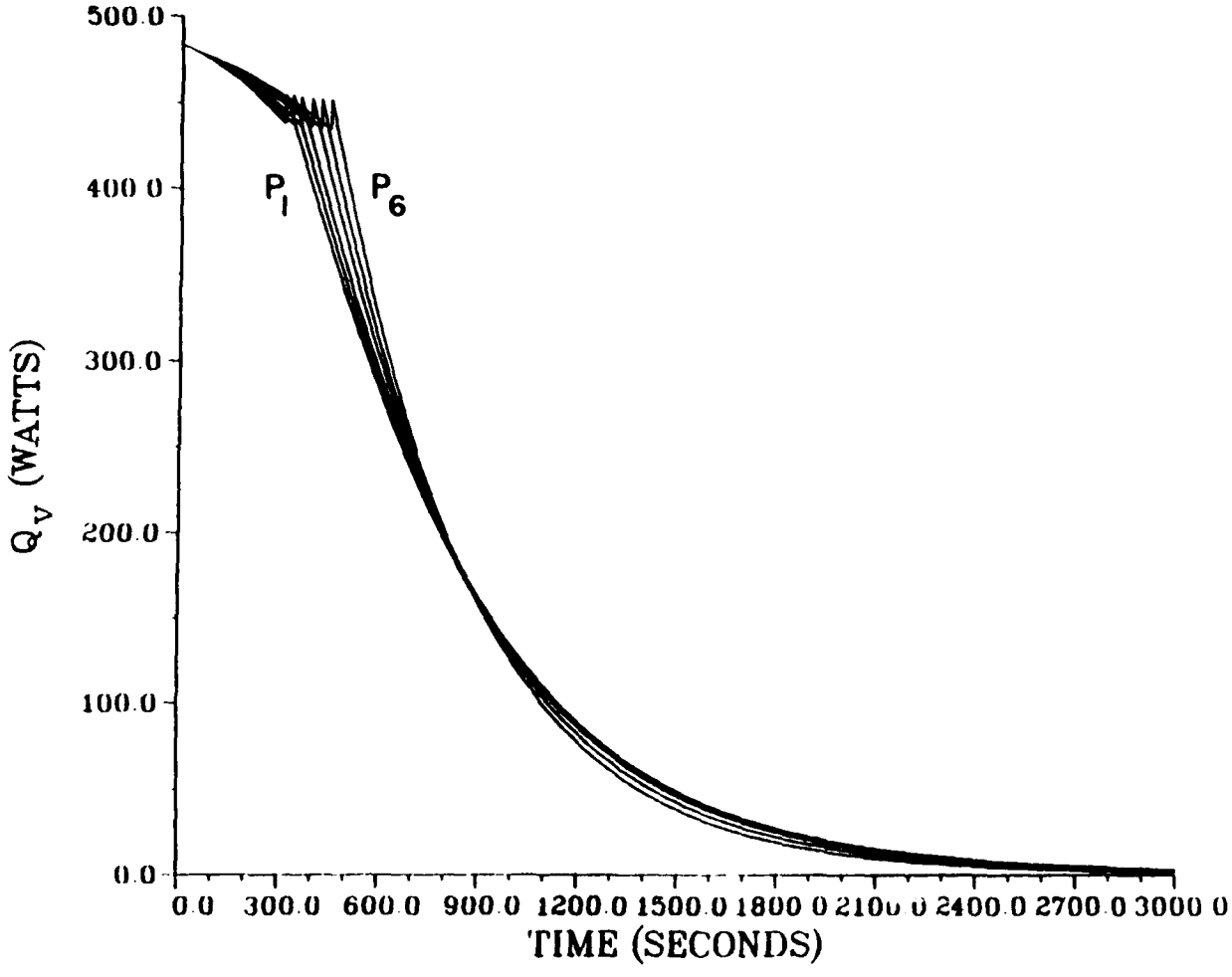

Figure 23. Q_V Versus t for 500 W

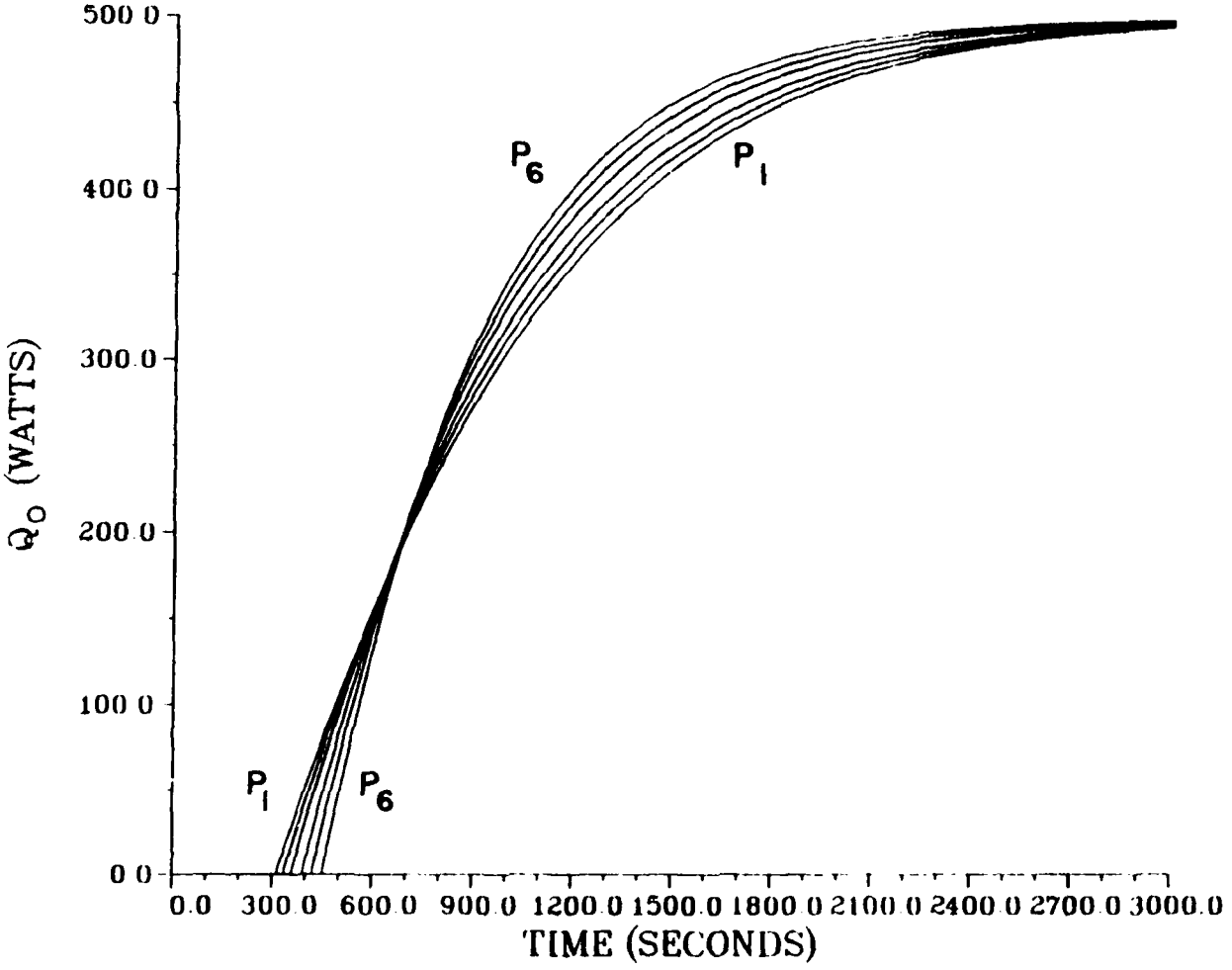

Figure 24. Q_O Versus t for 500 W

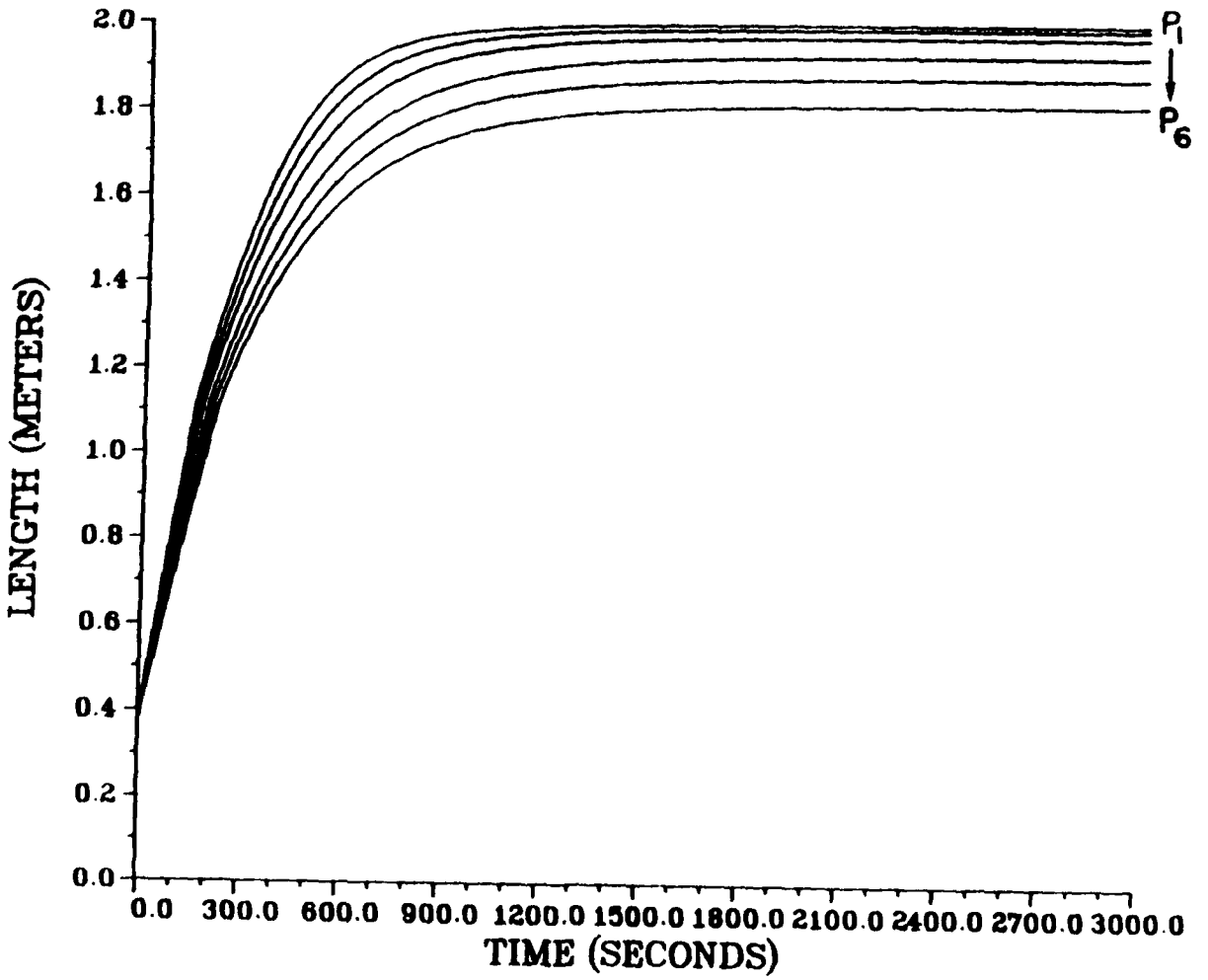

Figure 25. L Versus t for 1000 W

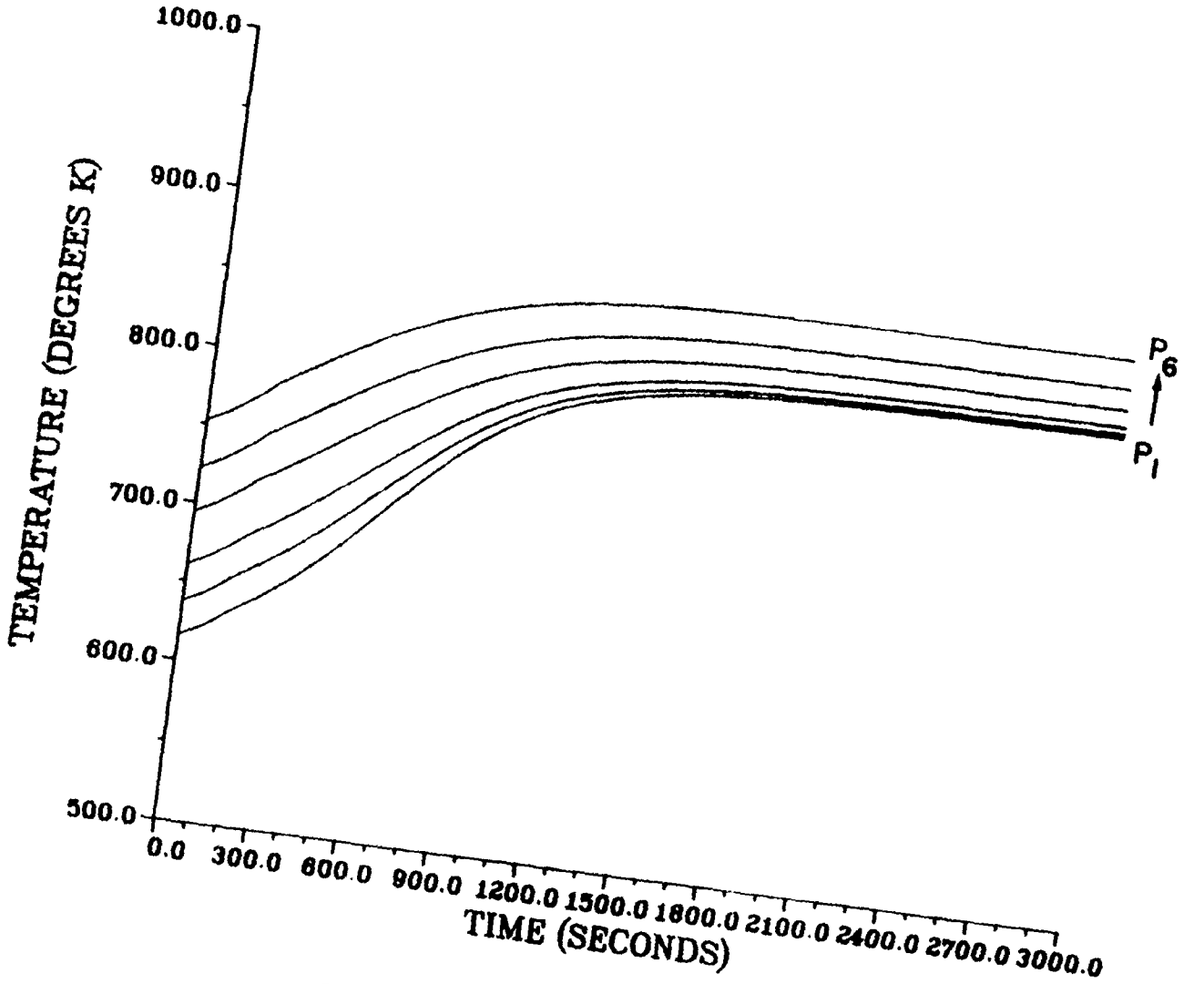

Figure 26. T Versus t for 1000 W

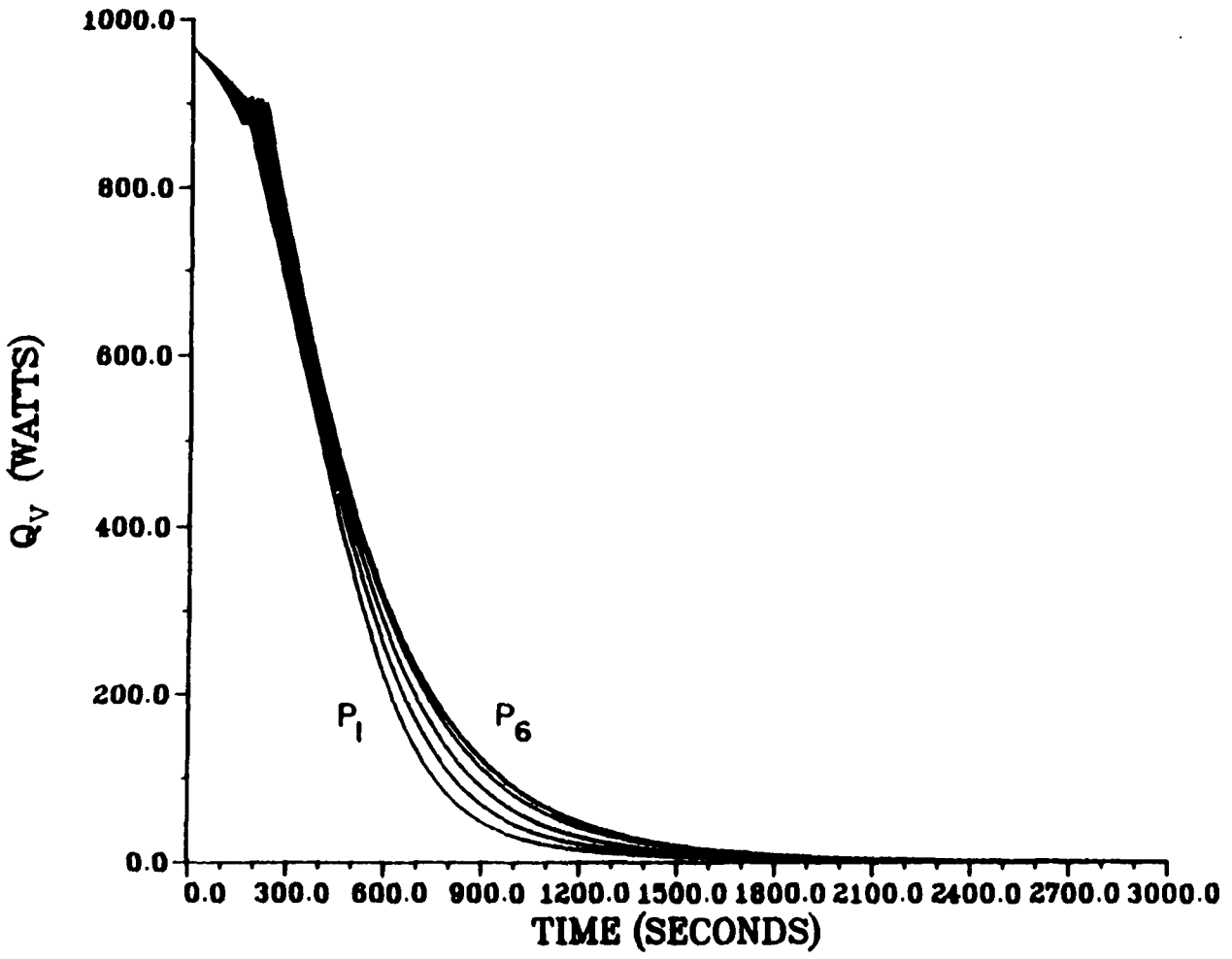

Figure 21. Q_V Versus t for 1000 W

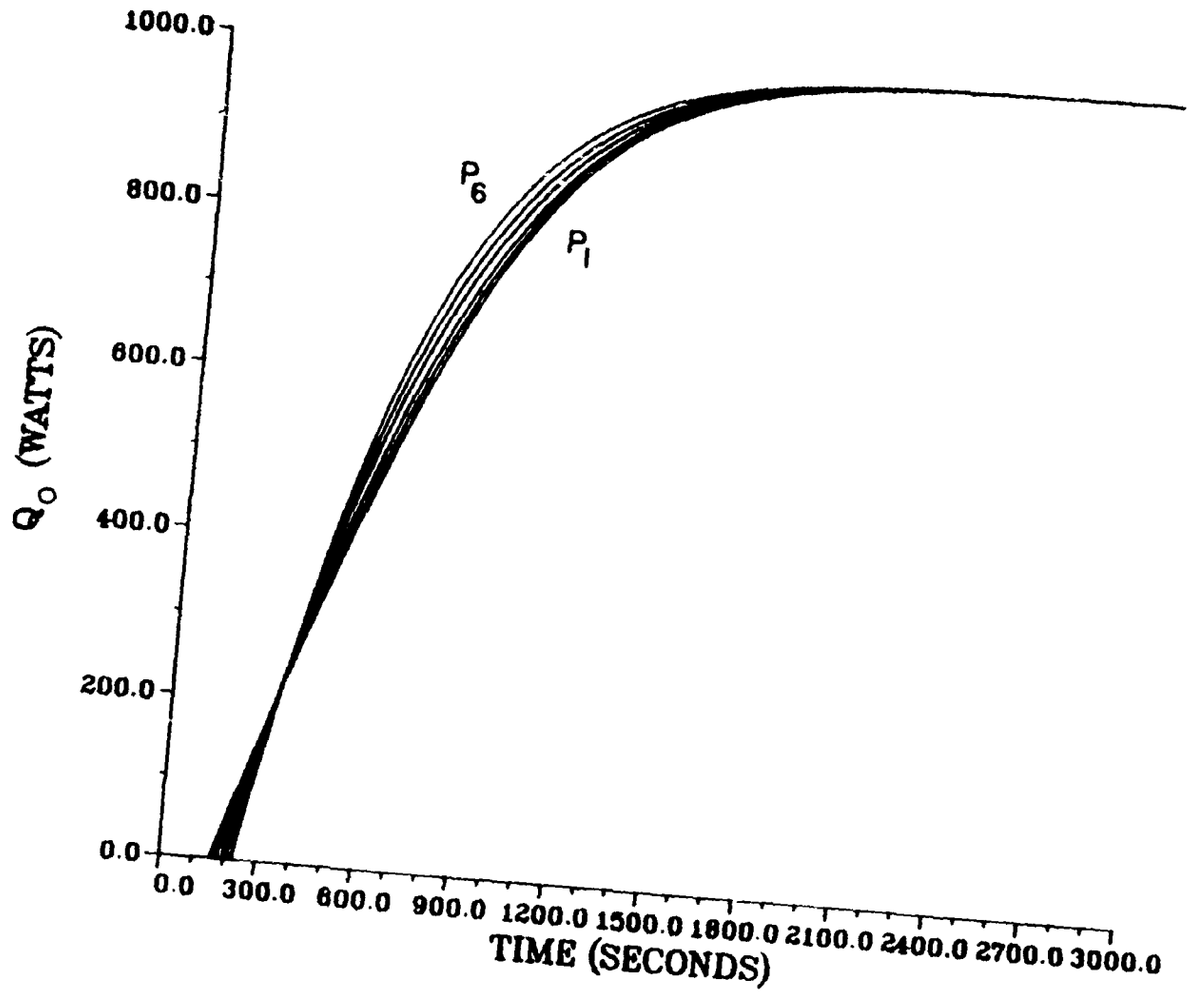

Figure 28. Q_o Versus t for 1000 W

CHAPTER III

DESIGN ANALYSIS OF THE EXPERIMENTAL HEAT PIPE

3.1. Design Constraints/Requirements

The starting point of any heat pipe design is to consider the operating temperature regime of interest, geometries and the heat transport capacity requirements. The objective of the present work is to investigate the startup characteristics of the high temperature DWAHP in the 1000 K regime with a selected nominal laboratory testable load of 2000 W. The most appropriate working fluid in the temperature range 400 1000°C is sodium and the compatible container easily available is stainless steel. An overall length of 2 m and a tube diameter of 2.22 cm was chosen for the physical dimensions for the heat pipe. The geometry of evaporator, adiabatic (transport) and condenser sections of the heat pipe is always dictated by the application requirements of the device. However, in a research device, the sizing of various sections is flexible. The evaporator length selected by the input heat flux limit, fixed the type of heating employed. Radial heat fluxes up to 100 W/cm^2 are common for sodium heat pipes. The condenser length is dictated by the type of heat transfer coupling available between the heat pipe and the sink. Radiative, convective, or conductive coupling is possible. In order to simulate space radiator conditions and for simplicity of laboratory

testing, radiative coupling with a cold shrouded vacuum chamber was chosen.

Since the present study is an offshoot of the 2 m copper water DWAHP, the mechanical design details such as the type of screen wick, artery groove size, double wall feature, etc., were kept the same as previous configurations for comparison purposes [10,11]. Some of the special features included in the experimental heat pipe design are:

(1) Single groove artery transport section to study the effects of orientation of the groove with respect to the gravity vector in 1 g testing;

(2) Noncondensible gas (NCG) loading to study the rapid startup from frozen state.

From a fabrication point of view, the geometrical shape and size of the groove, vent slots, end cap design, screen wick assembly, cleaning and filling procedures were chosen to be simple, safe and within the limits of available resources.

The basic design parameters available to start a detailed design are summarized as follows:

- Working fluid — Sodium
- Noncondensible gas — Argon
- Temperature range — 25-1000°C
- Heat load — 2000 W
- Container material — Stainless steel
- Wick material — Stainless steel screen
- Total length — 2 m

- Outer diameter — 2.22×10^{-2} m
- Heat input mode — Direct contact electrical resistance coil heating
- Heat removal mode — Radiation coupling to a cold shroud

3.2. Material Selection and Compatibility

Sodium: Sodium is a well characterized substance and is available in very pure analytical grades. It has high thermal conductivity in solid and liquid phases. The low vapor pressure even at high temperature (0.2×10^5 N/m^2 at 1000 K) makes sodium pressure containment easy since a relatively thin walled container is adequate. The liquid transport factor or figure of merit ($\sigma_\ell \rho_\ell \lambda / \mu_\ell$) for sodium is 3×10^5 kW/cm^2 at 1000 K. It is compatible with stainless steel, inconel, nickel and niobium which are candidate wall materials for high temperature heat pipes. The intrinsic drawbacks with sodium are its handling hazards and the frozen state at room temperature. Extreme care is required in handling sodium in order to ensure personnel safety and heat pipe working fluid purity. A list of selected properties is given in Appendix C.

Stainless Steel: The steel alloy chosen here is SS 304 which has the property of good corrosion resistance. While inconel may have been preferred over stainless steel from high temperature strength and corrosion resistance points of view, availability in required size tubings, bar stock and woven screen mesh dictated the selection. The ultimate tensile strength of SS 304 drops from 620×10^6 N/m^2 (90 kPSI) at 300 K to 207×10^6 N/m^2 (30 kPSI) at 1100 K.

The end cap size and wall thickness of the heat pipe envelope are governed by this high temperature strength limitations.

High Temperature Fill Valve: A valve at the condenser end of the research heat pipe is essential for processing such as evacuating, filling the working fluid or the noncondensible gas, and burping the excess fluid/gas if necessary. A high temperature, bellows type, all-metal (stainless steel), all welded construction valve manufactured by NUPRO was selected. This valve has a stellite tip for the valve stem. It is rated for service at 649°C and 17,200 kPa or at extended ratings of 816°C and 340 kPa if self lubricating fluids such as liquid metals are used. A secondary packing of grafoil, lubricated by moly disulfide base paste, seals the valve for protection of personnel in case of hazardous fluid leaks.

Argon: The noncondensible gas (NCG) chosen is the 99.99% pure, dry, oil and moisture free, laboratory grade 5.8 AIRCO supplied specialty gas, argon. The requirements of the NCG in the present application are low solubility and non reactivity with sodium even at high temperatures. The solubility constant (Ostwald coefficient) for argon and sodium at 500°C is 2.27×10^{-5} and it is considered that argon is insoluble in sodium for practical purposes. Also, argon is inert and does not form any compound with sodium. In contrast, nitrogen could be used as the NCG since the solubility constant is very low (3.11×10^{8} at 500°C); however, it is not considered because sodium is known to react with nitrogen at high temperatures (>300°C) forming sodium nitride.

3.3 Mechanical Design Details

A detailed design is carried out based on the available design parameters and constraints in order to determine the following:

(1) Vapor core diameter to provide a vapor Mach number of 0.2 which would eliminate vapor compressibility effects and sonic flow limitations.

(2) The container details such as evaporator, adiabatic and condenser section lengths, wall thickness, and end cap dimensions.

(3) The capillary wick details and flow pressure drops.

(4) The artery groove size (depth and width) and screen wrap details.

(5) The heat transport limits such as capillary, sonic, boiling, and condenser radiation limitations.

(6) The fluid inventory and NCG initial charge pressure.

3.3.1 Envelope Design

The chosen total length of 2 m is to be divided into evaporator, transport and condenser lengths. From the radiation limit calculations (refer to Section 3.5.1), it is found necessary to have a minimum of 0.91 m long condenser section. The heat pipe will be radiation limited if the condenser is shorter than 0.91 m. The lumped thermal capacity analysis (Section 3.4) is used to determine the length of evaporator needed mainly from the standpoint of working fluid requirement during startup. Accordingly, the evaporator length is 0.375 m which is divided into a reservoir wick length of 0.125 m and the heated evaporator length of 0.25 m. The

remaining heat pipe length of 0.745 m is available for the transport section which is sufficiently long for the experimental laboratory study. To summarize this design, the total length (L_p) and effective length (L_{eff}) are written as follows:

$$L_p = L_E + L_A + L_C \tag{35}$$

or $$2.03 \text{ m} = 0.375 \text{ m} + 0.745 \text{ m} + 0.91 \text{ m}$$

$$L_{eff} = 0.5\, L_E + L_A + 0.5\, L_C \tag{36}$$

$$= 1.388 \text{ m}$$

The minimum vapor core diameter required for an axial heat flux of 2000 W at 1000 K nominal operating temperature and vapor Mach number limit of 0.2 is obtained as $d_v = 8.32$ mm from Eq. (37).

$$d_v^2 = \frac{20\, Q_{max}}{\pi \rho_v \lambda \sqrt{\gamma_v R_v T_v}} \tag{37}$$

The vapor pressure of sodium at a possible maximum operating temperature of 1400 K is 0.6061×10^6 N/m^2 and the ultimate tensile strength of SS 304 at this temperature = 120.7×10^6 N/m^2 as given in Appendix D.

The diameter ratio of the container tube is obtained from Appendix E as $D_o/D_i = 1.05$ for $P_v = 0.606$ MPa and $f_u = 120.7$ MPa.

An available standard SS 304 tube stock of 2.22 cm OD, 1.89 cm ID, and 1.65 mm wall thickness is selected for the envelope. The extra wall thickness provides added safety for this design. However, the associated heavy thermal mass has to be tolerated. The flat end cap thickness is also obtained from the design chart of Appendix F as $t/D_o = 0.075$ for the above vapor pressure and strength values. Therefore, the minimum required end cap thickness is $t = 0.075 \times 2.22$ cm $= 1.67$ mm. Actual thickness used is 6 mm for the conveniences of machining and welding.

3.3.2 Wick Design

The wick configuration chosen is a version of the double walled artery concept researched by the author in the recent past [10,11]. A cross sectional view of the wick geometry is illustrated in Figure 29. In general, the double walled wick arrangement consists of:

(1) A cylindrical, selectively perforated and externally grooved (axial) inner tube wall;

(2) An inner annuli screen mesh wick; and

(3) An outer tube envelope with internally grooved evaporator all packaged in a single concentric assembly. The inner tube contains the artery transport groove wick and firmly presses the inner annuli evaporator supply screen wick against the outer tube. This feature ensures that the screen wick remains in good mechanical contact with the outer tube throughout its operating life, thereby enhancing the radial heat

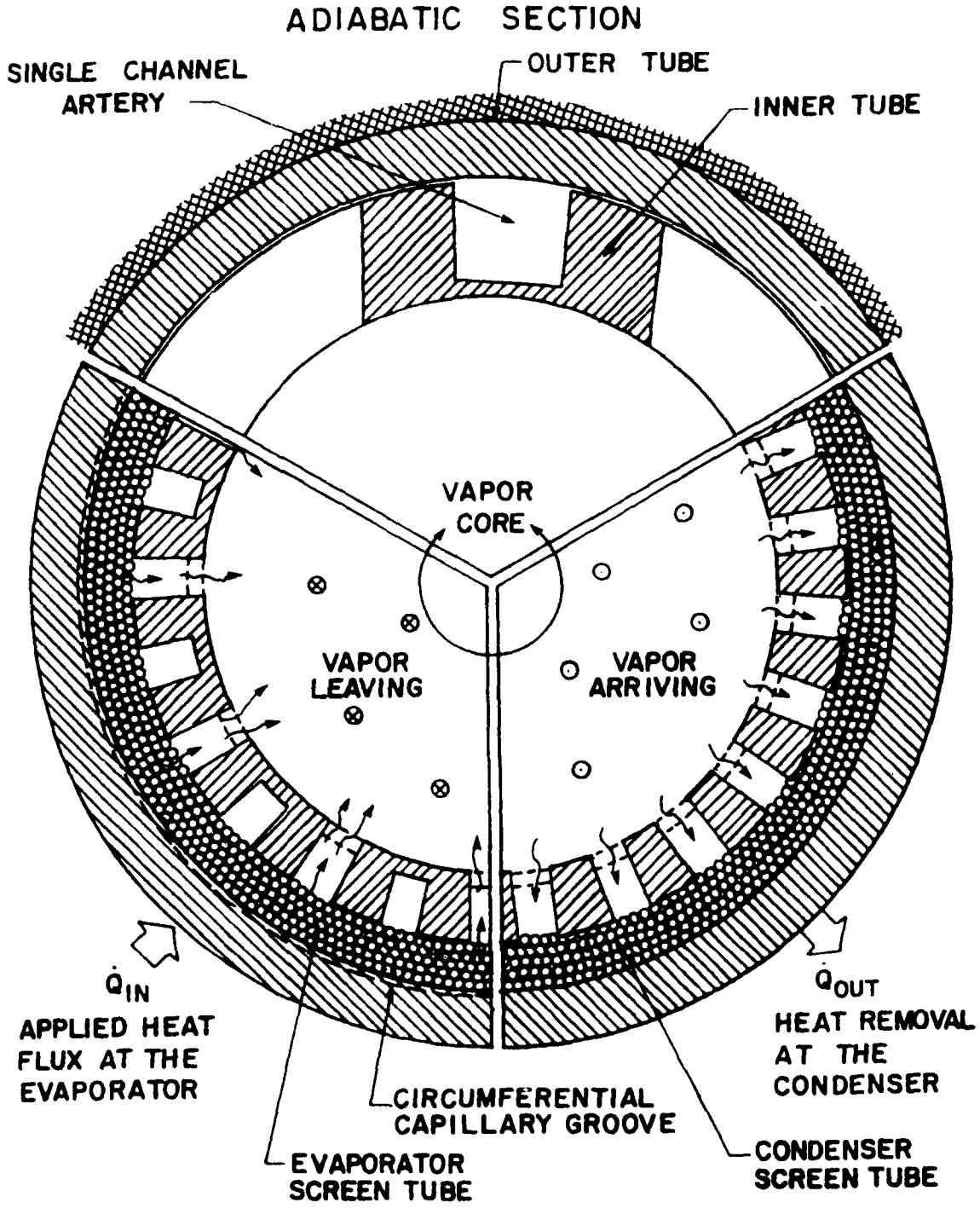

Figure 29. Cross Sectional View of the Wick Geometry

transfer in the evaporator and condenser sections. It is of particular importance in the liquid metal heat pipe evaporator since hot spot development due to the detachment of screen wick from the wall is common in conventional screen wick designs. Suitable vapor vent cut-outs along the axial grooves of the inner tube provide for the vapor injection from the evaporator and the vapor suction into the condenser screen wick. The screen wick is formed of spirally wrapped multiple layers of wire mesh with suitable pore size to give the required capillary head.

The special feature of this design is the entrainment-free vapor transport due to the physically separated vapor and liquid flows in the adiabatic section. Other characteristic features uniquely incorporated in the present wick design are:

(1) Single groove transport artery as opposed to multiple grooves;

(2) Screenless, ventless, and groove only transport section;

(3) Non constant groove widths for evaporator/condenser; and transport sections.

Inner and Outer Tubes: The inner tube diameter and the wall thickness are determined from the requirements of the vapor core diameter and the artery channel size, respectively. Also, the availability of standard tube stock dictates the choice of the dimensions. Hence, two standard seamless extruded tube sizes were picked. They are, 2.22 cm OD and 1.65 mm wall outer tube and 1.905 cm OD and 3 mm wall inner tube. The 12.7 mm ID of the inner

tube more than satisfied the 8.32 mm diameter required for the vapor core and the 3 mm wall was adequate to machine an artery groove of up to 2.4 mm (3/32 inch) square (see Section 3.3.3 for artery dimension).

Screen Wick: The screen or the capillary wick radial thickness depends on the radial temperature differences (ΔT) permissible at the evaporator and condenser sections. Larger wick thickness means higher thermal resistance and consequently larger ΔT across the wick. On the other hand, smaller wick thickness may not be sufficient to hold enough working fluid. In addition, the main parameter controlling the heat transfer across the wick is the effective thermal conductivity of the fluid saturated screen wick. Several analytical and empirical models are available in the heat pipe literature for effective thermal conductivity. Section 3.3.5 deals with this in detail. The screen wick tube diameter ratio can be obtained from the radial heat conduction equation for the cylindrical geometry given in Eq. (38).

$$Q_{r,s} = \frac{2\pi L_E k_{eff} \Delta T_{r,s}}{\ln (d_o/d_i)_s} \qquad (38)$$

Q_r = 2000 W, L_E = 0.25 m, k_{eff} = 39 W/m K (for sodium saturated stainless steel wick at 1000 K using series parallel model) and $\Delta T_{r,s}$ is assumed not to exceed 5 K. It may be noted on similar calculations, that the ΔT across the outer tube wall is about 15 K. For $\Delta T_{r,s}$ = 5 K, the above equation gives (d_o/d_i) = 1.166

and knowing d_o = 1.89 cm, d_i is evaluated as 1.62 cm. Hence, the total thickness of the screen layers is 0.135 cm. The wire diameter of the 40 x 40 cm^{-1} screen mesh, d = 0.1143 mm. Thickness of one layer of screen = 2d = 0.2286 mm. Number of layers of screen = 1.35 mm/0.2286 mm = 5.9. In order to be consistent with the previous copper water heat pipe design, a 4 layer screen tube was selected. This incidentally reduced the $\Delta T_{r,s}$ to 3.3 K.

Capillary Pumping Head: In a composite wick, the effective capillary radius is that of the pumping wick (screen) and hence, the capillary radius,

$$r_c = \frac{1}{2N} \tag{39}$$

$$= \frac{1}{2 \times 100} = 0.0005 \text{ in.} = 0.127 \text{ mm}$$

The maximum capillary pumping head provided by r_c is given as:

$$P_{cm} = \frac{2\sigma_\ell}{r_c} \tag{40}$$

At 400°C, $$P_{cm} = \frac{2 \times 0.159}{0.127 \times 10^{-3}} = 2503.9 \text{ N/m}^2$$

From the thermophysical property data given in table 4 for sodium, the capillary pumping head at various temperatures can be calculated. The normal and axial hydrostatic pressure drops given

TABLE 4. THERMOPHYSICAL PROPERTY DATA OF SODIUM

Sl. No.	Property	Temperature (°C)						
		400	500	600	700	800	900	1000
1	Latent Heat, λ (J/kg)	4.342×10^{6}	4.37×10^{6}	4.243×10^{6}	4.09×10^{6}	3.977×10^{6}	3.913×10^{6}	3.827×10^{6}
2	Liquid Density, ρ_{ℓ} (kg/m^3)	855.9	828.1	805.4	763.5	757.3	745.4	725.4
3	Vapor Density, ρ_{v} (kg/m^3)	0.242×10^{-3}	0.003	0.013	0.050	0.134	0.306	0.667
4	Liquid Thermal Conductivity, k_{ℓ} (W/mk)	72.669	70.08	64.62	60.81	57.81	53.35	49.08
5	Liquid Viscosity, μ_{ℓ} (kg/m sec) or $(\frac{N\cdot sec}{m^2})$	0.278×10^{-3}	0.24×10^{-3}	0.21×10^{-3}	0.19×10^{-3}	0.18×10^{-3}	0.17×10^{-3}	0.16×10^{-3}
6	Vapor Viscosity, μ_{v} ($N\cdot sec/m^2$)	0.169×10^{-4}	0.18×10^{-4}	0.19×10^{-4}	0.20×10^{-4}	0.22×10^{-4}	0.23×10^{-4}	0.24×10^{-4}
7	Vapor Pressure, P_{v} (N/m^2)	0.58×10^{2}	0.01×10^{5}	0.40×10^{5}	0.15×10^{5}	0.47×10^{5}	1.25×10^{5}	2.81×10^{5}
8	Vapor Specific Heat, C_{p_v} (J/kg K)	9.94×10^{2}	9.04×10^{2}	9.04×10^{2}	9.04×10^{2}	9.04×10^{2}	9.04×10^{2}	9.04×10^{2}
9	Liquid Surface Tension, σ_{ℓ} (N/M)	0.159	0.151	0.142	0.133	0.123	0.113	0.104
10	Transport Factor $(\sigma_{\ell}\rho_{\ell}\lambda/\mu_{\ell})$ (W/m^2)	2.126×10^{12}	2.277×10^{12}	2.311×10^{12}	2.186×10^{12}	2.058×10^{12}	1.939×10^{12}	1.804×10^{12}
11	Factor $\frac{\nu_{\ell}}{\lambda}$ or $\frac{\mu_{\ell}}{\lambda\rho_{\ell}}$ $(\frac{N\cdot m}{W})$	0.07478×10^{-12}	0.06632×10^{-12}	0.06145×10^{-12}	0.06084×10^{-12}	0.05976×10^{-12}	0.05825×10^{-12}	0.05763×10^{-12}

by Eqs. (41) and (42) are subtracted from P_{cm} to obtain maximum pumping head available.

$$\Delta P_L = \rho_\ell g\, d_w \cos\psi \qquad (41)$$

At 400°C

$$\Delta P_L = 855.9 \times 9.81 \times 1.89 \times 10^{-2} \times 1 = 158.7\ N/m^2$$

$$\Delta P_A = \rho_\ell g\, d_w \sin\psi = 0 \quad \text{(for horizontal heat pipe operation)} \qquad (42)$$

$$P_{pm} = P_{cm} - \Delta P_L - \Delta P_A \qquad (43)$$

Table 5 lists these values for various temperatures.

TABLE 5. CAPILLARY PUMPING HEAD AVAILABLE WITH 40x40 cm^{-1} MESH AND SODIUM

Temperature (°C)	P_{cm} (N/m^2)	ΔP_L (N/m^2)	P_{pm} (N/m^2)
400	2504	158.7	2345.3
500	2378	153.5	2224.5
600	2236	149.3	2086.7
700	2094	141.6	1952.4
800	1937	140.4	1796.6
900	1779	138.2	1640.8
1000	1638	134.5	1503.5

3.3.3 Artery Design

The artery channel design procedure followed here is the same as that used in the 2 m copper water heat pipe [4,11,55]. The groove sizes used for water heat pipe should work for the sodium heat pipe also since the liquid transport factor at the respective peak operating temperature for sodium is 4.2 times greater than that for water. In principle, even larger grooves than those used in water heat pipe may be employed for sodium heat pipe. However, for the sake of comparison and other considerations such as wettability, wetting angle, etc., the dimensions of grooves are retained the same. Accordingly, the number of grooves on the evaporator and condenser sections are 24 and their sizes are 0.79 x 1.4 mm. On the transport section, only one 2.4 x 2.4 mm groove is necessary as a liquid transport artery. Incidentally, this single groove arrangement helps in testing the heat pipe for artery orientation effects (with respect to gravity vector) and acts as a scaled down model for easy low power testing. The approximate scale down criterion used is as follows:

Theoretical transport capacity of the copper water heat pipe with 12 artery grooves = 5142 W

Capacity for 1 groove = 5142/12 = 428.5 W

For sodium heat pipe with 1 artery groove of the same size, the capacity = 428.5 x 4.2 (transport factor ratio)

= 1800 W

This is close to the nominal 2000 W capacity set as the design goal.

The inner tube groove and vapor vent details are shown in Figure 30. Alternate grooves in the evaporator are vented whereas all the grooves in the condenser are vented. No vent slots are provided in the adiabatic. A short capillary insert is installed within the adiabatic groove at the evaporator exit.

Self Priming Requirement: Arterial heat pipes should be capable of priming with the working fluid within the capillary spaces at all times. If an artery becomes depleted of working fluid due to external influences such as evaporator dryout or unfavorable tilt in 1 g environment, it should be able to reprime automatically once the external influence is removed. Such an artery is called a self priming artery. Self priming requirement can be satisfied by limiting the diameter of the heat pipe to within the maximum capillary height potential (H) given by the relation,

$$\rho_{\ell} gH = \frac{2\sigma_{\ell} \cos \theta}{r_c} \qquad (44)$$

For comparison purposes, H has been calculated for several wick structures as given in Table 6. In the present design, the circumferential fluid distribution is accomplished by the screen wick at the evaporator and condenser. The capillary grooves prime from the screen and the larger (2.4 x 2.4 mm) artery groove primes from the 0.79 x 0.79 mm grooves in the condenser section.

Artery Dimension: The artery in a heat pipe could be a screen tube, groove, annular space, or a circular tube. In the double wall design, it is convenient to machine square groove on the inner tube.

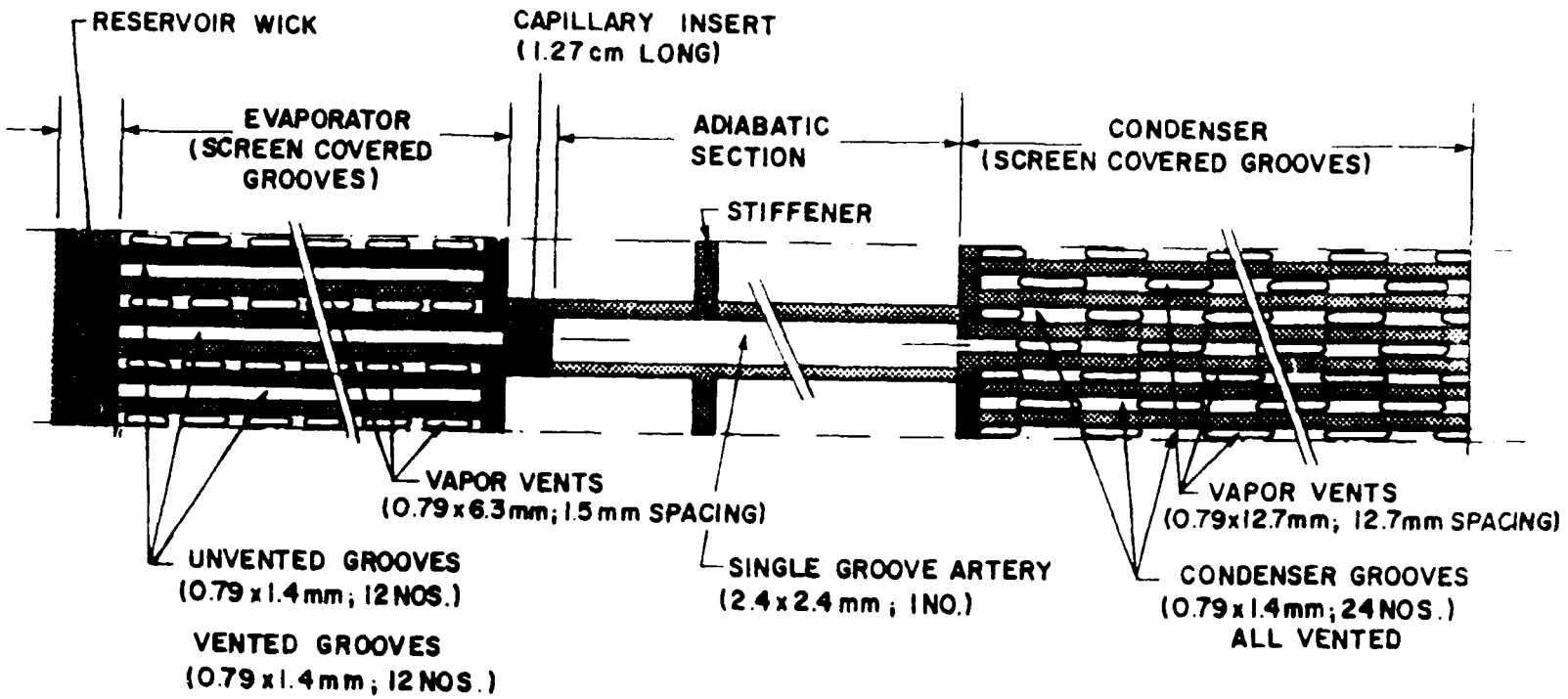

Figure 30. Inner Tube Groove and Vapor Vent Details

TABLE 6. COMPARISON OF WICKING HEIGHTS FOR SODIUM IN VARIOUS WICKS (SCREEN, GROOVE, AND CIRCULAR TUBE)

Temperature (°C)	Theoretical Wicking Height, H (cm)				
	40x40 cm^{-1} wire mesh r_c = 0.127 mm	0.79x0.79 mm groove r_c = 0.79 mm	1.59 mm dia. circular r_c = 0.79 mm	1.59x1.59 mm groove r_c 1.59 mm	2.38x2.38 mm groove r_c = 2.38 mm
500	29.27	4.68	4.68	2.34	1.56
600	28.30	4.53	4.53	2.26	1.51
700	27.96	4.47	4.47	2.24	1.49
800	26.07	4.17	4.17	2.09	1.39
900	24.34	3.89	3.89	1.95	1.29
1000	23.01	3.68	3.68	1.84	1.23

In order to arrive at the width of the groove, a conservative approach is used wherein the groove should be able to prime to the height at least equal to the diameter of the heat pipe. Table 7 gives the artery widths at various temperatures. At 700°C, the calculated value of w is 2.69 mm and the chosen width of 2.4 mm is well within this estimate. An optimistic estimate based on the priming height equal to the width or depth of the groove itself is also made and the numbers are given in Table 7.

TABLE 7. SQUARE GROOVE ARTERY SIZE FOR SODIUM

Temperature (°C)	Artery Width w = δ	
	Conservative Design (mm)	Optimistic Design (mm)
500	2.85	6.09
600	2.73	5.99
700	2.69	5.96
800	2.47	5.75
900	2.27	5.56
1000	2.12	5.41

Equations used:

1. Conservative Approach:
$$w = \frac{1}{2}\left[d_o - \sqrt{d_o^2 - \frac{8\sigma_\ell \cos\theta}{g(\rho_\ell - \rho_v)}}\right] \quad (45)$$

2. Optimistic Approach:
$$w = \sqrt{\frac{2\sigma_\ell \cos\theta}{g(\rho_\ell - \rho_v)}} \quad (46)$$

3.4. Lumped Thermal Capacity Analysis

3.4.1 Configuration Summary

- Design details as in Section 3.3.1
- $l_f/l_A/l_C$ 33/19/91 cm l_p 203 cm
  D_o 2.22 cm
- Single groove artery in adiabatic; multiple groove screen covered evaporator and condenser
- Reservoir wick in evaporator
- Excess metal in inner tube cut out in adiabatic
- Sodium working fluid; argon as the noncondensible gas
- Frozen start from room temperature (T_o)

3.4.2 Objective

To find the maximum length of adiabatic section that can be tolerated in the 2 m long heat pipe without drying out the evaporator. Also determine the size of the liquid reservoir wick at the evaporator end. The sketch of the heat pipe is shown in Figure 31.

3.4.3 Assumptions

(1) All the sodium in the evaporator is transferred in the form of saturated vapor (no superheat) to thaw the adiabatic section and to move the hot zone to the beginning of the condenser.

(2) No liquid return to the evaporator during startup.

(3) For a given noncondensible gas (NCG) charge pressure (P_i), there is a fixed evaporator temperature (T_H) to which the evaporator has to be heated up before the hot zone moved to the adiabatic section.

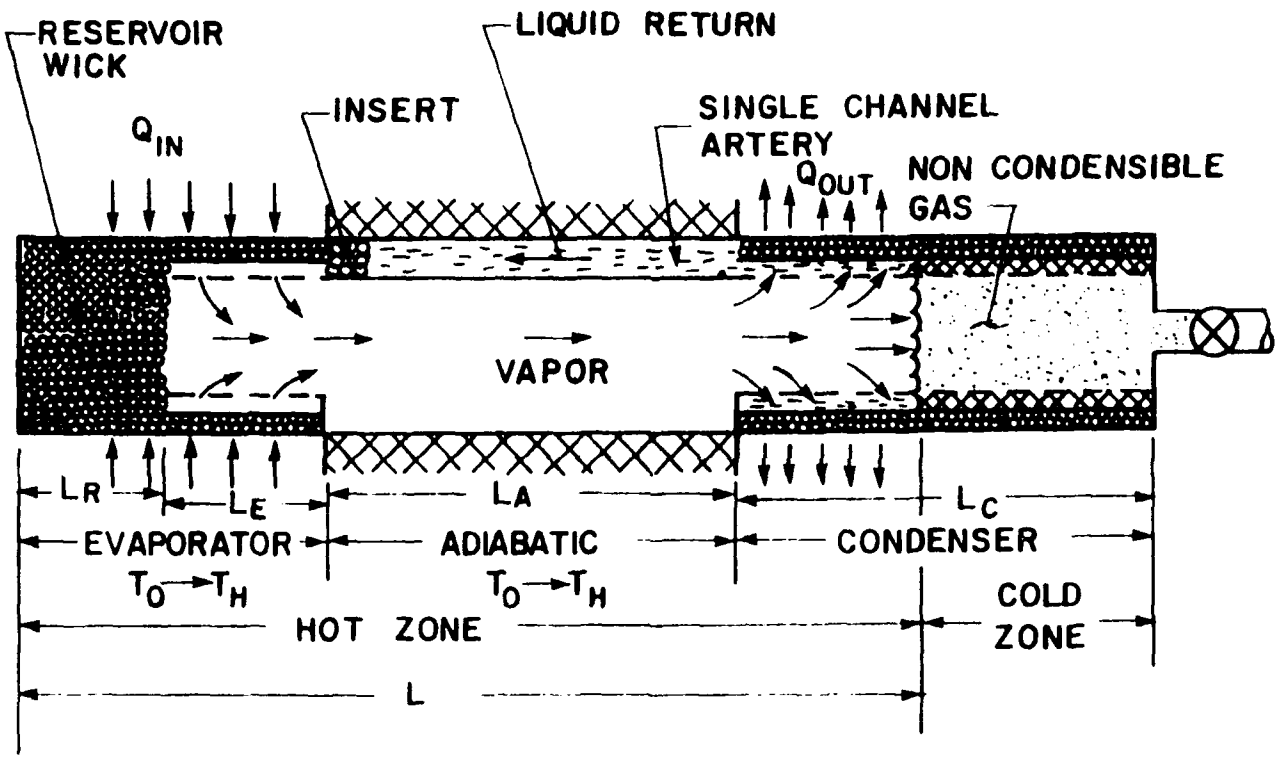

Figure 31. Single Channel Liquid Metal DWAHP with Reservoir Wick

(4) No heat losses in the adiabatic section.

(5) Only vapor diffusion is considered for energy transport. No axial conduction through wall.

(6) The initial power input is less than the sonic limit corresponding to the desired startup temperature (T_H).

(7) The reservoir wick is in good contact with the evaporator wick and there is fluid communication between the two wicks.

(8) Sodium working fluid is uniformly distributed within the wick structures (screen and grooves).

3.4.4 Energy Balance

For the hot front to move from evaporator exit to the beginning of the condenser, the energy supplied externally to the evaporator has to vaporize the sodium in the evaporator. The latent heat of vaporization stored in the vapor is transferred to the adiabatic section by condensation of the vapor. A lumped energy balance under steady state can be written as follows:

$$\left\{\begin{array}{l}\text{Energy input}\\ \text{to Evaporator}\end{array}\right\} \geq \left\{\begin{array}{l}\text{Energy carried by}\\ \text{the saturated sodium}\\ \text{vapor from evaporator}\\ \text{to adiabatic at}\\ \text{temperature } T_H\end{array}\right\} \geq \left\{\begin{array}{l}\text{Energy required to}\\ \text{raise the adiabatic}\\ \text{section from } T_o \text{ to}\\ T_H\end{array}\right\} \tag{47}$$

$$Q_i \geq m_{Na}\, \lambda_{Na}(T_H) \geq C_A(T_H - T_o) \tag{48}$$

For determining the exact quantities of sodium fill and the possible maximum l_A, Eq. (48) can be written as:

$$m_{Na}\ \lambda_{Na}\ (T_H) \quad C_A(T_H \quad T_o)$$

Expanding the terms we can write,

$$\left(m_{Na}\Big|_{\substack{\text{Evap}\\\text{screen}}} + m_{Na}\Big|_{\substack{\text{Evap}\\\text{groove}}} + m_{Na}\Big|_{\substack{\text{Reservoir}\\\text{wick}}} \right) \lambda_{Na}(T_H)$$

$$= (m_{ss}C_{p,ss}L_A + m_{Na}C_{p,Na}L_A)(T_H - T_o) \qquad (49)$$

where

m_{Na} — mass of sodium in the wick per unit length

m_{ss} — mass of stainless steel wall per unit length

$\lambda_{Na}(T_H)$ — heat of vaporization for sodium at temperature T_H

$C_{p,Na}$ — specific heat capacity of sodium liquid

$C_{p,ss}$ — specific heat capacity of stainless steel

L_A — adiabatic length

T_H — hot zone temperature

T_o — room temperature

The mass terms are written and simplified by substituting the cross sectional areas and wick porosities as follows:

$$m_{Na}\Big|_{\substack{\text{Evap}\\\text{screen}}} = A_w l_E \epsilon_s \rho_\ell$$

$$= 0.32535\, l_E \rho_\ell$$

$$m_{NA}\Big|_{\substack{\text{Evap}\\\text{groove}}} = A_g N\, l_E \rho_\ell$$

$$= 0.26613\, l_E \rho_\ell$$

$$m_{Na}\Big|_{\substack{\text{Reservoir}\\\text{wick}}} = A_R l_R \epsilon_R \rho_\ell$$

$$= 2.11629\, l_R \rho_\ell$$

The LHS of Eq. (49) becomes,

$$((0.32535 + 0.26613) l_E + 2.11629\, l_R) \rho_\ell \lambda_{Na}(T_H)$$

$$(0.59148\, l_E + 2.11629\, l_R) \rho_\ell \lambda_{Na}(T_H)$$

$$(0.54829\, l_E + 1.96618\, l_R) \lambda_{Na}(T_H)$$

The density of sodium $\rho_\ell = 0.927\ g/cm^3$ corresponding to the phase change temperature of 97.83°C has been used since only that much of sodium can be stored in the wick pores. The latent heat of sodium λ_{Na} depends on the startup temperature T_H which can be varying from 400°C to 800°C.

Similarly, substituting the specific heat and mass values and simplifying, we obtain:

The RHS of Eq. (49) = $(5.91343 + 0.075903)\, L_A(T_H - T_o)$

$$= 5.98934\, L_A(T_H - T_o)$$

Now, Eq. (49) can be written as:

$$(0.54829\, L_E + 1.9618\, L_R)\, \lambda_{Na}(T_H) = 5.98934\, L_A(T_H - T_o) \qquad (50)$$

For sodium vapor, the transitional flow regime (from free molecular flow) to continuum flow regime occurs at 340°C. In a gas filled heat pipe such as our present design, the vapor flow attains (presumably) continuum flow regime before the hot front at the gas vapor boundary starts moving away from the evaporator. Above 520°C, the sodium heat pipe switches to isothermal operations.

Substituting $T_H = 340°C$, $T_o = 25°C$ and $\lambda_{Na}(340) = 4393$ J/g in Eq. (50) we obtain,

$$0.54829\, L_E + 1.9618\, L_R = 0.42946\, L_A \qquad (51)$$

From the design details we have,

$$L_E + L_R + L_A = 112 \text{ cm} \qquad (52)$$

For practical considerations we can assume that,

$$T_I = 2\,T_R \tag{53}$$

Therefore, Eqs. (51) and (52) become

$$1.09658\,L_R + 1.9618\,L_R = 0.42946\,L_A$$

or
$$3.05838\,L_R = 0.42946\,L_A \tag{54}$$

and
$$3\,L_R + L_A \geq 112 \tag{55}$$

Solving Eqs. (54) and (55)

$$\left.\begin{aligned} L_R &= 11.06\ \text{cm} \\ L_A &= 78.80\ \text{cm} \\ L_E &= 22.12\ \text{cm} \end{aligned}\right\} \quad \text{for } T_H = 340°C$$

To give a factor of safety on the startup temperature T_H let us assume $T_H = 400°C$

$$\lambda_{Na}(400°C) = 4380\ J/g\ ;\ T_H - T_o = 375$$

Eq. (50) becomes,

$$0.54829\ L_E + 1.9618\ L_R - 0.512786\ L_A \qquad (51)'$$

Using Eqs. (52) and (53) as before, we obtain

$$\left.\begin{aligned} L_R &= 12.50\ \text{cm} \\ L_A &= 74.50\ \text{cm} \\ L_E &= 25.00\ \text{cm} \\ L_C &= 91.00\ \text{cm} \end{aligned}\right\} \quad \text{for } T_H = 400°C$$

We select this result for sizing the heat pipe. It may be noted that even though this analysis does not predict the movement of the hot front as a function of time, it is accurate enough to tell that the front can reach the condenser before the evaporator dried out.

3.5 Performance Limits

The performance of the heat pipe is judged by its ability to transport a desired amount of thermal energy supplied at the evaporator end to the condenser end with a minimum temperature drop and without causing a dryout. The temperature dependent heat transport capacity of the heat pipe under steady state conditions is limited by several other factors such as sonic limitation, capillary limitation, boiling limitation, entrainment limitation, and condenser radiation limitation. A quantitative estimate of each of the limitations is as follows.

3.5.1 Condenser Limitation

This is an external limitation due to the radiative coupling of the condenser to the cold wall of the chamber. The net radiant energy exchange from the heat pipe condenser to the cold chamber wall is given by Stefan's formula.

$$Q_r = A_C \epsilon_C \sigma (T^4 - T_s^4) \qquad (56)$$

Here, Stefan-Boltzmann's constant, $\sigma = 5.67 \times 10^{-12}$ W/cm^2 K^4; emissivity of the oxidized stainless steel, $\epsilon_C = 0.6$; area of the condenser, $A_C = \pi D_C L_C = 425.6$ cm^2 for $D_C = 2.22$ cm and $L_C = 60.96$ cm; the chamber temperature, T_s is assumed to be the average of the 25°C cooling water inlet and 80°C outlet temperature or $T_s = 52.5$°C; the heat pipe operating temperature, T can vary from 400-1000°C. Q_r has been calculated for $L_C = 30$, 60, and 90 cm and tabulated as shown in Table 8. This limitation is sketched in Figure 32 along with other limitations.

3.5.2 Sonic Limitation

Sonic limitation generally occurs when the heat pipe is operating at low vapor densities (that is at low temperatures) and high vapor velocities. Critical and choked flow conditions exist when the vapor velocity at the evaporator exit becomes sonic (M_v 1.0). In liquid metal heat pipes, the sonic limitation is very significant during the startup phase. At this limit there is a maximum axial heat transport rate due to the choked flow and a fixed axial temperature drop along the evaporator, which is associated

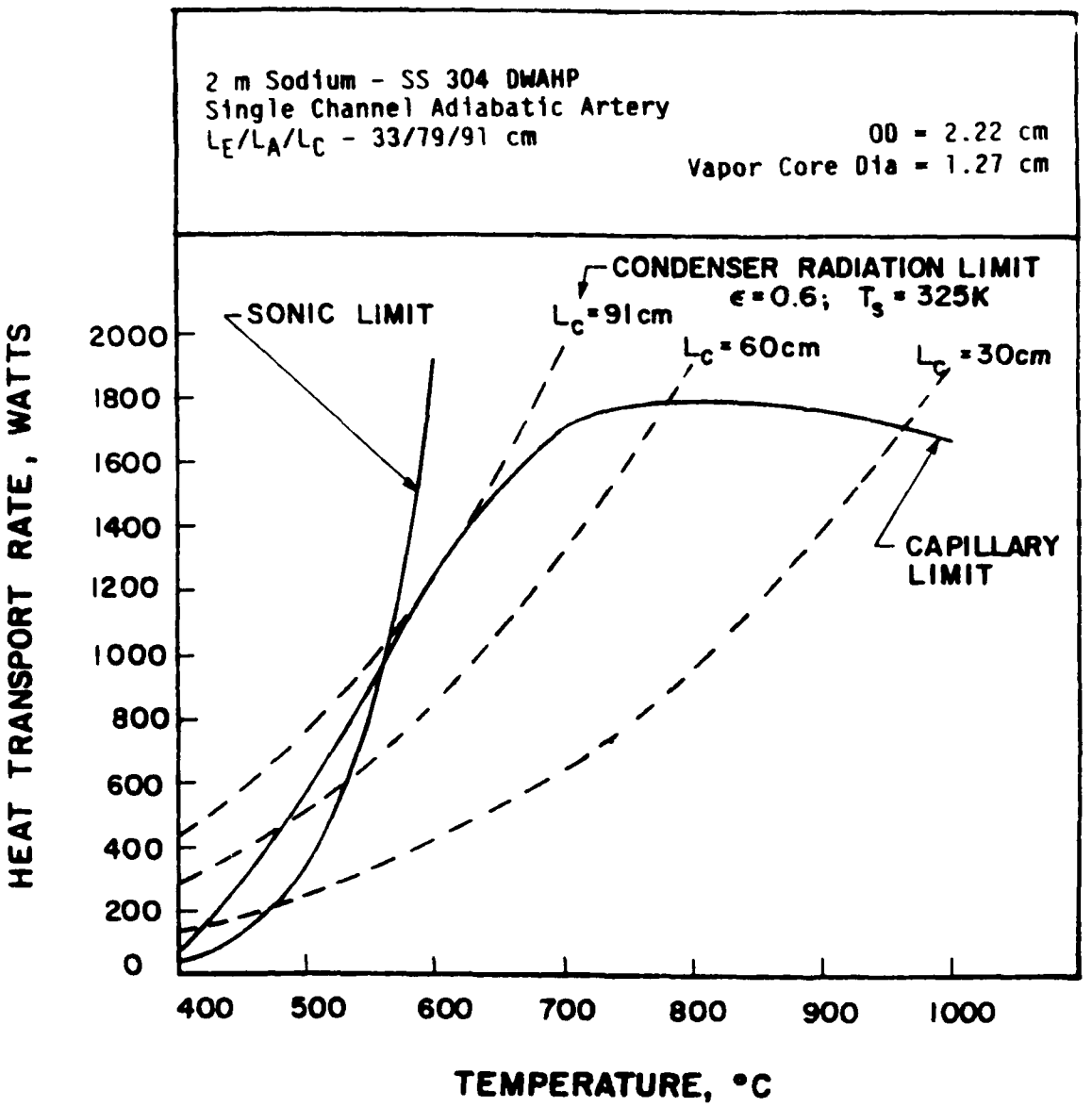

Figure 32. Heat Transport Limits Q Versus T

TABLE 8. CONDENSER RADIATION LIMITATION

Temperature		Radiation limit, Q_r (W)		
(°C)	(K)	L_c = 30 cm	L_c = 60 cm	L_c = 90 cm
400	673	140	280	421
500	773	250	500	751
600	873	413	825	1237
700	973	640	1281	1922
800	1073	951	1903	2854
900	1173	1362	1903	2854
1000	1273	1893	3786	5680

with any given evaporator entrance temperature. Increasing the heat rejection rate beyond the sonic limit lowers the condenser temperature, induces supersonic vapor flow, and creates very large axial temperature gradients along the pipe but it does not increase heat transport rate. Consequently, near isothermal operation is not possible. Levy's equation is used to calculate the sonic limit [4]. That is,

$$Q_{sonic} = A_v \rho_o \lambda \left(\frac{\gamma_v R_v T_o}{2(\gamma_v + 1)} \right)^{0.5} \quad \text{(Levy's Equation)} \qquad (57)$$

Subscripts v and o refer to the static and stagnation states of the vapor, respectively. For sodium $\gamma_v = 1.67$ and $R_v = R/M = 361$ J/kg K. The vapor core cross-sectional area $A_v = \pi d_i^2/4 = 1.267 \times 10^{-4} m^2$. Using the property table for sodium, Q_{sonic} has been calculated at various temperatures.

Temperature (°C)	Q_{sonic} (W)
402	36.8
452	122.3
502	343.9
552	849.3
602	1891.5

Sonic limit curve is plotted in Figure 32 along with the other limitations. It can be observed that the sonic limit determines the present sodium heat pipe transport capacity in the 400-560°C range.

The presence of NCG in the heat pipe may affect the sonic limit calculations based on Levy's equation. The effect is favorable to a frozen startup situation since the NCG slows down the vapor molecules and possibly prevents them from attaining sonic or supersonic velocity until the vapor pressure becomes equal to the NCG charge pressure. Once the vapor pressure exceeds the NCG charge pressure, then the sonic limit by Levy's equation will be applicable. Any variation in temperature varies the length of active condenser.

3.5.3 Capillary Limitation

Capillary wick priming considerations: In composite wicks, capillary pumping is achieved by surface tension forces created by the small pores of the screen wick at the liquid-vapor interface in the evaporator where the evaporation of the liquid takes place. Liquid from the condenser section flows through the artery channel into the evaporator grooves and then radially into the screen layers to make up for the depletion of fluid by evaporation. This process of saturating the wick is called the capillary priming and this has to be maintained at all times of the heat pipe working.

Capillary inserts: As evidenced by the low temperature visual tests on glass walled copper-water heat pipe, a possible vapor back flow into the liquid channel is prevented using a screen insert at the evaporator exit. However, this insert offers extra resistance to the return liquid flow.

Liquid Flow Resistance: The pressure drop associated with the liquid flow in various segments of the wick structure is modeled as a set of series and parallel resistance paths. The total pressure drop is calculated from these resistances. Eq. (58) gives the liquid flow pressure drop in the wick structure for elemental length dx.

$$\frac{dP_\ell}{dx} = -F_\ell Q + \rho_\ell g \sin\psi \qquad (58)$$

F_ℓ is the liquid friction coefficient defined as:

$$F_\ell = \frac{\mu_\ell}{K_w A_w \rho_\ell \lambda} \quad \text{or} \quad \frac{1}{K_w A_w}\left(\frac{\nu_\ell}{\lambda}\right) \qquad (59)$$

The capillary transport capacity of the heat pipe is inversely proportional to this factor F_ℓ. For horizontal operation of the heat pipe, $\psi = 0$ and Eq. (58) simplifies to:

$$\frac{dP_\ell}{dx} = -F_\ell Q \tag{60}$$

Upon integrating over the desired lenth Δx of flow in wicks,

$$-\Delta P_\ell = (F_\ell \Delta x) Q \tag{61}$$

The above equation is analogous to an electrical resistance circuit where ΔP_ℓ corresponds to voltage drop, Q corresponds to current, and $F_\ell \Delta x$ corresponds to resistance. Hence, the liquid flow resistance due to the various segments of the wick structure can be added in series to get the total resistance.

$$\begin{aligned}(F_\ell l)_{eff} &= (F_\ell \Delta x)_{total} \\ &= (F_\ell \Delta r)_{\substack{\text{evaporator}\\ \text{screen}\\ \text{radial}}} + (F_\ell L_E/2)_{\substack{\text{evaporator screen}\\ \text{and groove}\\ \text{axial effective}}} \\ &\quad + (F_\ell L_I)_{\substack{\text{inserts}\\ \text{axial}}} + (F_\ell L_A)_{\substack{\text{transport groove}\\ \text{axial}}} \\ &\quad + (F_\ell L_C/2)_{\substack{\text{condenser screen}\\ \text{and groove}\\ \text{axial effective}}} + (F_\ell \Delta r)_{\substack{\text{condenser}\\ \text{screen}\\ \text{radial}}}\end{aligned} \tag{62}$$

The individual resistances which are functions of the wick mechanical properties (permeability, area, etc.) and the fluid properties (kinematic viscosity and latent heat) are computed. The details are given in Appendix G. The result is,

$$(F_{\ell}L)_{eff} = 15.2085 \times 10^{12} \left(\frac{\nu_{\ell}}{\lambda}\right) \quad [(N/m^2)/W] \tag{63}$$

Approximate Capillary Limit Calculation:

An estimate of the capillary limit neglecting the vapor flow friction effects (F_v) is made in order to obtain a first-cut approximation using Eq. (64)

$$Q_{cl} = \frac{P_{Pm}}{F_{\ell}L_{eff}} \tag{64}$$

and the values are listed in Table 9.

Vapor Flow Friction Factor (F_v):

The applicable equations from Reference 4 are,

$$F_v = \frac{f_v Re_v \mu_v}{2 r_{h,v}^2 A_v \rho_v \lambda} \tag{65}$$

where $f_v Re_v = 16$ if $Re_v \leq 2300$ and $M_v \leq 0.2$

$$Re_v = \frac{2 r_{h,v} Q}{A_v \mu_v \lambda} \tag{66}$$

$$M_v = \frac{Q}{A_v \rho_v \lambda \sqrt{\gamma_v R_v T_v}} \tag{67}$$

TABLE 9. CAPILLARY LIMIT VERSUS TEMPERATURE

Sl. No.	Design Parameter	Temperature (°C)						
		400	500	600	700	800	900	1000
1	P_{cm} (N/m^2)	2504	2378	2236	2094	1937	1779	1638
2	$\Delta P_{\perp}$ (N/m^2)	158.7	153.5	149.3	141.6	140.4	138.2	134.5
3	P_{pm} (N/m^2)	2345.3	2224.5	2086.7	1952.4	1796.6	1640.8	1503.5
4	$F_{\ell}L_{eff}$ $(N/m^2/W)$	1.1373	1.0086	0.9346	0.9253	0.9088	0.8864	0.8765
5	$Q_{c1} = P_{pm}/F_{\ell}L_{eff}$ (W)	2062.2	2206	2233	2110	1977	1851	1715
6	F_vL_{eff} $(N/m^2/W)$	34.4510	3.0322	0.7607	0.2159	0.0911	0.0424	0.02076
7	$Q_{c2} = P_{pm} / (F_{\ell} + F_v)L_{eff}$ (W)	65.9	556.8	1243	1711	1797	1767	1676

The vapor core dimensions are,

$$r_{h,v} = r_v = 0.635 \times 10^{-2} \text{ m}$$

$$A_v = \pi r_v^2 = 1.2667 \times 10^{-4} \text{ m}^2$$

$$\therefore \quad Re_v = 100.255 \frac{Q}{\mu_v \lambda}$$

Re_v is calculated in terms of Q for various temperatures and listed in Table 10. The limit of heat transport rate allowed to satisfy laminar vapor flow condition is obtained by setting the condition, $Re_v \leq 2300$. Also, M_v is calculated in terms of Q by substituting $\gamma_v = 1.67$ and $R_v = 361$ J/kg K for sodium in Eq. (67) and listed for different temperatures in Table 10. Initially, Q is unknown to determine Re_v and M_v and hence the approximate estimates of Q_{cl} (Table 9) is used to start the calculations. The conditions,

$$M_v \leq 0.2 \quad \text{(Incompressible flow)}$$

$$M_v \geq 0.2 \quad \text{(Compressible flow)}$$

are used to determine the compressibility of the vapor. Based on the sonic limit and the operating power limit known, the vapor flow is found to be laminar in the entire range of operating temperature and compressible up to 600°C and incompressible at temperatures above

600°C. The applicable equations for f_v are,

TABLE 10. VAPOR FLOW FRICTION COEFFICIENT VERSUS TEMPERATURE

Sl. No.	Design Parameter	Temperature (°C)						
		400	500	600	700	800	900	1000
1	Vapor flow Reynolds number, Re_v	1.3663 Q	1.2745 Q	1.2436 Q	1.2256 Q	1.1459 Q	1.1139 Q	1.0915 Q
2	Heat transport rate to satisfy laminar vapor flow condition, Q (W)	≤1683	≤1805	≤1850	≤1877	≤2007	≤2065	≤2107
3	Re_v based on Q_{c2} from Table 9	90	710	1546	2097	2059	1968	1829
4	Turbulent or Laminar	Laminar (Based on sonic limit)			Laminar (Based on 2000 W operating limit)			
5	Vapor flow Mach Number, M_v	$1179.5 \times 10^{-5} Q$	$88.21 \times 10^{-5} Q$	$19.728 \times 100^{-5} Q$	$5.04 \times 10^{-5} Q$	$1.84 \times 10^{-5} Q$	$0.784 \times 10^{-5} Q$	$0.353 \times 10^{-5} Q$
6	M_v based on operating limit of Q	0.434	0.303	0.373 (Based on sonic limit)	0.106	0.036	0.014	0.006 (Based on Q_{c1} limit)
7	Compressible (C) or Incompressible (I)	C	C	C	I	I	I	I
8	Select Equation for F_v	Eq. (69)			Eq. (68)			
9	F_v ($N/m^2/Wm$)	25.1913	2.1180	0.5274	0.1532	0.06466	0.03008	0.01473

$$F_v = \frac{8\mu_v}{r_{h,v}^2 A_v \rho_v \lambda} \quad \text{for} \begin{cases} Re_v \leq 2300 \\ M_v \leq 0.2 \end{cases} \quad \text{(Laminar and incompressible)} \tag{68}$$

$$F_v = \left[\frac{8\mu_v}{r_{h,v}^2 A_v \rho_v \lambda}\right]\left[1 + \frac{\gamma_v - 1}{2} M_v^2\right]^{-0.5} \quad \text{for} \begin{cases} Re_v \leq 2300 \\ M_v > 0.2 \end{cases} \quad \text{(Laminar and compressible)} \tag{69}$$

$$Q_{c2} = \frac{P_{pm}}{(F_\ell + F_v) l_{eff}} \tag{70}$$

After calculating F_v, the capillary limit Q_{c2} is calculated using Eq. (70) and $L_{eff} = 1.41$ m. The results are given in Table 9 and Figure 32. It should be noted that the vapor flow friction is very high during the startup temperature regime (up to 540°C).

3.5.4 Boiling Limitation

The boiling limitation is a limitation of the radial heat flux density at the evaporator due to the formation of vapor bubbles within the wick structure. The bubble formation is undesirable because it can cause hot spots and obstruct fluid circulation. In liquid metal heat pipes, this limitation is not serious since liquid metals have high thermal conductivities. The series-parallel model given by Chi [4] for the effective thermal conductivity (k_{eff}) of sodium saturated stainless steel wick is given in Eq. (71).

$$k_{eff} = \frac{k_\ell[(k_\ell + k_s) - (1 - \varepsilon)(k_\ell - k_s)]}{[(k_\ell + k_s) + (1 - \varepsilon)(k_\ell - k_s)]} \tag{71}$$

The thermal conductivity of steel, k_s is 17.3 W/m K in the nominal operating temperature range of 500-1000°C while that of sodium liquid, k_ℓ varies from 70 49 W/m K. Substituting $\epsilon = 0.6289$ for the 40x40 cm^{-1} wire screen with 0.1143 mm wire diameter in Eq. (71), one obtains

$$k_{eff} = 44.42 \text{ W/m K at } 500°C$$

$$\text{or } 34.27 \text{ W/m K at } 1000°C$$

Boiling limit is given by

$$Q_b = \frac{2\pi L_E k_{eff} T_v}{\lambda_v \rho_v \ln (r_o/r_i)} \left(\frac{2\sigma}{r_n} - P_c\right) \qquad (72)$$

The nucleation radius, r_n, is determined using the nucleation theory of Rohsenow and Bergles [14] for smooth surfaces represented in Eq. (73).

$$r_n = \left(\frac{2\sigma T_{sat} k_\ell (V_v - V_\ell)}{\lambda q_r}\right)^{0.5} \qquad (73)$$

For sodium heat pipes, the radial heat flux density values reported in the literature range from 200-400 W/cm^2. Assuming the minimum value of 200 W/cm^2 for q_r, r_n for 500 and 1000°C are calculated as 7.899×10^{-4} m and 0.5045×10^{-4} m respectively. These values are much higher than or close to the wick pore sizes of 1.27×10^{-4} m for 40x40 cm^{-1} screen mesh and 1.466×10^{-4} m for the triangular grooves on the evaporator inner wall. For lower

radial heat fluxes of about 10 20 W/cm^2 applicable to the present heat pipe, r_n predicted by Eq. (73) will be very large. It is recommended by Marcus [14] that this equation not be used in such cases. Silverstein [56] has suggested that the effective nucleation site radius in properly wetted liquid metal heat pipes can be on the order of 10^{-6} m or less. An upper limit of r_n = 3 to 7 x 10^{-6} m corresponding to a burnout heat flux of 287 W/cm^2 is recommended by him [56]. Hence, the conservative values recommended by Chi [4], r_n = 2.54 x 10^{-5} m for gas loaded heat pipe and r_n = 2.54 x 10^{-7} m for conventional heat pipe have been considered. Using these values and setting L_t = 0.25 m and assuming that the pipe is operating at capillary limit ($P_c = P_{cm}$), Q_b is calculated from Eq. (72) at various temperatures and listed in Table 11. For convertional mode operation, the boiling limit is very very high whereas for gas loaded mode the limit drops sharply at and above 900°C.

Experimental Radial Heat Flux Data: The experimental data reported in the literature on the sodium heat pipe radial heat flux density for various wick structures are summarized below [6,8].

Wick	Temperature (°C)	Radial Heat Flux (W/cm^2)
1. Stainless Steel Mesh	760	230
2. Various Wicks	850 950	200 400
3. Stainless Steel Mesh (3 layer; 390 μm)	925	214
4. Stainless Steel Mesh	775	1250

TABLE II. BOILING LIMIT AND CRITICAL TEMPERATURE DIFFERENCE

Temperature, T_v (°C)	Wick Effective Thermal Conductivity, k_{eff}, (W/m K)	Boiling Limit, Q_b (W)		ΔT_{crit} (K)
		Conventional Mode	Gas loaded Mode	
500	44.42	12.24×10^6	98,131	560
600	41.81	2.908×10^6	23,316	142
700	39.98	0.7841×10^6	6,278	39.9
800	38.53	0.2959×10^6	2,368	15.6
900	36.36	0.1248×10^6	999	6.97
1000	34.21	0.5508×10^5	441	3.27

Boiling of sodium in sodium heat pipes is impeded as a result of high thermal conductivity of the liquid metal. Evaporation of the working fluid takes place at the free surface of the wick pores. Assuming a safe limit of 100 W/cm^2 radial flux, the radial limit for the present heat pipe is obtained as,

$$Q_{radial} = \pi D_E L_E q_r \qquad (76)$$

$$= \pi \times 2.22 \times 10^{-2} \times 0.25 \times 100 \times 10^4$$

$$= 17,435 \text{ W}$$

However, this limit is too high to be encountered since the capillary limitation will restrict the flow of liquid return to the evaporator. Radial heat flux density expected here is a maximum of 13 W/cm^2 based on A_E = 137 cm^2 and $Q_{C?}$ = 1797 W at 800°C.

3.5.5 Temperature Drop

Steady state temperture differences across various segments (pipe wall, wick, and vapor passage) of the heat pipe during normal mode of operation can be computed using Fourier's law for conduction through the pipe wall or wick and Clausius Clapeyron relation for vapor flow [1].

1. Pipe wall at evaporator:

$$\Delta T_{p,E} = \frac{\ln(r_o/r_i)}{2\pi L_E k_p} Q \qquad (77)$$

2. Wick at evaporator:

$$\Delta T_{w,E} = \frac{\ln(r_i/r_s)}{2\pi L_E k_{eff}} Q \qquad (78)$$

3. Vapor passage:

$$\Delta T_V = \frac{T_v (P_{v,E} - P_{v,C})}{\rho_v \lambda J Q} Q$$

$$\text{(or in terms of } T_V) = \frac{T_V T_V \left(\frac{L_E}{6} + \frac{L}{A} + \frac{L_C}{6}\right)}{\rho_v \lambda J} Q \qquad (79)$$

4. Wick at condenser:

$$\Delta T_{w,C} = \frac{\ln(r_i/r_s)}{2\pi l_C k_{eff}} Q \qquad (80)$$

5. Pipe wall at condenser:

$$\Delta T_{p,C} = \frac{\ln(r_o/r_i)}{2\pi l_C k_p} Q \qquad (81)$$

Maximum ΔT is expected at the highest power transporting conditions which is 1797 W at 800°C (Table 9). The ΔT's are computed using the physical dimensions and the property values at 800°C (Table 4) and the results are as follows.

$$\Delta T_{P,E} = 10.83 \text{ C}$$

$$\Delta T_{w,E} = 2.97 \text{ C}$$

$$\Delta T_{v} = 0.22 \text{ C}$$

$$\Delta T_{w,C} = 0.82 \text{ C}$$

$$\Delta T_{p,C} = 2.98 \text{ C}$$

The total temperature drop across the heat pipe is 17.82 C. In gas loaded mode, the condenser ΔT's will vary depending upon the active condenser length.

3.5.6 Entrainment Limitation

In conventional screen or groove wick heat pipes, the counter flowing liquid and vapor are in direct shear against each

other and this causes the vapor to entrain some liquid along with it causing a depletion of return liquid supply to the evaporator. The heat transport limit caused by this process is called the entrainment limitation. Here, in the double wall wick structure there is no direct shear between the liquid and vapor flows particularyly in the adiabatic section. Hence, there is no entrainment limitation for the DWAHP.

3.5.7 Fluid Inventory

The quantity of working fluid filled inside the heat pipe is determined on the basis of saturating the void volume available in the wick pore structure. Due to the variation in the density of liquid sodium with temperature, the wick may operate oversaturated or undersaturated depending upon the operating temperature. The calculation of the initial fill quantity is normally based on the optimum operating temperature at which the liquid transport number of sodium is the highest. This temperature is 700°C and the density is 0.7635 g/cm^3. However, overfilling is tolerated better than underfilling and the recommended overfilling is about 20% of the correct filling.

Fluid inventory,

$$m_{total} = m_{liquid} + m_{vapor} \tag{82}$$

$$m_{liquid} = m_{\substack{evaporator\\screen + groove\\wicks\\(A)}} + m_{\substack{evaporator\\reservoir\\wicks\\(B)}} + m_{\substack{adiabatic\\groove\\(C)}} + m_{\substack{condenser\\screen + groove\\wicks\\(D)}} \tag{83}$$

where,

(A) $m_{\substack{evaporator\\screen + groove\\wicks}} = (A_w \varepsilon + A_g n) L_E \rho_\ell$

(B) $m_{\substack{evaporator\\reservoir wick}} = A_R \varepsilon_R l_R \rho_\ell$

(C) $m_{\substack{adiabatic\\groove}} = A_A n_A l_A \rho_\ell$

(D) $m_{\substack{condenser\\screen + groove\\wicks}} = (A_w \varepsilon_s + A_g n) l_C \rho_\ell$

$m_{vapor} = A_v l_p \rho_v$

Substituting the physical dimensions, one obtains

$$m_{total} = (0.59148\ L_t + 2.11629\ L_R + 0.056704\ L_A + 0.59148\ L_C)\rho_\ell + (1.2668\ L_P)\rho_v \quad (84)$$

for L_t = 25 cm, L_R = 12.5 cm, L_A = 74.5 cm and L_C = 91 cm,

$$m_{total} = (14.787 + 26.454 + 4.224 + 53.825)\rho_\ell + 257.407\ \rho_v$$

or $$m_{total} = 99.29\ \rho_\ell + 257.407\ \rho_v \quad (85)$$

The total mass of fluid required will vary depending upon the temperature at which the density value is picked. In order to see the variation, a table of values are calculated at various temperatures of interest as shown in Table 12.

TABLE 12. FLUID INVENTORY VARIATION WITH TEMPERATURE

Temperature (°C)	ρ_ℓ (g /cm^3)	m_P (g)	ρ_v (g /cm^3)	m_v (g)	m_{total} (g)
97.83	0.9270	92.04	0	0	92.04
500	0.8281	82.22	0.003×10^{-3}	0.0011	82.22
600	0.8054	79.97	0.013×10^{-3}	0.0033	79.97
700	0.7635	75.81	0.050×10^{-3}	0.0128	75.82
800	0.7573	75.19	0.134×10^{-3}	0.0344	75.23
900	0.7454	74.01	0.306×10^{-3}	0.0781	74.09
1000	0.7254	72.02	0.667×10^{-3}	0.1711	72.19

Since the wick is to be fully saturated with liquid sodium just before freezing (97.83°C), the mass of liuqid to be filled should be determined at this temperature. If it is done so, the overfilling will be 21.4% more than the correct filling at 700°C.

3.6 Noncondensible Gas Loading

One of the means of facilitating the startup of a liquid metal heat pipe from frozen state is the introduction of noncondensible gases into the heat pipe. The amount of gas in the pipe in the initial (cold) state must be the minimum possible, but sufficient to achieve frontal heating on startup. Excessive amounts of gas would reduce the active condenser length by blocking the vapor flow into the condenser zone. A predetermination of the quantity of NCG charge is necessary in order to judge the active/inactive condenser lengths at a desired heat input rate or operating temperature.

A simple thermodynamic calculation is done to obtain the inactive condenser length (or NCG slug length) as a function of initial NCG charge pressure and the heat pipe hot zone temperature, T. Assume that initially the working fluid is frozen within the pores of the wick and the vapor core of volume V_1 is filled with NCG at a pressure P_i and temperature T_c. After the heat pipe is started and allowed to attain a steady state condition at temperature T, the NCG is compressed towards the condenser end by the hot vapor. Let the NCG volume which is still at the temperature T_c occupies an unknown volume V_2. The pressure of the vapor, $P_v(T)$ and that of the NCG are the same for equilibrium condition.

For an ideal gas the equation of state can be written for states 1 and 2 as,

$$P_1 V_1 = RT_1$$

$$P_2 V_2 = RT_2$$

$T_1 = T_2 = T_c$ since the gas temperature remains the same.

Therefore, $P_1 V_1 = P_2 V_2$

$$V_2 = \frac{P_1}{P_2} V_1 = \frac{P_i(T_c)}{P_v(T)} V_1$$

For cylindrical vapor core of uniform cross section, the volumes are proportional to the lengths. Hence,

$$L_{NCG} = L_p \frac{P_i(T_c)}{P_v(T)} \qquad (86)$$

where L_{NCG} = NCG slug length at any temperature T

L_p = total length of heat pipe (2 m)

P_i = Initial NCG charge pressure at temperature T_c

$P_v(T)$ Vapor pressure of sodium at temperature T

Figure 33 illustrates this model pictorially.

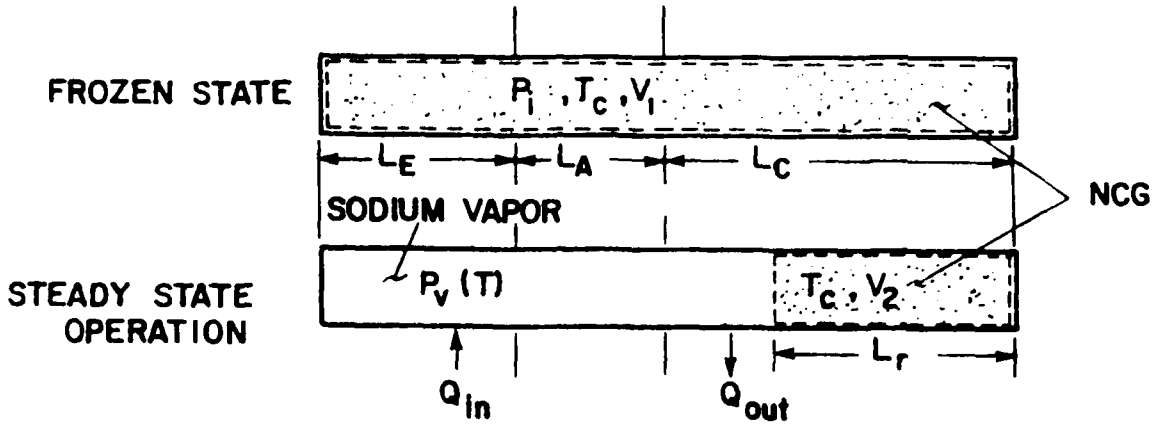

Figure 33. Noncondensible Gas Compression Model

The results of Eq. (86) are graphed as lengths of NCG slug versus temperature for a number of assumed NCG charge pressures as shown in Figure 34. For a typical operating temperature of 1000 K, the non condensible gas slug is compressed to negligible lengths of less than 1 cm if P_i is below 1 torr. If P_i is between 5 and 20 torr, the gas slug length varies from 5 to 25 cm. Above 50 torr, the pipe cannot operate below 1000 K. Thus, this graph facilitates the choice of selecting the proper NCG charge pressure.

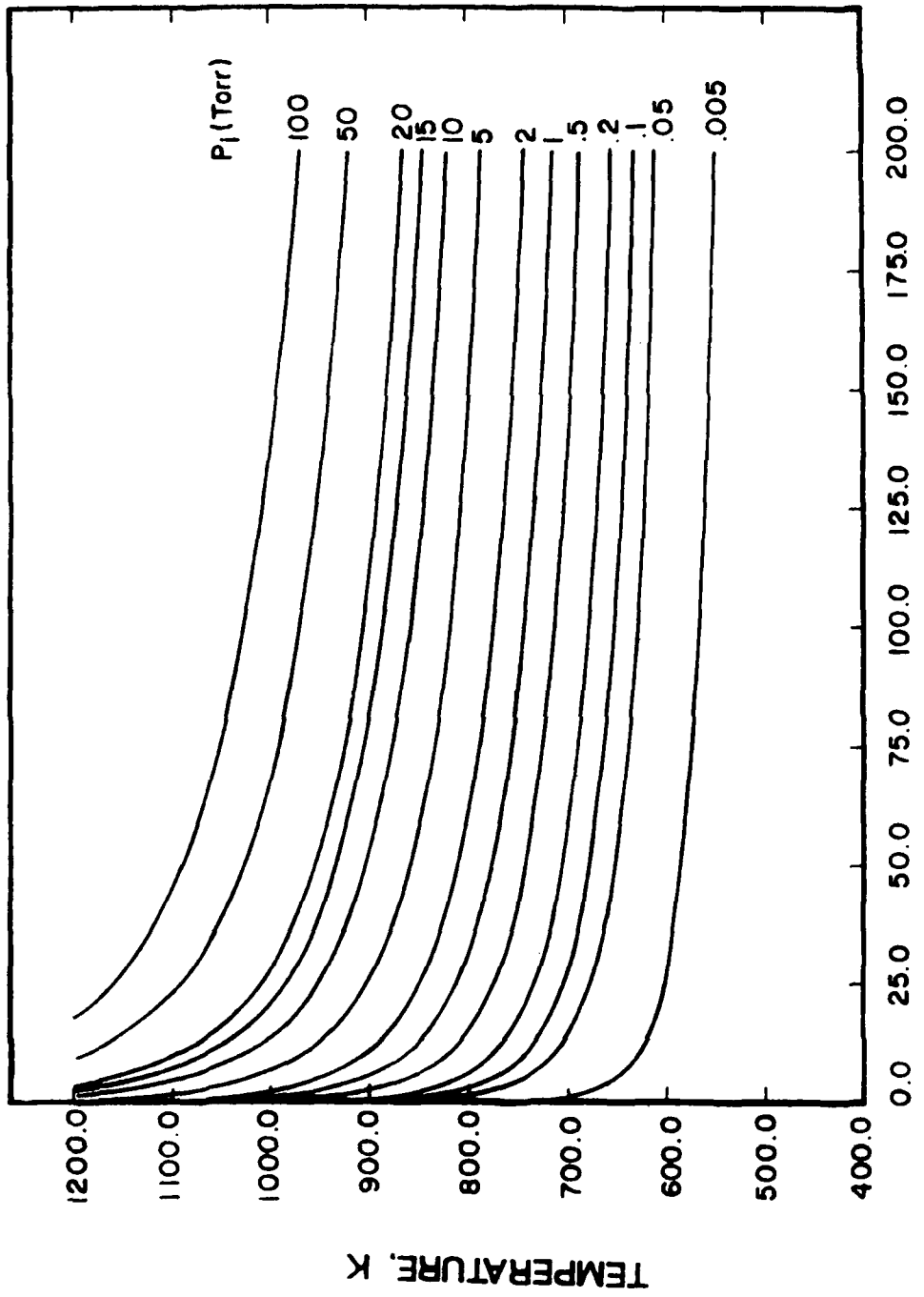

Figure 34. Effect of NCG Initial Charge Pressure on the Inactive Condenser Length as a Function of Temperature

From the point of view of sodium mass depletion (at the evaporator during startup) and the length of inactive condenser tolerable, it is recommended to use P_i 0.2 torr as the initial NCG charge pressure.

3.7 Design Summary

A summary of the pertinent design and performance numbers are listed in Table 13.

TABLE 13. GAS LOADED LIQUID METAL DWAHP (SINGLE ARTERY) DESIGN DETAIL SUMMARY

MATERIAL	
Outer tube, inner tube, end caps	Stainless steel 304
Screen wick	Stainless steel 304 wire mesh
Fill valve	Stainless steel bellows valve by NUPRO with stellite tip stem
Working fluid	Sodium
Noncondensible gas	Argon
OVERALL DETAILS	
Temperature range (operating)	400 850°C
Initial temperature	Room temperature (25°C)
Heat transport capacity (circulation limited)	1800 W at 800°C
Sonic limitation	Not applicable in gas loaded mode (controls transport upto 560°C in vacuum mode, refer Figure 32)
Effective length	1.388 m
Total length	2.03 m
Evaporator/Adiabatic/Condenser	0.375 m/0.745 m/0.91 m
Overall diameter	2.22×10^{-2} m
Vapor core diameter	1.27×10^{-2} m

TABLE 13. GAS LOADED LIQUID METAL DWAHP (SINGLE ARTERY)
DESIGN DETAIL SUMMARY (continued)

WICK

Type			Double walled construction with screen and groove wick for evaporator and condenser while adiabatic is screen less
Screen size (evaporator and and condenser)			40 x 40 cm^{-1} mesh
Number of spiral wraps			4
Evaporator reservoir wick			40 x 40 cm^{-1} SS 304 screen plug 1.89 cm dia. and 12.5 cm. long with porosity 75.25%.
Capillary insert			24x24 cm^{-1} mesh; 0.24x0.24x1.27 cm
Artery grooves:	Evaporator	Transport	Condenser
Number	24	1	24
Width, mm	0.79	2.38	0.79
Depth, mm	1.40	2.38	1.40
Vapor Vents:			
Number per groove	10 (cut on alternate grooves)	none	36 (cut on all grooves; staggered)
Size, mm	6.3 x 0.79		12.7 x 0.79
Axial spacing, mm	1.5		12.7

TABLE 13. GAS LOADED LIQUID METAL DWAHP (SINGLE ARTERY)
DESIGN DETAIL SUMMARY (concluded)

HEAT TRANSPORT LIMIT (Horizontal mode of operation)		
	Available capillary pumping head at 800°C	1796.6 N/m^2 or Pa
	Liquid pressure drop in wicks at 800°C	0.9088 Pa per W
	Vapor pressure drop in vapor core of 800°C	0.0911 Pa per W
	Maximum capillary transport limit at 800°C	1797 W
FLUID INVENTORY (Analytical grade sodium)		
	Optimum fill for operation at 1000 K (67.52 g in screen & grooves; 24.52 g in reservoir wick)	92.04 g
NONCONDENSIBLE GAS	Argon pressure	0.05-2.0 Torr at 25°C

CHAPTER IV

EXPERIMENTAL WORK

4.1 Fabrication of Parts

The experimental heat pipe assembly consists of an outer tube, an inner tube, two screen tubes, a reservoir screen plug, two end caps, a capillary insert plug, and a process valve with a fill tube as shown in Figure 35. The tube and bar stocks used in fabricating the parts are certified stainless steel material (1304 Alloy) supplied by Kilsby Roberts Company. The outer and inner tubes are cut in straight and continuous lengths and machined to form the assembly. The inner tube contains 24 equally spaced longitudinal small rectangular grooves each on the evaporator and condenser sections with a single large artery groove on the center section (adiabatic) connecting them. These grooves are machined using precision saw cutters on a horizontal milling machine. The rectangular vent slots (as shown in Figure 30) are cut by electro discharge machining. The screen tubes and reservoir screen wick are formed of stainless steel 304 wire mesh by carefully trimming along the edges and rolling on the mandrel. A bellows type high temperature valve with 649°C at 1700 kPa rating supplied by NUPRO Company is used to process the working fluid and inert gas. The end caps, fill tube and valve are tungsten inert gas (TIG) welded in a dry-box, circulated with argon. The evaporator section

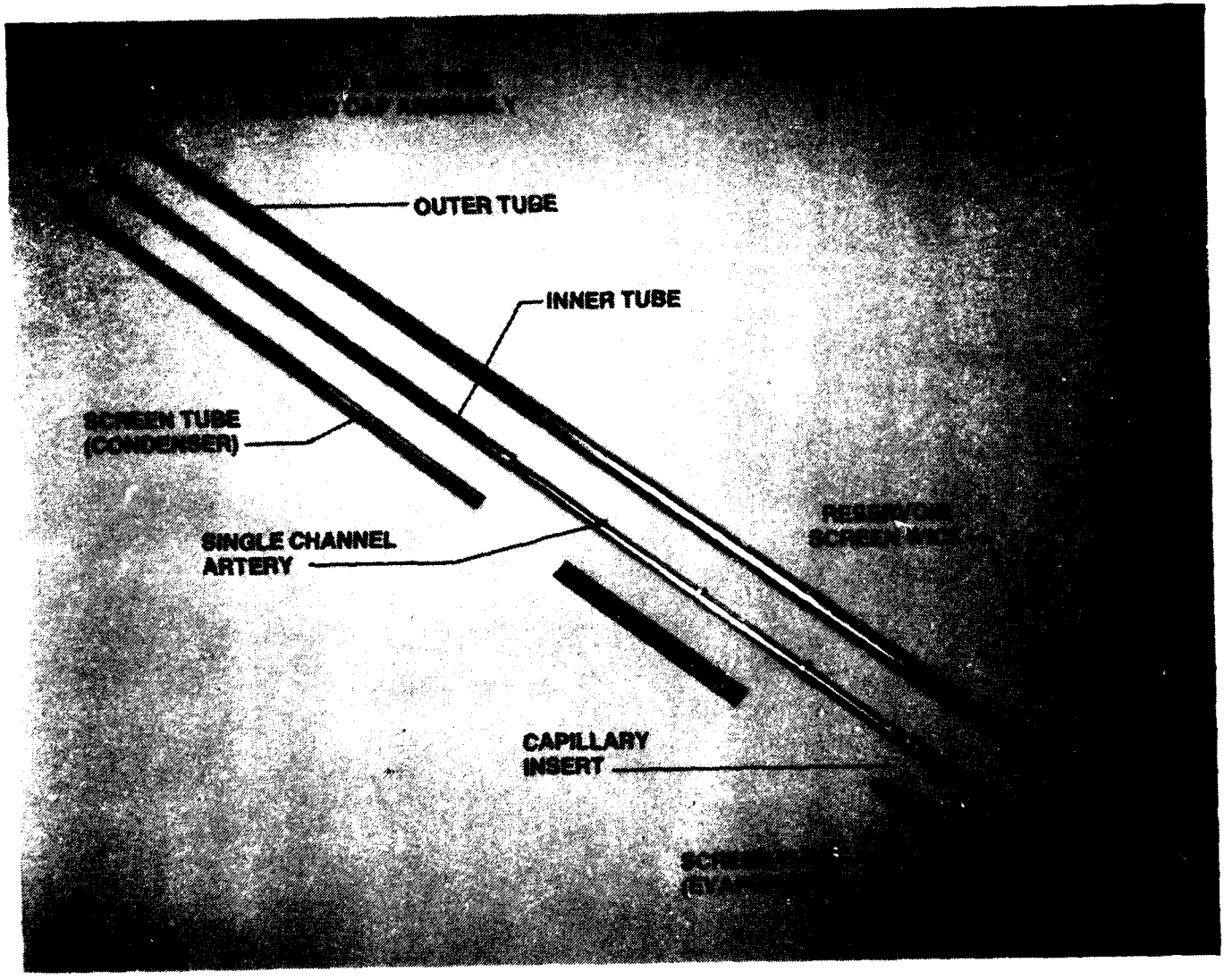

Figure 35. Photograph of the Heat Pipe Parts Laid Out Before Assembly

of the outer tube contains fine circumferential threads on the inner wall to a length of 37.5 cm. The inner tube wall material is machined out selectively to reduce the thermal mass. The tolerances on the various parts are such that there will not be any gap between mating parts after assembly. A closeup view of some of the parts are shown in Figure 36.

4.2 Cleaning of Parts, Assembly and Welding

It is very essential to clean all the parts of the heat pipe before assembling. Machined parts and tubes have contaminations such as oil, grease and scales. Those are rough-cleaned initially with vapor degreasing by trichloroethylene and followed by metal wire brush scrubbing and thorough cleaning using the procedure given below.

(a) Immerse in stainless steel deoxidizer solution (50% dilute) for 20 minutes;

(b) Rinse in deionized water;

(c) Dry with clean air;

(d) Rinse with isopropyl alcohol and dry with air.

For screen mesh cleaning, ultrasonic agitation is used.

The assembly procedure consists of rolling the screen tubes over the inner tube and inserting the composite wick structure thus formed into the outer tube. The inner edges of the screen mesh are spot welded on the inner tube at several locations in order to get a good grip of the screen while rolling to form a tube. A number of short sleeve tubes are slid over the screen tubes to hold them in place. Sterile gloves are worn while handling the cleaned parts and

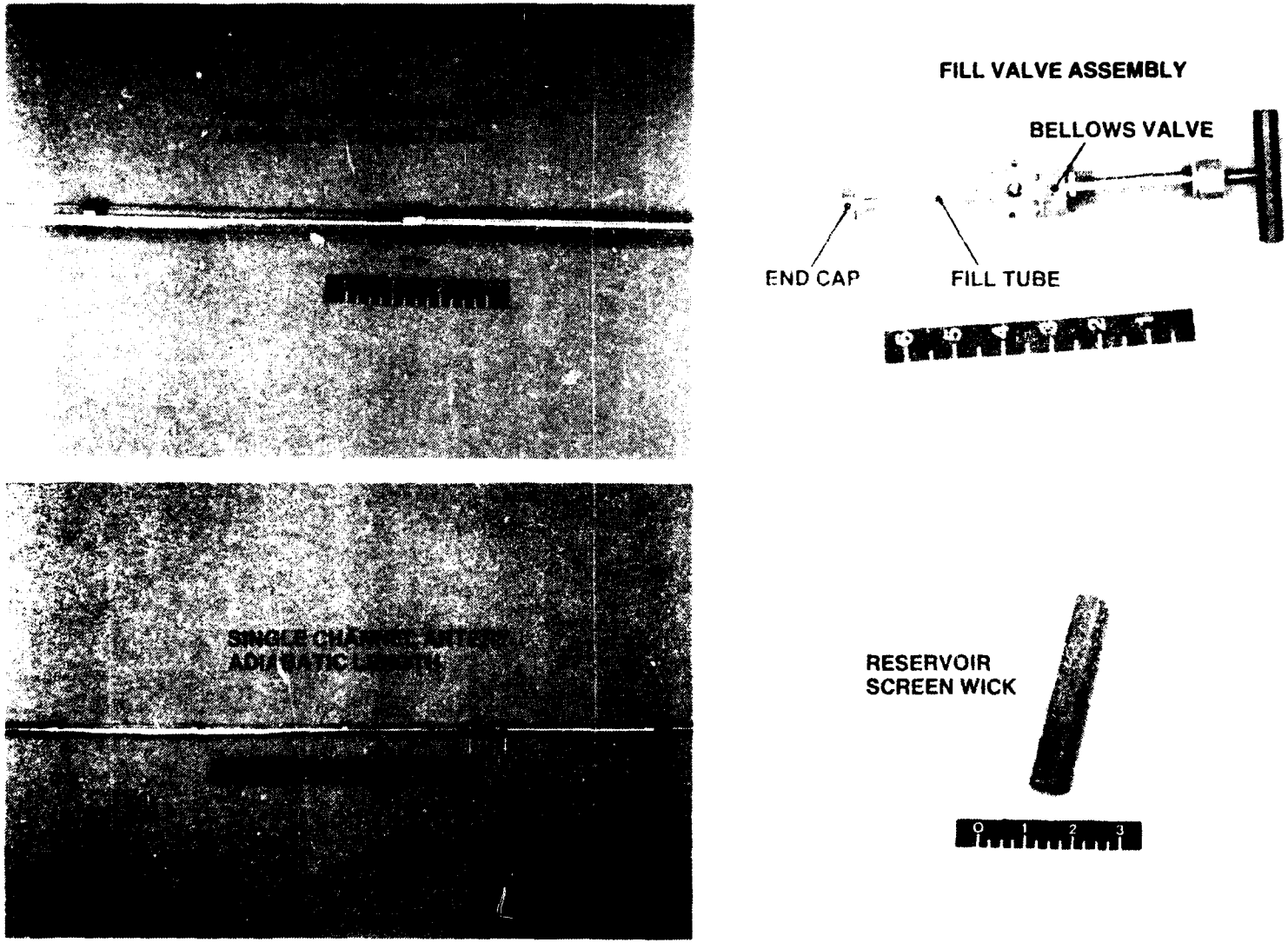

Figure 36. Photograph of Closeup Views of the Parts

the assembly is done in a clean room. As the inner tube composite is inserted into the outer tube, the sleeve tubes are progressively slid along and removed at the other end. This way, the assembly is accomplished without damaging or displacing the screen tube. A short pin on the condenser end cap locks into one of the 24 grooves cut on the inner tube and prevents rotation of the inner tube composite with respect to the outer tube. Also, a reference mark corresponding to the position of the single adiabatic groove is made on the outer tube for locating the groove orientation after the ends are sealed.

The end caps, reservoir screen plug and fill valve are assembled in place and the heat pipe is made ready for final seal welding. These TIG weldings are very crucial and are done within a dry box circulated with argon of purity <5 ppm oxygen and <0.5% water vapor in order to avoid oxidation or contamination. A number of practice weldings were done on samples similar to the heat pipe end-seal welding and examined for weld penetration and grain structure prior to the heat pipe welding. A weld penetration of about 1.5 mm was obtained which is considered satisfactory for the 1.65 mm walled outer tube.

4.3 Vacuum Baking and Sodium Loading

The heat pipe thus assembled and welded is connected to a sodium filling rig shown in Figure 37 which also serves as a baking and oxidizing setup. This rig consists of a graduated glass cylinder, a vacuum pump, an argon gas cylinder and heating tapes/heaters with a suitable valving arrangement. Initially, the

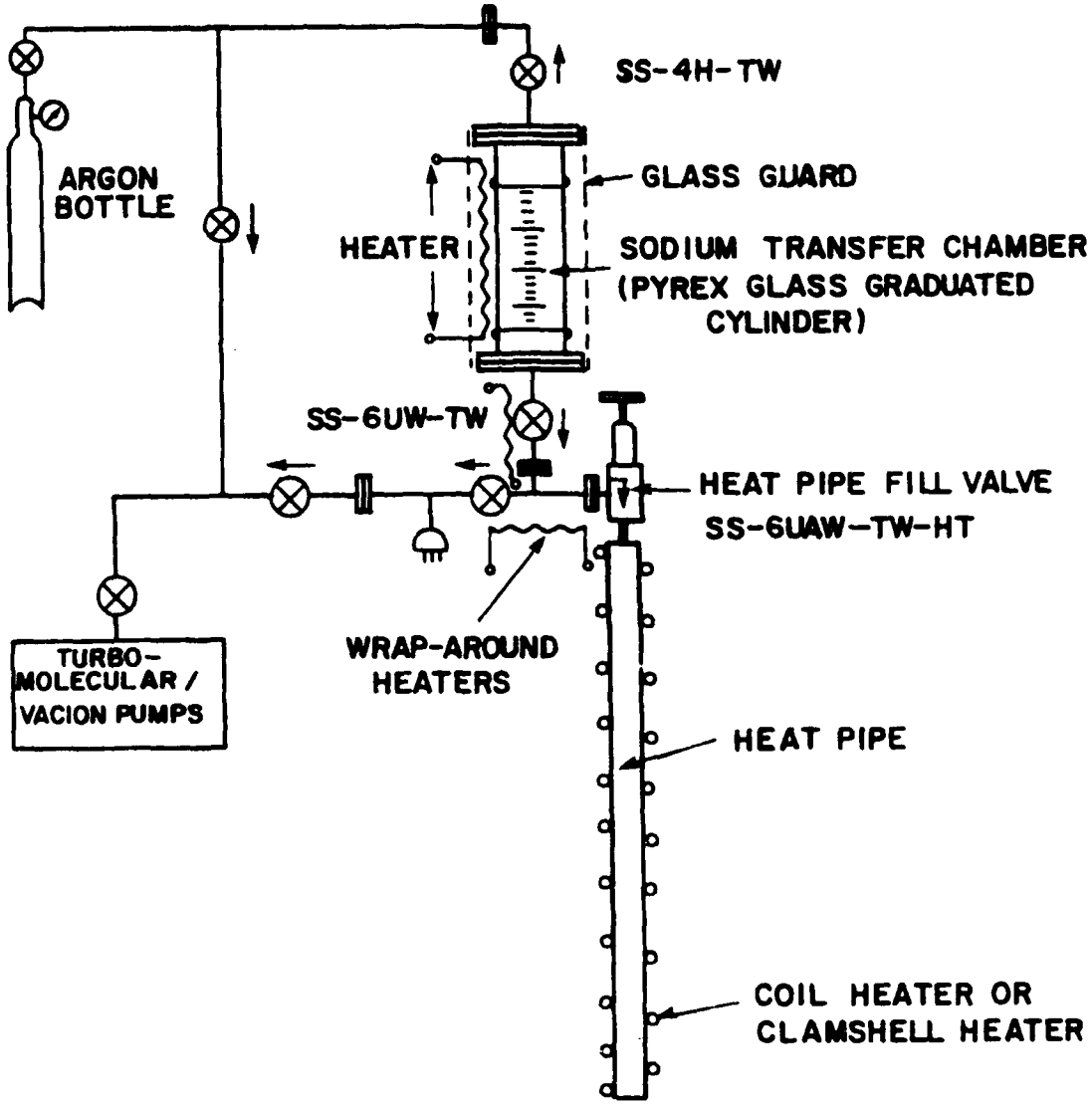

Figure 37. Sodium Filling Rig Schematic

heat pipe is pumped down to about 10^{-6} torr for three days and then heat is applied gradually over the entire heat pipe, fill valve and the plumbing connecting to the glass jar for thoroughly baking and degassing of the internal surfaces. The pipe is heated to 900°C for 4-6 hours maintaining the vacuum at 10^{-7} torr or better. This process helps to solutionize the welds and also oxidizes the external surface to improve the emissivity needed for the condenser heat rejection. After cooling to room temperature and making sure that the glass jar is leak tight, the pipe is valved off and the glass jar is removed for sodium loading.

The sodium loading to the jar is done within the dry box by melting and draining pure analytical grade sodium from glass vials. Four vials of 50 grams each are transferred to the glass jar and sealed. The glass jar is taken out of the dry box and mounted on the sodium filling rig. The entire lines in the rig including the heat pipe are evacuated to 10^{-7} torr or better when the sodium is in frozen condition. Now, the heat pipe is ready to be filled with sodium. The sodium jar, heat pipe and the lines including valves are heated to 150°C which is ~50°C higher than the melting point of sodium. The heat pipe fill valve and the vacuum isolation valve are shut off and the line, up to the valve is primed with sodium by opening the valve at the bottom of the sodium jar. Argon gas pressure is necessary at the top of the sodium level to push the sodium into the line. The meniscus position of sodium in the jar is noted and required volume of the Sodium liquid is made to flow into the heat pipe by slowly opening the fill valve and observing the

drop in meniscus level. The vacuum pressure in the pipe and the gravity head available to the sodium are sufficient to complete the filling process. Once the filling is successfully completed, the fill valve is shut off tight and the valve handle is removed to prevent accidental opening of the valve.

The filled heat pipe is removed from the sodium filling rig and weighed to countercheck the exact quantity of sodium filled in. The sodium sticking to the flange joints and lines is cleaned with suitable solvent. Now, the heat pipe is ready to be instrumented and tested.

4.4 Test Setup Description

The test setup consists of several subsystems which include (1) the mechanical support and mounting, (2) the vacuum chamber and the vacion pump, (3) the cooling fluid circulation and the constant temperature cool bath, (4) the electrical resistance heaters and the power regulating, controlling and measuring circuit, (5) the thermocouple temperature measuring circuit and data logging instrumentation, (6) the radiation shields and the condenser load regulating shutters, and (7) the NCG filling rig. Figure 38 shows the schematic of the test setup representing all these subsystems. The heat pipe is completely contained inside the vacuum chamber in order to thwart the exposure of sodium to the ambient in case of a leak at high temperature testing. Photographic views of the test setup are shown in Figure 39.

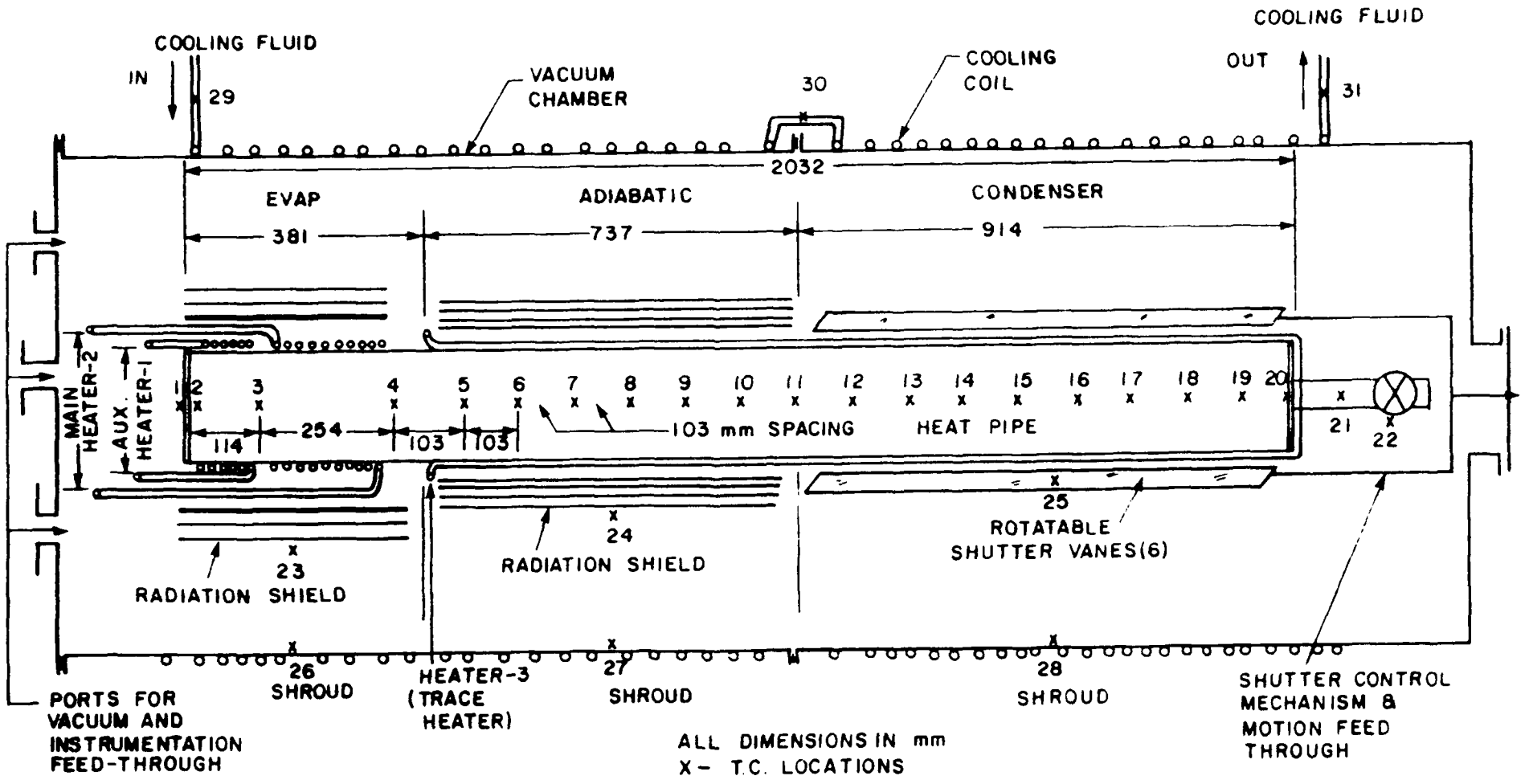
COOLING FLUID
IN
29
VACUUM CHAMBER
30
COOLING COIL
COOLING FLUID
OUT
31
2032
EVAP
ADIABATIC
CONDENSER
381
737
914
MAIN HEATER-2
AUX. HEATER-1
1
2
3
4
5
6
7
8
9
10
11
12
13
14
15
16
17
18
19
20
114
254
103
103
103 mm SPACING
HEAT PIPE
21
22
25
ROTATABLE SHUTTER VANES(6)
24
RADIATION SHIELD
23
RADIATION SHIELD
26
SHROUD
HEATER-3 (TRACE HEATER)
27
SHROUD
28
SHROUD
SHUTTER CONTROL MECHANISM & MOTION FEED THROUGH
PORTS FOR VACUUM AND INSTRUMENTATION FEED-THROUGH
ALL DIMENSIONS IN mm
X- T.C. LOCATIONS

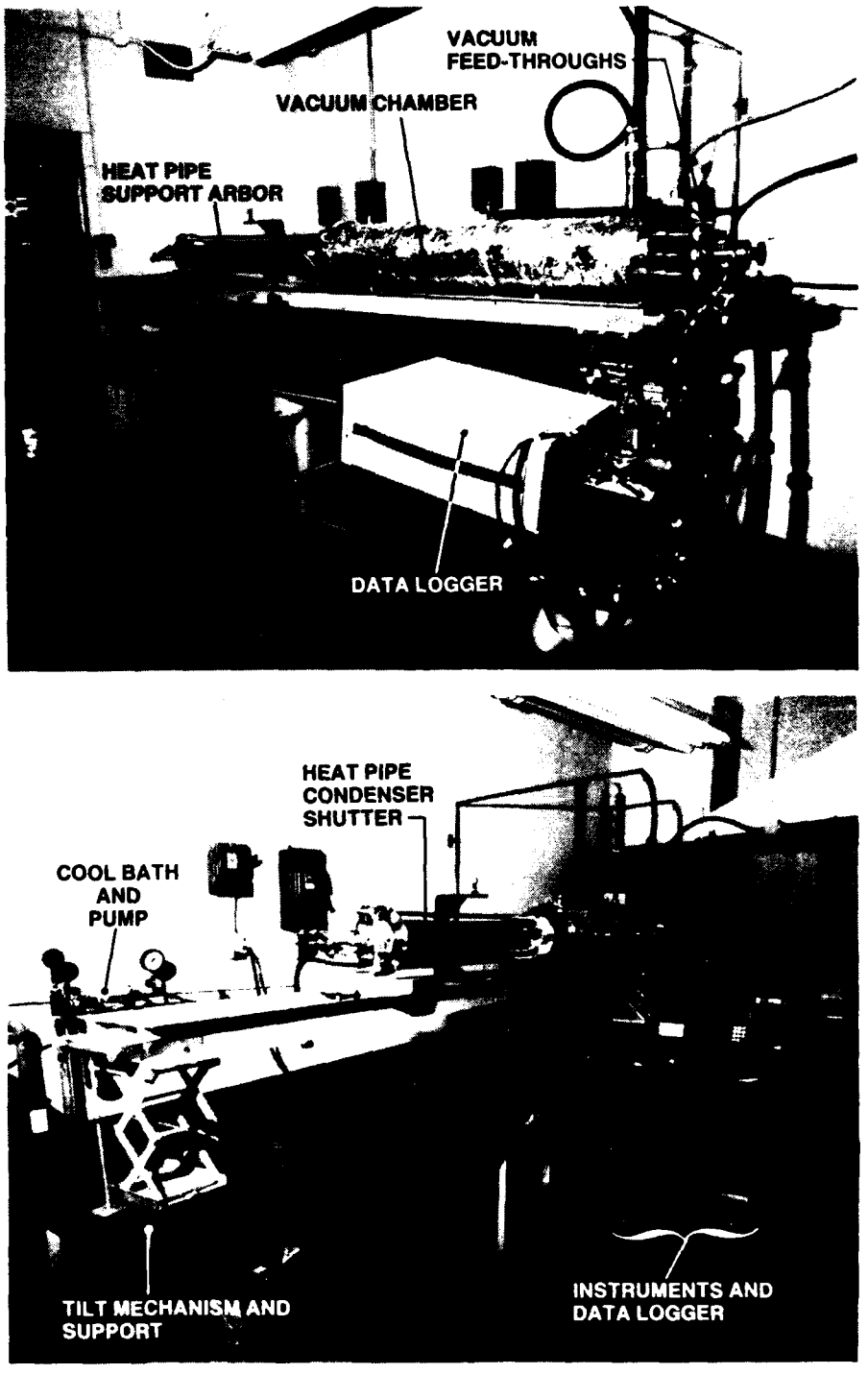

Figure 39. Photographic Views of the Experimental Setup

4.4.1 Mechanical and Vacuum System

The heat pipe is supported at three positions spaced at lengths of the evaporator, adiabatic and condenser end points on brackets having ceramic supports. These brackets are supported from two horizontal, stepped down arbors welded to the vacuum chamber flange. Two 20 cm diameter stainless steel tubular chambers each 122 cm long and bolted together encase the heat pipe assembly and provide the vacuum environment. A turbo molecular pump and vacion pumping unit pump the chamber to 10^{-6} torr or better vacuum. One end of the chamber provides the necessary vacuum port and electrical and thermocouple feedthrough ports. The other end houses the rotary motion feedthrough for regulating the shutter opening. A few view ports fitted with quartz windows on the side of the chamber enable viewing the heat pipe assembly. The whole chamber assembly is mounted on a metal frame with a fulcrum at the center point and either end has an adjusting screw rod for adjusting the level of the frame and the chamber. The level of the heat pipe assembly is initially checked with that of the frame before assembling the chamber. This way, the level maintained on the frame or chamber represents that of the heat pipe. The inside wall of the chamber is painted with a special diffuse black paint having an absorptance (solar) value of >95%. This treatment helps to obtain good calorimetric data on the chamber wall. The vacuum environment is necessary to eliminate convection heat losses and to prevent oxidation of the heat pipe at high temperatures.

4.4.2 Cooling System

The vacuum chamber wall is maintained at room temperature by circulating chilled water from a constant temperature bath through the copper coil (6.35 mm diameter tubing) wrapped around the chamber at 25.4 mm intervals. The coil is tightly wrapped and soldered to the chamber using soft solder. A continuous duty centrifugal pump circulates water through the coil up to a maximum flow rate of 5.75 liters/minute and a rotameter type flowmeter monitors the flow rate. Three thermocouples mounted on the cooling coil at the evaporator end of the chamber, the condenser beginning and the end of the chamber provide temperature data for the calorimetry. The chamber is insulated externally with fiberfrax insulation.

4.4.3 Electrical Heating System

There are three electrical resistance coil heaters mounted on the heat pipe as shown in Figure 38. The main heater is a 20 cm long, closely coiled sheathed coil heater and is mounted directly over the 25 cm evaporator screen wick. The auxiliary heater (10 cm long and similar to the main heater) is mounted on the reservoir wick portion at the starting end of the evaporator. The third heater is mounted on a linear trace from the beginning of the adiabatic section to the condenser and back. Each heater is powered from separate variacs and each of them has a power measuring circuit. The main heater has a current shunt (standard 0.01 ohm resistance) and a signal conditioner circuit to measure the current through the heater. This circuit also has a relay to cut off the

power in case of an over temperature alarm at the evaporator. Figure 40 shows the circuit diagram.

4.4.4 Thermocouple Circuit and Data Logging

There are 28 chromel alumel (type K) high temperature thermocouples mounted internal to the vacuum chamber (22 on the heat pipe, 3 on the shields, and 3 on the chamber wall) as shown in Figure 38. In addition, there are two other control thermocouples (channels 3c and 4c) attached on the heat pipe and positioned on either side of the evaporator main heater. These thermocouple junctions are formed by TIG welding and the lead wires are insulated with porcelain tubing. The junctions are positioned on the small dents created on the heat pipe wall and spot welded by resistance welding. After this, the junctions are covered with a thin bead of high temperature cement (Sauereisen Cement No. 78) which is further covered with a radiation shield. All the thermocouple lead wires are run along the heat pipe to the nearest strip connector block from which the extension leads are taken to the data logger through the vacuum glass-to-metal seal feedthroughs. Three other type K thermocouples of the sheathed type are used to measure the cooling fluid temperatures at the inlet, midpoint and the outlet locations. All the thermocouples are connected to a multichannel programmable data logger (Fluke Model 2280A).

4.4.5 Radiation Shields and Shutter

Multiple layers of polished stainless steel thin sheet metal are used to shield the radiation losses from the heat pipe at the evaporator and adiabatic sections. Four concentric layers of

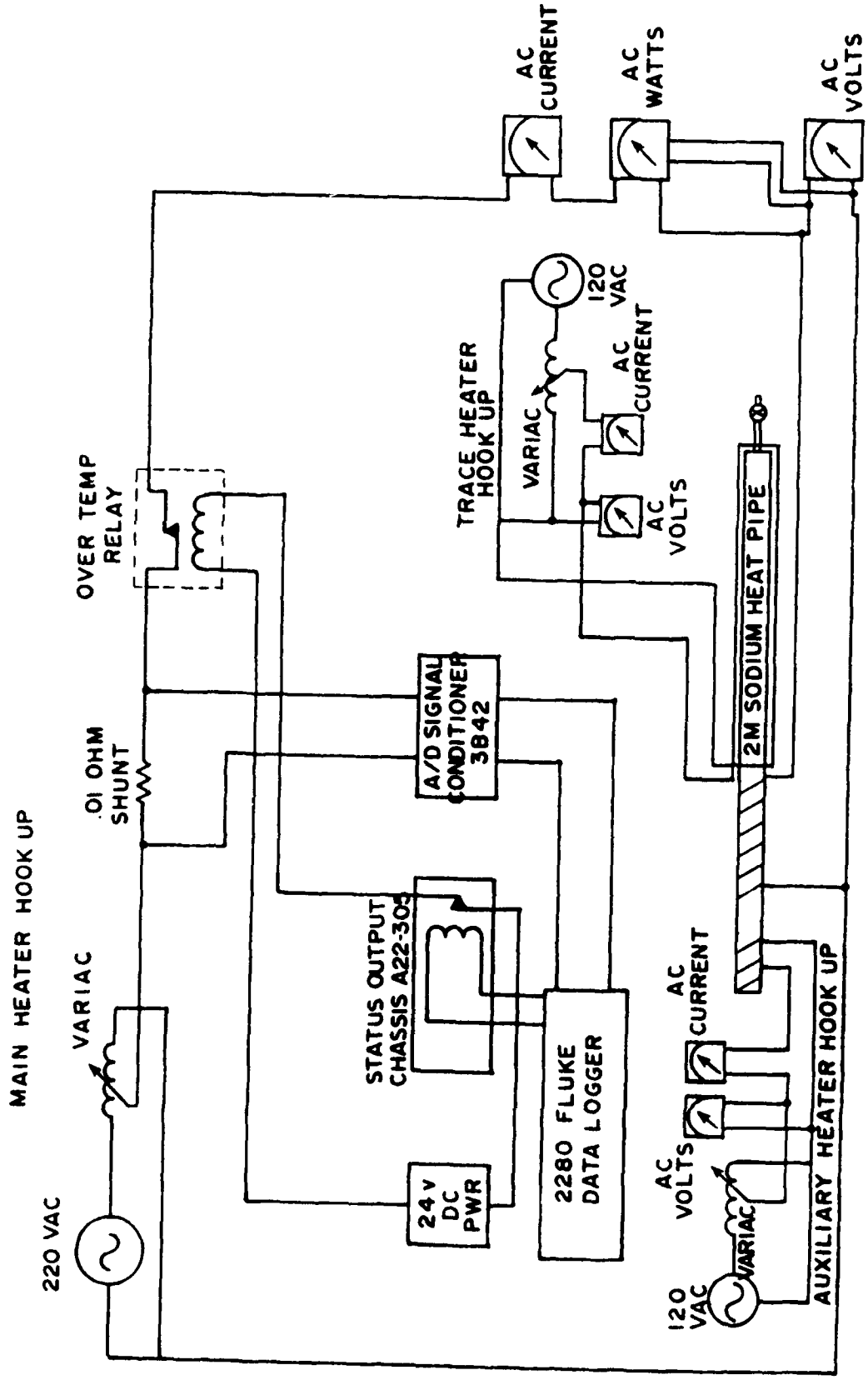

Figure 40. Circuit Diagram of the Heater Power Input

0.25 mm thick SS304 foil separated by 6.35 mm (89 mm diameter to 127 mm diameter) and 73.7 cm long shields in two hemicylindrical halves cover the adiabatic section. Five layers of similar construction in full cylindrical form cover the 37.5 cm evaporator. A radiation loss calculation based on the shield emissivity value of 0.08 and pipe operating temperature of 1000 K shows only 5% loss through the shield, compared to the direct black body emission from the pipe. The 91 cm long condenser section is covered with a set of six twin layer shutter blades to form a hexagonal cage around the condenser. The shutters are individually pivoted on either end by their central shafts supported from the heat pipe support brackets. All these shafts are connected to a circular disc with arc-like slots through L shaped cranks. The disc is in turn connected to a rotary motion feedthrough (MFT) mounted on the chamber end flange. The rotation of the MFT actuates the shutter blades in unison. The blades can be positioned in fully open or fully closed or any intermediate positions and thus the condenser radiation load can be varied as desired.

4.4.6 NCG Filling Rig

The noncondensible gas is filled into the heat pipe through the fill valve in-situ using the filling rig while the free end section of the chamber is dismantled. A schematic diagram of this system is shown in Figure 41.

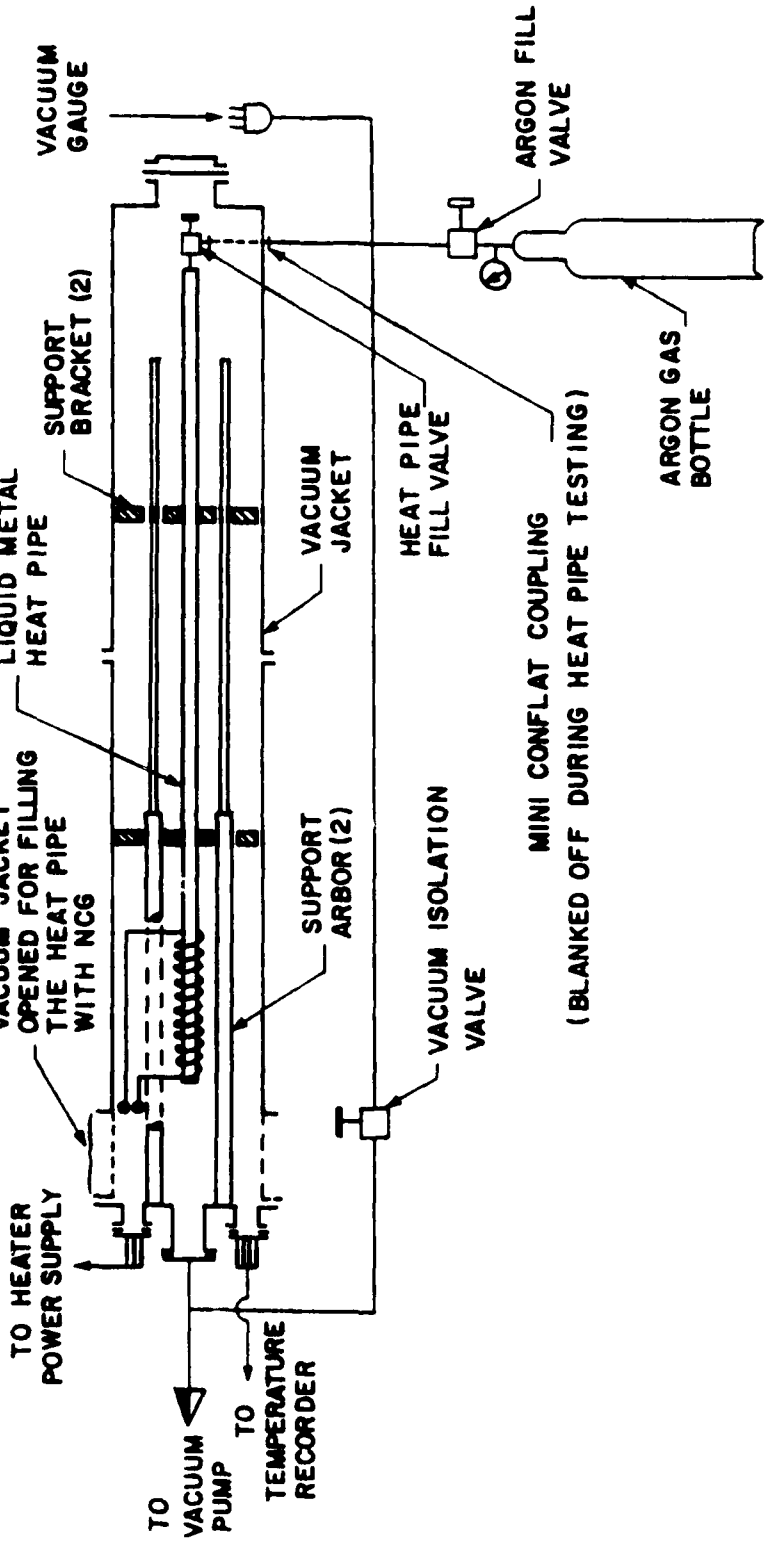

Figure 41. Noncondensible Gas Filling Rig

4.5 Test Procedure

4.5.1 System Checkout and Preliminary Test

A thorough system check is done on each and every subsystem before the vacuum jacket is assembled. All the internal parts are checked for cleanliness and greasy spots are cleaned with alcohol. Any outgassing material such as adhesive tape and plastic ties are removed. The alignment of the heat pipe is checked with a leveling instrument and adjusted to remain horizontal with respect to gravity vector. It is important to check the continuity of all the thermocouples and the heaters (in order to detect possible breakage during assembly or harnessing the wires) and to repair if necessary. After the chamber jacket is assembled, the turbo molecular pumping unit is used to rough the system until the vacion pumping unit could take over pumping. If any leakage at the vacuum joints is found, these joints are tightened further. A vacuum level of 10^{-6} torr or better is acceptable for this test. The cooling fluid circulation is checked out by switching on the centrifugal pump and circulating the coolant through the coil around the vacuum chamber. Any leak in the line or joints is easily detectable and repairable. The rotameter type flowmeter is calibrated using stop watch and measuring jar. The room temperature readings of all the thermocouples are checked against a known reference thermometer. The heater circuit current measurement using the shunt resistance of 0.01 ohm and the data logger is verified using analog meters in the circuit.

The initial configuration of the heat pipe is vacuum mode. Initially, it is necessary to bake out the heat pipe and the internal parts of the chamber by slowly warming up the pipe. About 100 W on each of the three heaters will be sufficient to raise the temperature to ~500°C for the baking purpose. The power to heaters may be increased or decreased as necessary to maintain the temperature at a constant level for about 8 hours. In this process, the outgassing rate of the vacuum parts is accelerated and more importantly, the heat pipe "wets in" with the working fluid. The main purpose of including the trace heater is to uniformly warm up the pipe. An added advantage of this is to redistribute sodium from the condenser and adiabatic area to the evaporator section after an unfavorable shutdown or cooldown of the pipe from a previous test. After these tests, the vacuum level in the chamber should improve. At this point, the pipe is ready for performance tests.

The objectives of the performance test, transient as well as steady state are limited to two modes of the heat pipe internal configuration, namely, (1) vacuum mode and (2) noncondensible gas (NCG) filled mode. Further, the tests are limited to the level condition (axis of the pipe is horizontal) and to the horizontal orientation (3 o'clock position with respect to gravity vector) of the artery groove for both of the above modes of internal configuration.

4.5.2 Vacuum Mode Testing

The vacuum mode represents that the heat pipe does not contain any NCG within its vapor core and the wick structure contains pure

sodium in its pores. The objectives of this test are twofold. Firstly, the initial burn-in test for wetting and distribution of the working fluid throughout the wick structure is done soon after the heat pipe is instrumented. This is followed with the steady state performance tests to verify the transport capacity, operating temperature and overall temperature difference (ΔT) for a given power input for a number of input powers (250 W, 500 W, 1000 W, etc.). The steady state axial temperature plots and calorimetric input/output measurements to determine the losses are done. During these tests, the pipe's priming ability and restart capabilities after a cooldown (frozen fluid) period are evaluated. The above tests form the basis for design verification.

Secondly, the transient tests at several power inputs are performed to characterize the frontal nature of startup of a sodium heat pipe. The frontal startup behavior is mapped by temperature versus time plots using the thermocouples attached to the heat pipe. An important aspect of this study/test is to understand the startup behavior of a heat pipe with long adiabatic section (the present pipe has 74.5 cm long adiabatic section without vapor-liquid direct contact as opposed to traditional heat pipes).

4.5.3 Noncondensible Gas Filled Mode

The heat pipe, after characterization in vacuum mode as described above, is filled with a noncondensible gas (argon) to an initial predetermined pressure (in the range 0.05-2.0 Torr at room temperature) and sealed.

The main objective of the test in this mode is to conduct transient startup tests from frozen state and to determine:

(a) the rise time and temperature,

(b) the startup time and temperature,

(c) the position of the hot front as a function of time,

(d) the hot zone temperature as a function of time, and

(e) active/inactive condenser lengths (after steady state)

for any given power input to the evaporator. These startups are attempted from liquid as well as frozen state of the working fluid. A trace heater attached on the adiabatic and condenser sections enables the thawing of sodium when powered. The measured heat pipe temperature versus time data are used to determine the rate of hot front propagation from the evaporator into its transport and condenser sections. These experimental results are corroborated with the results of the theoretical analysis done using the binary vapor gas diffusion model. Adjustments to theoretically calculated or assumed parameters (such as evaporator and transport heat losses, unaccounted losses through support brackets, emissivity values, diffusivity values, etc.) and modeling errors are done as necessary.

CHAPTER V

RESULTS AND DISCUSSION

As described in the test procedure section (Chapter IV), the 2 m sodium heat pipe was first tested in vacuum mode and then in gas filled mode with 1.35 Torr argon. Three sets of test results were obtained. Test Sets 1 and 2 correspond to the gas filled mode tests with the condenser shutter closed and partially open condition, respectively. Test Set 3 corresponds to the vacuum mode tests. All test sets cover steady state and transient tests as well. The transient tests preceded the steady state tests for every power input level. The repeatability of results was good. The orientation of the pipe axis was horizontal to the gravity vector, and the artery groove was at the 3 o'clock position as shown in Figure 42 in solid lines. Both frozen state startup and liquid state startup tests were carried out in the gas filled mode. The results follow.

5.1 Vacuum Mode Test Results

5.1.1 Steady State Test Results

The steady state test data were used to obtain the axial temperature profiles and calorimetric heat loss at various evaporator power input levels. These results were used to determine the heat transport performance of the pipe.

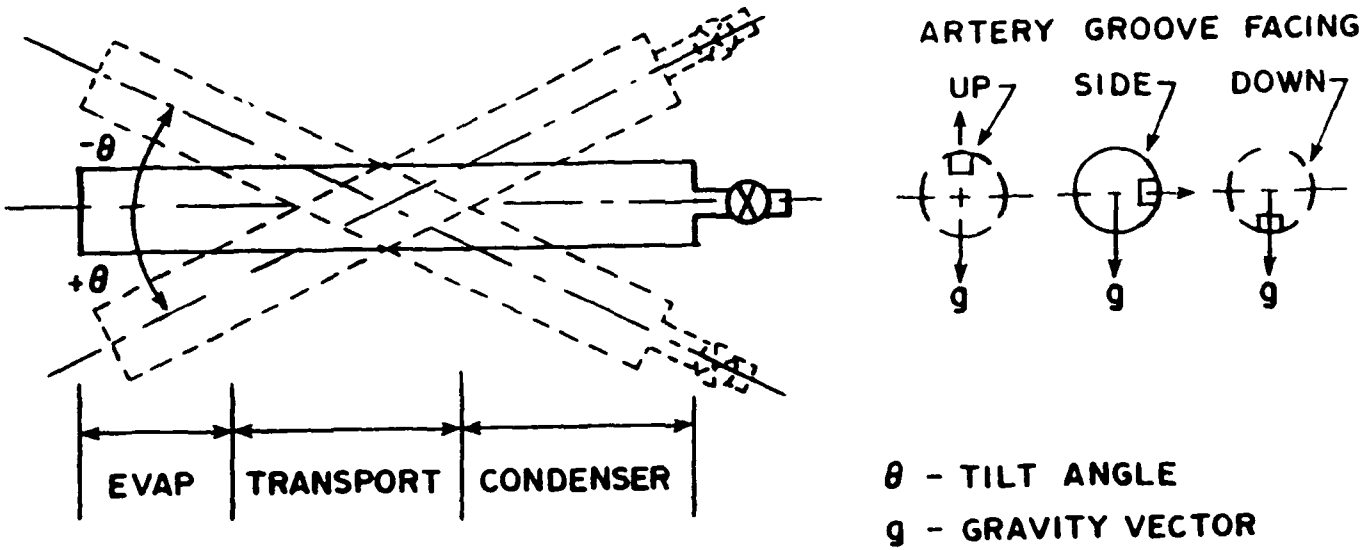

Figure 42. Heat Pipe Test Orientation

Calorimetry: The heat input (Q_i) to the evaporator was split three ways as the heat pipe transported energy along its length. Eq. (87) gives the heat balance for steady conditions.

$$Q_i = Q_E + Q_A + Q_o \tag{87}$$

The quantities Q_E, Q_A, and Q_o are the portions of the heat lost radially from the evaporator, adiabatic and condenser zones, respectively. Thus, Q_o is the actual quantity of heat transported by the heat pipe and this quantity has to be compared with the input Q_i while comparing with the theoretical results. Q_E and Q_A are considered as losses since these quantities are lost along the way when the pipe is transporting. Four thermocouples mounted on the coolant line at the entrance and exit locations of each of the heat pipe zones, monitored the temperatures for calorimetric calculations. Figure 43 shows the percentages of heat loss in each zone as a function of the heat input. At low heat inputs (<600 W) losses in the evaporator and adiabatic zones were higher than the transported energy which was less than 50%. At high inputs (>600 W), Q_o was stable at 55-60%. The heat carried by the coolant was calculated using Eq. (88).

$$Q_{cal} = \dot{V} \rho C_p \Delta T_{coolant} \tag{88}$$

Coolant flow rate, $\dot{V}$ = 2.3 liters/minute; specific gravity, ρ = 1.0; and specific heat, C_p = 4.2 J/g K for water. Substituting in

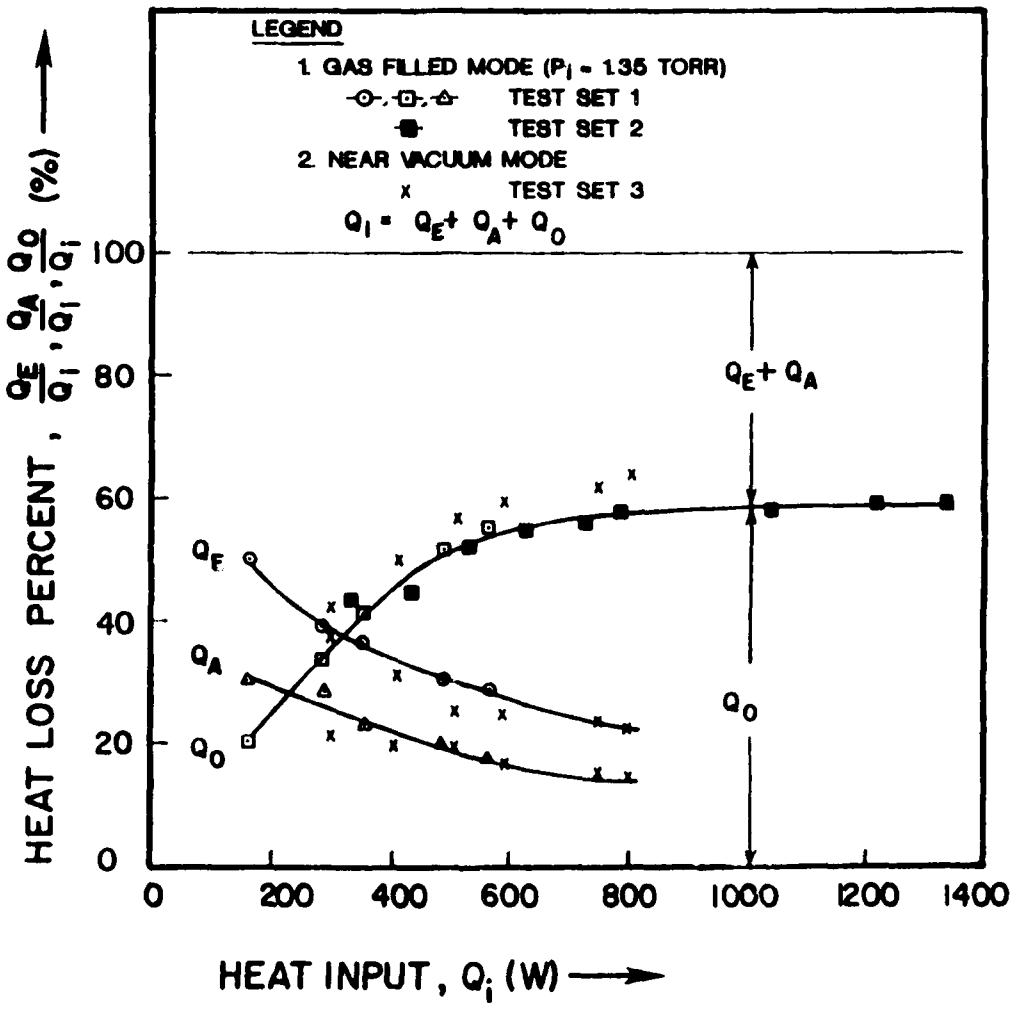

Figure 43. Heat Loss Distribution from Steady State Calorimetric Test Data

Eq. (88), $Q_{cal} = 161.07\ (\Delta T_{coolant})$ watts. There was good agreement between Q_i (power measured in the current shunt circuit) and Q_{cal} for all the steady state test data reported in Figure 43. The errors were within the instrument uncertainty limits. Appendix H shows the list of numerical data obtained in the steady state tests.

Axial Temperature Profile: Figure 44 shows the axial temperature profiles for different transported power levels (129-515 W). The pipe operated near-isothermal from end-to-end at $Q_o = 467$ W and 515 W. The average temperatures of the evaporator and condenser for $Q_o = 515$ W were 558.1°C and 534.6°C, respectively, and the total ΔT was 23.5 C. As seen from Figure 44, at power levels below $Q_o = 467$ W, the hot front did not reach the condenser end. This indicates the presence of a trace amount of gas in the pipe. Hence, the vacuum mode tests actually represent near-vacuum mode. The trace amount of gas could have been trapped within the sodium during filling and was not pumped out subsequent to the filling of the pipe.

Transport Capacity: The transport capacity data attained experimentally are plotted on the theoretically predicted capillary and sonic limit curves in Figure 45. The experimental points correspond to the average hot zone temperature, $\bar{T}_H$ and the transported power, Q_o. The pipe operated along the border of the sonic limit curve. High capacity and high temperature test data were not available since the heater could not be operated beyond

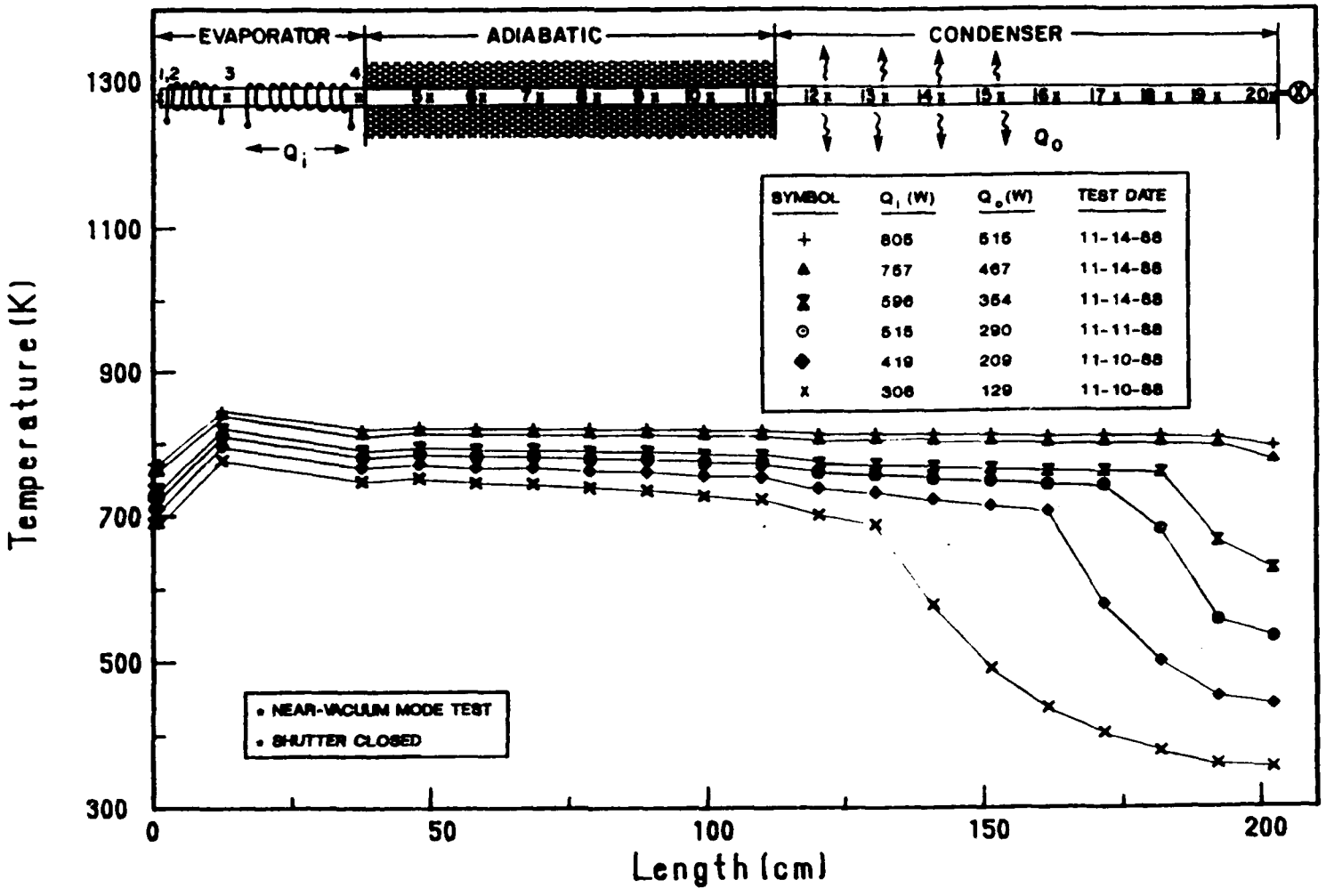

Figure 44. Steady State Test Axial Temperature Profiles (Vacuum Mode)

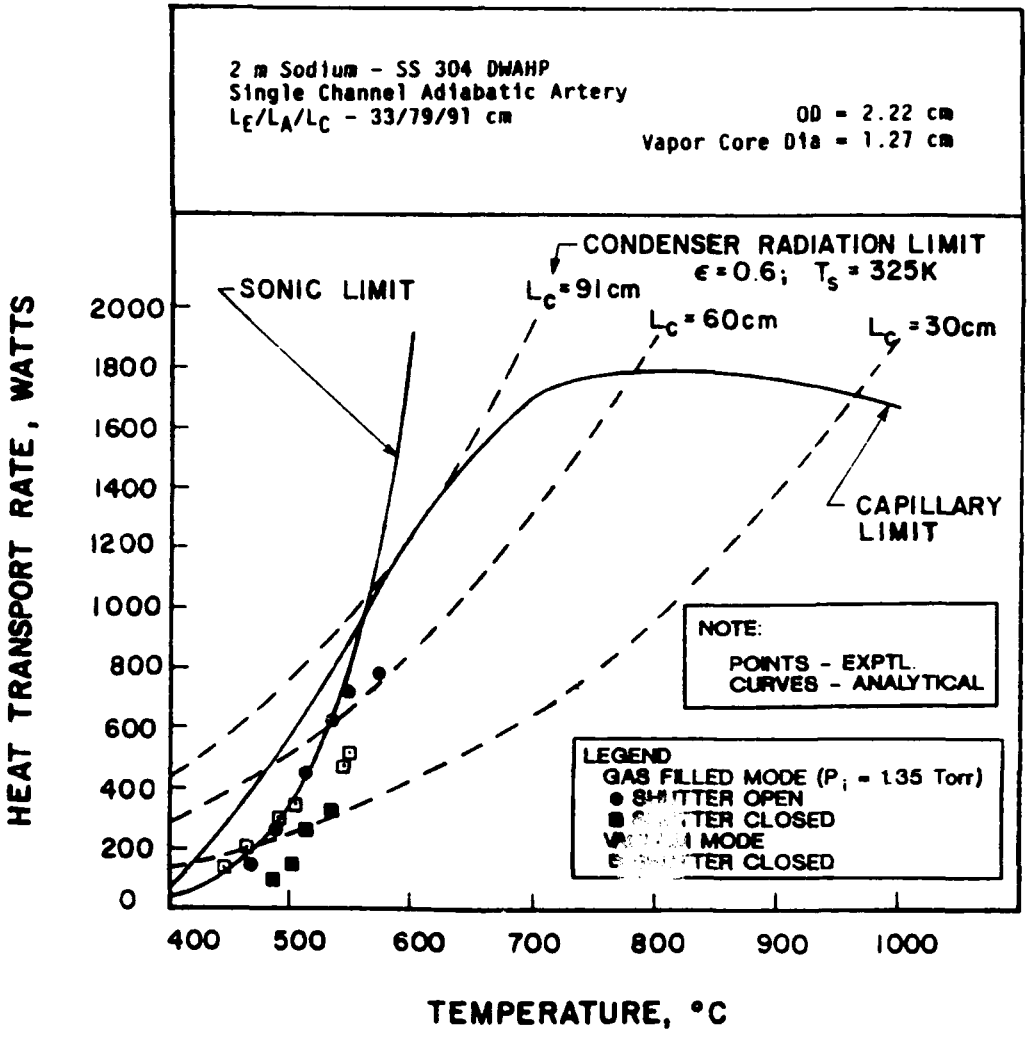

Figure 45. Heat Transport Rate Versus Temperature (Q_o vs $\bar{T}_H$) - Experimental Data

1000°C for fear of melt down. Induction heater or tantalum heater could solve this problem.

5.1.2 Transient Test Results

Frozen State Startup: In the vacuum mode, the pipe was nearly free of noncondensible gas. The pipe was started from frozen state of the working fluid which was at room temperature. Figures 46 and 47 show the axial temperature profiles at 20, 30, 60, and 150 minutes after the application of the power input for Q_o = 289.6 W and 354.4 W, respectively. Figures 48 and 49 show the transient temperature profiles at a few specified axial locations for the same power levels mentioned above. It may be observed that the hot zone was not isothermal during startup.

5.2 Noncondensible Gas Filled Mode Test Results

5.2.1 Steady State Tests

Two sets (Test Sets 1 and 2) of tests were conducted corresponding to the NCG charge pressure of 1.35 Torr at various input power levels up to 1337 W. The calorimetric heat loss distribution and the heat transport capacity with the repeatability of some test runs have been shown in Figures 43 and 45 (Section 5.1.1) along with the vacuum mode test results. The numerical data are listed in Appendix H.

Axial Temperature Profile: Figure 50 shows the axial temperature profiles for various transported power levels (Q_o from 145 to 718 W). The adiabatic zone temperatures are isothermal at each power level and the position of the hot front lies at different axial locations in the condenser zone. The frontal nature of the

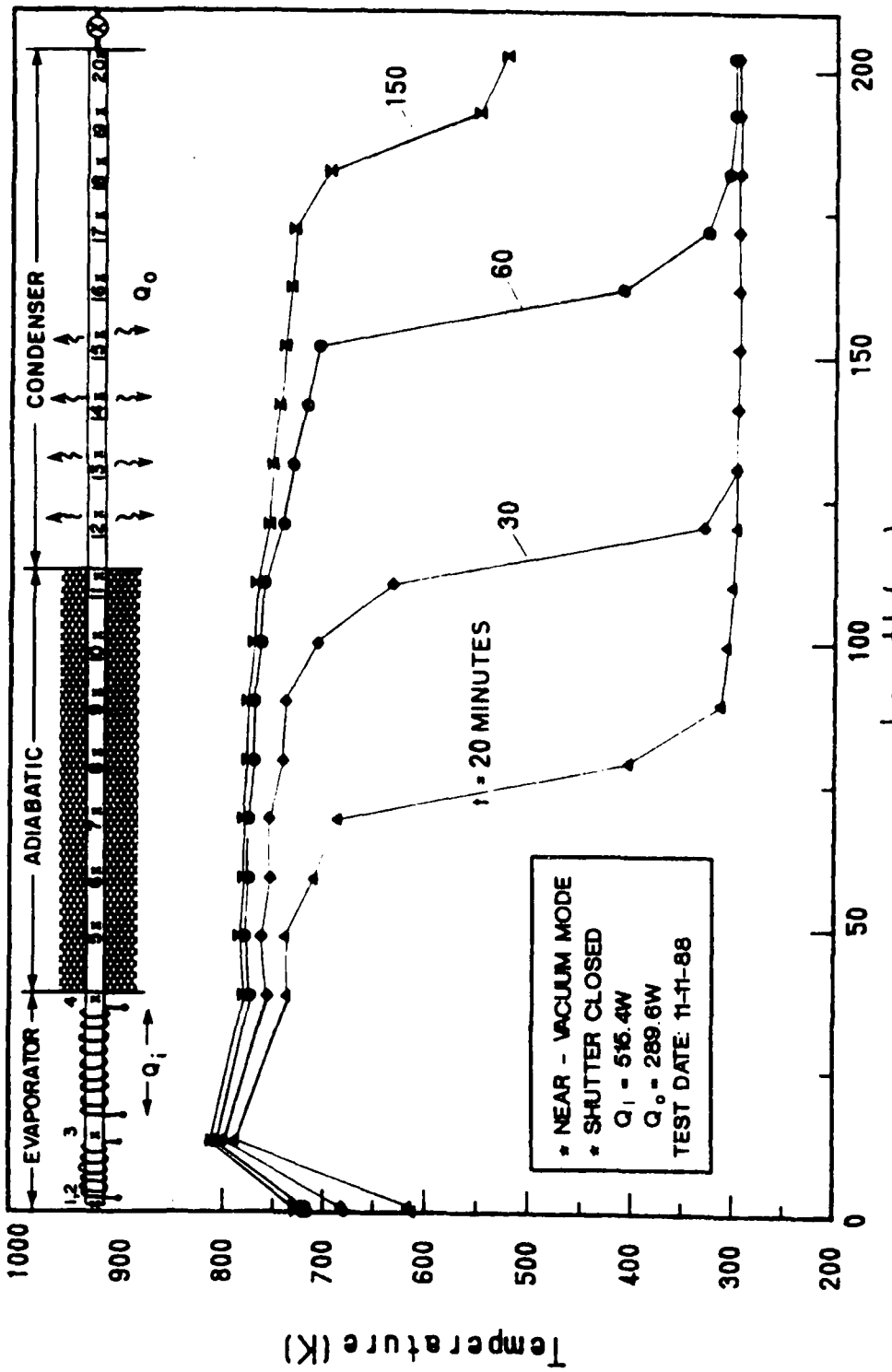

Figure 46. Axial Temperature Profiles at Specified Time from 0-150 Minutes after Power Input (Q_o = 289.6 W)

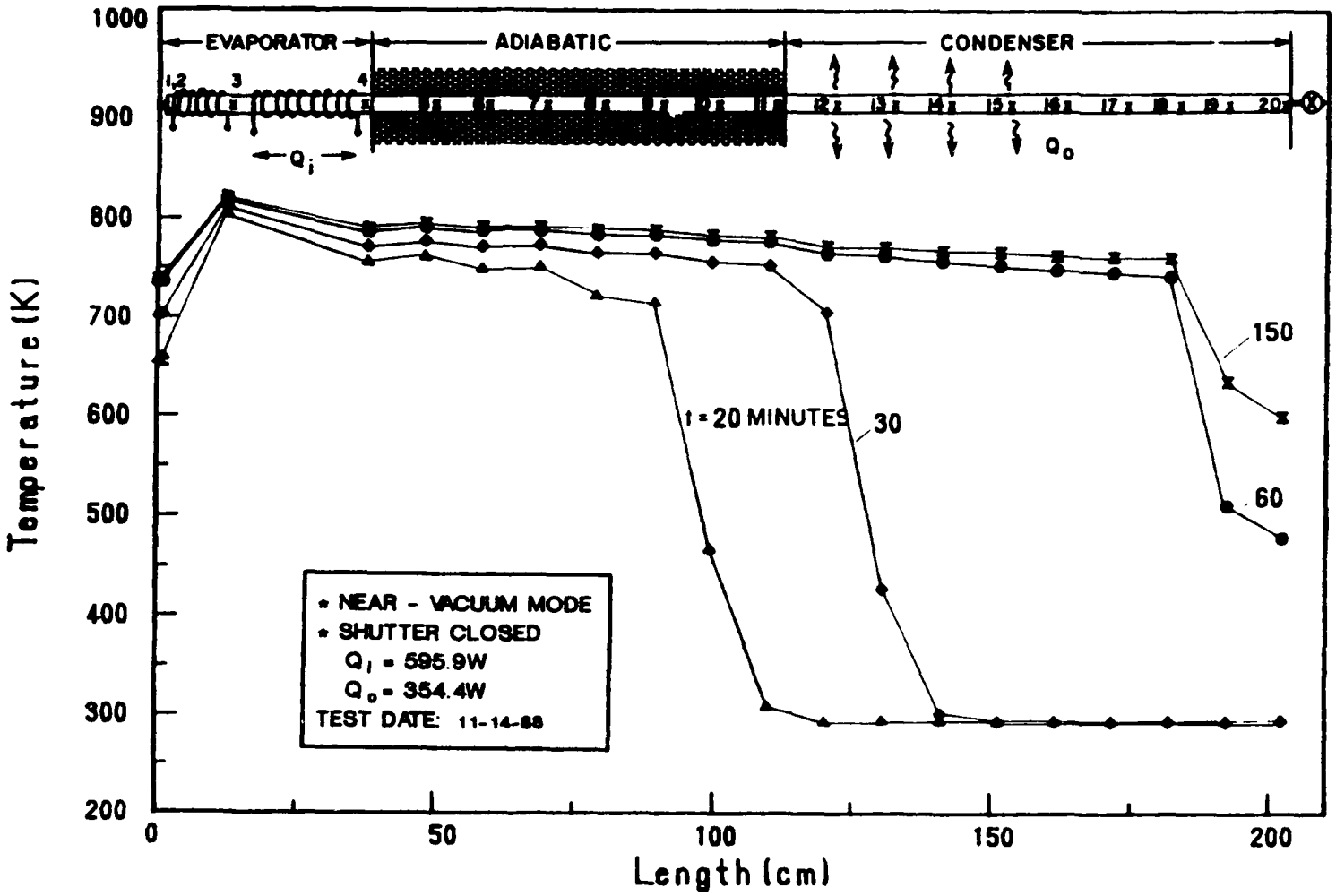

Figure 47. Axial Temperature Profiles at Specified Time from 0-150 Minutes after Power Input (Q_o = 354.4 W)

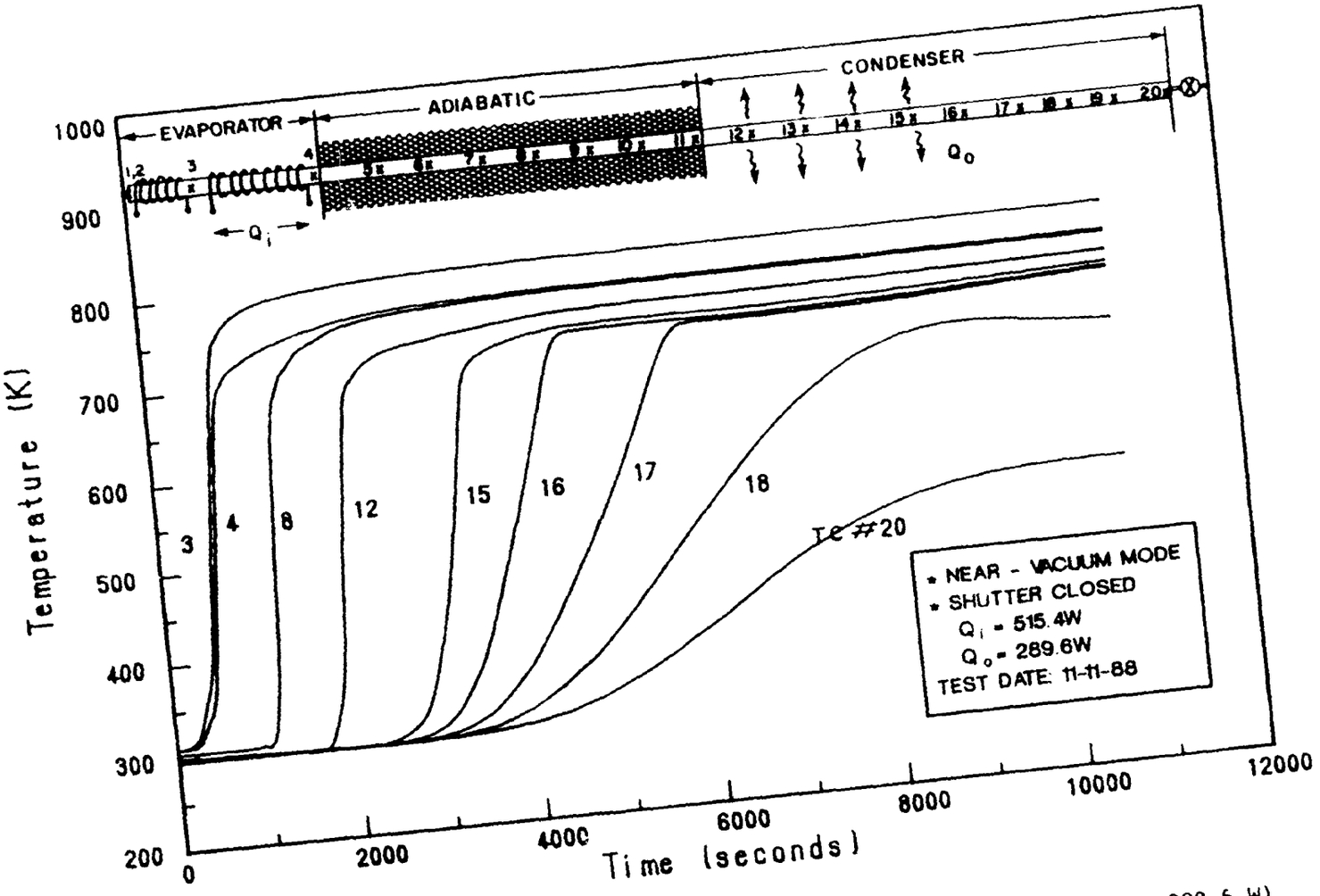

Figure 48. Transient Temperature Profiles at Specified Axial Locations (Q_o = 289.6 W)

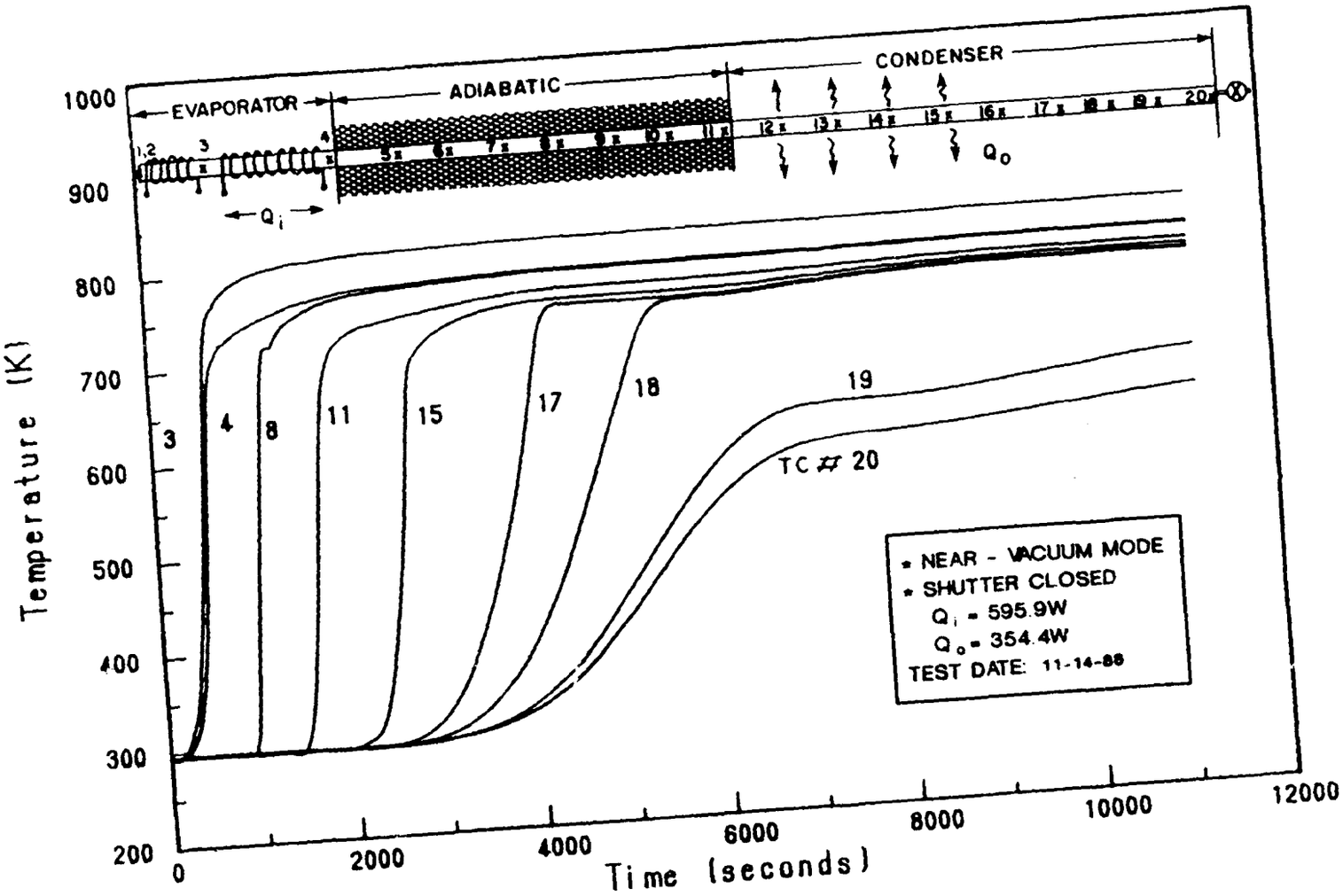

Figure 49. Transient Temperature Profiles at Specificed Axial Locations (Q_o = 354.4 W)

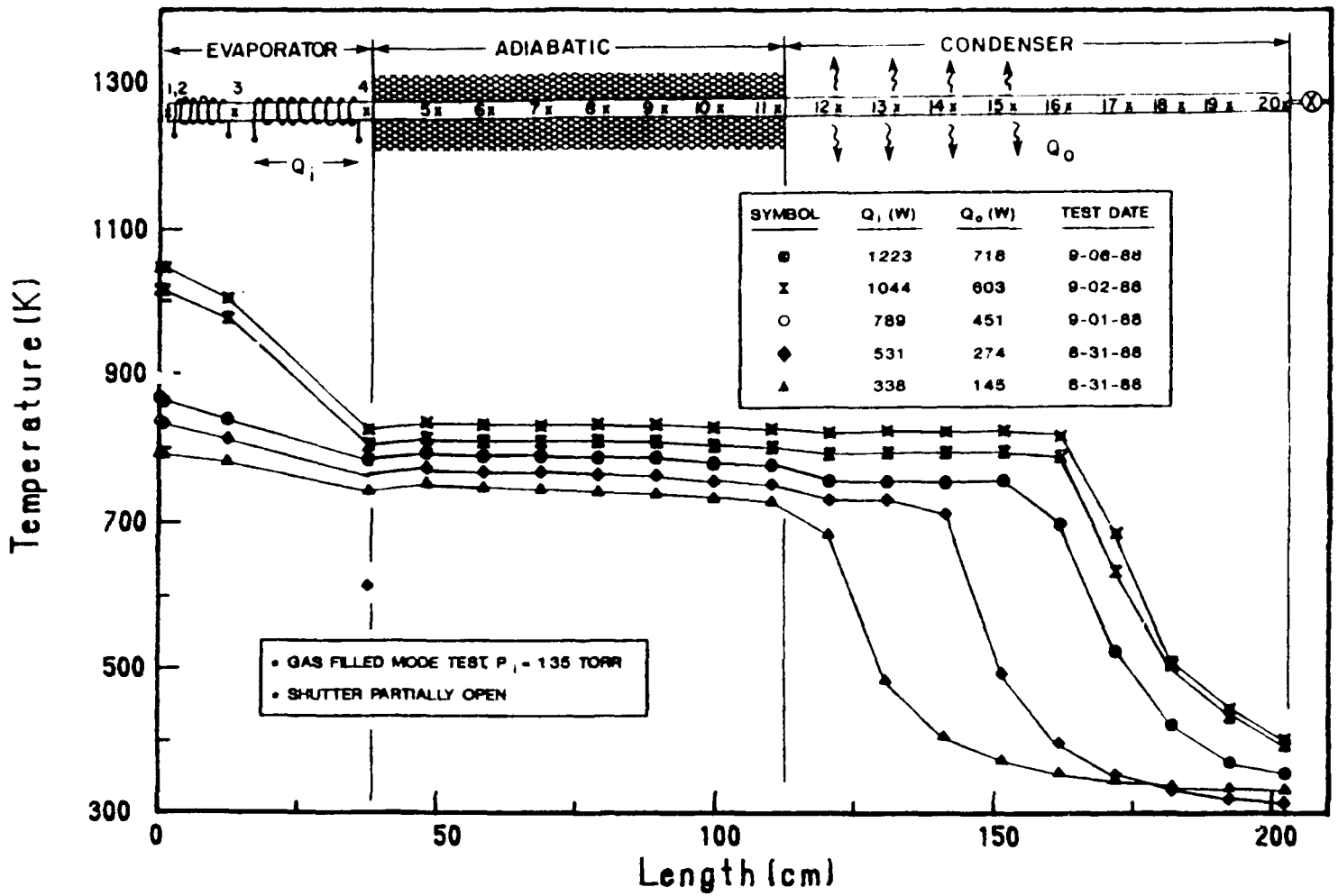

Figure 50. Steady State Test Axial Temperature Profiles (Gas Filled Mode)

temperature front is evident from this figure. The slant of the front is off vertical and the temperature of the cold zone is progressively high with Q_o. This signifies the dominance of axial conduction over the diffusion mechanism at the steady state condition where $Q_v = 0$. It should be noted that the marginal rise in cold zone temperature will cause corresponding pressure rise in the gas slug which, in turn, will affect the position of the hot front.

Inactive Condenser Length: The steady state test data are plotted on the operating temperature versus the inactive (gas slugged) length of the condenser graph as shown in Figure 51 to compare with the theoretical values. The experimental points lie in the vicinity of the theoretical curve corresponding to $P_i = 1.0$ Torr. More data points fell above the 1.0 Torr curve than those below it. This closely agrees with the 1.35 Torr initial gas charge pressure. The gas slug length varied from 121 cm to 28.3 cm for the transport power (Q_o) variation of 32.2 W to 782.8 W (see tables in Appendix H). It should be noted that this plot is not directly dependent on the power level; instead, it is directly dependent on the temperature. For a given power level if the pipe is operated at a higher temperature, the gas slug length will be reduced. The experiment could not be run at high temperatures (>850 K) due to heater limitation. The experimental data uncertainty is ±0.05 m in the length determination and ±4.5 K for temperature measurements.

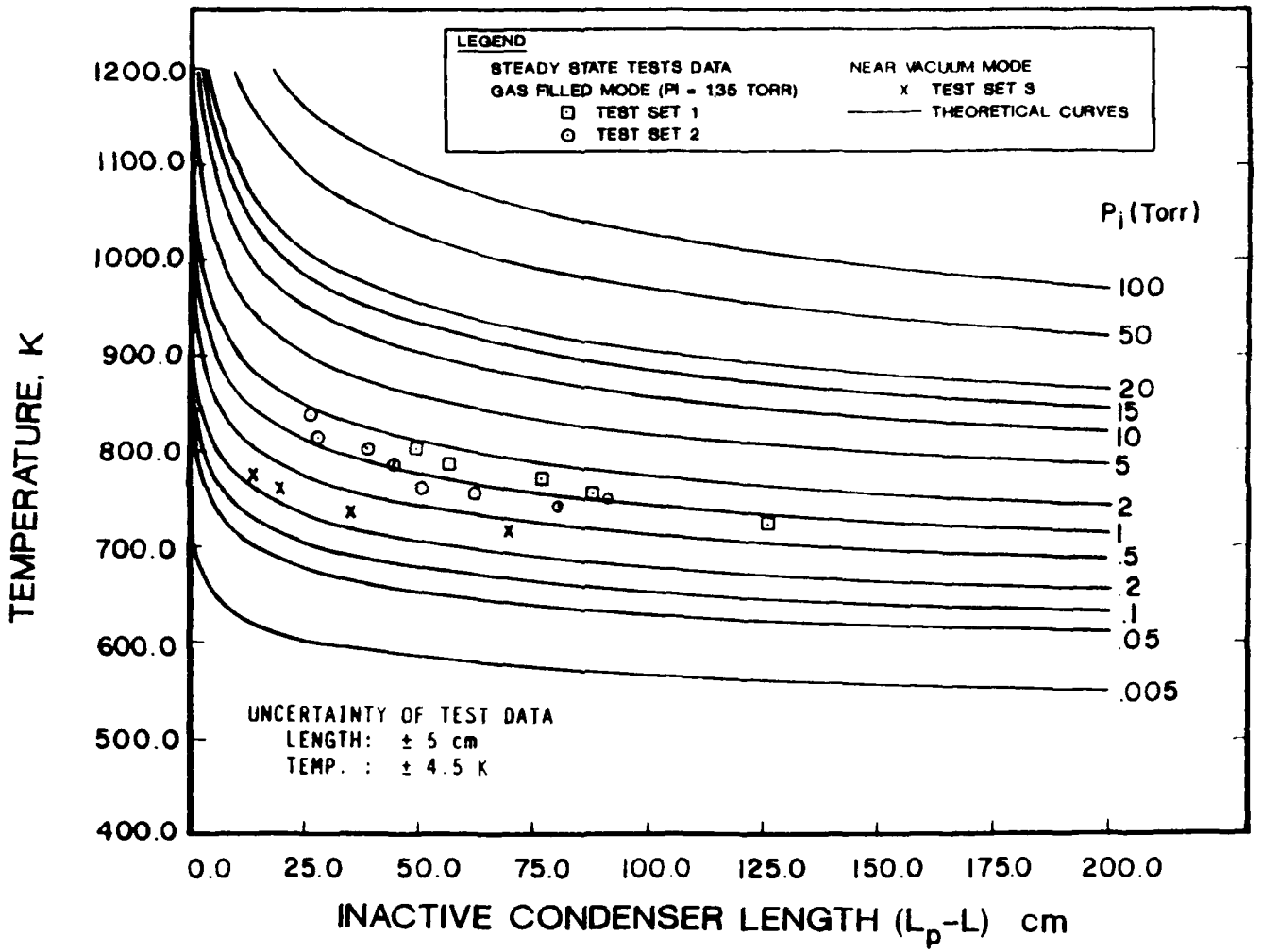

Figure 51. Steady State Inactive Condenser Lengths (T vs L_{NCG})

Hot Front Length: The steady state test data are also plotted on the L vs Q_o graph as shown in Figure 52. The experimental points lie within the band of P_i = 0.5 and 2.00 Torr curves and the mean curve appears to fall along P_i = 1.35 Torr which is the actual charge pressure of the gas.

5.2.2 Transient Tests

Temperature Profiles: Transient tests were conducted in order to map the startup behavior of the heat pipe. The temperature variations along the length as a function of time were graphed for various power levels. Figures 53 and 54 show the axial profiles at 20, 30, 60, and 150 minutes after the application of power input for Q_o = 96.6 W and 258 W, respectively. The temperature front at 20 minutes is in the adiabatic zone and the profile of the front is relatively flatter than that in the condenser zone. At 150 minutes, the front is completely in the condenser zone and is more slanted. This is the expected behavior and it agrees with the hypothesis proposed in the analysis section (Section 2.3) very well. The vapor diffusion activity is strong during the transient state and the axial conduction is dominant in the steady state. Figures 55 and 56 show the transient temperature profiles at a few specified axial locations for Q_o = 96.6 W and 258 W, respectively. The number shown along each of the curves represents the thermocouple location. The rise time (t_i) for the given power level is obtained from this plot by finding the time (after power on) at which T.C #4 attained a temperature close to the rise temperature (T_{Hi}) within 2 K. Also, the startup time (t_s) is obtained in a

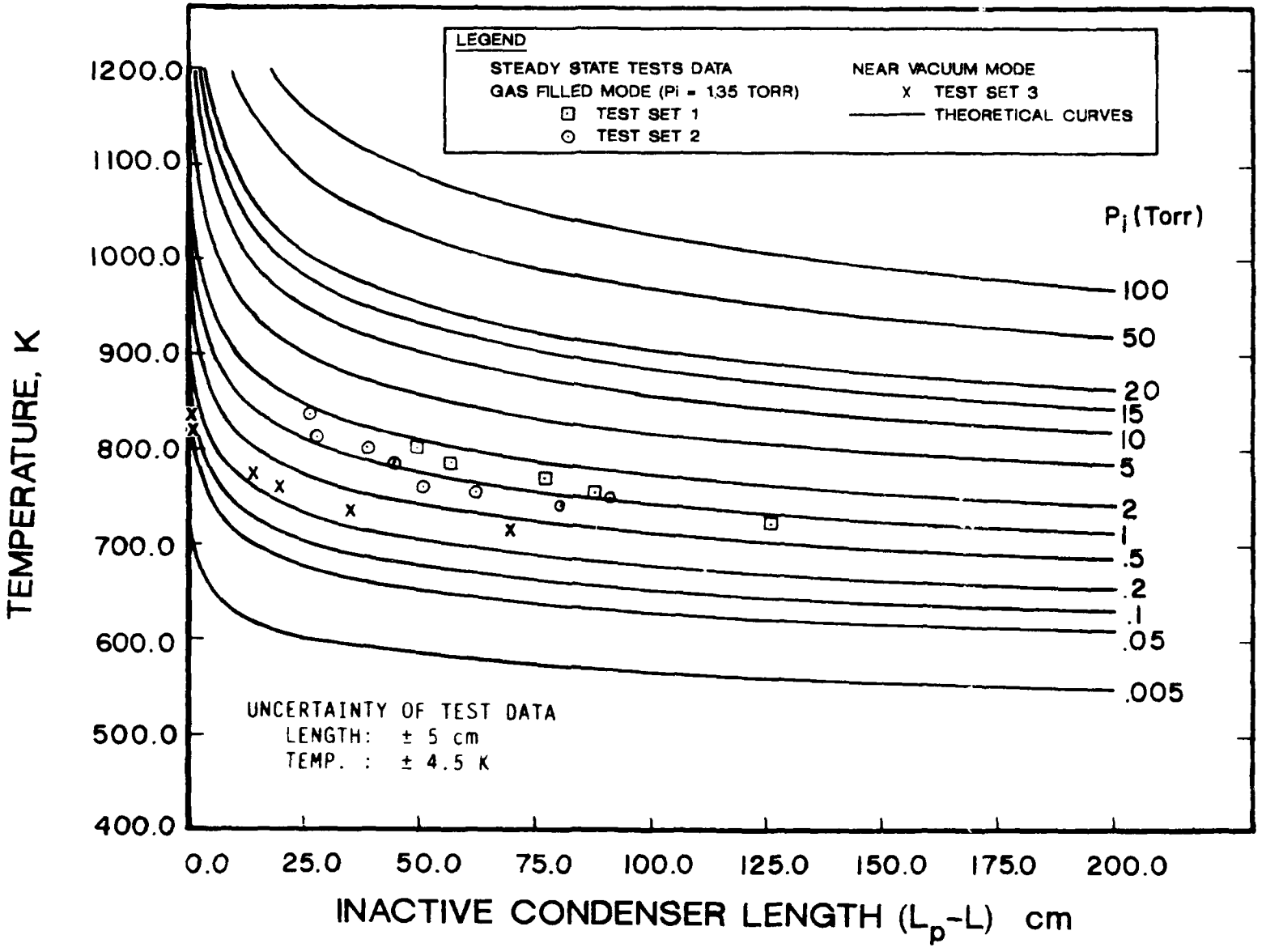
LEGEND
STEADY STATE TESTS DATA
GAS FILLED MODE (Pi = 1.35 TORR)
TEST SET 1
TEST SET 2
NEAR VACUUM MODE
X TEST SET 3
THEORETICAL CURVES
P_i (Torr)
100
50
20
15
10
5
2
1
.5
.2
.1
.05
.005
UNCERTAINTY OF TEST DATA
LENGTH: ± 5 cm
TEMP. : ± 4.5 K
TEMPERATURE, K
1200.0
1100.0
1000.0
900.0
800.0
700.0
600.0
500.0
400.0
0.0
25.0
50.0
75.0
100.0
125.0
150.0
175.0
200.0
INACTIVE CONDENSER LENGTH (L_p-L) cm

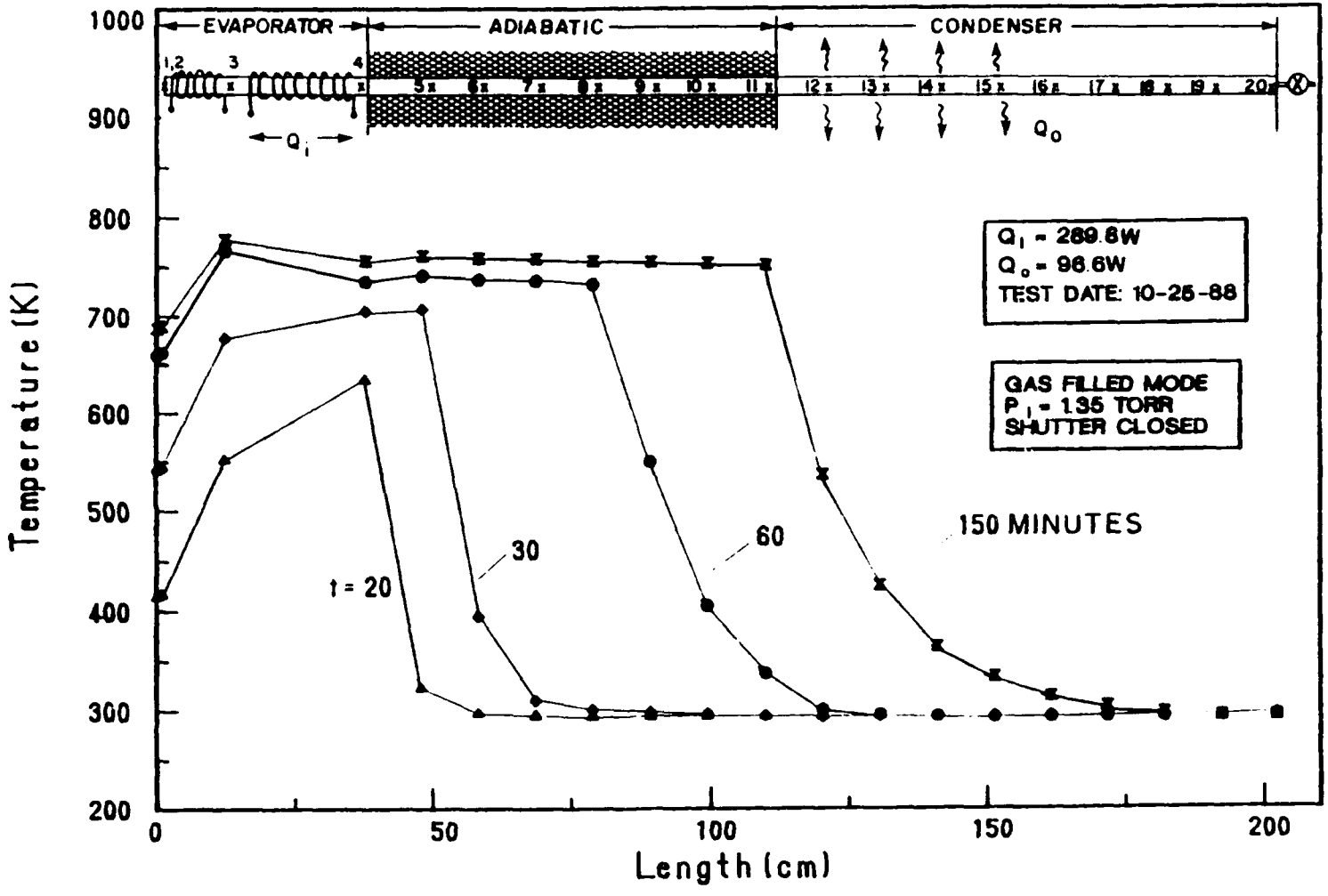

Figure 53. Axial Temperature Profiles at Specified Time from 0-150 Minutes after Power Input T vs L for Q_o = 96.6 W

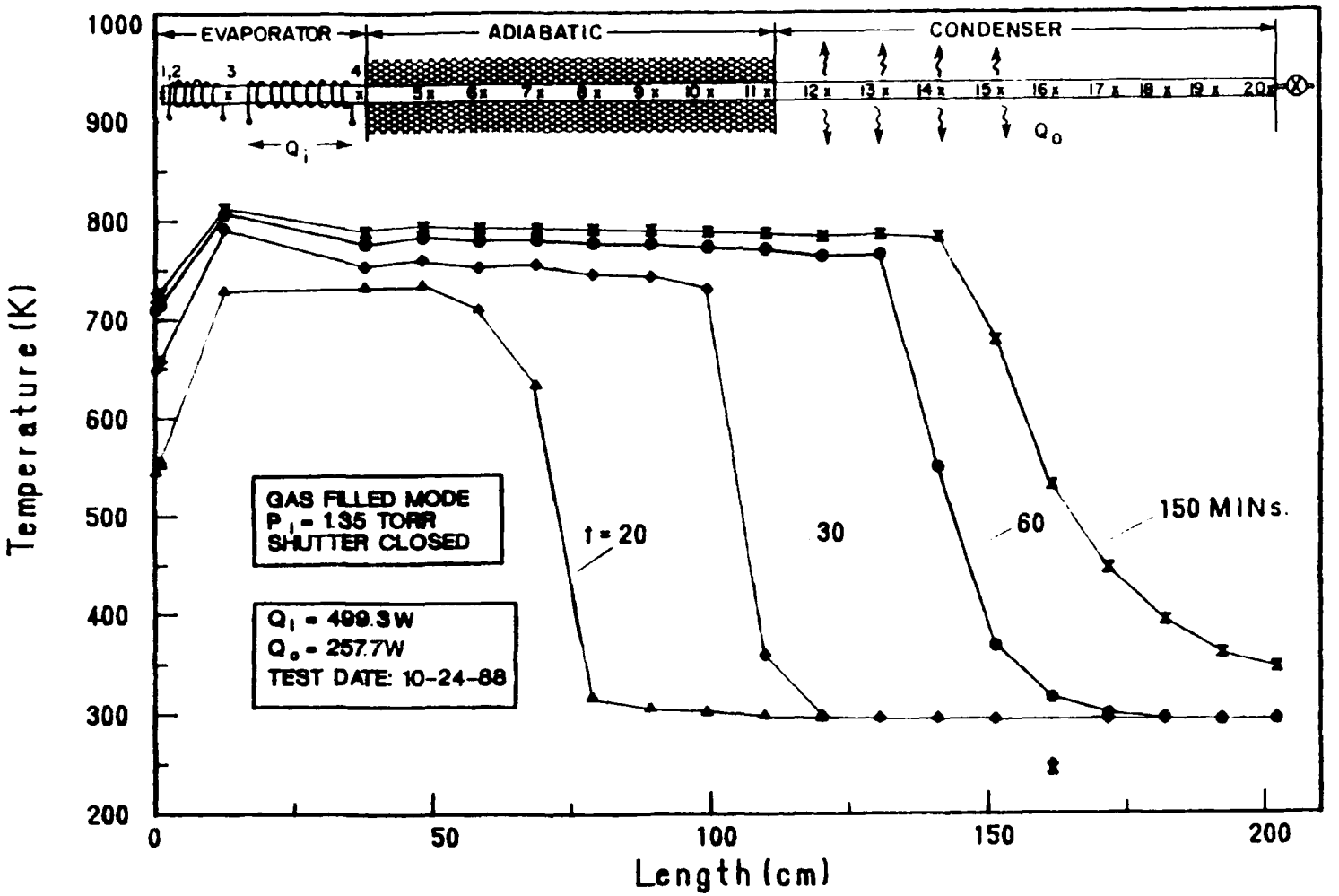

Figure 54. Axial Temperature Profiles at Specified Time from 0-150 Minutes after Power Input T vs L for Q_o = 258 W

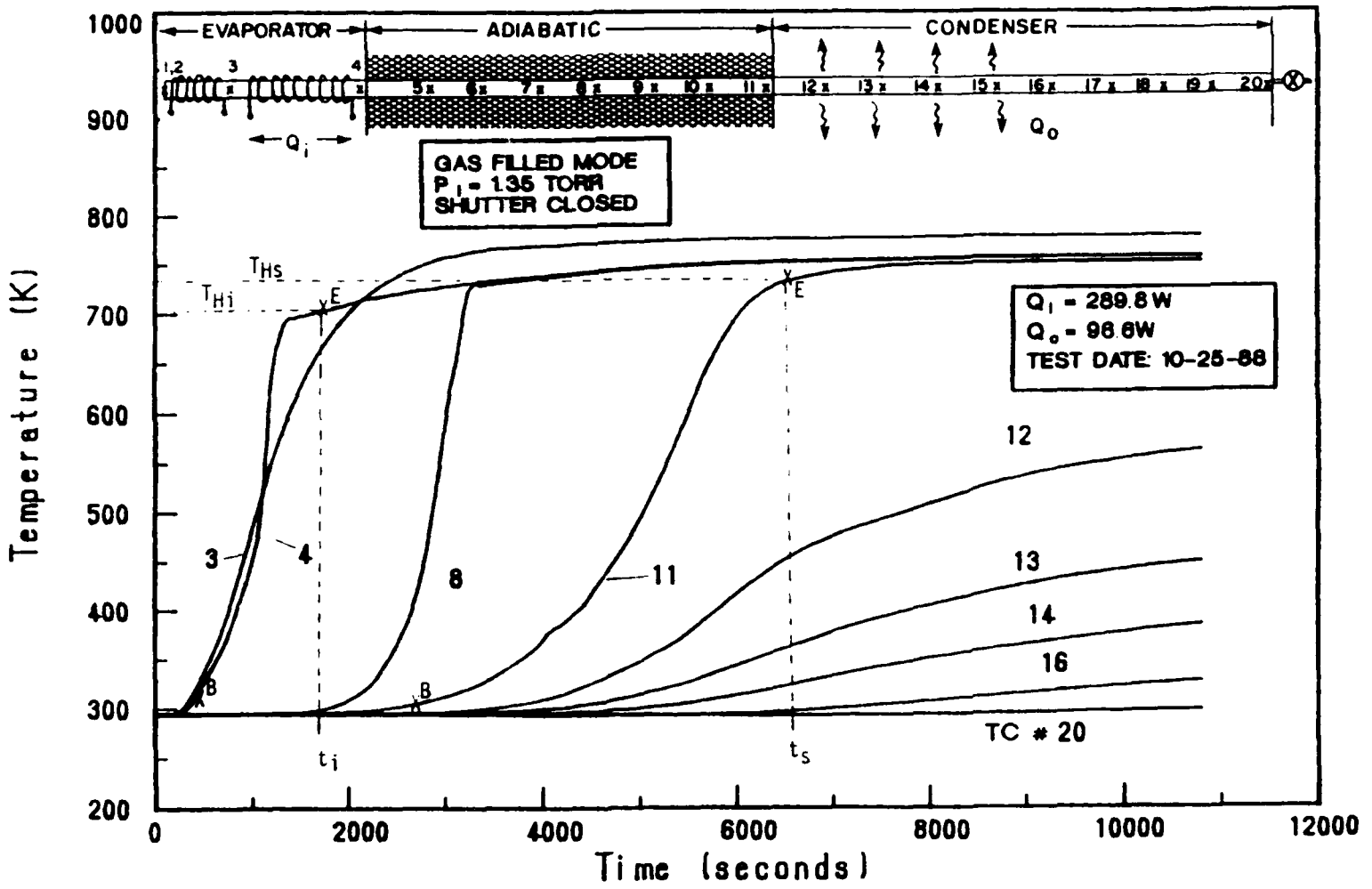

Figure 55. Transient Temperature Profiles at Specified Axial Locations T vs t for Q_o = 96.6 W

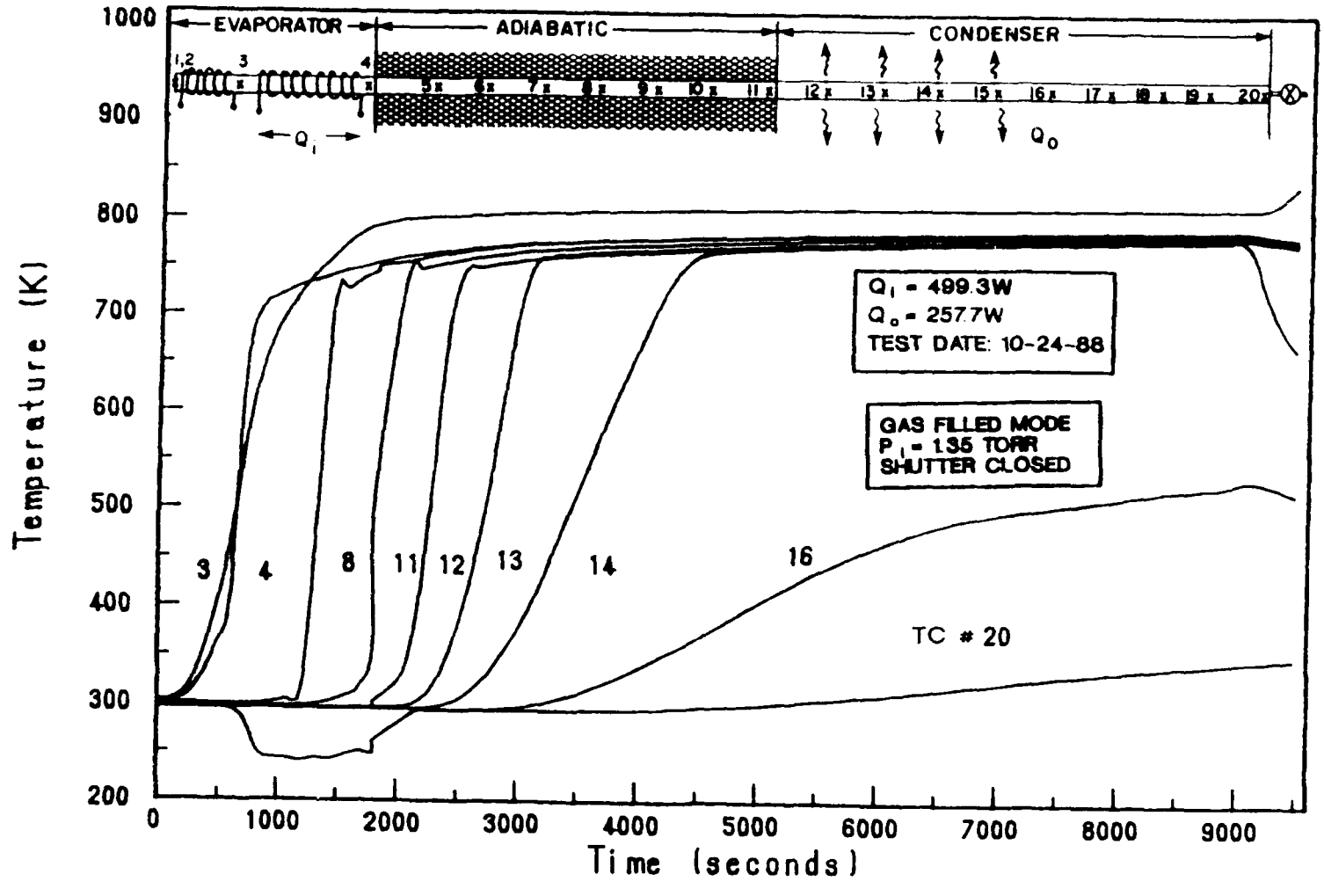

Figure 56. Transient Temperature Profiles at Specified Axial Locations T vs t for Q_o = 258 W

similar procedure applied to T.C. #11 and counting the time from the rise time. The startup temperature corresponds to the temperature T.C. #11 reached at the startup time. During startup, each T.C. location registers a sharp rise in temperature in the adiabatic zone and somewhat slow rise in the condenser zone due to the heat loss in that zone. As the beginning and the end of the heating at a T.C. location take place over a period of time, it is hard to judge the location of the hot front precisely. This gives rise to a small deviation in comparing the experimental data with the theory. This deviation is explained later in connection with the L vs t plots.

The pipe started up from the frozen state for all power inputs up to Q_i = 564 W (Q_o = 306 W) when applied as a suddenly applied load. Beyond this power level, only gradual increments of 25 W were possible. In addition, the heater operating temperature limitation (1000°C) restricted the heat input level.

Comparison of Liquid State and Frozen State Startup: The liquid state startup is faster and smoother than the frozen state startup. For a typical power input of Q_i = 564 W, these two startups were conducted. The results are shown in Figures 57 through 60. It is evident from Figure 59 that T.C. #3 registered very high temperature and the power had to be reduced slightly to continue the test. However, in the liquid state startup, there is no overshooting of temperature indicating smooth startup (Figure 60).

Hot Zone Temperature Variation: The experimental temperature variations of the hot zone are plotted for Q_o = 96.6 W, 257.7 W, and 306 W in Figures 61, 62, and 63, respectively. The experimental

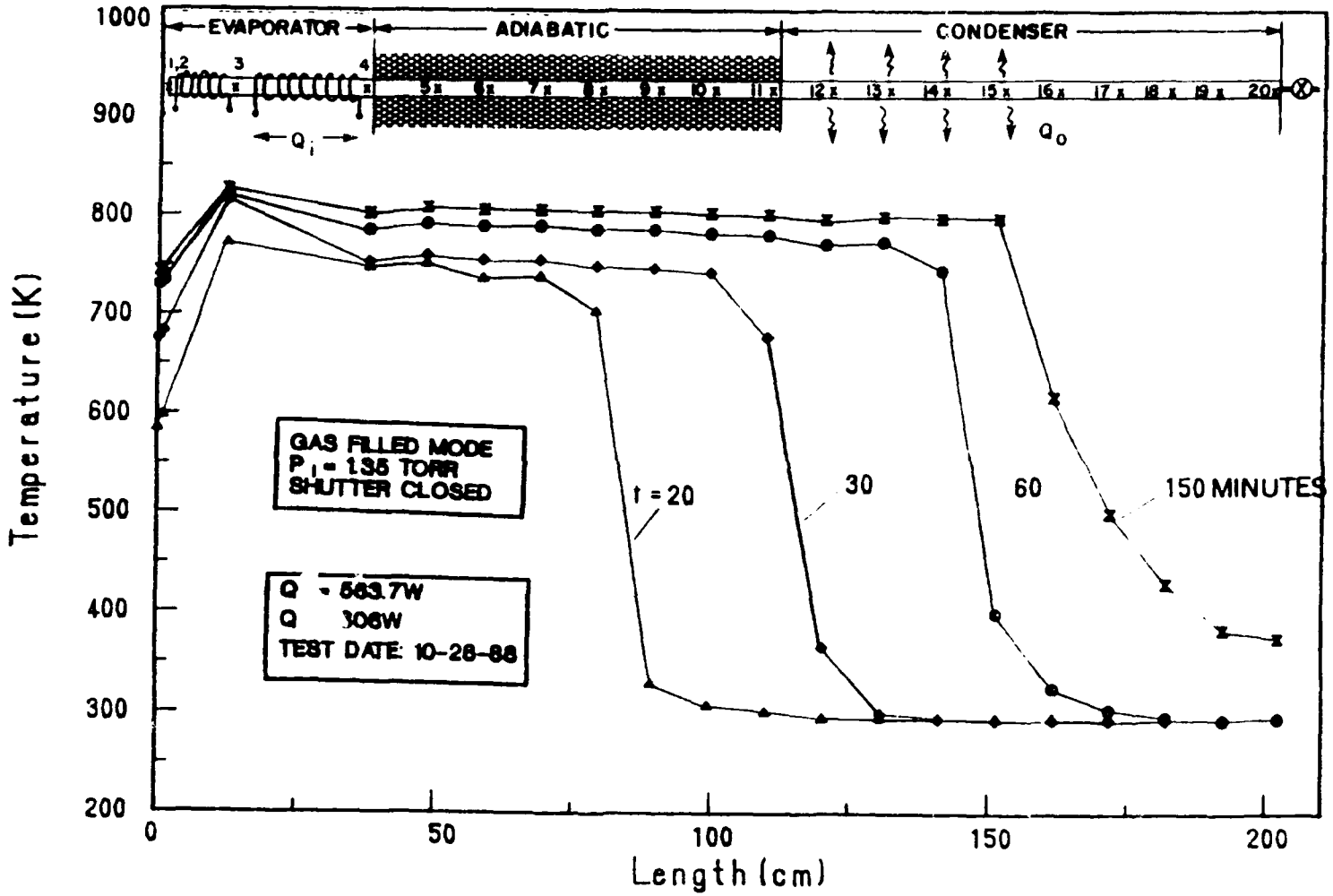

Figure 57. Comparison of Temperature Profiles for Liquid and Frozen State Startup
T vs L for Q_c = 306 w - Frozen State Startup

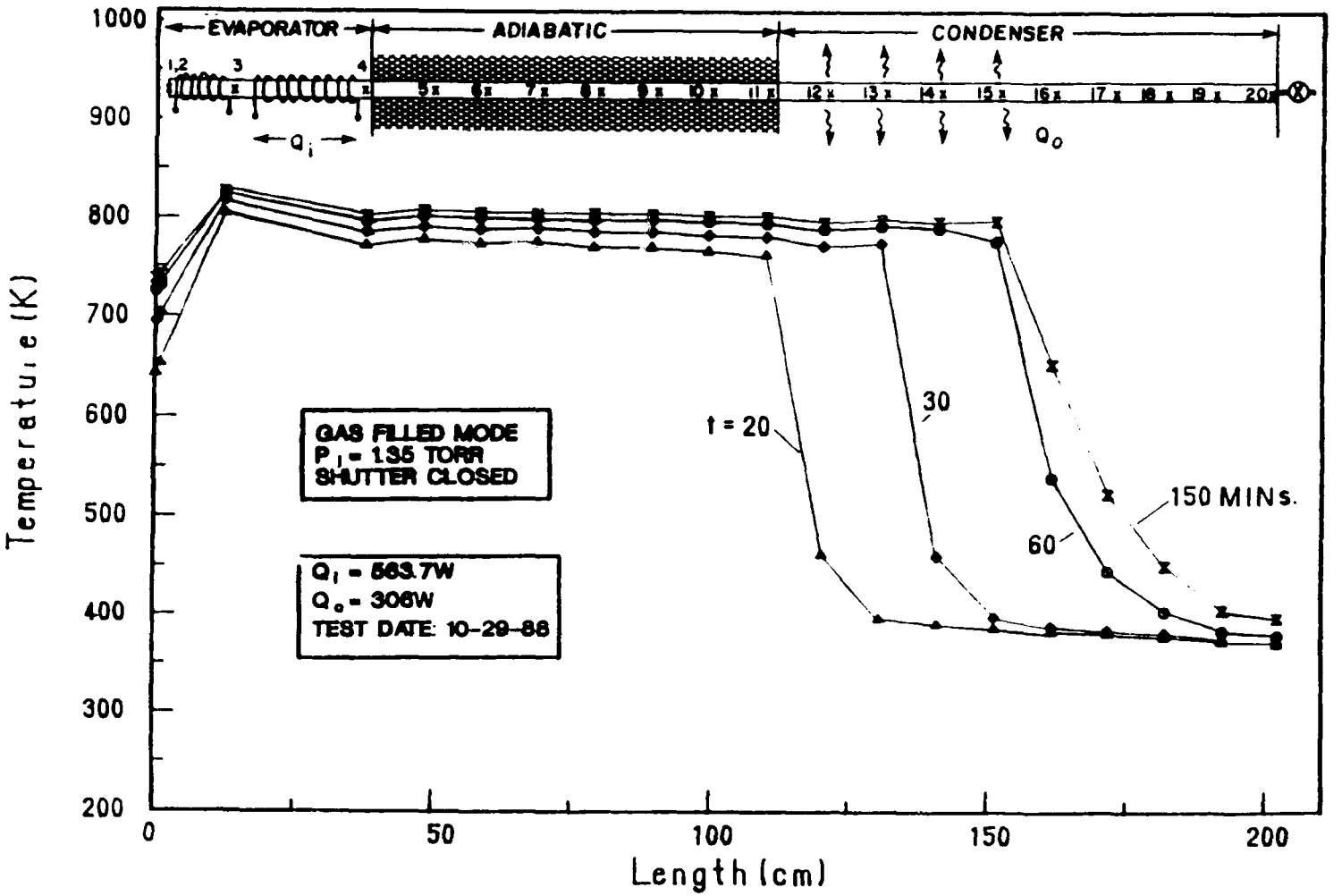

Figure 58. Comparison of Temperature Profiles for Liquid and Frozen State Startup
T vs L for Q_o = 306 W - Liquid State Startup

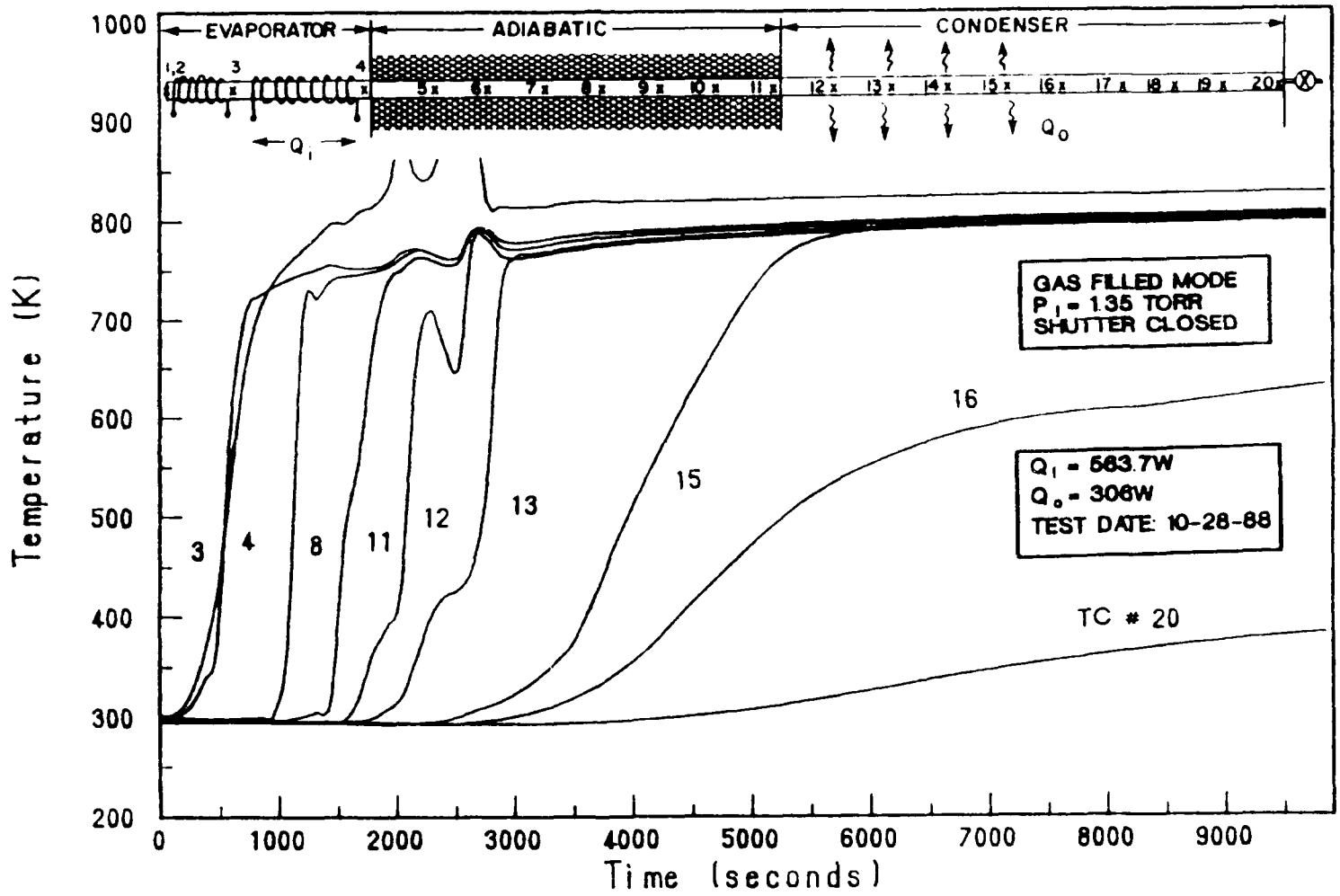

Figure 59. Comparison of Temperature Profiles for Liquid and Frozen State Startup
T vs t for Q_o = 306 W - Frozen State Startup

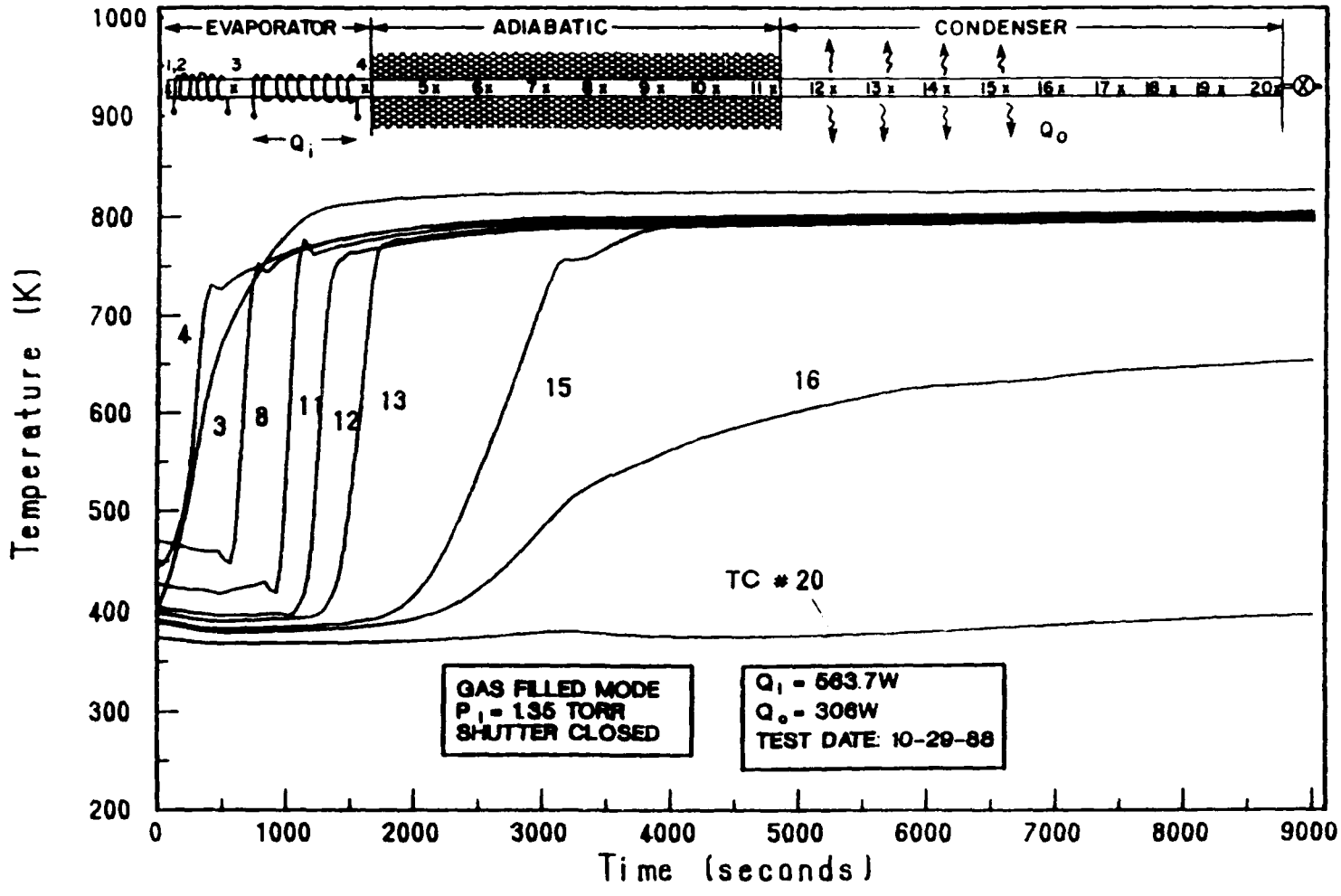

Figure 60. Comparison of Temperature Profiles for Liquid and Frozen State Startup
T vs t for Q_o = 306 W - Liquid State Startup

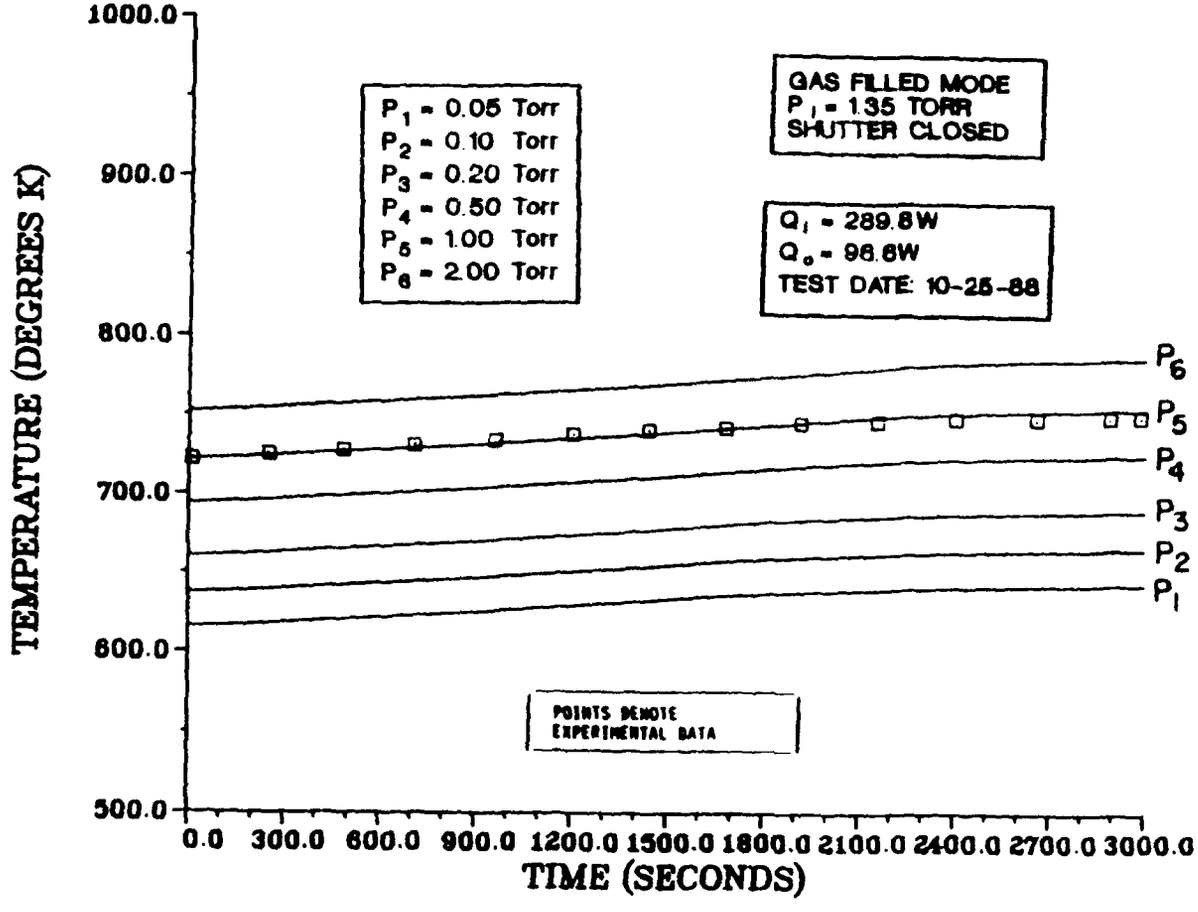

Figure 61. Hot Zone Temperature Variation During Startup T vs t for Q_O = 96.6 W

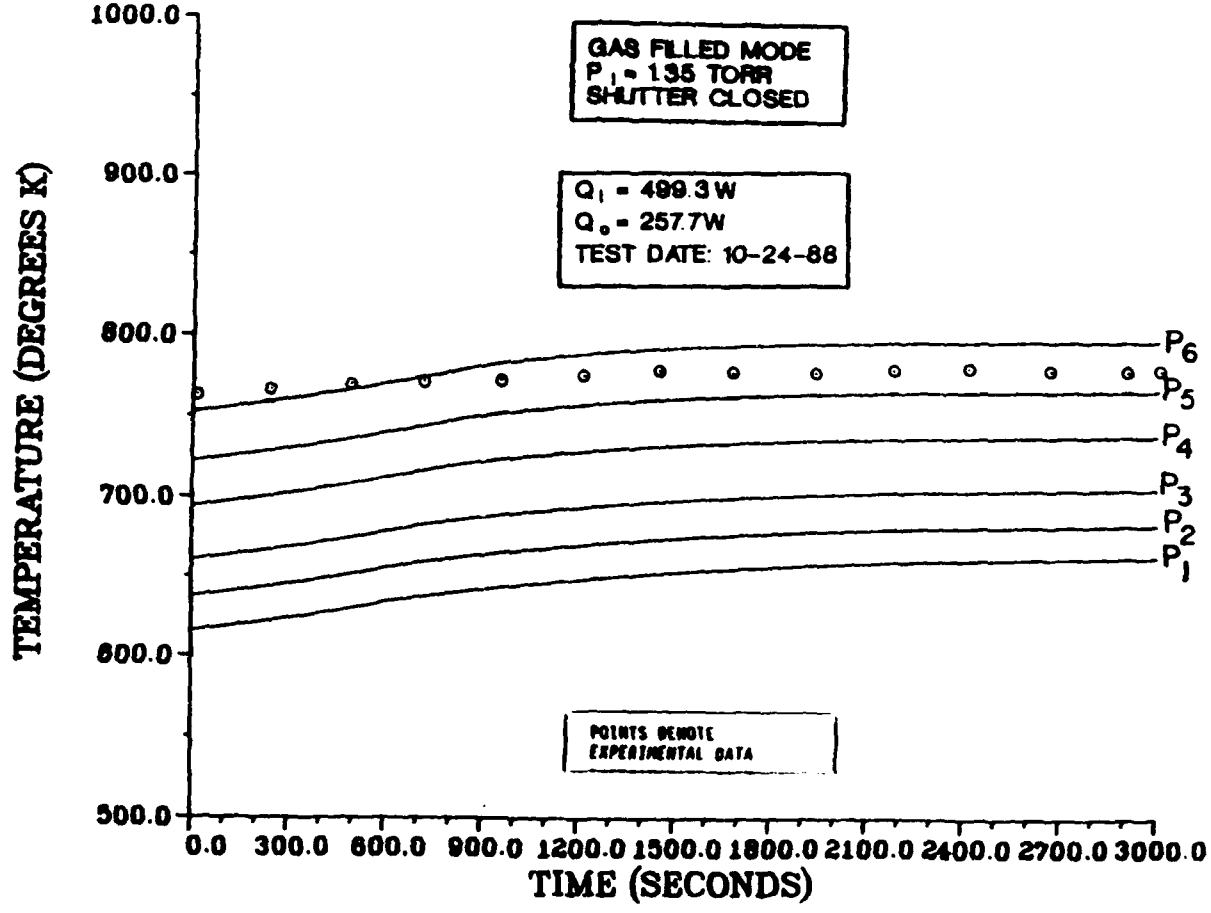

Figure 62. Hot Zone Temperature Variation During Startup T vs t for Q_0 = 257.7 W

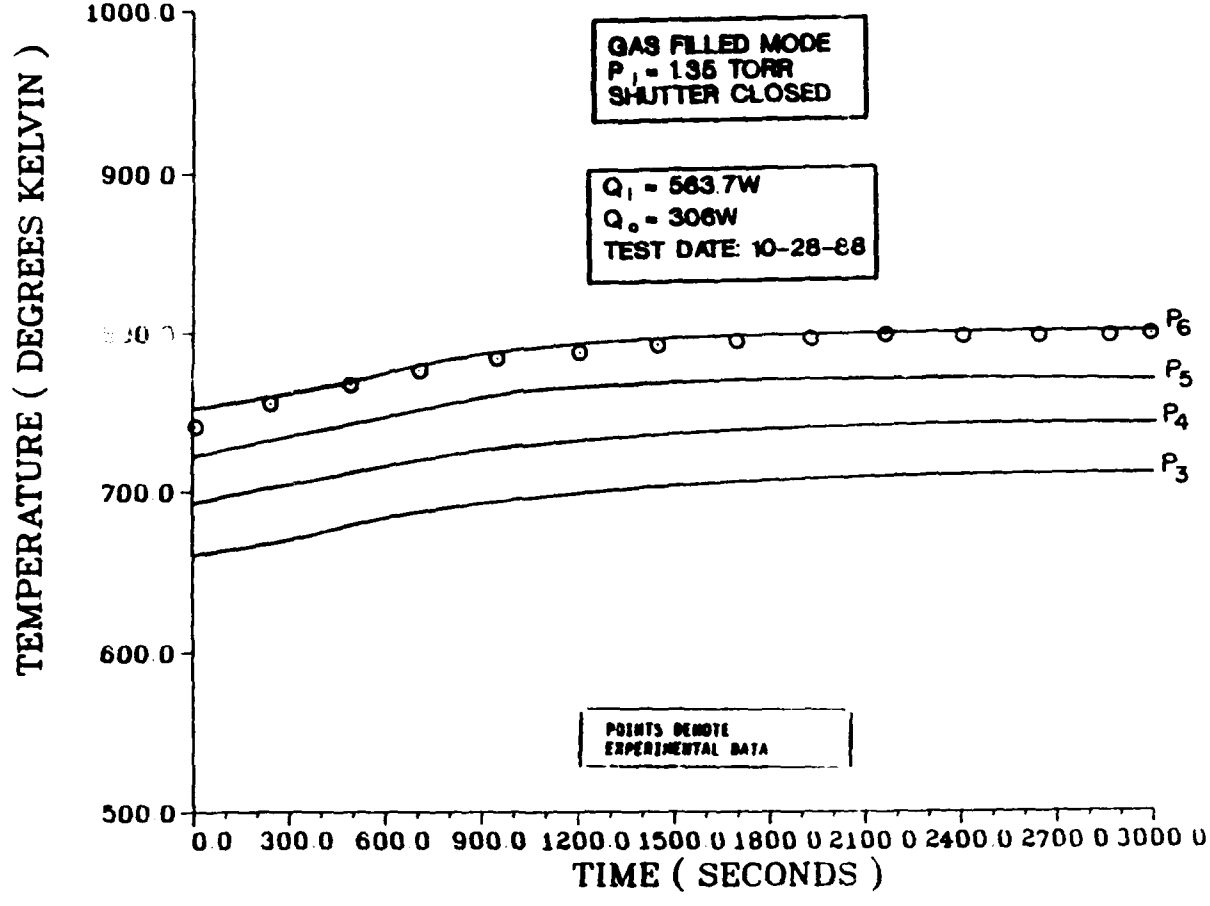

Figure 63. Hot Zone Temperature Variation During Startup T vs t for Q_o = 306 W

data very well match the theoretically calculated values. All the points lie along the P_i = 1.0 to 2.0 Torr band of the theoretical curves. In the time axis, t = 0 corresponds to the rise time, t_i. The 3000 seconds of transient test are counted after the lapse of t_i.

Hot Front Propagation: The transient experimental data for plotting the L vs t plot were processed from the two-minute scan group data recorded in the data logger/computer during the test. The raw data available in the form of degrees celcius for each thermocouple location at two-minute time intervals for 2 to 3 hours of test were processed to obtain the length versus time data. The thermocouple positions were translated into axial lengths from the evaporator end. Table 14 lists the input data used in the computer program. Since the hot front travels at varying velocities depending upon the input power and inert gas charge pressure, the heating of a particular spot along the length to the startup temperature will take a finite amount of time. The beginning of the heating process is marked by a sudden rise in temperature (designated as point "B" in Figure 55) and the ending of the heating is marked by more or less constant temperature (variation within 2 K) designated by point "E" in Figure 55. In the present work, the ending point "E" is taken as the reference to locate the hot front of the diffusing front. The "B" and "E" point designation applies to all the thermocouple positions whether the slope of the temperature profile is steep or otherwise. However, the point "E"

TABLE 14. THERMOCOUPLE POSITIONS MEASURED FROM THE END OF THE EVAPORATOR

T.C. Number	Position (cm)	T.C. Number	Position (cm)
1	0	11	109.85
2	0.79	12	120.24
3	12.22	13	130.56
4	37.62	14	140.96
5	48.02	15	151.35
6	58.26	16	161.59
7	68.58	17	171.75
8	78.81	18	181.99
9	89.21	19	192.3
10	99.45	20	202.2

will not be applicable if a particular T.C. has not reached the startup temperature.

Figures 64 through 66 show the comparison of the experimental results with the analytical predictions for Q_o = 96.6 W, 257.7 W, and 306 W, respectively. The agreement between the experimental and analytical results is good. It may be observed that the experimental curves lie along a mean theoretical curve between P_i = 1.0 and 2.0 lorr. The small deviation in each graph is attributed to the limitations of length determination (±0.05 m uncertainty) and temperature measurement (±4.5 K uncertainty).

In the l vs t plots, t = 0 corresponds to the rise time (t_i) and the 3000 seconds of transient time is not counting the rise time duration.

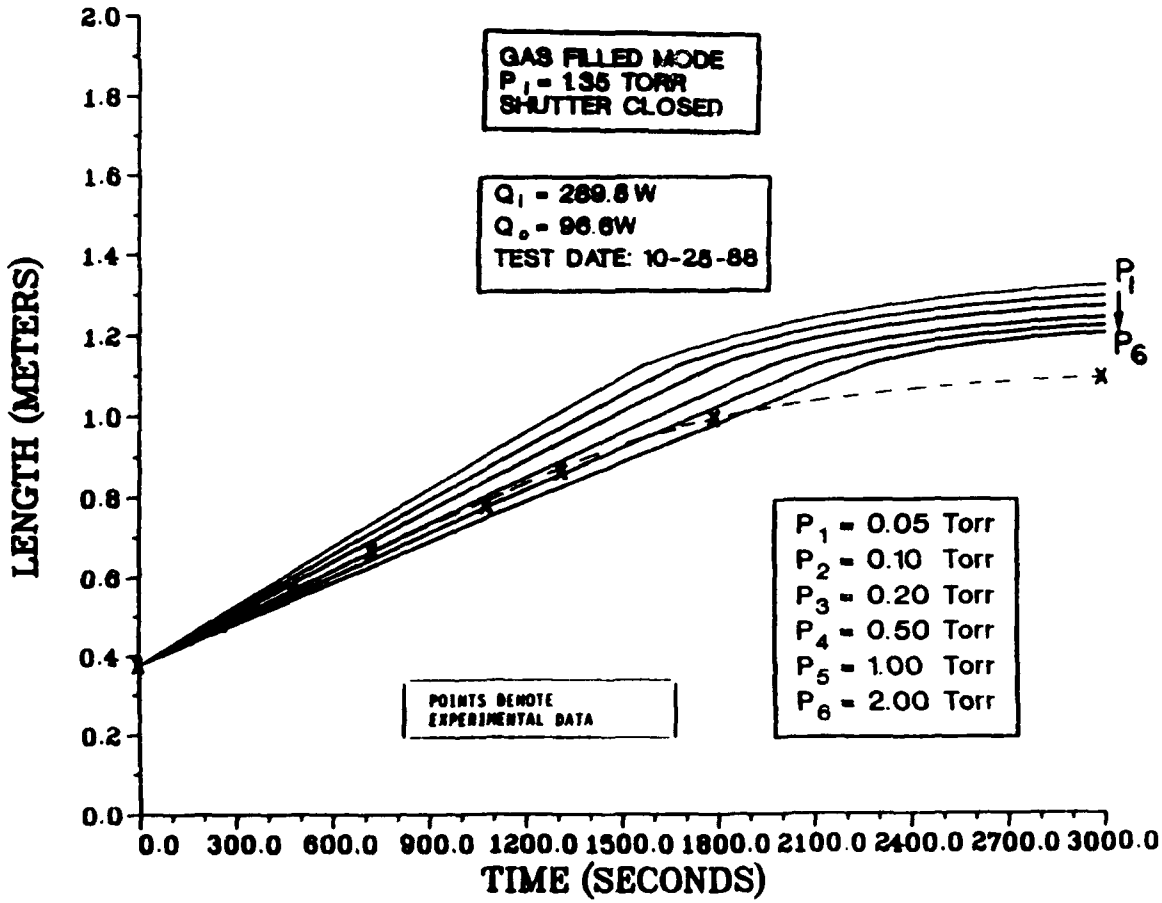

Figure 64. Hot Zone Length Variation During Startup L vs t for Q_0 = 96.6 W

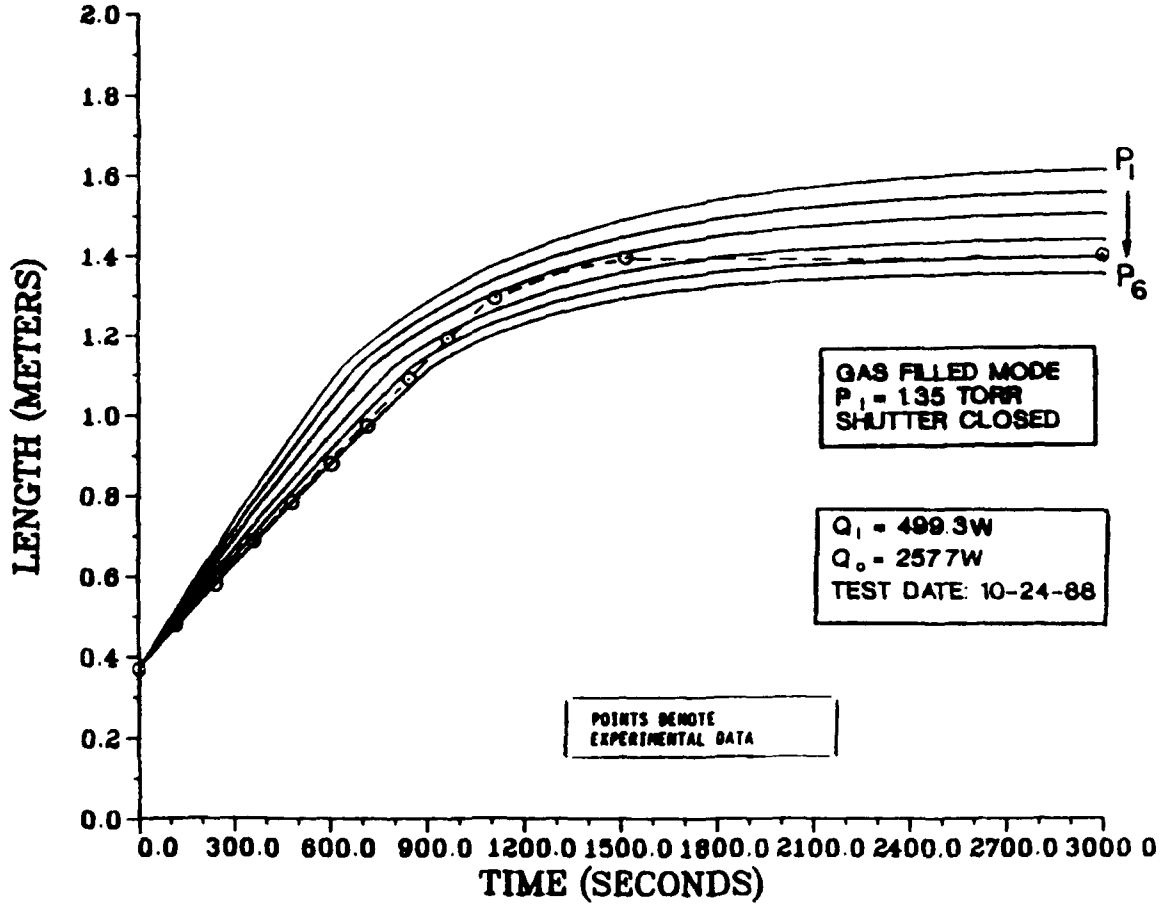

Figure 65. Hot Zone Length Variation During Startup L vs t for Q_0 = 257.7 W

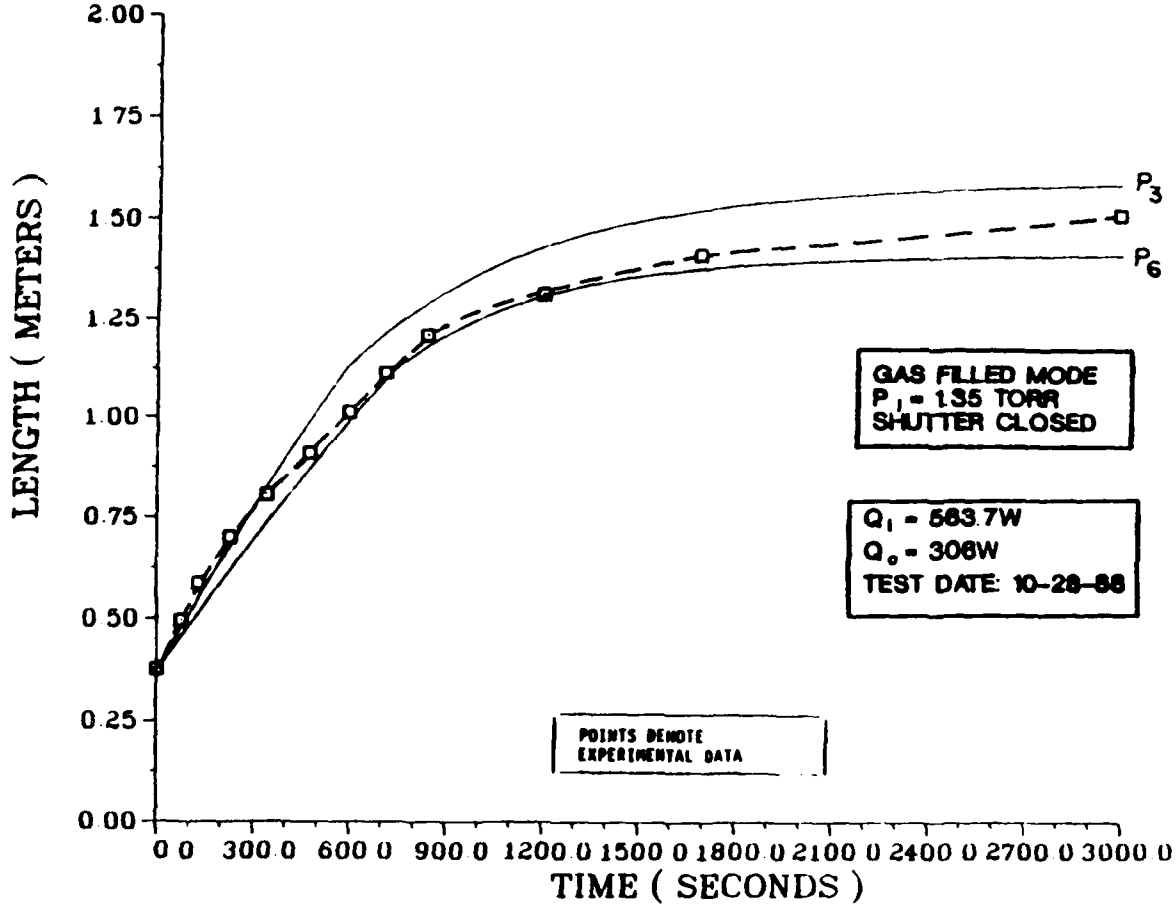

Figure 66. Hot Zone Length Variation During Startup L vs t for Q_0 = 306 W

Rise Time, Rise Temperature, Startup Time, and Startup Temperature: The experimental values for these parameters were determined from the output data for every transient test. For a typical transient test, the rise time corresponded to the time at which T.C. #4 reached the peak temperature. The power "switch on" time was considered as t = 0. As explained earlier, the point "E" (Figure 55) corresponds to the rise time. The rise time data for various power levels are listed in Table 15. With increase in power, the rise time decreased as predicted. Comparing these results with the predicted values in Table 3, it is found that the experimental values are almost twice that of the theoretical ones. The reason for this discrepancy is the unaccounted thermal mass (in the form of heater coil, thermocouples, clamps, support, etc.) attached on the evaporator length.

The rise temperature, startup time, and startup temperature data are also determined as shown in Figure 55. The heat pipe is supposed to have started successfully if the hot front has crossed T.C. #11. These three parameters are in good agreement with the predicted values as can be seen in Table 15. This table also lists the results for the location of the front in 3000 seconds after the rise time which match the predictions given in Table 3.

5.3 Experimental Uncertainty Data

The experimental data were subject to the following uncertainty in measurement due to systematic or instrumental errors.

TABLE 15. TRANSIENT STARTUP TEST RESULTS

SI No.	STARTUP PARAMETERS	TEST SET 1 P_i = 1.35 Torr		TEST SET 2 P_i = 1.35 Torr	
		Q_o (W)	STARTUP PARAMETER RESULTS		Q_o (W)
1	Rise Time, t_i (sec)	32.2	3000		
		96.6	2880	2640	96.6
		145	1920		
		257	1200	1200	241
		306	960		
2	Startup Time t_s (sec)	32.2	-		
		96.6	3000	3840	96.6
		145	1200		
		257	840	960	241
		306	840		
3	Rise Temperature T_{Hi} (K)	32.2	691		
		96.6	726	726	96.6
		145	732		
		257	732	731.5	241
		306	840		
4	Startup Temperature T_{Hs} (K)	32.2	-		
		96.6	751	757	96.6
		145	756		
		257	774	761.6	241
		306	753.3		
5	location of hot front in 3000 seconds after rise time L (cm)	32.2	59-69		
		96.6	99-110	99-110	96.6
		145	110-120		
		257	141	130-141	241
		306	141-151		

NOTE: The experimental settings for both Test Set 1 and 2 were the same except for the following:

Test Set 1: Condenser shutters closed; zircar ceramic shield over evaporator.

Test Set 2: Condenser shutters partially open; stainless steel radiation shield on the evaporator.

1. Temperature measurement using chromel alumel thermocouples:

   0-1250°C ... ±2.2°C or ±0.75% of the reading whichever is the largest.

2. Electrical power measurement through current shunt and signal conditioner:

   0 2000 W ... ±1% maximum

3. Water flow meter (rotometer type) calibration:

   0 5 liters/min ... ±0.25% maximum

4. Pressure measurement using thermocouple type convectron gage calibrated in torr of argon:

   1 999 Torr ... ±0.5%

   0 999 mTorr ... ±0.5%

All instruments were calibrated before use in the test setup. By periodic checks, it was found that the instruments maintained their calibration within specification.

CHAPTER VI

CONCLUSIONS AND RECOMMENDATIONS

6.1 Conclusions

The aspects of starting up a liquid metal heat pipe from frozen state of the working fluid have been investigated in detail, both analytically and experimentally. The idea of gas loading the liquid metal heat pipe for easy startup was recognized and explored. A vapor-gas diffusion model was developed to predict the transient startup behavior rather than the axial conduction model used in the low temperature variable conductance heat pipe (VCHP) theory. A computer code to predict the propagation of the startup front much faster than the state of the art codes in the industry has been developed. A typical run in the CDC 3600 mainframe computer took only 220 cpu seconds. Experimental results corroborate very well with the predicted results.

The project was carried out in three phases. In the first phase, called the preliminary design and analysis phase, a rough design of the 2 m stainless steel sodium heat pipe was worked out. This was followed by a lumped thermal capacity calculation based on steady state energy balance to size the length and thermal capacity parameters. The need for a 12.5 cm long reservoir wick in the evaporator to meet the fluid supply during the startup was determined. The two dimensional quasi steady state binary vapor-gas

diffusion model determined the predominantly diffusion controlled energy transport mechanism of the vapor at the diffusion front. Axial wall conduction was neglected. The key point in this model was that the hot vapor front did not move until the vapor pressure became equal to the initial charge pressure of the inert gas filled in the pipe. The one dimensional transient thermal model coupled the diffusion and the thermal problems because of the diffusive heat transfer coupling between the hot and cold zones. A computer code called SODART was written to solve the first order, nonlinear, ordinary differential equations with a set of known initial and boundary conditions. The code determined the time rate of change of hot front lengths and temperature of the hot front. The mass depletion of sodium from the evaporator by evaporation during startup was also computed in the code in order to limit the evaporator heat input from causing a dryout.

In phase two, called the detailed design and fabrication phase, a scaled down single channel artery double walled heat pipe with 2.22 cm outer diameter (1.27 cm vapor core) and 74.5 cm long adiabatic section was designed and fabricated. The pipe was capable of transporting 1800 W at 1000 K and capillary limited at high temperature and sonic limited at low temperature. The pipe was filled with 93.4 grams of sodium and 1.35 torr argon at room temperature. The pipe was instrumented and tested in a vacuum chamber for easy calorimetry and safety.

In the final phase of the study, the heat pipe was tested in vacuum and gas filled modes and the results were compared with the analytical/computational results.

In summary, the following major conclusions were reached from this study:

(1) Noncondensible gas loading of the liquid metal heat pipe helped the pipe to start easily even from frozen state. Large power inputs (>600 W), if suddenly applied, caused evaporator dryout. The gas charge pressure could be predetermined to minimize the inactive condenser length.

(2) The long adiabatic artery without a fine capillary surface did not pose any priming problem in the presence of noncondensible gas.

(3) In gas loaded mode, the heat front propagation during startup was found to be solely diffusion controlled, while in the steady state, axial conduction determined the temperature profile of the front. The axial conduction rate accounted for approximately 15 W which was only 2-10% of the condenser radiated power.

(4) The variable conductance feature would be an added benefit of the startup solution.

(5) The theoretical predictions of the rise time, rise temperature, startup time, startup temperature, heat front versus time plot, and hot zone temperature versus time plot and the experimental verification were in good agreement.

(6) The computational time required for the transient predictions was small.

(7) The unheated evaporator lengths and the reservoir wick kept the evaporator end relatively cooler than the evaporator exit.

(8) The temperature of the hot zone remained more isothermal in the gas loaded mode than in the vacuum mode. As expected, the startup from the liquid state of the working fluid was smoother compared to that from the frozen state.

(9) The steady state transport performance data followed very closely with the predicted sonic limit curve.

(10) A completely gas free mode (perfect vacuum mode) of the present heat pipe could not be achieved due to experimental setup limitations. Hence, the difficulty of frozen state startup in the vacuum mode was not demonstrated to contrast the easy gas loaded mode startup. The nicrome resistance heating was another drawback which restricted the heater temperature to less than 1000°C.

6.2 Recommendations

(1) The heater temperature limitation could be overcome by using tantalum or induction heating.

(2) The radiation shield at the adiabatic section must also be a ceramic (zircar) type for better insulation.

(3) A gas venting arrangement similar to the one used for the gas filling rig may be needed in order to vent the pipe in hot condition without losing the working fluid.

(4) The thermocouples on the pipe may have to be placed at closer intervals to determine the exact lengths of the diffusion zone during startup.

(5) The thermal capacities of the heater coil, thermocouples, and support/mounting brackets should be taken into account in the analytical calculations. Also, the heat losses in the transport section should be accounted in theory.

(6) In order to avoid lengthy iterative calculation procedure of the design section, an integrated computational approach to couple the hydrodynamics of the heat pipe into the transient analysis may be adopted.

(7) The possible follow-on tests and study should include aspects such as pulse or programmed heat loads, artery orientation, pipe tilt angle, NCG pressure variation, variable radiance, shut down tests, condenser load variation, etc.

REFERENCES

1. R. S. Gaugler, Heat Transfer Devices, U.S. Patent 2350348, 1944.

2. G. M. Grover, T. P. Cotter, and G. F. Erickson, "Structures of very High Thermal Conductivity," J. Applied Physics, Vol. 35, pp. 1190-1191, 1964.

3. T. P. Cotter, Theory of Heat Pipes, Los Alamos Scientific Laboratory, Report No. LA-3246-MS, February 1965.

4. S. W. Chi, Heat Pipe Throry and Practice: A Source Book, McGraw-Hill Book Co., New York, NY, 1976.

5. B&K Engineering Inc., Heat Pipe Design Handbook, Vol. I and II, Co-authored by P. J. Brennan, and E. J. Kroliczek, NASA Contract No. NAS-23406. NTIS No. N81-7012, June 1979.

6 P. D. Dunn and D. A. Reay, Heat Pipes, Pergamon Press, 2nd Edition, 1978.

7. ESDU, Heat Transfer, Heat Pipes, Vol. 3, Engineering Sciences Data Unit, ESDU International Inc., London, 1979.

8. M. N. Ivanovskii, V. P. Sorokin, and I. V. Yagodkin, The Physical Principles of Heat Pipes, Translated by R. Berman and G. Rice. Clarendon Press, Oxford, 1982.

9. M. A. Merrigan, "Heat Pipe Technology Issues," Space Nuclear Power Systems 1984, Vol. 2, Orbit Book Co., Malabar, FL, Edited by M. S. El Genk and M. D. Hoover, 1985, pp. 419-426.

10. R. Ponnappan and E. T. Maheikey, "Development of a Double-Wall Artery High Capacity Heat Pipe," Spacecraft Thermal Control, Design, and Operation, Progress in Astronautics and Aeronautics, Vol. 86, 1983, pp. 202-221.

11. R. Ponnappan, J. E. Beam, and E. F. Mahafkey, "Improved Double Wall Artery High Capacity Heat Pipe," J. Spacecrafts and Rockets, Vol 22, No. 6, December 1985, pp. 592-597.

12. T. P. Cotter, "Heat Pipe Startup Dynamics," 1967, Thermionics Conversion Specialist Conference, Palo Alto, CA, October 1967.

13. R. Forman and P. M. Sockol, "Re-examination of Heat Pipe Startup," 9th IEEE Annual Thermionic Conversion Specialist Conference, Miami Beach, FL, October 26-29, 1970.

14. B. D. Marcus, "Theory and Design of Variable Conductance Heat Pipes," NASA CR-2018, April 1972.

15. G. I. Fleischman and B. D. Marcus, "Steady State and Transient Performance of Hot Reservoir Gas Controlled Heat Pipes," NASA CR-73420, 1970.

16. L. K. Tower, "Theoretical Analysis of Oxygen diffusion at startup in an Alkali Metal Heat Pipe, with Gettered Alloy Walls (Oxygen Diffusion in Gettered Tantalum Alloy Heat Pipes at Startup)," NASA-TM-X-2793, May 1973.

17 P. M. Sockol, "Startup Analysis for a High Temperature Gas Loaded Heat Pipe," NASA-TM X-2840, July 1973.

18. B&K Engineering, Inc., Towson, MD, "Design and Analysis of a Cryogenic Variable Conductance Axial Grooved Heat Pipe," NASA-CR-137882, March 1976.

19. C. J. Camarda, "Analysis and Radiant Heating Tests of a Heat Pipe Cooled Leading Edge," NASA-TN D-8468, August 1977.

20. Gene T. Colwell, "Prediction of Cryogenic Heat Pipe Performance," NASA-CR-152710, 31 March 1977.

21. R. J. Williams, "Parametic Performance of a Spiral-Artery, Liquid-Trap-Diode Heat Pipe," NASA-TM-78448, October 1977.

22. M. Groll and W. D. Munzel, "Design and Development of a Heat Pipe Diode, Phase 1: Design," ESA-CR(P)-979, July 1977.

23. M. Groll and W. D. Munzel, "Design and Development of a Heat Pipe Diode, Phase 2: Development and Performance Testing," ESA CR(P) - 1134, May 1978.

24. J. Alario, "Cryogenic Thermal Diode Heat Pipes," NASA-CR-152268, February 1979.

25. R. J. Williams, "Transient Shutdown Analysis of Low-Temperature Thermal Diodes," NASA-TP-1369, March 1979.

26. M. Groll, W. D. Munzel, and W. Supper, "Development of a Liquid Trap Heat Pipe Thermal Diode," J. Spacecraft and Rockets (USA), Vol. 16, No. 4, July-August 1979.

27. K. N. Shukla, "Transient Response of a Gas Controlled Heat Pipe," AIAA Journal, Vol. 19, No. 8, pp. 1063 1070, August 1981.

28 M. Groll and W. Supper "Transient Shutdown of an Axial Groove Liquid Trap Heat Pipe Thermal Diode," Heat Transfer Sov. Res. (USA) Vol. 13, No. 6, pp. 26 33, November December 1983.

29. P. I. Bystrov, V. F. Goncharov, V. N. Kharchenko, and A. N. Shul'ts, "Transient Heat and Mass Transfer in Liquid Metal Pipes," Heat Transfer Sov. Res. (USA), Vol. 14, No. 3, pp 18 23, May June 1982.

30. P. I. Bystrov and V. F. Goncharov, "Starting Dynamics of High Temperature Gas Filled Heat Pipes," High Temperature (USA), Vol. 21, No. 6, pp. 929 936, November December 1983.

31. G. T. Colwell and W. S. Chang, "Measurements of the Transient Behavior of a Capillary Structure Under Heavy Thermal Loading," INT. J. Heat and Mass Transfer (GB), Vol. 27, NO. 4, pp. 541 551, April 1984.

32. W. S. Chang and G. T. Colwell, "Mathematical Modeling of the Transient Operation Characteristics of a Low Temperature Heat Pipe," Numer. Heat Transfer (USA) (11 Refs), Vol. 8, No. 2, pp. 169 186 1985.

33. G. T. Colwell and J. G. Hartley, "Modeling of Transient Heat Pipe Operation," NASA CR 175496, 20 February 1985.

34. J. E. Beam, "Transient heat pipe analysis, "Paper No. 85 0936, AIAA 20th Thermophysics Conference, Williamsburg, VA, June 19-21, 1985, June 1985.

35. B. A. Cullimore, "Modeling of Transient Heat Pipe Effects Using a Generalized Thermal Analysis Program," AIAA Paper 86 0938, Thermophysics Conference, 20th, Williamsburg, VA, June 19 21, 1985.

36. J. Ambrose, L. C. Chow, and J. E. Beam, "Transient Heat Pipe Response and Rewetting Behavior," AIAA Paper No. 86 1359 AIAA/ASME 4th Thermophysics and Heat Transfer Conference, Boston, MA, June 2 4, 1986.

37. D. Tilton, L. S. Chow, and F. T. Mahefkey, "Transient Response of a Liquid Metal Heat Pipe Subjected to External Thermal Loading at the Condenser." AIAA Paper No. 86 1271. AIAA/ASME 4th Thermophysics and Heat Transfer Conf., Boston, June 2 4, 1986.

38. M. A. Merrigan, E. S. Keddy, and J. T. Sena, "Transient Performance of a Space Power System Heat Pipe," AIAA-86-1273, AIAA/ASME 4th Joint Thermophysics and Heat Transfer Conference, Boston, MA, June 1986.

39. R. P. Bobco, "Variable Conductance Heat Pipes: A First Order Model," J. Thermophysics and Heat Transfer, Vol. 1, No.1, Janurary 1987, pp.35-42.

40 F. A. Costello, et al. "Detailed Transient Model of a Liquid Metal Heat Pipe," Transactions of the 4th symposium on space nuclear power systems, held in Albuquerque, NM, 12-16 January 1987, pp. 393-402.

41. M. L. Hall and J. M. Doster, "Transient Thermohydraulic Heat Pipe Modeling," Transactions of the 4th symposium on space nuclear power systems, held in Albuquerque, NM, 12-16 January 1987, pp. 307-310.

42. G. T. Colwell, J. H. Jang, and C. J. Camarda, "Modeling of Startup from the Frozen State," Proceedings of the 6th International Heat Pipe Conference, Grenoble, France, May 25-29, 1987, pp. 94-99.

43. M. S. El-Genk and J. T. Seo, "A Transient Model for Liquid Metal Heat Pipes," in transactions of the 5th Symposium on Space Nuclear Power Systems held in Albuquerque, NM, January 11-14, 1988.

44. P. F. Peterson and C. L. Tien, "Numerical and Analytical Solutions for Two-Dimensional Gas Distribution in Gas-Loaded Heat Pipes," paper to be published in J. Heat Transfer (ASME), submitted December 1987.

45. P. F. Peterson, "Diffusion and Convection of Non-Condemible Gas in Heat Pipe Condensation," Ph.D. Thesis, U. California, April 1988.

46. E. T. Mahefkey, "Military Spacecraft Thermal Management: The Evolving Requirements and Challenges," Spacecraft Thermal Control, Design, and Operation, Progress in Astronautics and Aeronautics, Vol. 86, 1983, pp. 3-16.

47. E. T. Mahefkey, "Overview of Thermal Management Issues for Advanced Military Space Nuclear Reactor Power Systems," Space Nuclear Power Systems 1984, Vol. 2, Orbit Book Co., Malabar, FL, Edited by M. S. El Genk and M. D. Hoover, 1985, pp. 405-407.

48. W. A. Ranken, "Heat Pipe Development for the Spar Space Power System," Advances in Heat Pipe Technology, Proceedings of the Fourth IHPC, September 1981, London, England, pp. 561-574, Ed. by D. A. Reay, Pergamon Press, 1982.

49. R. C. Hendricks, "Heat Transfer in Space Power and Propulsion Systems," Mechanical Engineering, February 1986, pp. 41-52.

50. E. W. Saaski, "Gas Occlusions in Arterial Heat Pipes," Thermophysics and Spacecraft Thermal Control, Progress in Astronautics and Aeronautics (AIAA), Vol. 35, 1974, pp. 353-370.

51. R. B. Bird, W. E. Stewart, and E. N. Lightfoot, Transport Phenomena, John Wiley & Sons Inc., New York, NY, 1960.

52. G. E. Forsythe, M. A. Malcolm, and C. D. Moler, Computer Methods for Mathematical Computations, Prentice-Hall, Inc., NJ 1977.

53. Marshall Sittig, Sodium-Its Manufacture, Properties and Uses, Reinhold Publishing Corp., New York, NY, 1956.

54. Nupro Manually Operated Bellows Valves, Catalog No. N-881A, Nupro Co., 4800 E. 345th Street, Willoughby, OH 44094.

55. R. Ponnappan, J. E. Beam, and E. T. Mahefkey, "Performance of the 2m DWAHP with Artery Priming Enhancements," Proceedings of the 6th International Heat Pipe Conference, Grenoble, France, May 1987, pp. 117-122.

56. C. C. Silverstein, "Surface Heat Flux for Incipient Boiling in Liquid Metal Heat Pipes," Nuclear Technology, Vol. 12, September 1971, pp. 56-62.

12511

APPENDIX A

MASS DIFFUSIVITY CALCULATION FOR SODIUM-ARGON MIXTURE

The mass diffusivity D_{AB} for binary mixtures of nonpolar gases[†] is predictable within about 5% by kinetic theory [51]. For gases A and B at low density, the Chapman-Enskog relation is given as

$$cD_{AB} = 2.2646 \times 10^{-5} \quad \frac{T(1/M_A + 1/M_B)}{\sigma_{AB}^2 \, \Omega_{D,AB}} \qquad (A.1)$$

where

c = molar density of the mixture, g-moles/cm^3

D_{AB} = mass diffusivity of the system A B, cm^2/sec

T = temperature of the system, K

M_A, M_B = molecular weight of A and B respectively, g/mole

σ_{AB} = collision diameter, Angstrom units

$\Omega_{D,AB}$ = collision integral, dimensionless function of temperature

[†]Nonpolar gases at low density have rigid, nonattracting, spherical molecules with no charge. Example: Ar, Na, Li, K. Polar gases, on the other hand, have positively and negatively charged ends and have highly elongated molecules. Example: H_2O, NH_3, CH_3OH, NOCl.

If ideal gas law is applied to this binary gas system, $c = P/RT$ where P = pressure in atm. and R is the gas constant = 82.05 cm^3 atm./g mole K, then Eq. (A.1) becomes

$$D_{AB} = 0.0018583 \frac{T^3 (1/M_A + 1/M_B)}{P \sigma_{AB}^2 \Omega_{D,AB}} \qquad (A.2)$$

In order to determine D_{AB} from Eq. (A.1) or (A.2) as a function of temperature, σ_{AB} and $\Omega_{D,AB}$ are to be found out first.

$\Omega_{D,AB}$ is a dimensionless function of the temperature and of the intermolecular potential field for one molecule of A and one of B. Tabulated values of $\Omega_{D,AB}$ are available as a function of $\kappa T/\epsilon_{AB}$, where κ is the Boltzmann's constant = 1.380 x 10^{-23} Joules/K and ϵ_{AB} is one of the Lennard Jones parameters (the other is σ_{AB}).

The Lennard-Jones (L-J) parameters σ_{AB} and ϵ_{AB} could be estimated fairly satisfactorily for nonpolar, nonreacting molecular pairs by combining the L-J parameters of species A and B empirically using the following relationships:

$$\sigma_{AB} = 1/2 (\sigma_A + \sigma_B) \qquad (A.3)$$

$$\epsilon_{AB} = \epsilon_A \epsilon_B \qquad (A.4)$$

The σ and ϵ, the collision diameter and the characteristic energy of interaction between the molecules respectively are in turn estimated from the properties of the particular fluid (gas) at the critical point.

$$\epsilon/\kappa \quad 0.77\ T_c \tag{A.5}$$

$$\epsilon = 2.44\ (T_c/P_c)^{1/3} \tag{A.6}$$

For sodium:

$$T_c = 2500\ K;\ P_c = 370 \times 10^5\ N/m^2$$
$$= 365.16\ atm.$$

$$\therefore \quad \epsilon_{Na} = 0.77\ T_c\ \kappa$$
$$= 0.77 \times 2500 \times 1.38 \times 10^{-23}$$
$$2656.5 \times 10^{-23}\ J$$

and $$\sigma_{Na} \quad 2.44\ (T_c/P_c)^{1/3}$$
$$= 2.44\ (2500/365.16)^{1/3}$$
$$= 4.6331\ \text{Å}$$

For argon:

$$T_c = 151\ K;\quad P_c = 48\ atm.$$

$$\sigma = 3.418\ \text{Å};\quad \varepsilon/k = 124\ K$$

[Note: Data taken from Table B 1 of Reference 51.]

$$\therefore \quad \varepsilon_{Ar} = 124 \times \kappa$$

$$= 124 \times 1.38 \times 10^{-23}$$

$$= 171.12 \times 10^{-23}\ J$$

and $$\sigma_{Ar} = 3.418\ \text{Å}$$

Now for the binary mixture of sodium and argon

$$\varepsilon_{AB} = \varepsilon_{Na.Ar} = \varepsilon_{Na}\,\varepsilon_{Ar}$$

$$= (2656.5 \times 10^{23} \times 171.12 \times 10^{-23})^{1/2}$$

$$= 674.225 \times 10^{23}\ J$$

$$\sigma_{AB} = \sigma_{Na.Ar} = 1/2\ (\sigma_{Na} + \sigma_{Ar})$$

$$= 1/2\ (4.6331 + 3.418)$$

$$= 4.0256\ \text{Å}$$

Table B-2 of the Reference [51] lists $\Omega_{D,Na.Ar}$ for various values of $(\kappa l/\varepsilon_{Na.Ar})$ which has a range of 0.3 to 100.

Now, in the present work, the operating temperature range is 300 K to 1200 K. $cD_{Na.Ar}$ for the sodium-argon mixture is calculated for this temperature range interpolating the values given in Table B 2 of the Reference [51]. Table A.1 gives the data thus calculated using Eq. (A.1) and used in the numerical computation of the startup analysis.

TABLE A.1. MASS DIFFUSIVITY VALUES FOR SODIUM ARGON GAS MIXTURE

T (K)	$\frac{\kappa T}{\epsilon_{Na.Ar}}$ (N.D)	$\Omega_{D,Na.Ar}$ (N.D)	$cD_{Na.Ar}$ (g-moles/cm sec)
300	0.6140	1.861	3.4035×10^{-6}
400	0.8187	1.592	4.5941×10^{-6}
500	1.0234	1.424	5.7424×10^{-6}
600	1.2281	1.309	6.8431×10^{-6}
700	1.4328	1.221	7.9241×10^{-6}
800	1.6374	1.157	8.9398×10^{-6}
900	1.8421	1.107	9.9104×10^{-6}
1000	2.0468	1.067	10.8381×10^{-6}
1100	2.2515	1.033	11.12×10^{-6}
1200	2.4562	1.005	12.6049×10^{-6}

units: $c \equiv \frac{g \text{ moles}}{cm^3}$

$D : \frac{cm^2}{sec}$

APPENDIX B

LISTING OF THE FORTRAN PROGRAM SODART, SUBROUTINES AND SAMPLE DATA INPUT

```
      PROGRAM SODART ( TAPE5,TAPE3,TAPE7,TAPE1,TAPE2,TAPE4,INPUT,OUTPUT)
C
C     THIS PROGRAM NUMERICALLY ESTIMATES THE RATE AT WHICH
C     ENERGY TRANSPORT OF VAPOR OCCURS BETWEEN THE HOT AND
C     COLD ZONES OF THE PIPE. THE VAPOR TRANSPORT IS
C     CALCULATED USING A SIMPLE MODEL OF THE STARTUP OF
C     A RADIATION - COOLED HEAT PIPE.
C
C      THIS VERSION WAS CREATED ON FEBRUARY 1988
C     IT CALCULATES PV USING A NEW CURVE FIT EQN.
C     SODIUM MASS DEPLETION DURING STARTUP IS
C        COMPUTED  IN THIS VERSION AS DELM
C
C
C     SODAR2  IS  THE CORRECTED  VERSION OF
C           SODAR1  WITH  NEWER EQUATIONS
C
C
C     ***16 FEB 1988****   THIS VERSION  STORES
C    OUTPUT DATA  IN TAPES FOR  PLOTTING ON  TEKTRONICS
C    MACHINE  WITH PLOTTER  HARD COPIER
C
C    ***15MARCH1988***  SODARTS  IS THE VERSION OF
C    SODART WITH SHORT TIME STEP AND PRINT INTERVAL
C
C     ****18MARCH1988****SODARTC REVISED VERSION OF
C     SODARTS TO INCLUDE CD AT AVERAGE TEMP.
C     OF HOT AND COLD ZONES.
C
C
C
C     REFERENCE:
C
C
C
C
      REAL L,LE,LP,MV,LI
      DIMENSION PV(10),HFG(10),CD(10),TMP(10)
      COMMON / PON1 / RW, D, LE, LP, PAI, QNORM
      COMMON / PON2 / C, MV, TC,TS
      COMMON / PON3 / GAMMA, EPSILON, SIGMA
      COMMON / PON4 / BETA1, AR, AO, PI
      COMMON / PON5 / NSET, TMP(10),HFG(10),CD(10),PV(10)
      COMMON / PON6 / QHEAT(10), QTIME(10)
      COMMON / PON7 / LI,LC,CE,CI,CC,EPSR,FHC,THETAS4,S1,S2
C
C
      REWIND 1
      REWIND 2
      REWIND 4
      REWIND 3
      REWIND 7
C
C
C
```

```
      CALL INPSUB ( Q, TFINAL )
C
C
C
      BETA1 = 2.4048255577
      ITRACK = 1
C
      TSTEP  = 0.001
      PAI    = 4.0 * ATAN ( 1.0 )
      TIME   = 0.0
      ICOUNT = 1
          TC = 300
      IRESET = 0
        NUMB = 1
      DELM = 0.0
C
C
C       NORMALIZE VARIABLES
C
      DO 20 J = 1, NSET
   20 TMP (J) = TMP (J) / TC
      PVBAR = PI * LP / ( LP - LE )
      AAA = PAI  * SIGMA * ( TC ** 3 ) / CE
      AO =  D* EPSILON * AAA
      AR = 2.0 * RW * FHC * EPSH * AAA
       L = LE
C
      CALL STARTMP ( PVBAR, THETA )
C
      ITOTAL = ITHEAT + 1
      TO=THETA*TC
      RLLE = LE * RW
      TIMSU=CE*RLLE*(TO-TC)/Q
      WRITE ( 3, 100 ) PVBAR, TO
  100 FORMAT ( //10X, * INITIAL VALUE OF PV  = *,F15.5,* BAR*,/
     +           10X, * RISE TEMPERATURE= *,F15.5,* K *)
      WRITE(3,30) TIMSU
   30 FORMAT (10X, *RISE TIME BEFORE STARTUP =*,F15.5,
     +*  SECONDS *,///)
      Q = Q / QNORM
      QTIME (ITOTAL) = TFINAL
      WRITE(3,444)
  444 FORMAT(/3X,*TIME*,6X,*HEAT FRONT*,5X,*TEMP        *,
     +6X,*G*,10X,*MASS*,9X,*QV*,12X,*QO*,12X,*QR*,/)
      DO 600 IT = 1, ITOTAL
      TFINAL = QTIME (IT)
C     Q = QHEAT(IT) / QNORM
  150 CONTINUE
      IF ( IRESET .EQ. 1000 ) TSTEP = TSTEP * 10.0
      CALL RUNGE ( THETA, L, TSTEP, TIME, Q,NUMB)
      IRESET = IRESET + 1
      IF ( TIME . GE . TFINAL ) GO TO 500
      CALL CALC ( L, THETA, G,QV,HFGBAR, QR, QO, NUMB)
C
C       DE-NORMALIZE
```

```
      QV = QV * QNORM
      DELM = DELM + ( QV/HFGBAR ) * TSTEP
      QR = QR * QNORM
       QO = QO * QNORM
      REALL = L * RW
      ADIL = (LE + LI) * RW
      TEMPR = THETA * TC
C
C
C
      IF ( ICOUNT .LT. 500 ) GO TO 165
      IF ( REALL .GT. ADIL ) DELM = 0.0
C
      WRITE ( 3, 300 ) TIME, REALL, TEMPR, G,DELM,QV, QO,  QR
  300 FORMAT (8(F10.4,3X))
      WRITE ( 1,888 ) TIME , REALL
      WRITE (2,888 )  TIME , TEMPR
      WRITE ( 4,888 ) TIME , QV
      WRITE (7 ,888 ) TIME , QO
888   FORMAT (5X, 2F15.4)
  162 CONTINUE
      ICOUNT = 0
  165 ICOUNT = ICOUNT + 1
      GO TO 150
  500 CONTINUE
      IF (IT.EQ.ITOTAL) GO TO 600
      Q = QHEAT(IT) / QNORM
      IRESET = 0
      TSTEP = TSTEP / 10.0
  600 CONTINUE
       WRITE(1,889)
       WRITE(2,889)
       WRITE(4,889)
       WRITE(7,889)
 889   FORMAT(5X,*/*,//)
      STOP
      END
C
C
      SUBROUTINE INPSUB ( Q, TFINAL )
C
      REAL LE,LP,MV, LI, LC
C
      COMMON / PON1 / RW, D, LE, LP, PAI, QNORM
      COMMON / PON2 / C,MV,TC,TS
      COMMON / PON3 / GAMMA, EPSILON, SIGMA
      COMMON / PON4 / BETA1, AR, AO, PI
      COMMON / PON5 / NSET, TMP(10), HFG(10), CD(10),PV(10)
      COMMON / PON6 / QHEAT (10), QTIME(10)
      COMMON / PON7 / LI,LC,CE,CI,CC,EPSH,FHC,THETAS4,S1,S2
C
      DO 10 I = 1,10
      QHEAT(I) = 0.0
      QTIME(I) = 0.0
      PV(I)    = 0.0
```

```
   10 CONTINUE
C
      READ (5,*) NSET
      READ (5,*) (TMP(I),I=1,NSET)
      READ (5,*) (HFG(I),I=1,NSET)
      READ (5,*) (CD (I),I=1,NSET)
C
C
C
C
      READ (5,*) RW
      READ (5,*) D
      READ (5,*) LE,LI,LC,CE,CI,CC
      READ (5,*) LP
      READ (5,*) MV
      READ (5,*) EPSILON,EPSH
      READ (5,*) SIGMA, FHC, TC, TS
C
      READ (5,*) PI,Q
      READ (5,*) ITHEAT
C
C
      IF ( ITHEAT .EQ. 0 ) GO TO 118
      DO 114 J = 1,ITHEAT
      READ (5,*) QHEAT (J), QTIME (J)
  114 CONTINUE
  118 CONTINUE
C
C
      READ (5,*)  TFINAL
C
      CALL WRITEUP ( PI, Q, TFINAL )
C
      LE = LE / RW
      LP = LP / RW
      LI = LI / RW
      THETAS = TS / TC
      QNORM = TC * CE * RW
      THETAS4 = THETAS ** 4
      S1 = CI / CE
      S2 = CC / CE
C
C
      RETURN
      END
C
C
C
C
C
C
C
      SUBROUTINE RUNGE ( TOLD, LOLD, DT, T, Q,NUMB)
C
C
```

```
      REAL L, LOLD
      DIMENSION Y(2), YDRV (4,2)
C
C
      Y(1) = TOLD
      Y(2) = LOLD
      YINC = 0.5 * DT
      DO 100 I = 1, 4
      GO TO (10, 20, 20, 30 ) I
C
   10 THETA = TOLD
      L = LOLD
      CALL DERV ( I, L, THETA, YDRV, Q,NUMB)
      GO TO 100
C
   20 THETA = Y(1) + YINC * YDRV (I-1,1)
           L = Y(2) + YINC * YDRV (I-1,2)
      CALL DERV ( I, L, THETA, YDRV, Q,NUMB)
      GO TO 100
C
   30 THETA = Y(1) + DT * YDRV (I-1,1)
           L = Y(2) + DT * YDRV (I-1,2)
      CALL DERV ( I, L, THETA, YDRV, Q,NUMB)
  100 CONTINUE
C
C
      DO 120 I = 1, 2
      SUM = Y(I)
      DO 110 J = 1, 4
      FACTOR = DT / 6.0
      IF ( J.EQ.2 .OR. J.EQ.3 ) FACTOR = DT / 3.0
  110 SUM = SUM +YDRV (J,I) * FACTOR
      Y(I) = SUM
  120 CONTINUE
      TOLD = Y(1)
      LOLD = Y(2)
      T = T + DT
      RETURN
      END
C
C
C
C
      SUBROUTINE CALC ( LENG, TEMP, G,QV,HFGBAR, QR,QO, NUMB)
C
      REAL LENG,LP,LE,LI,MV,LC
      COMMON / PON7 / LI,LC,CE,CI,CC,EPSH,FHC,THETAS4,S1,S2
      COMMON / PON1 / RW, D, LE, LP, PAI, QNORM
      COMMON / PON4 / BETA1, AR, AO, PI
      COMMON / PON2 / C,MV,TC,TS
C
      TCN = TC/TC
       TAVG = ( TEMP + TCN )/2.0
      CALL INTPOLT ( TEMP , TAVG, HFGBAR, CDBAR, NUMB)
      CALL PVCALC ( TEMP, PVBAR )
```

```
C
      PVBAR = PVBAR * 1.0E-05
C
      EXTRA1 = LP - LENG - ( LP * PI ) / PVBAR
      EXTRA2 = 1.339 + BETA1 * EXTRA1
      G = 0.0
      IF ( ABS(EXTRA2) .LT. 20 ) G = EXP (EXTRA2)
      AV = PAI * MV * CDBAR * HFGBAR  / (TC * CE )
      QV = AV * G
      QR = AR * (TEMP * * 4 - 1.0 ) * LENG
      QO = AO * ( LENG - LI - LE ) * (( TEMP**4)-THETAS4)
      IF ( LENG .LE. (LE+LI)) QO = 0.0
C
      RETURN
  999 WRITE ( 3,111 )
  111 FORMAT ( // * ########## VALUE OF LOG ( PV ) IS LARGE ##### *,/)
      STOP
      END
C
C
C
C
      SUBROUTINE DERV ( I, LENG, TEMP, YD, Q,NUMB)
C
      REAL LENG,LE,LI,LELI
      COMMON / PON1 / RW,D,LE,LP,PAI, QNORM
       COMMON / PON7 / LI,LC,CE,CI,CC,EPSN,FHC,THETAS4,S1,S2
C
      DIMENSION YD (4,2)
C
C
      CALL CALC ( LENG, TEMP, G,QV,HFGBAR ,QR,QO,NUMB )
      DENM1 = LE + S1 *(LENG - LE)
      DENM2 = LE+S1*LI+S2*(LENG-LE-LI)
      LELI = LE + LI
       QQQ = Q - QV - QR
       IF ( LENG.GT.LELI ) GO TO 20
       YD (I,1) = QQQ / DENM1
      YD(I,2) = QV/(S1*(TEMP-1.0))
      GO TO 30
   20  YD (I,1) = (QQQ-QO)/DENM2
      YD(I,2) = QV/(S2*(TEMP-1.0))
   30  CONTINUE
      RETURN
      END
C
C
      SUBROUTINE INTPOLT (  A,B, C, D, NUMB)
C
C
      COMMON / PON5 / NSET, TMP(10), HFG(10), CD(10),PV(10)
C
      IF ( A .LE. TMP(1) ) GO TO 100
      IF ( A .GT. TMP(NSET) ) GO TO 300
      I = NUMB
```

```
    5 CONTINUE
      TBEGIN = TMP (I)
      IF ( I .EQ. NSET )  GO TO 300
      TEND = TMP (I+1)
      IF ( A .LE. TEND ) GO TO 10
      I = I+1
      NUMB = I
      GO TO 5
   10 TDIFF = TEND - TBEGIN
      SLOPE = ( A - TBEGIN ) / TDIFF
      SLOPE2 = ( B - TBEGIN ) / TDIFF
      C = HFG(I) + (HFG(I+1) - HFG(I)) * SLOPE
      D = CD(I) + (CD(I+1) - CD(I)) *SLOPE2
      RETURN
  100 CONTINUE
      A = TMP(1)
      C = HFG(1)
      D = CD(1)
      RETURN
  300 CONTINUE
      WRITE ( 3,111 ) A
  111 FORMAT (//3X,* ######### ERROR ############ *,
     +          /3X,* # TEMPERATURE IS OUT OF     # *, /
     +           3X,* #  RANGE OF THE TABLE      # *,/
     +           3X,* ################################ *,/)
      STOP
      END
C
C
C
      SUBROUTINE WRITEUP ( PI, Q, TFINAL )
      COMMON / PON1 / RW, D, LE, LP, PAI, QNORM
      COMMON / PON3 / GAMMA, EPSILON, SIGMA
      COMMON /PON2 /C,MV,TC,TS
      COMMON / PON5 / NSET, TMP(10), HFG(10), CD(10),PV(10)
      COMMON / PON6 / QHEAT(10), QTIME(10)
      COMMON / PON7 /LI,LC,CE,CI,CC,EPSH,FHC,THETAS4,S1,S2
C
      WRITE (3,111)
  111 FORMAT ( ////5X,* ------   STARTUP ANALYSIS    ------ *,/5X,
     +                 * ---  FOR A HIGH - TEMPERATURE ----- *,/5X,
     +                 * ----  GAS - LOADED HEAT PIPE   ---- *,////)
C
C
       WRITE (3,112)
  112  FORMAT (///5X,*   INPUT  DATA  LIST  :    *,///)
C
C
       WRITE (3,777 ) RW,D,LE,LI,LP,CE,CI,CC,MV,SIGMA
  777  FORMAT (/3X,* INSIDE RADIUS OF WICK   = *,F15.5,* M *,
     +         /3X,* PIPE OUTSIDE DIAMETER     = *,F15.5,* M *,
     +         /3X,* LENGTH OF EVAPORATOR      = *,F15.5,* M *,
     +         /3X,* LENGTH OF INSULATED SECTION   = *,F15.5,* M *,
     +         /3X,* LENGTH OF HEAT PIPE       = *,F15.5,* M *,
     +         /3X,* HEAT CAPACITY PER UNIT EVAP.LENGTH=*,F15.5,* J/M-K*,
```

```
     +        /3X,* HEAT CAPACITY PER UNIT ADIA LENGTH =*,F15.5,* J/M-K*,
     +         3X,* HEAT CAPACITY PER UNIT COND LENGTH =*,F15.5,* J/M-K*,
     +         /3X,* MOLECULAR WEIGHT OF VAPOR = *,F15.5,
     +         /3X,* STEFAN-BOLZMANN CONSTANT = *,E15.5,* W/SQ CM-K^4*,/)
C
      DO 220 I=1,NSET
      TEMP = TMP(I)/ TC
      CALL PVCALC (TEMP , PVBAR )
      PVBAR = PVBAR * 1.0E-05
      PV(I) = PVBAR
220   CONTINUE
C
C
      WRITE (3,222) TMP,PV,HFG,CD
  222 FORMAT(/3X,*TEMP. K  =*,10F12.4/3X,*PV BAR  = *,
     +10E12.4/3X,*HFG J/G = *,10F12.4/1X,*CD G-M/CM-S=*,
     +10E12.4///)
C
      WRITE (3,333) PI,Q,EPSILON,EPSH,FHC,TC,TS,ITHEAT,TFINAL
  333 FORMAT (3X,* INITIAL NCG CHARGE PRESSURE      = *,F15.5,* BAR *,
     +        /3X,*   HEAT INPUT  TO EVAPORATOR     =*,F15.5,* W *,
     + /3X,* EMISSIVITY OF CONDENSER WALL = *,F15.5,
     + /3X,*EMISSIVITY OF HOT ZONE INNER WALL =*,F15.5,
     + /3X,* SHAPE FACTOR OF HOT TO COLD ZONE =*,F15.5,
     + /3X,* AMBIENT TEMPERATURE            =*,F15.5,* K *,
     + /3X, * COLD SHROUD TEMP. AT COND.ZONE =*,F15.5,* K *,
     + /3X, * NUMBER OF HEAT INCREMENT STEPS =*,F15.5,
     + /3X,* SOLUTION  END TIME      = *,F15.5,* SECONDS*,///)
C
      WRITE(3,443)
  443 FORMAT (//10X, * OUTPUT  DATA :    *,//)
      RETURN
      END
C
C
      SUBROUTINE PVCALC (TIN,PVOUT )
C
      COMMON / PON2 /C,MV,TC,TS
C
      TIN = TIN*TC
      TSQ =TIN ** 0.5
      TD = 5567.0/TIN
      COEF = 2.29E+11
      TD = COEF/(10.0**TD)
      PVOUT = TD/TSQ
      TIN = TIN/TC
      RETURN
      END
C
C
C
      SUBROUTINE STARTMP ( PVBAR, THETA )
      COMMON / PON2 / C, MV, TC,TS
C
C
```

```
      TINC =  0.2
      ERRLMT = 0.001
      TOLD =  5./3.
      ITER = 0
   10 CONTINUE
      CALL PVCALC ( TOLD, PVOLD )
      PVOLD = PVOLD * 1.0E-05
      IF ( PVOLD .GT. PVBAR ) GO TO 20
      ITER = ITER + 1
      TOLD = TOLD + TINC
      GO TO 10
   20 ERR = ( PVBAR- PVOLD ) / PVBAR
      ERR = ABS ( ERR )
      IF ( ERR .LE. ERRLMT ) GO TO 30
      ITER =ITER + 1
      TOLD = TOLD -TINC
      TINC = TINC / 10.0
      IF (ITER .GE. 100) GO TO 222
      GO TO 10
   30 THETA = TOLD
      RETURN
  222 WRITE 333
  333 FORMAT (/2X,* INITIAL TEMPERATURE DID NOT CONVERGE *)
      STOP
      END
```

INPUT DATA

```
 10
 300,400,500,600,700,800,900,1000,1100,1200
4600,4550,4474,4401,4322,4234,4139,4040,3949,3847
3.4035E-06,4.5941E-6,5.7424E-6,6.8431E-6,7.9241E-6,8.9398E-6,9.9104E-6,
10.8381E-6,11.7412E-6,12.6049E-6,
.00635,.022225,.375,.745,.910,.911,.717,.598,.934,.886,.340,2.03,23,.66,.1,
5.6696E-8,.01159,300,300,66,661E-5,250,0,3000
END OF FILE
```

APPENDIX C

SELECTED PROPERTY DATA FOR SODIUM

Atomic number	11
Atomic weight	23
Specific heat ratio	1.67
Melting point	370.83 K
Boiling point	1152.2 K
Critical temperature	2500 K
Critical pressure	370×10^5 N/m^2

Density:

Solid at 294 K	0.9684 g/cm^3
Solid at 370.83 K	0.9514 g/cm^3
Liquid at 370.83 K	0.0270 g/cm^3
Liquid at 1150 K	0.740 g/cm^3

Ditchburn and Gilmour relation for vapor pressure [51]:

$$p_v = 2.29 \times 10^{11} (T^{-0.5})(10^{-5556/T})$$

where p_v is in N/m^2 and T in degrees Kelvin.

Temperature (K)	P_v (N/m^2)	h_{fg} (J/g)
300	0.3670×10^{-8}	4600
400	0.1385×10^{-3}	4550
500	0.1522×10^{-1}	4474
600	0.4925×10^{1}	4401
700	0.9648×10^{2}	4322
800	0.8903×10^{3}	4234
900	0.4979×10^{4}	4139
1000	0.1963×10^{5}	4040
1100	0.6001×10^{5}	3949
1200	0.1511×10^{6}	3847

Heat capacity (C_p) at 97.83°C: Solid: 1.3642 kJ/kg K
Liquid: 1.3850 kJ/kg K

(Nearly constant in the range 25-1125°C)

Prandtl Number (liquid): 0.011 0.004
(100 700°C)

Maximum liquid transport: 2.3×10^{12} W/m^2 at 600°C
factor ($\rho_\ell \lambda \sigma_\ell / \mu_\ell$)
or merit number

APPENDIX D

ULTIMATE TENSILE STRENGTH OF SEVERAL SOLID MATERIALS

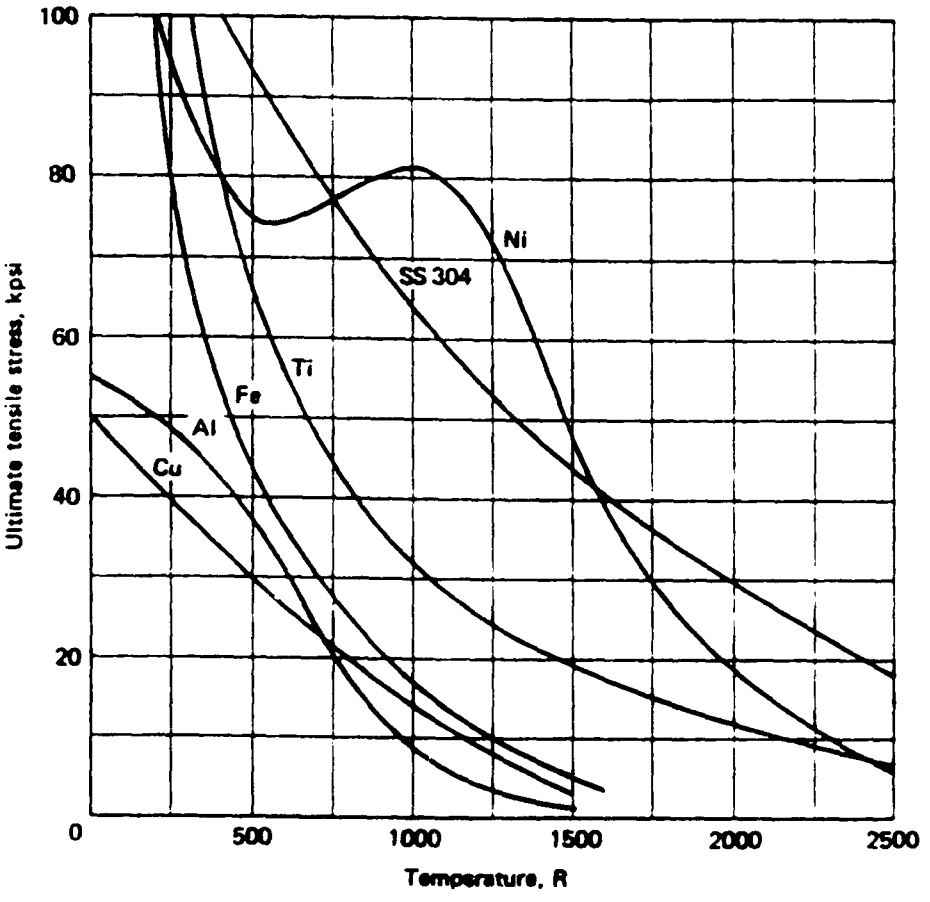

Ultimate Tensile Strength of Several Solid Materials.
(1 deg R = 0.5556 K, 1 kspi = 6.895 x 10^6 N/m^2)
[Reproduced from Reference 4.]

APPENDIX F

DESIGN CHART FOR HEAT PIPE CONTAINER TUBES

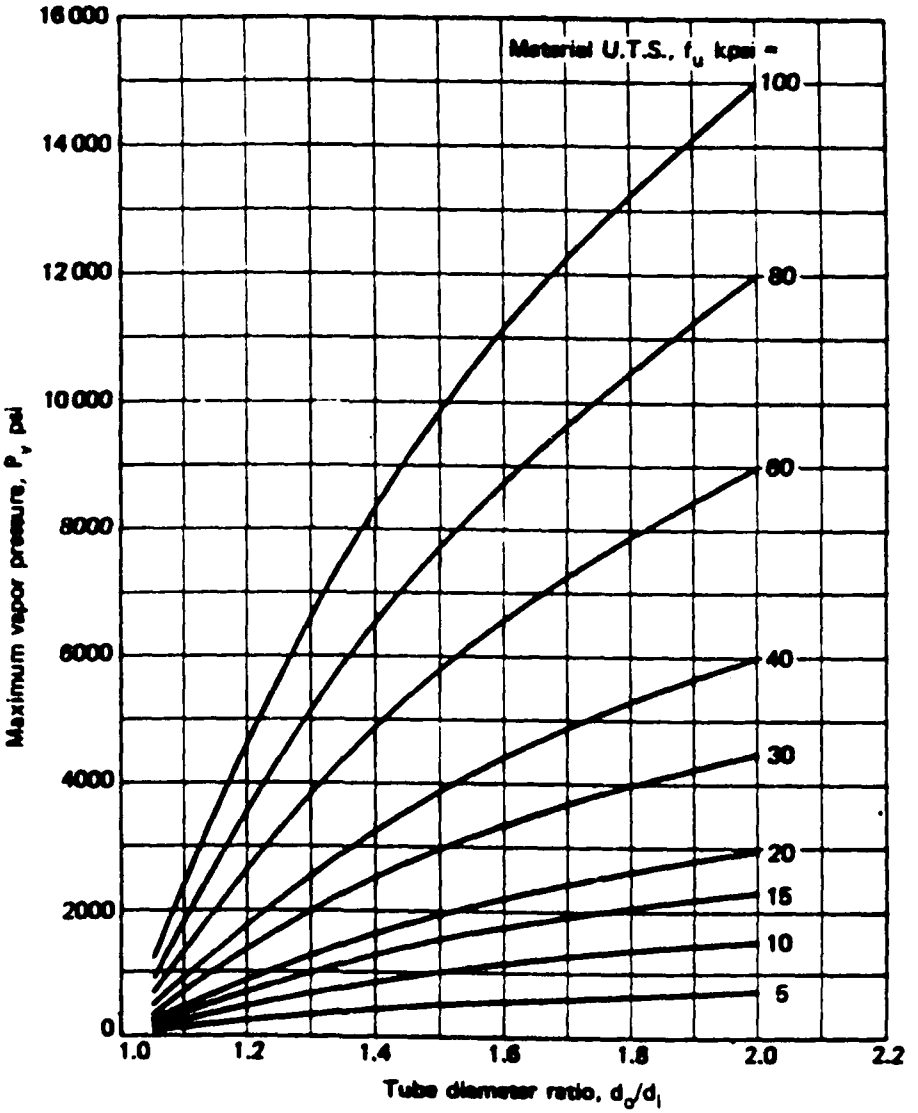

Design Chart for Heat Pipe Container Tubes.
(1 psi $\quad 6.95 \times 10^3$ N/m^2, 1 kpsi $\quad 6.895 \times 10^6$ N/m^2)
[Reproduced from Reference 4.]

APPENDIX F

DESIGN CHART FOR HEAT PIPE END CAPS

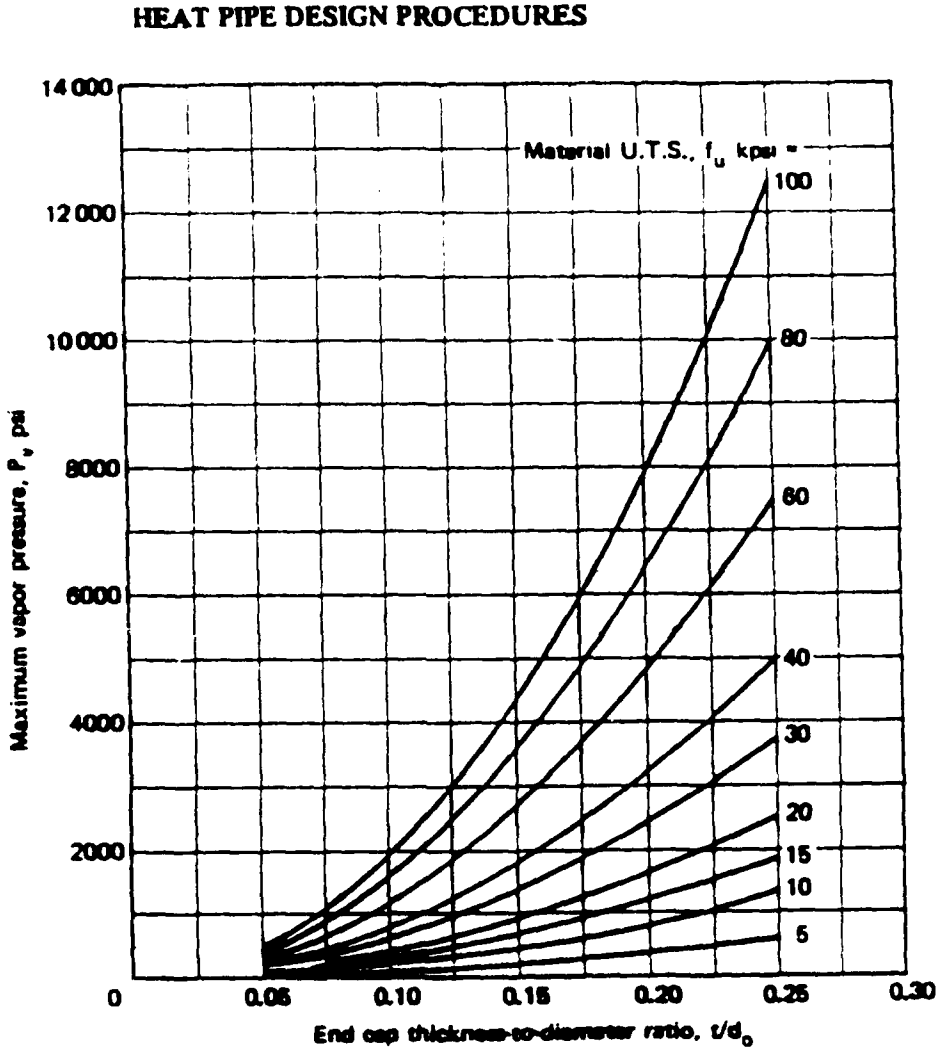

Design Chart for Heat Pipe End Caps.
(1 psi = 6.895×10^3 N/m^2, 1 kpsi = 6.895×10^6 N/m^2)
[Reproduced from Reference 4.]

APPENDIX G

RESISTANCE MODEL FOR LIQUID FLOW IN THE DWAHP

The liquid flow resistance network is sketched in Figure G.1.

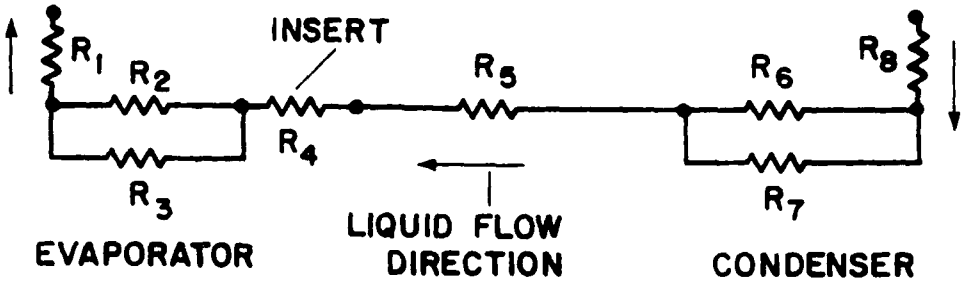

Figure G.1

Definition

R_1 = Radial flow resistance through 4 layers of 40 x 40 cm^{-1} screen wick in evaporator.

R_2 = Axial flow resistance in the evaporator screen tube.

R_3 = Axial flow resistance in evaporator grooves.

R_4 = Axial flow resistance in capillary insert.

R_5 = Axial flow resistance in adiabatic groove.

R_6 = Axial flow resistance in condenser screen tube.

R_7 = Axial flow resistance in condenser grooves.

R_8 = Radial flow resistance in condenser screen tube.

$$R_1 = F_\ell \Delta r = \frac{\Delta r \ln(d_o/d_i)}{2\pi K_s L_E \Delta r} \left(\frac{\nu_\ell}{\lambda}\right) \qquad (G.1)$$

With $d_o = 1.89$ cm, $d_i = 1.71$ cm, $k_s = 1.9342 \times 10^{-10}$ m^2, $L_E = 0.33$ m and $\Delta r = 0.091$ cm

$$R_1 = 2.5343 \times 10^{8} \left(\frac{\nu_\ell}{\lambda}\right) \quad N/m^2 \text{ per watt}$$

$$R_2 = \frac{L_E/2}{k_s A_s} \left(\frac{\nu_\ell}{\lambda}\right) \qquad (G.2)$$

The cross-sectional area (A_s) used here is 1/12th of the total screen tube area in order to account for 2 out of 24 grooves in the evaporator. $A_s = 0.04311 \times 10^{-4}$ m^2.

$$R_2 = 197.878 \times 10^{12} \left(\frac{\nu_\ell}{\lambda}\right) \quad N/m^2 \text{ per watt}$$

$$R_3 = \frac{L_E/2}{k_g A_g} \left(\frac{\nu_\ell}{\lambda}\right) \qquad (G.3)$$

Mean radius of grooves (Figure G.2),

$$r_m = \frac{d_o}{2} - \frac{\delta}{2}$$

$$= \frac{1.71. - 0.14}{2} = 0.785 \text{ cm}$$

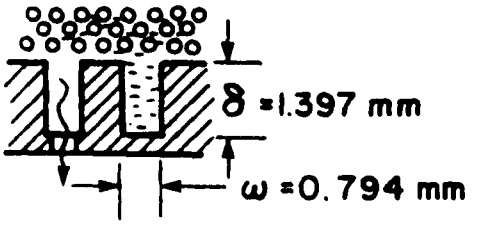

Figure G.2

Porosity, $\varepsilon = \frac{nw}{(2\pi_m r)/12}$ $n = 1$ (assume flow through single groove only)

$= 0.1931$ (19.31%)

Hydraulic radius, $r_{h,\ell} = \frac{w\delta}{w+\delta} = 0.5063 \times 10^{-3}$ m

Permeability, $k_g = \frac{2\varepsilon r_{h,\ell}^2}{f_\ell Re_\ell}$

For $w/\delta = 0.568$ and laminar flow, $f_\ell Re_\ell = 15.5$ from Figure G.3.

$\therefore$ $k_g = 0.6325 \times 10^{-8}$ m^2

$A_g = \frac{2\pi r_m \delta}{n} = 0.05742 \times 10^{-4}$ m^2

$\therefore$ $R_3 = 4.5432 \times 10^{12} \left(\frac{\nu_\ell}{\lambda}\right)$ N/m^2 per watt

$$R_4 = \frac{L_I}{K_I A_I} \left(\frac{\nu_\ell}{\lambda}\right) \qquad (G.4)$$

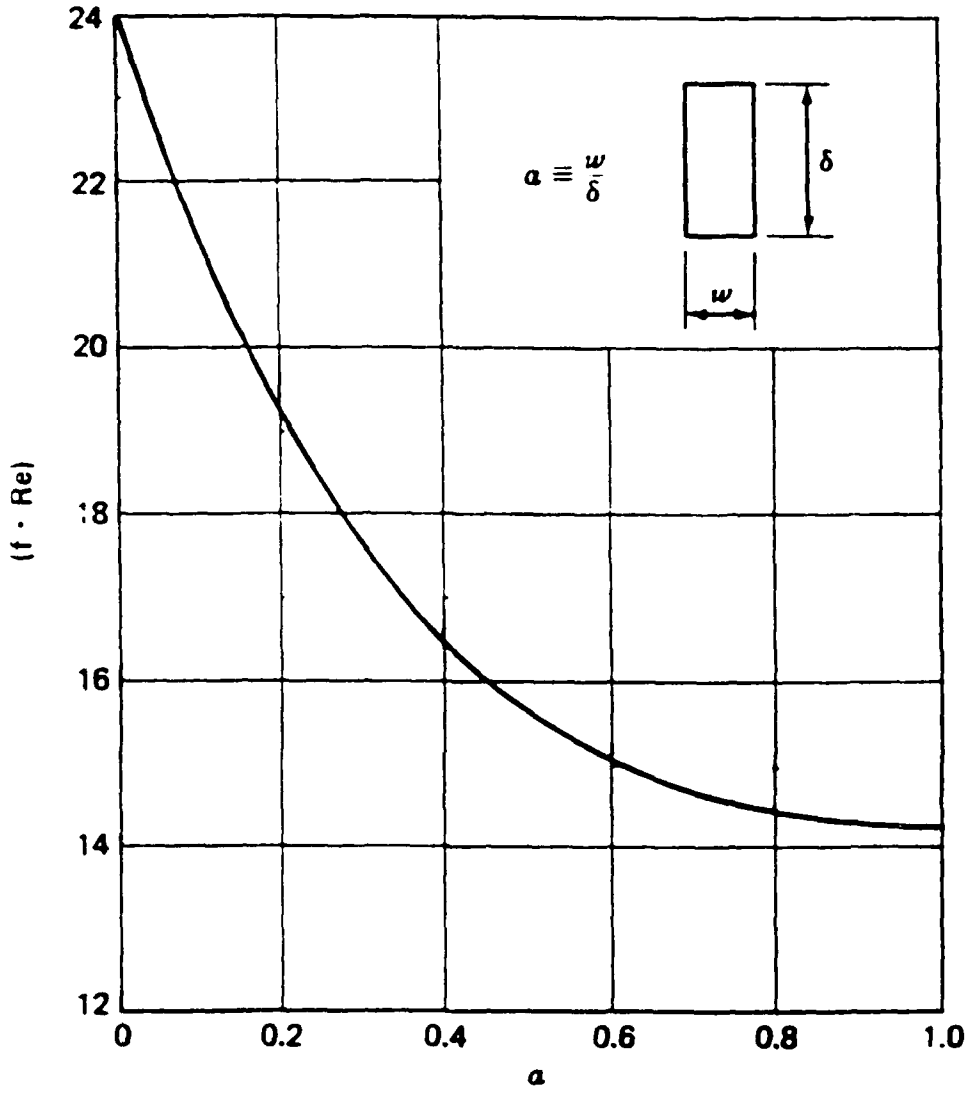

Figure G.3

Frictional Coefficients for Laminar Flow in Rectangular Tubes.
[Reproduced from Reference 4.]

$L_I = 0.0127m$, $K_I = 6.1432 \times 10^{-10}\ m^2$ for 24 x 24 cm^{-1} screen and $A_I = A_G = 5.67 \times 10^{-6}\ m^2$ for one groove.

$$R_4 = 3.3215 \times 10^{12} \left(\frac{\nu_\ell}{\lambda}\right) \quad N/m^2 \text{ per watt}$$

$$R_5 = \frac{L_A}{K_G A_G} \left(\frac{\nu_\ell}{\lambda}\right) \tag{G.5}$$

$L_A = 0.79$ m, $K_G = 1.1115 \times 10^{-7}\ m^2$ for 2.38 mm square groove using $f_\ell Re_\ell = 14.25$ (Figure G.3) if $w/\delta = 1$ and $r_{h,\ell} = \delta/2$ in the permeability equation, and $A_G = 5.67 \times 10^{-6}\ m^2$ for one groove (Figure G.4).

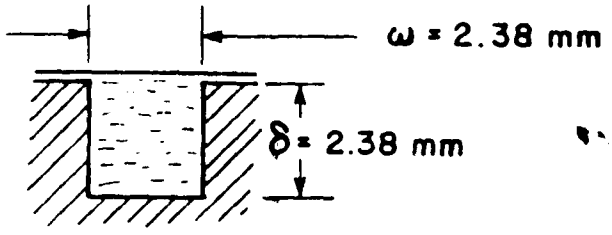

Figure G.4

$$\therefore \quad R_5 = 1.2528 \times 10^{12} \left(\frac{\nu_\ell}{\lambda}\right) \quad N/m^2 \text{ per watt}$$

$$R_6 = \frac{L_C/2}{K_s A_s} \left(\frac{\nu_\ell}{\lambda}\right) \tag{G.6}$$

The condenser screen and groove geometry is the same as that of the evaporator except the length. Here, $L_c = 0.91$ m, $K_s = 1.9342 \times 10^{-10}$ m^2 and A_s is same as in R_1.

$$\therefore \quad R_6 = 545.6635 \times 10^{12} \left(\frac{\nu_\ell}{\lambda}\right) \quad N/m^2 \text{ per watt}$$

$$R_7 = \frac{L_c/2}{K_g A_g} \left(\frac{\nu_\ell}{\lambda}\right) \tag{G.7}$$

Mean radius of grooves shown in Figure G.5 (same as in R_3)

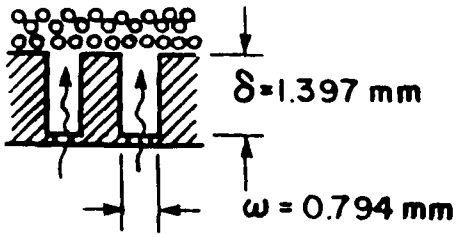

Figure G.5

$$r_m = 0.785 \text{ cm}$$

Porosity, $\varepsilon = \dfrac{nw}{(2\pi r_m)/12}$ $\quad n = 2$ (Effectively two condenser grooves feed to one adiabatic groove)

$= 0.3863$

or 38.63%

Hydraulic radius, $r_{h,\ell} = 0.5063 \times 10^{-3}$ m (same as in R_3)

Permeability $k_g = \dfrac{2 \varepsilon r_{h,\ell}^2}{f_\ell \, Re_\ell} = 1.265 \times 10^{-8}$ m^2 (twice as that of R_3)

Axial flow area is same as in R_3. Hence,

$$R_7 = 6.2641 \times 10^{12} \left(\frac{\nu_\ell}{\lambda}\right) \quad N/m^2 \text{ per watt}$$

$$R_8 = \frac{\Delta r \, \ln(d_o/d_i)}{2\pi K_s L_c \Delta r} \left(\frac{\nu_\ell}{\lambda}\right) \qquad (G.8)$$

This is computed similar to R_1.

$$R_8 = 0.9190 \times 10^{8} \left(\frac{\nu_\ell}{\lambda}\right) \quad N/m^2 \text{ per watt}$$

Summarizing,

$$R_1 = 2.5343 \times 10^{8} \left(\frac{\nu_\ell}{\lambda}\right)$$

$$R_2 = 197.878 \times 10^{12} \left(\frac{\nu_\ell}{\lambda}\right)$$

$$R_3 = 4.5432 \times 10^{12} \left(\frac{\nu_\ell}{\lambda}\right)$$

$$R_4 = 3.3215 \times 10^{12} \left(\frac{\nu_\ell}{\lambda}\right)$$

$$R_5 = 1.2528 \times 10^{12} \left(\frac{\nu_\ell}{\lambda}\right)$$

$$R_6 = 3.3215 \times 10^{12} \left(\frac{\nu_\ell}{\lambda}\right)$$

$$R_7 = 6.2641 \times 10^{12} \left(\frac{\nu_\ell}{\lambda}\right)$$

(R_1 and R_8 are orders of magnitude small compared to the rest and hence may be neglected)

$$R_8 = 0.919 \times 10^{8} \left(\frac{\nu_\ell}{\lambda}\right)$$

Since R_2 and R_3 are in parallel, their equivalent resistance is

calculated as $R_{\substack{2-3 \\ equi}} = \dfrac{R_2 R_3}{R_2 + R_3}$

Thus $R_{\substack{2-3 \\ equi}} = 4.4412 \times 10^{12} \left(\frac{\nu_\ell}{\lambda}\right)$

Similarly, $R_{\substack{6-7 \\ equi}} = 6.193 \times 10^{12} \left(\frac{\nu_\ell}{\lambda}\right)$

The total liquid flow resistance is,

$$F_\ell L_{eff} = R_1 + R_{\substack{2-3 \\ equi}} + R_4 + R_5 + R_{\substack{6-7 \\ equi}} + R_8 \qquad (G.9)$$

i.e., $F_\ell L_{eff} = 15.2085 \times 10^{12} \left(\frac{\nu_\ell}{\lambda}\right)$ N/m^2 per watt

APPENDIX H

STEADY STATE EXPERIMENTAL TEST DATA

TEST SET 1

TEST SET 2

TEST SET 3

TEST SET 1
GAS FILLED MODE (P_i = 1.35 TORR; CONDENSER SHUTTER CLOSED)

TEST DATE	HEAT INPUT			Q_E		Q_A		Q_D		AVG TEMP. (°C)		HOT FRONT LOCATION		INACTIVE CONDENSER
	Q_i MEASURED (W)	$\Delta T_{coolant}$ E + A + C (K)	Q_i CALORIMETER (W)	(W)	% Q_i	(W)	% Q_i	(W)	% Q_i	$\bar{T}_H$	$\bar{T}_C$	T.C. #	L (cm)	L_{NCG} (cm)
10/24/88	284	0.7+0.5+0.6=1.8	289.8	112.8	38.9	80.5	27.8	96.6	33.3	485	85	11/12	115	85
10/24/88	506	0.9+0.6+1.6=3.1	499.3	145	29	96.6	19.4	257.7	51.6	516	126	14/15	145	55
10/25/88	289	0.7+0.5+0.6=1.8	289	112.8	38.9	80.5	27.8	96.6	33.3	488	103	11/12	115	85
10/26/88	358	0.8+0.5+0.9=2.2	354	128.9	36.4	80.5	22.7	144.9	40.9	502	105	12/13	125	75
10/27/88	153	0.5+0.3+0.2=1.0	161	80.5	50	48.3	30	32.2	20	456	105	8	79	121
10/28/88	566	1.0+0.6+1.9=3.5	563.4	161.1	28.6	96.6	17.1	306	54.3	533	210	15	151	49

NOTE: $Q_{cal} = 161.07\ \Delta T_{coolant}$

TEST SET 2
GAS FILLED MODE (P_i = 1.35 TORR; CONDENSER SHUTTER PARTIALLY OPEN)

TEST DATE	HEAT INPUT			$Q_E + Q_A$		Q_O		AVG TEMP. (°C)		HOT FRONT LOCATION		INACTIVE CONDENSER
	Q_i MEASURED (W)	$\Delta T_{coolant}$ (E + A) + C (K)	Q_i CALORI-METER (W)	(W)	% Q_i	(W)	% Q_i	$\bar{T}_H$	$\bar{T}_C$	T.C. #	L (cm)	L_{NCG} (cm)
08/15/88	350	1.0 + 0.7 = 1.7	280.5	165	58.8	115.5	41.2	475	129	12	120.2	79.8
08/15/88	620	1.4 + 1.7 = 3.1	511.6	231	45.2	281	54.8	500	207	15	151.4	48.6
08/31/88	502	1.6 + 1.7 = 3.3	531.5	257.7	48.5	273.8	51.5	490	93.5	14	140.1	59.9
08/31/88	299	1.2 + 0.9 = 2.1	338.2	193.3	57.2	144.9	42.8	467	96.4	11/12	115	85
09/01/88	752	2.1 + 2.8 = 4.9	789.2	338.2	42.9	451	57.1	513	143	15/16	156.4	43.6
09/02/88	1009	2.7 + 3.7 = 6.4	1043	440.3	42.2	603.4	57.8	535	208	16	161.6	38.4
09/06/88	1211	3.1 + 4.4 = 7.5	1223	505.6	41.4	717.6	58.6	568	176	17	171.7	28.3
09/06/88	1328	3.4 + 4.8 = 8.2	1337	554.5	41.5	782.8	58.5	575	175	17+	171.7+	28.3-
10/04/88	280	1.3 + 0.6 = 1.9	306	209.4	68.4	96.6	31.6	490	120	11	110	90

NOTE: $Q_{cal} = 161.07\ \Delta T_{coolant}$

TEST SET 3
NEAR-VACUUM MODE (SHUTTER CLOSED)

TEST DATE	HEAT INPUT			Q_E		Q_A		Q_D		AVG TEMP. (oC)	
	Q_i MEASURED (W)	$\Delta T_{coolant}$ E + A + C (K)	Q_i CALORI-METER (W)	(W)	% Q_i	(W)	% Q_i	(W)	% Q_i	$\bar{T}_H$	$\bar{T}_C$
11/10/88	293.7	0.7+0.4+0.8=1.9	306	112.6	36.8	64.4	21.05	128.8	42.15	445.5	153.3
11/10/88	409.2	0.8+0.5+1.3=2.6	418.8	129	30.8	80.4	19.2	209.4	50.0	463.5	220
11/11/88	517.6	0.8+0.6+1.8=3.2	515.4	128.9	25	96.9	18.8	289.6	56.2	489.3	316
11/14/88	590.8	0.9+0.6+2.2=3.7	595.9	144.9	24.3	96.6	16.2	354.4	59.5	502.8	371
11/14/88	757.9	1.1+0.7+2.9=4.7	757.9	177.2	23.4	112.7	14.9	467.1	61.7	544.9	501.4
11/14/88	757.9	1.1+0.7+2.9=4.7	757.9	177.2	23.4	112.7	14.9	467.1	61.7	544.9	501.4

NOTE: $Q_{cal} = 161.07\ \Delta T_{coolant}$

U.S. GOVERNMENT PRINTING OFFICE: 1989 - 648-036/00447